
The University Of Sheffield.

# Composite cement systems for encapsulation of barium sulphate scale from oil industry and application as high density support matrix

**Oday Hadi Hussein**

**A thesis submitted to the Faculty of Engineering in partial fulfilment of the requirements for the degree of Doctor of Philosophy**

**Department of Materials Science and Engineering**

**University of Sheffield**

**November 2013**

# Dedication

To my dad, Hadi Hussein Al- Subaiee, who died before I finished my project.

To my mum, and my lovely family

# Acknowledgments

This research project would not have been possible without the support of many people. Firstly, I wish to express my gratitude to my supervisor, Dr. Hajime Kinoshita for his support throughout the project and for the great amount of time and effort he spent to help me to finish my project. He has always believed in my abilities and provided whatever advice and resources necessary for me to accomplish my goals. Deepest gratitude is also to my previous supervisor Dr. Michel Ojovan for his support during the first year, and added much more meaning to my work. Special thanks also to Dr. Claire Utton, Dr. Susan Bernal, and Professor John Provis for their many invaluable inputs, suggestions and comments to the project.

I would like to thank the technical and administrative staff in the Department of Materials Science and Engineering for providing laboratory facilities, in particular Bev Lane, Andrew Mould, Dean Haylock, Ben Palmer and Karen Burton.

Great appreciation is for staff and students in the Immobilisation Science Laboratory (ISL) for their advice, guidance and support throughout the project.

The residents of L6, thank you who have given me wonderful advices, inspiration and friendship over the years.

Also, I would like to convey thanks to the Iraqi ministry of high education and scientific research and to Iraqi cultural attach for providing the financial means.

A big thank go to Dr. Yousif Zayir from the Iraqi ministry of science and technology for her support to start my research project.

Finally, I wish to express my love and gratitude to my beloved family; for their understanding & endless love, who have always given me their support through the duration of my studies. My wife and my children Laith, Maream, Hassan, and Fatima, I love you all.

# Abstract

Radioactive barium sulphate scales raise a serious concern in the oil and gas industries. They are often classified as low level radioactive waste, but there are no clear methodologies established world widely to deal with this well know issue. The present study investigates a potential use of composite cement systems based on Portland cement to encapsulate the barium sulphate scales, aiming to provide a feasible option for safe handling, storage and disposal. The investigation was conducted on three different aspects: basic formulation, wasteform development and potential use as a high density support matrix.

The first part studied the basic formulation to clarify the impact of $BaSO_4$ loading and water contents on the physical properties of the composite cementing system. Fine $BaSO_4$ powders and excess water were found to influence the product phases whereas coarse $BaSO_4$ particles showed larger impact on strength of the products. The second part investigated the effect of mineral admixtures to develop practical wasteform formulations. Fine $BaSO_4$ powder, metakaolin and quartz were found to improve the workability of the pastes as well as the microstructure by eliminating highly porous interfacial transition zone, resulting in the higher compressive strength and reasonable leaching rates of elements. Addition of quartz was found to be most effective to minimise the degradation caused by the high temperature environment, by initiating the formation of stable tobermorite phase.

# List of abbreviations

Commonly used symbols and notations are presented below. Others are defined in the text as they appear.

**Cement Nomenclature**

| | | |
|---|---|---|
| C | $CaO$ | Calcium oxide |
| S | $SiO_2$ | Silicon dioxide |
| A | $Al_2O_3$ | Aluminium oxide |
| F | $Fe_2O_3$ | Iron oxide |
| H | $H_2O$ | Water |
| $\overline{S}$ | $SO_3$ | Sulphate |
| C | $CO_2$ | Carbon dioxide |

**Roman letters**

| | |
|---|---|
| BFS | Blast furnace slag |
| BSE | Backscattered electron imaging |
| DBGD | Deep Bore hole Geological Disposal |
| EDS | Energy Dispersive X-ray Spectroscopy |
| EPA | U.S. Environmental Protection Agency |
| HDSM | High Density Support Matrix |
| HLW | High level waste |
| IAEA | International Atomic Energy Agency |
| ICP-MS | Inductively coupled plasma optical emission spectroscopy |
| ILW | Intermediate level waste |
| LLW | Low level waste |
| LSA-scale | Low Specific Activity scale |
| MIP | Mercury Intrusion Porosimetry |
| NORM | Naturally Occurring Radioactive Materials |
| PC | Portland cement |
| SCM | Supplementary Cementing Materials |
| SEI | Secondary electron imaging |
| SEM | Scanning electron microscopy |
| TGA | Thermal gravimetric analysis |
| XRD | X-ray diffraction |

# Table of Contents

# List of Figures

# List of Tables

# Chapter 1: Introduction

## 1.1 Background

Some petroleum industry operations have been responsible for environmental radioactive pollution [1, 2]. Pollutants include radioactive scale waste known as naturally occurring radioactive materials (NORM). This NORM scale waste is arising from processing oil and gas extraction processes as by-products of formation water and crude oil [1, 3, 4]. The management and disposal of NORM scale is becoming a significant environmental in recent years [5-8]. Therefore, the development of techniques for the disposal of this kind of radioactive waste is an area of increasing importance and concern. The NORM scale wastes are classified as low level radioactive waste (LLW) [9]. Cements are inorganic binder commonly used for encapsulation of LLW [10]. The cement matrix may be used for the encapsulation of NORM scale, because of the historically successful application in the nuclear industry and its flexibility with different types of additives [11].

## 1.2 Scope of the project

The aim of this research project is to provide experimental data on the fundamental properties of PC-$BaSO_4$ systems. The effect of $BaSO_4$ loading, particle size, water content and mineral admixtures on PC cement paste were evaluated, in order to develop commercially feasible cementing systems to encapsulate scales containing NORM from oil and gas industry. This project also investigated the applicability of the PC-$BaSO_4$ system for the high-density support matrix (HDSM) in the deep bore hole geological disposal system (DBGD) for nuclear wastes [12].

The main objectives of the project are the following:

1) To establish the fundamental understanding on the effect of basic formulation on the PC-$BaSO_4$ system, in particular $BaSO_4$ loading and water content on the product phases, microstructure and compressive strength using $BaSO_4$ powder and coarse granules. Such fundamental data would be useful to develop the formulation of the system for the encapsulation of $BaSO_4$ NORM scale from oil and gas industry.
2) To optimise the formulation of cement wasteform with the industrial application in mind. The effects of water content, $BaSO_4$ loading and different mineral admixtures were studied focusing on setting time and the rheological properties of the cement pastes. The mechanical property, microstructure and leaching behavior of the products were also studied.
3) To study the feasibility of PC-$BaSO_4$ system as HDSM for DBGD. Preliminary investigation was conducted to establish the effect of high temperature on hardened PC-$BaSO_4$ system, and the effect of hydrothermal curing of PC-$BaSO_4$ in closed system was further studied with or without addition of mineral admixtures. The investigation focused on the phase evolution, microstructure alteration, and mechanical property change in the products.

The materials to be used may not be exactly the same as the tailing materials arising from the oil industry. Substitute materials were used as a representative, keeping the properties similar to that of tailing materials.

## 1.3 Organisation of the thesis

The thesis comprises the following chapters:

**Chapter 1** introduces the brief background, the aims and objectives of the study, and thesis organisation.

**Chapter 2** reviews the literature information on the related areas currently available. The first part from this review introduces the issues of NORM scale, by-product waste streams from the oil and gas industry and summarises the use of cementitious materials for waste disposal. The second part of this review focus on the applicability of PC-$BaSO_4$ system as HDSM in DBGD.

**Chapter 3** describes the materials and experimental methods used in the project. This chapter is divided into three sections: the first section characterise the raw materials used in the experiments. The second section describes the sample preparation whereas the last section is an outline of the analytical techniques used to study the properties of the products.

**Chapter 4** covers the fundamental characterisation of PC-$BaSO_4$ systems. Experimental data are presented, and the effect of $BaSO_4$ loading, water contents, size of $BaSO_4$ are discussed focusing on product phases, microstructure, and compressive strength.

Chapter 5 optimise the formulation of the PC-$BaSO_4$ systems for industrial application of this system for encapsulation of $BaSO_4$ NORM scale. A good range of formulation and possible mineral admixture were tested.

**Chapter 6** covers the experimental data on the behaviour of PC-$BaSO_4$ systems under high temperature conditions.

**Chapter 7** summarises the obtained results, provides the conclusion of this thesis and offers recommendation.

**Chapter 8** summarises the future work.

## 1.4 References


1. A. Liland, P. Strand, I. Amundsen, H. Natvig, M. Nilsen, R. Lystad, and K. E. Frogg, *Advances in NORM management in Norway and the application of ICRP's 2007 Recommendations.* Annals of the nternational Commission on Radiological Protection ( ICRP I2011 Proceedings), 2012. **41**(3-4): p. 332-342.
2. M. S. Hamlat, S. Djeffal, and H. Kadi, *Assessment of radiation exposures from naturally occurring radioactive materials in the oil and gas industry.* Applied Radiation and Isotopes, 2001. **55**: p. 141–146.
3. M. S. Al-Masri and H. Suman, *NORM waste management in the oil and gas industry: The Syrian experience.* Journal of Radioanalytical and Nuclear Chemistry, 2003. **256**(1): p. 159–162.
4. M. B. Cooper, *Naturally Occurring Radioactive Materials (NORM) in Australian Industries - Review of Current Inventories and Future Generation*. 2005: Australia.
5. D. Read, B. Rabey, S. Black, F. P. Glasser, C. Grigg, and A. Street, *Implementation of a strategy for managing radioactive scale in the China clay industry.* Minerals Engineering, 2004. **17**: p. 293-304.
6. D. L. Blunt and K. P. Smith, *Dose Assessment for Management Alternatives for NORM - Contaminated Equipment within the Petroleum Industry*, in *Third Annual Conference on the Recycle and Reuse of Radioactive Scrap Metal*. 1995: Knoxville,Tennessee.
7. T. Strand. *Handling and disposal of NORM in the oil and gas industry*. in *WM99*. 1999. Phoenix- AZ-US: WM99.
8. IAEA. *Naturally Occurring Radioactive Material (NORM VI)*. in *Proceedings of an International Symposium*. 2010. Marrakesh, Morocco: IAEA.
9. H. Stensrud, T. Gäfvert, T. D. Bergan, I. Amundsen, T. Strand, and P. Strand, *Regulating Discharges from Non-nuclear Industry in Relation to Environmental elation to Environmental Radiological Protection*. 1995: Grini Næringspark,Norway.
10. C. R. Wilding, *The performance of cement based systems.* Cement and Concrete Research, 1992. **22**(2-3): p. 299-310.
11. J. H. Sharp, J. Hill, N. B. Milestone, and E. W. Miller. *Cementitious Systems for Encapsulation of Intermediate Level Waste*. in *Radioactive Waste Management and Environmental- ICEM03*. 2003. Oxford.
12. F. G. F. Gibb, N. A. McTaggart, K. P. Travis, D. Burley, and K. W. Hesketh, *High-density support matrices: Key to the deep borehole disposal of spent nuclear fuel.* Journal of Nuclear Materials 2008. **374** p. 370–377.

# Chapter 2: Literature review

## 2.1 Introduction

The following review introduces the issues of naturally occurring radioactive materials (NORM), a by-product waste stream from the oil and gas industry and summarises the use of cementitious systems to encapsulate the NORM scale and dispose as radioactive wasteforms. The usefulness of cement systems in terms of physical and chemical properties as well as that of the hardened composite cements for this application and their limitations are presented. Particular attention is given to Portland cement (PC), either alone or in conjunction with mineral admixtures to encapsulate the NORM scale in the form of barium sulphate ($BaSO_4$). The review also extends to the alternative methodology to dispose of high level radioactive waste (HLW) using deep bore hole geological disposal system (DBGD) with the view to apply the PC-$BaSO_4$ system as a high density support matrix (HDSM) in DBGD.

## 2.2 Naturally Occurring Radioactive Materials (NORM)

### 2.2.1 NORM scale

In many countries, a significant radioactive contamination in the oil and gas industrial processes occurs due to the solid precipitate scales containing natural radioactive elements, commonly known as Naturally Occurring Radioactive Materials (NORM), which are by-products present in varying concentrations in the hydrocarbon reservoirs [1-3]. For example, According to U.S. Environmental Protection Agency (EPA), about 25,000 tons of NORM scale are generated each year by the petroleum industry in the United States only [4]. As shown in Figure 2.1, NORM scales are deposited in processing equipment and vessels

[5], e.g. wellheads, tubular, and surface facilities including pipelines and plant equipment.

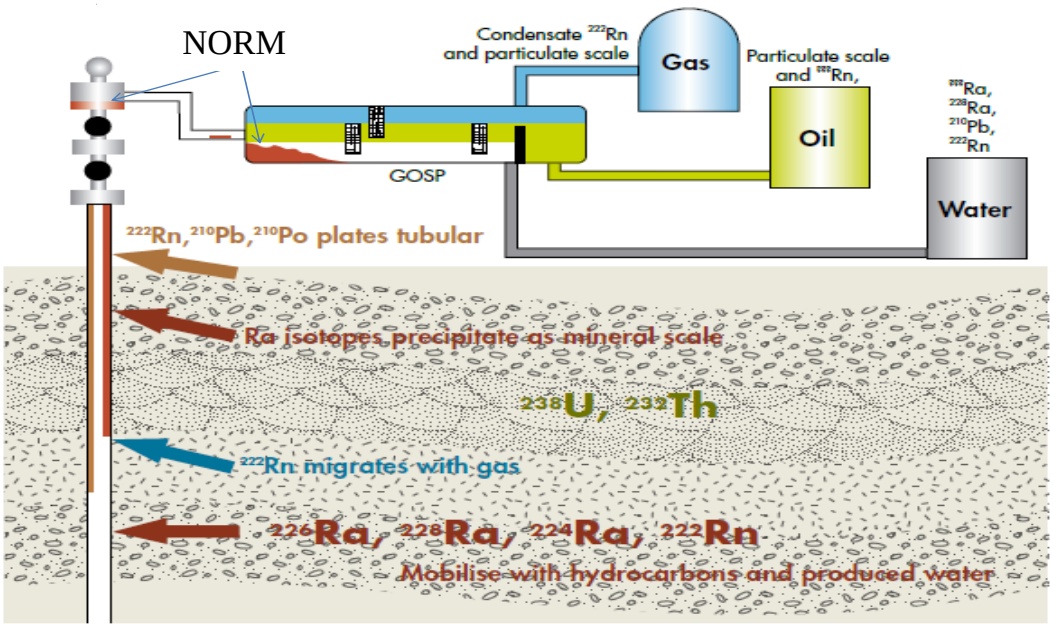


Figure 2.1 Schematic of oil and gas recovery process [5].

### 2.2.2 NORM radioactivity

The petroleum industry has recognized that the deposit of $BaSO_4$ and $SrSO_4$ can give a rise to the radioactive scale during the oil and gas production [6, 7]. The ionizing radiation originating from the $BaSO_4$ and $SrSO_4$ scales is derived from the radioactive decay of naturally occurring radium isotopes ($^{226}$Ra and $^{228}$Ra) and their decay products [3, 8, 9]. The sources of the radium in oil and gas NORM scales are long-lived isotopes of uranium-238 ($^{238}$U) and thorium-232 ($^{232}$Th). As shown in Figure 2.2, the $^{226}$Ra isotope is the sixth member of the $^{238}$U decay series, and the $^{228}$Ra isotope is the second member of the $^{232}$Th decay series as shown in Figure 2.3. Both uranium and thorium are present in

the oil environment with the activity concentration depending on the geologic formation and type of rock [2], which can produce several daughter radioisotopes through their decay series. Both of them are relatively insoluble and remain in the place of the subsurface formation. The decay products of these series are, however, more soluble and can become mobile in the produced water waste stream [8].

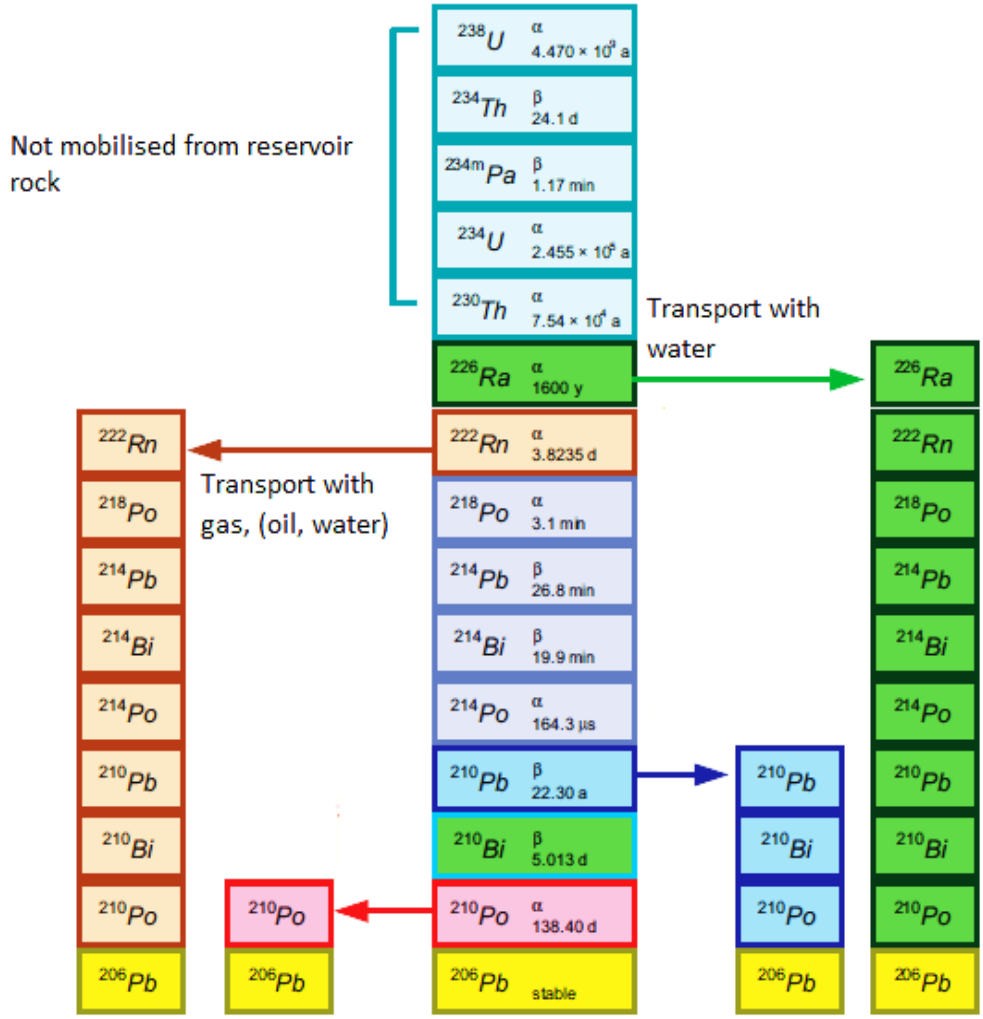


Figure 2.2 Uranium-238 decay series [8].

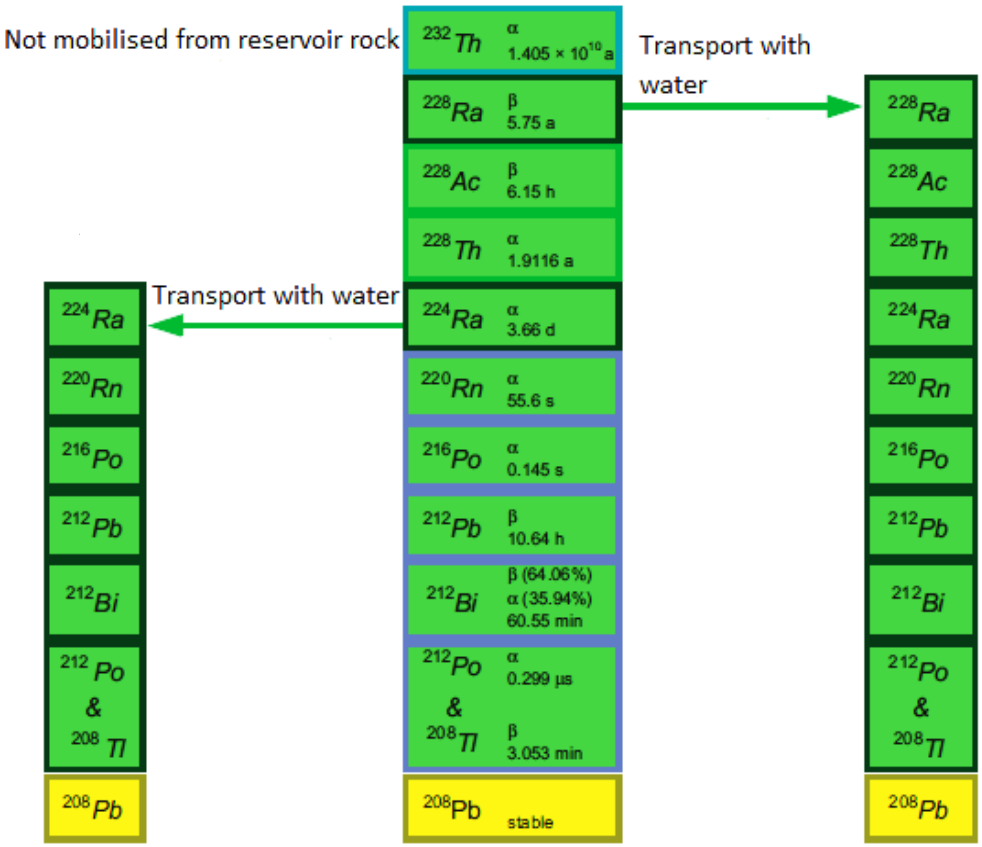


Figure 2.3 Thorium-232 decay series [8]

The scale, also known as Low Specific Activity scale (LSA-scale) or low radioactive waste [5, 10, 11] emits alpha (α), beta (β), and gamma radiation (ϒ) [5], which can cause problems when the equipment containing the radioactive scale has to be handled or removed from service. For example, the NORM materials may become an inhalation risk (Figure 2.4) when the material is removed by mechanical forces, such as wire brushing [5]. Therefore, these scales require appropriate handling and disposal. These radiation and their potential health risks are:

**Alpha (α)** particle is a heavy particle which is equivalent to a helium nucleus that is positively charged. It interacts strongly with matter and can be stopped by a thin sheet of paper [5]. The primary health concern associated with alpha particles is that, when the alpha-emitting materials are ingested or inhaled, energy from the alpha particles is deposited in internal tissues [12].

**Beta (β)** particles have either one positive (+1) or negative (-1) charge. They are small, over 7000 times lighter than the alpha particles. The beta particles travel farther through the solid material than the alpha particles, which interacts slowly with the matter. It can be stopped by thin layers of metal or plastic [5]. The health concerns associated with beta particles arise primarily when beta-emitting materials are ingested or inhaled [12].

**Gamma (ɣ)** rays can pass completely through the human body. It is a form of high energy electromagnetic radiation similar to X-rays but much more energetic that interacts lightly with matter and may cause ionization in any organ in the body [5]. Gamma rays are best shielded by thick layers (six inches) of lead or three feet of concrete. It is considered as an external hazard to the living tissues [12].

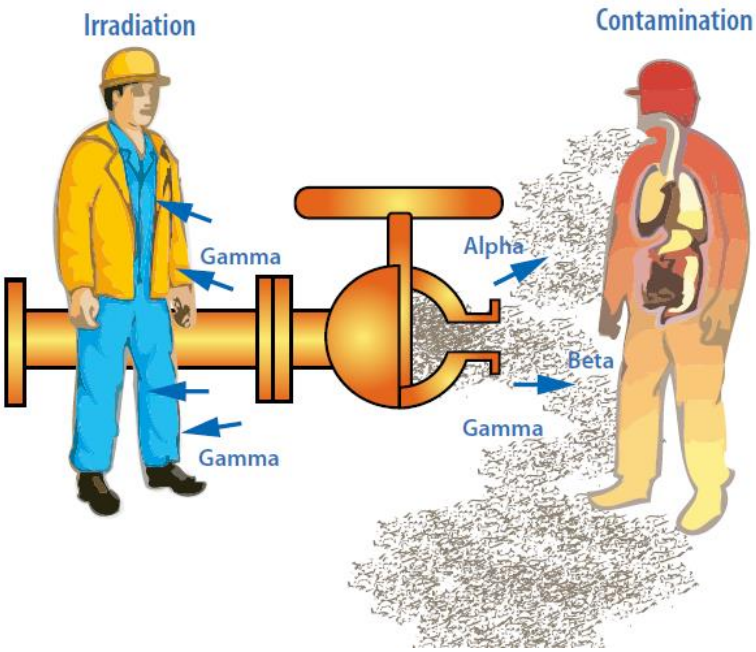


Figure 2.4 The potential NORM scale exposure scenarios [5]

### 2.2.3 Scale formation

The formation of scales in the oil and gas industry is due to the chemical-physical processes which take place in the reservoir's production waters [2]. Figure 2.5 shows the mechanism of scale formation: (i) In order to keep the oil production stable and to maintain the well integrity with the production time, it is necessary to inject seawater into the wells; (ii) then the injection seawater which contains of sulphate ion $SO_4^{2-}$ is mixed with the formation water which contains ions of the alkali earth elements including radium; (iii) the mixture of these incompatible water reaches the surface, and the change in the pressure, temperature or pH can lead to the radium isotopes ($^{226}Ra$ and $^{228}Ra$) to precipitate [1, 13-15].

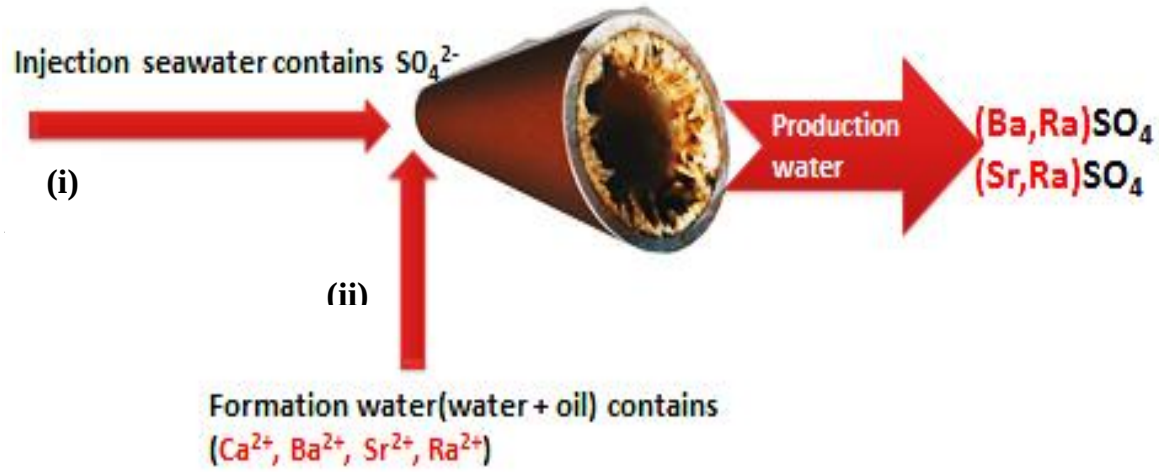


Figure 2.5 Mechanism of radioactive scale formation

Usually radium co-precipitates with divalent cations, barium and strontium, to form neutral compounds (primarily sulphates), i.e. $(Ba,Ra)SO_4$ and $(Sr,Ra)SO_4$ solid solutions [1, 13-15] via Equation 2.1 and 2.2

$$(Ba, Ra)^{2+}_{(formation\ water)} + SO_4^{2-}{}_{(seawater)} \rightarrow (Ba, Ra)SO_{4\ (scale)} \quad (2.1)$$

$$(Sr,Ra)^{2+}_{(formation\ water)} + SO_4^{2-}{}_{(seawater)} \rightarrow (Sr, Ra)\ SO_{4\ (scale)} \quad (2.2)$$

The affinity of radium with barium and strontium in the crystal lattice comes from the similar chemical properties [16, 17], and is most similar to barium [17]. Therefore, radium is expected to be well accommodated in their crystal structures [7, 18, 19]**.** Szabo et al. reported that both Ra and Ba do not undergo redox transformation, and they can form a neutral or anionic $SO_4$ complex at high pH (near 10) [17]. Grandia et al. reported that the sulphate solid solution of $(Ba, Ra)SO_4$ is thermodynamically more stable than the simple mechanical mixture between the solid end-members ($BaSO_4$ and $RaSO_4$) due to the

reduction of the Gibbs free energy when a solid solution of (Ba,Ra)$SO_4$ forms [19].

### 2.2.4 Concentration of radium in the scale

According to the literature, the scale found in the piping and any other equipment used in the oil and gas stream processes do not contain $^{238}U$ or $^{232}Th$ [20]. As noted before these elements are relatively insoluble and remain as the solid phase in the place of the subsurface formation. The scale contains only alkali earth elements such as barium, strontium, calcium and radium [20]. It has been known that barium and strontium sulphate precipitation will lead to a radium co-precipitation [5, 17]. A study by Al-Masri and Aba 2005 [13] reported the correlation among the concentration of these elements Ba, Sr and Ra in scale as shown in Figure 2.6. The concentration of radium in the scale increases in proportion with the concentration of barium and strontium increase.

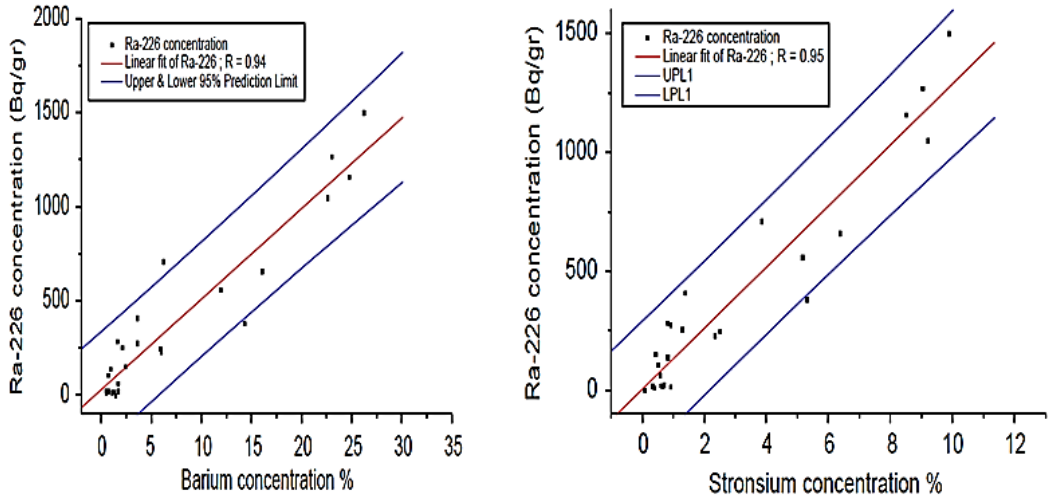


Figure 2.6 Correlation between Ra concentration and Ba, Sr concentration [13]

The chemical composition of various scales and the activity levels of $^{226}$Ra and $^{228}$R from different oil and gas fields are presented in Table 2.1. Available data shows that the specific activity of $^{226}$Ra ranges from less than 0.1 Bq/g up to 15000 Bq/g [8, 21, 22]. The values for $^{228}$Ra in scales are, in general, not much lower than that for $^{226}$Ra. The average of specific activity of scales can exceed the exemption level of 10 Bq/g for $^{226}$Ra and $^{228}$Ra recommended by the International Basic Safety Standards for protection against ionizing radiation and for the safety of radiation sources [23, 24]. The scale can be classified as radioactive when the concentration of $^{226}$Ra, $^{228}$Ra exceeds 10 Bq/g scale [10, 21], and should be handled as low level radioactive wastes (LLW) or low specific wastes (LSW) [10].

Table 2.1 Concentration of $^{226}Ra$ and $^{228}Ra$ in different scale samples

| Materials | Specific activity Bq[1]/g | | Chemical content in scale (ppb) | | location | Ref |
|---|---|---|---|---|---|---|
| | $^{226}Ra$ | $^{228}Ra$ | $^{226}Ra$ | $^{228}Ra$ | | |
| $(Ba,Sr)SO_4$ | 106 | 78 | 2.8 | 2.1 | Brazil | [14] |
| $BaSO_4$, $CaCO_3$ | 1-1000 | - | 0.02-27 | | | [25] |
| $(Ba,Sr)SO_4$ | 174 | 91 | 4.7 | 2.46 | Syria | [13] |
| | 1050 | - | 28.3 | - | | [26] |
| $(Ba,Sr)SO_4$, $CaCO_3$ | 1–950 | - | 0.02 25.6 | - | Algeria | [26] |
| Scale | 7.54-143.26 | - | 0.2-3.87 | - | Egypt | [27] |
| $(Ba,Sr)SO_4$, $CaCO_3$ | 4.3–658 | - | 0.11-17 | - | Tunis | [28] |
| $BaSO_4$ | 21-250 | 48-300 | 0.56-6.75 | 1.3-8.1 | Australia | [20] |
| scale | 114.3-187.7 | 130-206 | 3 -5 | 3.5-5.5 | Malaysia | [15] |
| scale | 76.1 | - | 2 | - | Oklahoma | [29] |
| | 15.4 | - | 0.4 | - | Michigan | |
| $(Ba,Sr)SO_4$, CaCO3 | 3700 | - | 100 | - | USA | [26] |
| $(Ba,Sr)SO_4$, $CaCO_3$ | 1–1000 | - | 0.027-27 | - | UK | [30] |
| Scale | 0.1–15000 | - | 0.0027-405 | - | - | [8] |

## 2.3 Options for disposal of NORM in oil and gas industry

### 2.3.1 Current technologies

Disposal of oil and gas industry NORM scale is not simple due to its content of hazardous and radioactive materials. Although the presence of NORM in oil and gas wastes has been recognized since 1930s [31], the NORM was not recognized as a waste management issue until the mid-1980's, when the

[1] 1 Bq = 1 disintegration per second

industry and regulators realised that NORM occurrence was more widespread than originally thought and that radioactivity levels can be high [32]. This leads the petroleum industry to adopt more restrictive methods for the management and disposal of NORM-contaminated wastes than those previously accepted, which are likely to provide greater isolation of the radioactivity [32]. In Syrian oil companies for example, NORM scale waste from the decontamination of equipment and removal from the piping (Figure 2.7 a) using high pressure water system or mechanical cleaning are currently stored in standard storage barrels as shown in (Figure 2.7 b) in a controlled area prior to the transfer to the radioactive waste facilities [33].

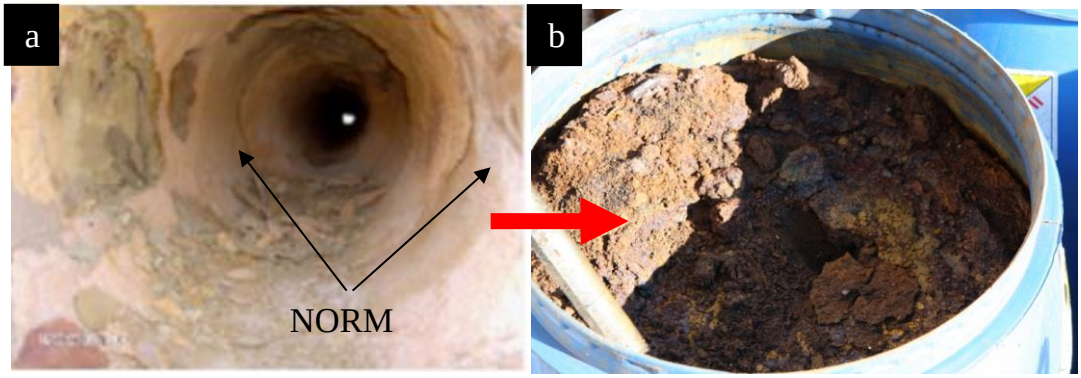


Figure 2.7 NORM scales [34, 35]

Some of the current options used by oil and gas companies for management and disposal of NORM are briefly outlined below.

- Land spreading: This method has been available to the petroleum industry and used world widely. In this method NORM scales having an

activity concentration higher than the acceptation level are mixed with clean soil to decrease the Ra concentration lower than the required level. The mixture is then disposed in a large area. However, the present use of this method is limited due to the increase of the Ra in ground water [36, 37].

- Landfill disposal: The burial of the wastes surrounded by a concrete barrier is one of the NORM disposal options. However, this method has remediation problems leading the negative human and environmental impacts, including long-term implications arising from groundwater contamination [38].
- Well injection: This method put the NORM wastes back to the place they come from. In this method the NORM scale is mixed with water and then injected to old well. After the NORM injection, the well is usually plugged with cement to prevent the migration of fluids in the wellbore. Studies have shown that these solution are very safe [39]. However, the method is only available when no longer the well is used [40].
- Deep underground disposal: The NORM scale is stored, usually in the mined repositories, tunnels or other types of low level radioactive waste facilities [37, 39].

### 2.3.2 Cementation of LLW

As already mentioned, NORM scale can be categorised as LLW. Radioactive wastes are classified by the level of radioactivity worldwide, e.g. Low Level Wastes (LLW), Intermediate Level Wastes (ILW) and High Level Wastes (HLW). In the UK, LLW, ILW, HLW are defined as following [12]:

- **LLW** has a radioactivity of less than 4000 Bq/g alpha activity or 12000 Bq/g beta or gamma activities and does not require shielding in handling or storage [12].
- **ILW** is highly radioactive, but is not significantly heat generating [12] such as the cladding of fuel rods.
- **HLW** is highly radioactive, which generate heat and will be vitrified. HLW contains over 95% of the entire radioactivity in wastes from the generation of electricity by the nuclear power [12].

Cementitious, or cement-based, wasteforms are commonly used worldwide for storage and disposal of LLW and ILW, hazardous and mixed wastes [41]. Portland cement (PC), with or without Supplementary Cementing Materials (SCM), is being used in the UK to encapsulate the LLW and ILW [41-44]. The reasons for converting the raw wastes into more formal wasteforms are to allow a safer transport of the wastes to a repository using the existing transportation system and to reduce the probability of the total system failure. Therefore, the immobilisation of the waste ions in wasteform is the key to prevent diffusion of contaminants and making a manageable product. Cement has been studied extensively for incorporating wastes as there are many advantages, both physically and chemically, with the main points being as follows [41, 43]:

1. The raw materials are readily available economically
2. The products have a good durability and strength.
3. The low temperature mixing process is simple and can provide a good workability [41, 43].

4. Cements can be combined with all kinds of additives that alter the products' final properties, making them a flexible material.
5. Hydrated cement has a reasonable chemical and thermal stability, also stable when irradiated and can provide a shield against radiation when it is thick enough [42, 45].
6. Cements can easily handle wet wastes because they need water for their solidification itself.
7. The solid products are relatively non-toxic and non-flammable.

In the UK, an PC-based cement matrix inside stainless steel containers has been used to encapsulate and immobilise LLW and ILW [44]. The waste is poured into 500 L stainless steel drums, followed by cement grout infilling as shown in Figure 2.8

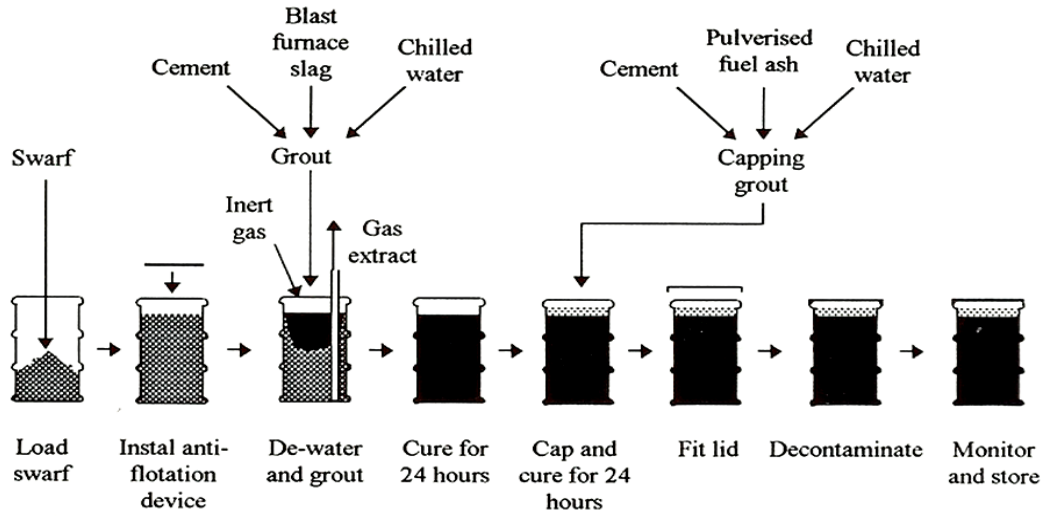


Figure 2.8: Schematic of encapsulation of ILW in composite cement [44]

The long-term durability and stability of the cement wasteform is of importance due to the long lifetime requirement for the hardened radioactive cement wasteforms. The waste packages may be stored above ground for a period of up to 200 years before ultimate disposal [46]. Figure 2.9 shows an example of ILW encapsulated in cement matrix.

Figure 2.9 Cement-encapsulated solid ILW in 500 L drums. [47]

### 2.3.3 Feasibility of cementation for $BaSO_4$ NORM scale

In general, the handling and disposal of waste from the oil and gas industry varies very much around the world. However, most of the methods described in the former section which have been used for long time to dispose the NORM waste do not fulfil the current regulatory regime of radiation protection and

environmental protection [48]. The NORM–contaminated scale can be treated before disposal, by solidification or chemical stabilisation to reduce the mobility of radionuclides.

Radioactive waste is typically immobilised to provide higher safety of handling and transportation, and hardened Portland cement paste has been known as suitable medium for the immobilisation of low level radioactive wastes [41]. Cement is a complex material and when it hydrates, it produces many phases which can be either crystalline or amorphous. Some of these phases have very flexible structures and can accommodate many ions into their structures. Some of the radioactive species from the wastes have been shown to be contained in the structure of these cement phases and hence are considered immobilised [49, 50]. The interaction between the hardened cement matrix and the waste is strongly dependent on the chemical reactivity of the waste and cement paste and hydration reactions involving the waste and composite cement systems. These areas have generally been reviewed by Glasser 1992 [42], Gougar et al [51], and Sharp et al [41] among others. By controlling the conditions during hydration (i.e. curing temperature or composite cement composition) it is possible to form an efficient immobilising matrix with a desirable microstructure, physical properties and internal chemical environment for a specific ion encapsulation.

R. Wang et.al [52] studied the feasibility of cement system containing $BaSO_4$ for the $^{226}Ra$ immobilisation and concluded, based on the compressive strength data and the solubility of sulfates, that their cement system could be an effective barrier for $^{226}Ra$ disposal in the geological repository. More recently, Read et al. [1] has compared three cementing systems based on PC and recommended a

blend of Portland cement, fly ash and metakaolin with water to solid (w/s) ratio of 0.50 as a preferred encapsulant for the $BaSO_4$-containing scale they studied up to 14 wt% owing to its good leach resistance.

## 2.4 Cementing system

### 2.4.1 Portland cement (PC)

Cements are usually manufactured by heating a mixture of limestone and clay at an approximate temperature of 1450°C, producing an assembly of crystalline and amorphous phases known as clinker which are combinations of oxides [53]. The cement clinker is ground with few per cent of gypsum ($CaSO_4.2H_2O$) to a fine powder. The final product is called Portland Cement (PC) [49, 54, 55]. The four major constituents of clinker are alite (tricalcium silicate, $3CaO.SiO_2$, $C_3S$), belite (dicalcium silicate, $2CaO.SiO_2$, $C_2S$), the aluminate phase (tricalcium aluminate, $3Ca.Al_2O_3$, $C_3A$) and the ferrite phase (tetracalcium aluminoferrite, $4CaO.Al_2O_3.Fe_2O_3$, $C_4AF$). Approximately 50-70% of Portland cement clinkers consist of alite, 15-30% belite, 5-10% aluminate and 5-15% ferrite.

### 2.4.2 Hydration of clinker phases

Cement powder (anhydrous cement) and gypsum when mixed with water forms a paste that sets and hardens by means of hydration reactions and retains its strength after hardening. The overall hydration is exothermic and is generally addressed according to the hydration of clinker phases. Alite ($C_3S$) is the most important phase as it reacts with water quickly for the strength development at the age up to 28 days. The reaction of belite ($C_2S$) with water is very similar to

that of alite. However, belite reacts slower than alite, thus contributes significantly to the later strength development [49]. These two silicate phases react with water in the following manner:

$$2C_3S + 6H \Rightarrow C_3S_2H_3 + 3CH \quad (2.3)$$

$$2C_2S + 4H \Rightarrow C_3S_2H_3 + CH \quad (2.4)$$

Gel Portlandite

The C-S-H gel is a calcium silicate hydrate phase, which is the major binding phase in cements and constitutes up 60 to 70% of mass of the hardened Portland cement paste [56]. It is an essentially amorphous material, although it can be semi-crystalline based on the mineral structures of tobermorite and jennite [57, 58]. Portlandite, $Ca(OH)_2$, composes about 20% of the volume of the hydrated cement product [56]. This phase is highly crystalline. The amount produced is different between the alite and belite. In the belite, the amount of CH has been reported to be between a fifth to a third of that produced in the alite [59].

The aluminate phase ($C_3A$) reacts very rapidly with water unless controlled by the addition of gypsum. These crystals could provoke a flash set of the hardening cement [56].. As shown in Eq. 2.5, the product of hydration is a trisulphoaluminate known as ettringite and commonly referred to as AFt.

$$C_3A + 3C\bar{S}H_2 + 26H \rightarrow C_6A\bar{S}_3H_{32} \quad (2.5)$$

Aluminate Gypsum water Ettringite (AFt)

It has been reported that AFt is the most common substitutes for calcium with other divalent cations, such as magnesium, strontium, and barium [60]. Usually the amount of substitution is no more than a few percent [51]. If there is not enough sulphate available, ettringite is progressively replaced by a calcium monosulphoaluminate phase, known as monosulphate and commonly referred to as AFm [49] as shown in Eq. 2.6.

$$2C_3A + C_6A\bar{S}_3H_{32} + 4H \rightarrow C_4A\bar{S}_3H_{12} \quad (2.6)$$

Aluminate Ettringite (AFt) water Monosulphate (AFm)

The last part of hydration involves calcium aluminoferrite ($C_4AF$), which is considered to be similar to that of $C_3A$. However, the kinetics of the reaction are much slower, and the hydration products formed have a substitution in a part of their $Al^{3+}$ by $Fe^{3+}$ [61, 62]. This phase is deficient in lime but if lime form from the hydration of alite then hexagonal hydrates ($C_4(A,F)H_{13}$) and cubic hydrogarnet ($C_3(A,F)H_6$) can be formed [63]. Figure 2.10 shows a typical example of the phase composition in the hardened PC.

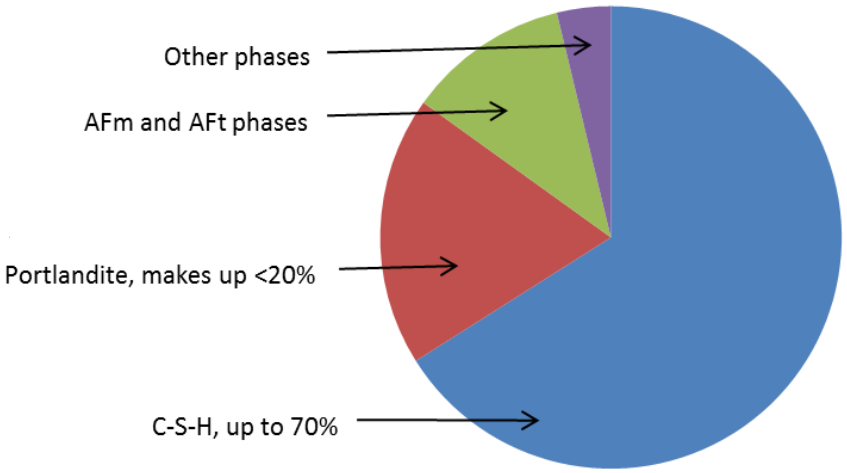


Figure 2.10 Typical compositions of cement hydration products

### 2.4.3 Hydration of cement

Cement hydration is the sum of the reactions given above and can be characterised by four different stages. The works of Taylor [56], Scrivener [64] provide a comprehensive explanation of the microstructural development of hydrating PC which is represented graphically in Figure 2.11.

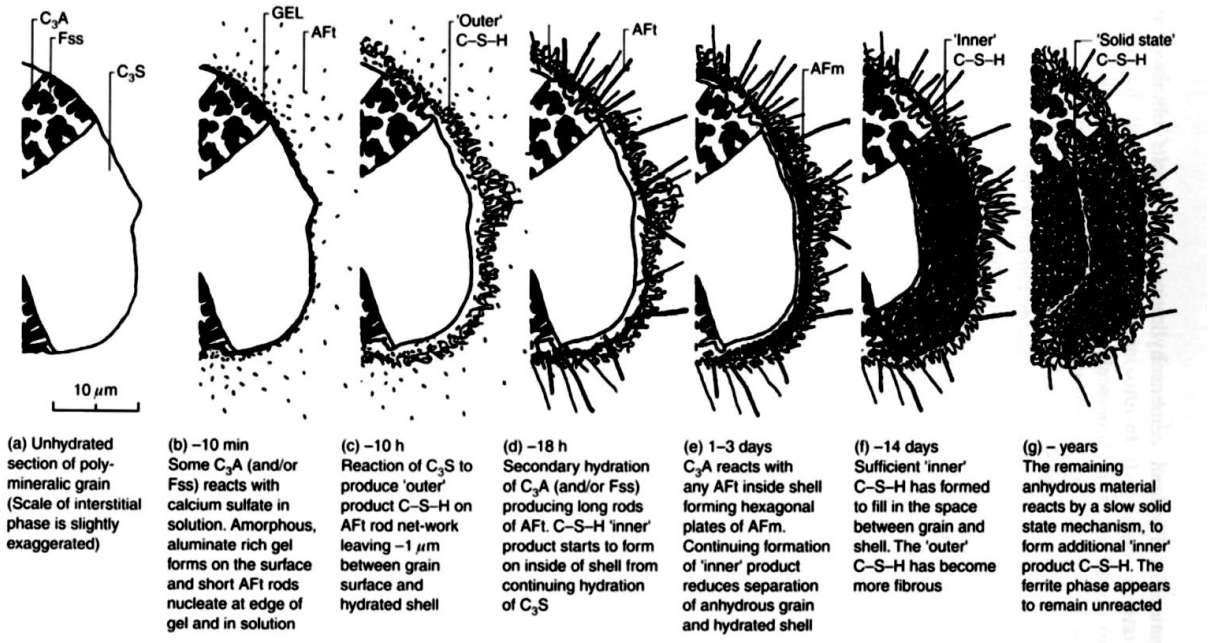


Figure 2.11: Diagrammatic hydration of PC [56]

**Pre-induction period (first minutes after mixing):** When cement is mixed with water, there is nearly an immediate reaction associated with the release of heat. Alkali sulphates dissolve completely, producing $K^+$, $Na^+$ and $SO_4^{2-}$ ions. The solution becomes supersaturated with respect to calcium hydroxide, and this hydroxide starts to precipitate.

**Induction period (first few hours):** During the early period (up to approximately 3 hours hydration), $C_3A$, reacts very fast with the sulphate from gypsum to form gelatinous ettringite, allowing the cement paste to maintain most of its plasticity. This amorphous surface gel layer is formed around the particles of cement, forming a layer which partially prevents water from gaining access to grains for further hydration [56]. In this period, the reaction is continuing, but very slowly compared with the faster reactions involved at the start of the hydration reaction. At this stage of hydration, little needles of calcium sulfoaluminate hydrate (ettringite) appear within a few minutes at the surface of the cement grains and in the pore solution away from the hydrating cement grains [56].

**Acceleration period (3-12 hours):** After approximately between 3 and 12 hours the unstable protective film formed around the cement grains is ruptured. The silica-rich solution inside the protective film can react with the $Ca^{2+}$ in the external solution, and C-S-H and CH form rapidly accompanied by a large heat output [65]. This allows the mechanisms of hydration to resume at a normal rate. According to Taylor, the growth of the C-S-H shell layers outwards into the pore solution, forming a gap between the anhydrous cement grain and this shell layer, is considered to be the induction period [53]. After 24 hours, the rate of ettringite formation is accelerated, increasing in the reactivity of $C_3A$ with

sulphate, and inner C-S-H product starts to form from the continuing hydration of the $C_3S$ on the inside of the shell, which is usually poorly crystallised [49, 54, 62].

**Post-acceleration period (12 hours and later):** The rapid progress of the previous stage slows down while the setting and hardening occur during this period. The ettringite initially formed transforms to monosulphate as a consequence of the decrease in the $SO_4^{2-}$:$Al^{3+}$ ratio with the progressive hydration reaction of the $C_3A$ during the first week of curing [54, 56]. The hydration is progressing, with continuing formation of inner C-S-H product. After approximately 2 weeks, the space between the grains is reduced and completely filled with the various hydrates, replacing the initial solution, and more outer C-S-H and CH are formed [56]. Within 4 weeks, the overlap structure of the various hydrates causes the hardening and the development of mechanical strength. In general, Portland cement attains most of its final strength after 4 weeks [46, 56].

### 2.4.4 Heat evolution

The heat evolution during the hydration of PC is graphically shown in Figure 2.12 as determined by isothermal conduction calorimetry (ICC) curve [66]. Peak I is associated with the initial reaction of the hydration and is attributed to a combination of wetting and the initial interaction between the cement powder and the water [56]. Peak II is the main exothermic reactions and corresponds to the hydration of $C_3S$ and the formation of C-S-H and CH [56], then the heat evolution gradually decreases after 24 h due to the limited ability of CH to interact with the available water through the outer layer (rim) [56]. Peak III has

often been associated with the replacement of Aft by Afm phases but it can also be associated with renewed formation of ettringite [56]. Peak IV has been associated with the conversion of Aft to Afm or the hydration of $C_4AF$ which continues as slowing exothermic reactions [56]. Peaks III and IV are not always observed.

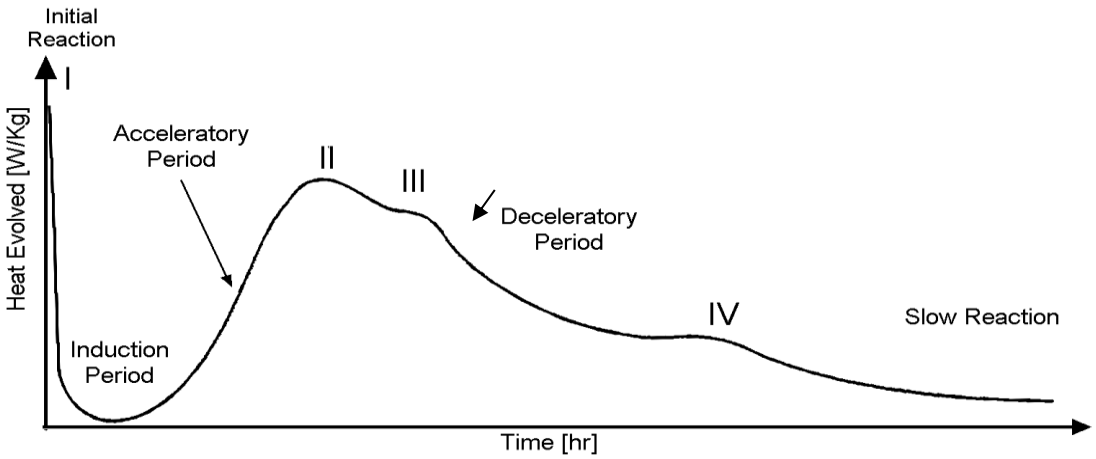


Figure 2.12: Graphical representation of heat evolved during hydration of PC [57]

## 2.5 Composite cement systems relevant to the project

### 2.5.1 PC- $BaSO_4$ system

Even if a small amount of $BaSO_4$ is dissolved, barium has chemistry similar to that of calcium, and therefore, its incorporation in cement based waste forms is not expected to present a problem when considering cement hydration chemistry and mechanisms [67, 68]. According to the data found in the literature, $Ba^{2+}$ will be released less easily because of its incorporation, or sorption, in or on the major cement hydrates, especially hydrated calcium aluminates [59, 68, 69]. Although, most of barium compounds are soluble in

alkaline solution, barium sulphate salt is very insoluble, only 3.11 mg/L($H_2O$) at 20°C, pH7 [70]. The reaction of $BaSO_4$ with cement is expected to be very little due to the strong bond between barium and sulphate [19].

On the other hand, there are numbers of reports available on the concrete systems containing barite (a mineral based on $BaSO_4$). Because of its high density (4.48 g/cm$^3$ [70]), barite is usually used as an aggregate to produce heavyweight concretes, applied for nuclear utilities to provide radiation protection [71]. Due to this specific application, many of the studies concern the interaction of PC-barite concrete systems with different types of radiations [72-75] and the physical properties of the system relevant to the practical usage as the structural materials, in particular workability and mechanical properties [75-79]. Kilincarslan et al. [77] reported that it was possible to use barite as a part of aggregates without reducing the hardness of concretes. Khan [78] compared cement pastes and mortars blended with different amount of barite powder (5, 10, 15 and 20 wt%), and reported that 5 and 10 wt% blends were the best based on the compressive strength data. Topcu [79] studied the effect of water to cement (w/c) ratio on the physical and mechanical properties of barite containing heavyweight concrete and reported that the most favourable w/c ratio was 0.40 based on the compressive strength and Schmidt hardness data. These data are useful for the specific products, but it is often difficult to understand the effect of barite (or $BaSO_4$) or water content on the reported properties due to the other variables i.e., different amount of other aggregates co-existing in the system [77], the wide range of barite particle size [77, 79] or the varying w/c ratio to keep the consistency of the cement paste and mortar [78].

### 2.5.2 PC- metakaolin system

As previously mentioned, Read et al. used a cementing system containing metakaolin [1]. Metakaolin (MK) is very fine powder produced from the calcination of kaolinite (clay) at the temperature between 650-800ºC [80]. The final product contains high reactive silica and alumina which is ready to react with cement hydration products [80]. When such fine powder is added to cement, the early strength is enhanced due to the filler effect [80]. Moreover, the filler effect of MK can improve the pore structure and increase the resistance to the harmful solution [80]. It has been reported that the inclusion of MK in the cement wasteform induces the formation of a larger amount of hydrated products as a consequence of pozzolanic reaction taking place between MK and the portlandite derived from cement hydration. The main hydration product of this reaction is C-S-H and a complex calcium aluminosilicate hydrate ($C_2ASH_8$) that can coexist with hydrogarnet-katoite ($C_3AH_6$) solid solutions phases [80, 81]**.** MK can also raise the crystallinity of C-S-H [82, 83]. However, PC-MK system may not be suitable for the applications under high curing temperatures, where the $C_2ASH_8$ produced during the pozzolanic reaction of MK with the cement hydration products can transform to more stable $C_3AH_6$ phase with volume reduction, leading to a more porous structure which can decrease the materials integrity [84]. In addition, it has been reported that MK adversely affects the workability of cement due to the water demand of MK [80].

### 2.5.3 PC- quartz system

Introduction of quartz to the cementing system may bring a variety of advantages. Glasser pointed out that the inclusion of quartz as a supplementary material to cement wasteform decreases permeability and increases sorption of metals and non-metals [42]. It has been reported that quartz can increase the thermal stability of the autoclaved cement systems by producing type (I) C-S-H with a low Ca:Si ratio [42, 85], which is closely related to the natural mineral tobermorite. Alhozaimy et al. studied the effect of two types of quartz on compressive strength of concrete in the normal and autoclave curing at 180ºC for 4-5 hours. They observed an improvement of compressive strength in both systems and suggested that the temperature has increased the reactivity of quartz to form C-S-H from the CH released during cement hydration [86].

## 2.6 High density support matrices

### 2.6.1 Deep bore hole geological disposal (DBGD)

Deep borehole geological disposal is an alternative methodology for the disposal of nuclear wastes to increase the geological barriers for the transport of the radionuclide to the geosphere [87]. Figure 2.13 shows a schematic of DBGD suggested by Gibb et al [87]. In this method, the waste canisters are stack at the bottom of deep bore hole, and the space is grouted by high density support matrix (HDSM). One of the main challenges for this design is the accurate stacking of the containers in the borehole without creating stresses that could lead to the release of the radionuclides to the environment. Gibb et al. [88] suggested that, to reduce the risk in the deformation of the nuclear waste containers without any ruptures, a substantial clearance between the

canisters and casing is required. It was recommended to situate the canisters individually and grout the space with the cement, allowing them to set safely, and then placing the next canister on the top. One of the very important aspects of such a grouting system is the density, which has to be as high as 4 g/cm$^3$ to support waste canister(s) [87], to prevent blow-out of the cement slurries.

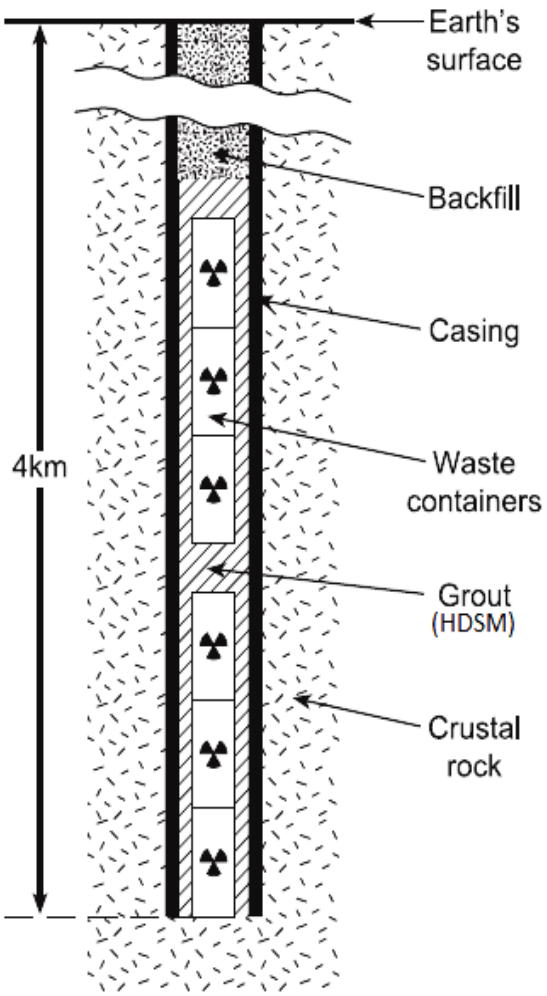


Figure 2.13 Schematic diagram of deep borehole geological disposal [87]

### 2.6.2 High density support material (HDSM)

In the deep borehole geological disposal systems, HDSM is used to surround the HLW containers and should flow into the voids and set under the predicted

temperature and pressure condition [88]. Cementitious grout is one of the candidate materials, which can be used to surround the containers so they can withstand deformation when the HDSM has solidified around them. The heat produced from radioactive decay waste can reach about 180ºC within 28 days of emplacement [88]. Also, the horizontal stresses in the borehole region will increase after waste containers emplacement due to the containers weight itself, meaning that the cement matrix has to withstand these conditions. In addition, the cement system for HDSM in DBGD has to be an optimal setting time and the cement slurry should have expectable viscosity to make it pump-able [89].

The cement properties required in such an application are similar as to in the oilwell cements. Oilwell cements are exposed to such high temperatures and pressure, and there has been variety of investigations on oil well cement systems [89-91]. The American Petroleum Institute (API) has defined the specifications for the materials and testing for the well cements. Class G and class H has been used for oil well cement in 2 km depth for high sulphate and high temperature (about 160ºC) resistance [90, 92]. In terms of properties, high mechanical strength is required to maintain the integrity during the operational life of the well at downhole conditions [89]. Oilwell cement slurries also need their densities to be raised so as to prevent blow-out of the cement slurries in such high pressure conditions. In addition to Portland cement, oil well cement is mixed with additives in order to tailor it to serve various purposes such as, providing support and protection of the casing, or preventing the blow-out of the cement slurries [89, 90]. The blow-out of cement slurries is usually overcome by the use of heavyweight additives such as barite ($BaSO_4$) to increase the density

of the final cement mix [93, 94]. Therefore, PC-$BaSO_4$ containing $BaSO_4$ scale may be utilised for this application.

## 2.7 Potential issues of PC-$BaSO_4$ system

### 2.7.1 Sedimentation

One of the main problems in the cement paste with high density particles is the sedimentation which can occur before the initial setting of cement paste takes place [95]. As the $BaSO_4$ particles are much denser (4.48 g/cm$^3$) [70] than the cement slurry (2 g/cm$^3$) [63]. Sedimentation of $BaSO_4$ granule is expected [96]. The phenomenon is related to many factors but the main reason is that the suspending fluid is not able to "carry" its particles [96]. Many researchers have studied the rheological properties of fresh cement pastes [97-102] in order to evaluate the effect of different factors, concentration, specific surface area, age and presence of mineral admixture on the viscosity and yield stress. Shaughnessy and Clark [98] reported that the rheological properties of cement pastes changed with the cement chemical composition, specific surface area of cement powder, hydration time, mixing procedures and curing temperatures. The literature shows that the incorporation of mineral admixtures such as metakaolin and quartz can help cement slurry to carry its particles and reduce the risk of sedimentation [100-102]. Shahriar pointed out that MK was found to enhance the yield stress of cement slurries and the intensity of this behaviour varied with amount of MK [103]. Felekoğlu et al. [104] reported that in general all finer powders increased the initial viscosity of the pastes compared with the plain cement paste. The mineral admixtures increase viscosity of the paste not

only through the added interparticle forces due to its fine particle size but also through the hydrodynamic interactions [96].

The rheological properties of fresh cement pastes are very important, since they affect the consistency, workability, and setting characteristics of cement paste. Cement pastes, from the industrial application point of view, have to be as fluid as possible to ensure that it would fill the formwork under its own weight. On the other hand, it has to be a stable mixture. Therefore, a compromise between the stability and fluidity has to be reached. The most straightforward approach is to find the minimum fluidity (or workability) that will guarantee the adequate filling of the formwork and assume that this minimum fluidity will ensure an acceptable stability.

### 2.7.2 High temperature strength regression

Due to the change in the microstructure during the curing at elevated temperatures, the physical properties of the cement also change. At elevated temperatures the initial strength of PC increases significantly, due to the faster rate of hydration of clinker phases [105]. However, at longer curing times, it has been reported that the strength was less than that of a sample cured at ambient temperatures, believed to be due to the higher porosity and the coarser and heterogeneous microstructure [61]. According to the literature, neat PC starts to lose its compressive strength at temperatures above 110ºC as a result of the breakdown of the main binding phase (C-S-H) at such temperatures [106]. This would render the Portland cement unusable for high temperature applications. It has been reported that the hydration of PC under high temperature resulted in the formation of lime-rich crystalline phases, such as alpha-dicalcium-silicate

hydrate ($\alpha$-$C_2SH$), which are known to weaken the mechanical strength of cements [106]. In order to avoid strength loses, crystalline silica, or quartz, is often added [106]. The addition of the crystalline silica or quartz allows the formation of silica-rich cement phases, such as tobermorite and xonotlite, which would not result in the significant strength regression in the cement [106].

## 2.6 Summary

The review showed that scale contains NORM is one of the main radioactive contaminations in the oil and gas industrial processes. The formation of scales is due to chemical-physical processes which take place in the reservoir's production water. Barium sulphate (barite) was the main constituents found in the scales, and the abundant information from early researches indicates that Ra (II) is mainly associated with $BaSO_4$ precipitation. Available data shows that the specific activity of $^{226}Ra$ in scale ranged from less than 0.1 Bq/g up to 15000 Bq/g. Therefore, NORM scale can be classified as LLW, and hence requires an appropriate handling and management. Also, the review has outlined the current usage of cement for radioactive waste management. As described previously, encapsulation of a variety of waste materials in cements is the favoured method in the UK, due to the favourable chemical and physical properties of cementitious systems. The hydration products favour the ion adsorption and substitution, and the overall microstructure decreases the mobility of waste species.

NORM scale containing cement wasteform has been studied by Read et al. [1] and by Wang et.al [52]. It was concluded from these studies that the cement materials based on PC could be an effective barrier for $BaSO_4$ scale, and it is

preferred encapsulant for $BaSO_4$-containing scale up to 14 wt%. The important question as a next step is whether it is possible to increase the loading of $BaSO_4$ scale without decreasing the integrity of the final products. It would be advantageous if the loading of $BaSO_4$ scale is further increased, as it would reduce the volume of the produced wasteforms. To optimise the amount of $BaSO_4$ scale loading, it is necessary to clarify the effect of increased $BaSO_4$ scale loading, as well as that of water content in the system on the properties of the products. There are numbers of reports available on the concrete system containing barite (or $BaSO_4$) to produce heavyweight concretes. These data are useful for specific product, but it is often difficult to understand the effect of barite or water content on the reported properties due to the other variables.

The sedimentation of $BaSO_4$ granules is expected due to its density being significantly higher than the cement slurry. More research in this area is needed to develop cement formulations with low sedimentation of $BaSO_4$ particles.

High density grouting system is important to reduce the risk in the deformation of the nuclear waste containers in DBGD. In order to use the PC-$BaSO_4$ system as the cement support matrix in DBGD, it is important to study the effect of high temperatures on the cement system in such environment. The interaction between a cement systems and $BaSO_4$ and the changes in the microstructure of the hardened cement paste in such temperatures have not been studied, and more research in this area is needed to fully understand these effects.

## 2.7 References


1. D. Read, B. Rabey, S. Black, F. P. Glasser, C. Grigg, and A. Street, *Implementation of a strategy for managing radioactive scale in the China clay industry.* Minerals Engineering, 2004. **17**: p. 293-304.
2. D. Chriss, *A study of the relationship of the geological formation to the NORM*, in *Naturally Occurring Radioactive Materials and Chmical Analysis of Produced Water Samples*. 2002, Southern University-center for energy and environmental studies Baton Rouge.
3. M. S. Hamlat, H. Kadi, and H. Fellag, *Precipitate containing norm in the oil industry: modelling and laboratory experiments.* Applied Radiation and Isotopes, 2003. **59**: p. 95–99.
4. U. S. E. P. Agency, *Draft Diffuse NORM-Waste Characterization and Preliminary Risk Assessment*. 1993, U.S. Environmental Protection Agency, Office of Radiation and Indoor Air: Washington, DC.
5. OGP, *Guidelines for the management of Naturally Occurring Radioactive Material (NORM) in the oil & gas industry*. 2008.
6. A. L. Smith, *Radioactive-scale formation.* Journal of Petroleum Technology, 1987. **June**: p. 697–706.
7. R. Fisher, *Geologic , geochemical and geographic controls on NORM in produced water from Texas oil, gas and geothermal reservoirs*. 1995, The University of Texas at Austin: Austin.
8. IAEA, *Radiation protection and the management of radioactiv waste in the oil and gas industry*, in *Safety reports series, No.34*. 2003, IAEA: Vienna.
9. M. B. Cooper, *Naturally Occurring Radioactive Materials (NORM) in Australian Industries - Review of Current Inventories and Future Generation*. 2005: Australia.
10. H. Stensrud, T. Gäfvert, T. D. Bergan, I. Amundsen, T. Strand, and P. Strand, *Regulating Discharges from Non-nuclear Industry in Relation to Environmental elation to Environmental Radiological Protection*. 1995: Grini Næringspark,Norway.
11. E. Commission, *Radiation Protection 122 – Practical Use of the Concepts of Clearance and Exemption (Part II), Application of the Concepts of Exemption and Clearance to Natural Radioactive Sources*. 2000.
12. M. I. Ojovan and W. E. Lee, *An introduction to nuclear waste immobilisation*. 2005, London: Elsevier Ltd.
13. M. S. Al-Masri and A. Aba, *Distribution of scales containing NORM in different oilfields equipment.* Applied Radiation and Isotopes, 2005. **63**: p. 457-463.
14. J. M. Godoy and R. P. d. Cruz, *226Ra and 228Ra in scale and sludge samples and their correlation with the chemical composition.* Journal of Environmental Radioactivity, 2003. **70**: p. 199-206.
15. M. Omar, H. Ali, M. Abu, K. Kontol, Z. Ahmad, S. H. S. S. Ahmad, I. Sulaiman, and R. Hamzah, *Distribution of radium in oil and gas industry wastes from Malaysia.* Applied Radiation and Isotopes, 2004. **60**: p. 779-782.
16. F. Leeuwen, *Selective Extraction of Naturally Occurring Radioactive Ra2+ from Aqueous Waste: Extractants Based on Thiacalix[4]arene and (iso)guanosine Streams*. 2005, Enschede: University of Twente. 144.
17. Z. Szabo, V. T. dePaul, J. M. Fischer, T. F. Kraemer, and E. Jacobsen, *Occurrence and geochemistry of radium in water from principal drinking-water aquifer systems of the United States.* Applied Geochemistry, 2012. **27**: p. 729–752.
18. T. F. Kraemer and D. F. Reid, *The occurrence and behavior of radium in saline formation water of the US Gulf Coast region.* Isotope Geoscience, 1984. **2**(2): p. 153-174.

19. F. Grandia, J. Merino, and J. B. Amphos, *Assessment of the radium-barium co-precipitation and its potential influence on the solubility of Ra in the near-field*, in *Technical Report* 2008: Stockholm.
20. A. P. P. E. A. Limited, *Guidelines for naturally occurring raddioactive materials*. 2002, Austrian petroleum production and exploration assusiation limited: Canberra. p. 6-26.
21. N. R. P. Authority, *Deposition of Naturally Occurring Radioactivity in Oil and Gas Production*, in *Strålevern hefte No. 12*. 1997: Norway.
22. IAEA, *International Basic Safety Standard for the Protection against Ionizing Radiation and for the Safety of Radiation Sources*, in *IAEA Safety Series No. 115*. 1996: Vienna.
23. IAEA, *Naturally occurring radioactive material (NORM V)*, in *proceedings of the Fifth International Symposium on Naturally Occurring Radioactive Material*. 2008, IAEA: Vienna. p. 383.
24. A. Liland, P. Strand, I. Amundsen, H. Natvig, M. Nilsen, R. Lystad, and K. E. Frogg, *Advances in NORM management in Norway and the application of ICRP's 2007 Recommendations.* Annals of the nternational Commission on Radiological Protection ( ICRP I2011 Proceedings), 2012. **41**(3-4): p. 332-342.
25. M. H. P. Gazineu, C. A. Hazin, and J. M. O. Godoy, *Chemical and minerlogical characterization of waste generated in the petroleum industry and its correlation with 226Ra and 228Ra contents.* Radioprotection, 2005. **40**: p. 753-758.
26. M. S. Hamlat, S. Djeffal, and H. Kadi, *Assessment of radiation exposures from naturally occurring radioactive materials in the oil and gas industry.* Applied Radiation and Isotopes, 2001. **55**: p. 141–146.
27. S. Shawky, H. Amer, A. A. Nada, T. M. A. El-Maksoud, and N. M. Ibrahiem, *Characteristics of NORM in the oil industry from Eastern Western deserts of Egypt.* Applied Radiation and Isotopes, 2001. **55**: p. 135-139.
28. B. Heaton and G. Lambley, *TENORM in oil and gas industry* Appl. Radiat., 1995: p. 577-581.
29. G. J. White and A. S. Rood, *Radon emanation from NORM-contaminated pipe scale and soil at petroleum industry sites.* Journal of Environmental Radioactivity, 2001. **54**: p. 401-413.
30. E. a. p. forum, *Low specific activity scale origin treatment and disposal*. 1987: London. p. 25-38.
31. W. F. Bakr, *Assessment of the radiological impact of oil refining industry.* Journal of Environmental Radioactivity, 2010 **101**: p. 273-243.
32. K. P. Smith, D. L. Blunt, G. P. Williams, and C. L. Tebes, *Radiological Dose Assessment Related to Management of Naturally Occurring Radioactive Materials Generated by the Petroleum Industry*. 1996, Argonne National Laboratory: Argonne. p. 69.
33. M. S. Al-Masri and H. Suman, *NORM waste management in the oil and gas industry: The Syrian experience.* Journal of Radioanalytical and Nuclear Chemistry, 2003. **256**(1): p. 159–162.
34. P. Varskog, N. Decom, E. Kvingedal, and W. Halsvik, *End disposal of petroleum industry NORM in Norway -Stangeneset NORM Disposal Site.* 2009.
35. A. S. Habib, D. A. Bradley, P. H. Regan, A. L. Shutt, B. Heaton, and G. Lambley, *The use of MCNP and gamma spectrometry in supporting the evaluation of NORM in Libyan oil pipeline scale.* Nuclear Instruments and Methods in Physics Research, 2010. **619** (A ): p. 245–251.
36. K. Smith, D. Blunt, and J. Arnish, *Potential Radiological Doses Associated with the Disposal of Petroleum Industry NORM via Landspreading*, in *Rep. DOE/BC/W-31-109-ENG-38-5*. 1998, Argonne National Laboratory

37. J. A. Veil, K. P. Smith, D. Tomasko, D. Elcock, D. L. Blunt, and G. P. Williams, *Disposal of NORM-Contaminated Oil Field Wastes in Salt Caverns*. 1998, Argonne National Laboratory: Argonne.
38. IAEA, *Operational Experience in Shallow Ground Disposal of Radioactive Wastes*. 1985: Vienna.
39. T. Strand. *Handling and disposal of NORM in the oil and gas industry*. in *WM99*. 1999. Phoenix- AZ-US: WM99.
40. K. P. Smith, *An overview of natrally occurring radioactive materials (NORM) in the petroleum industry*. 1992, Argonne national laboratory.
41. J. H. Sharp, J. Hill, N. B. Milestone, and E. W. Miller. *Cementitious Systems for Encapsulation of Intermediate Level Waste*. in *Radioactive Waste Management and Environmental- ICEM03*. 2003. Oxford.
42. F. P.Glasser, *Progress in the Immobilization of Radioactive Wastes in Cement.* Cement and Concrete Research 1992. **22**: p. 201-216.
43. C. R. Wilding, *The performance of cement based systems.* Cement and Concrete Research, 1992. **22**(2-3): p. 299-310.
44. P. Wilson, ed. *Waste treatment in The Nuclear Fuel Cycle; from Ore to Waste*. 1996, Oxford University Press. 161-183.
45. J. D. Palmer and G. A. Fairhal, *properties of cement system containing intermediate leve waste.* Cement and concrete Research, 1992. **22**: p. 325-330.
46. N. Collier, *The encapsulation of iron hydroxide floc in composite cement* in *Department of Engineering Materials*. 2006, The University of Sheffield: Sheffield.
47. Nirex, *The 2004 United Kingdom Radioactive Waste Inventory-Main Report*. 2005.
48. IAEA. *Naturally Occurring Radioactive Material (NORM VI)*. in *Proceedings of an International Symposium*. 2010. Marrakesh, Morocco: IAEA.
49. H. Taylor, *Chapter 1: Portland cement and its major constituent phases*, in *Cement chemistry*. 1990, Thomas Telford London. p. 1-28.
50. H. Taylor, *Chapter 9: Composite cements*, in *Cement Chemistry*. 1990, Thomas Telford Publishing: london. p. 261-294.
51. M. L. D. Gougar, B. E. Scheetz, and D. M. Roy, *Ettringite and C-S-H Portland cement phases for waste ion immobilisation,a review.* Waste Management, 1996. **16**(4): p. 295-303.
52. R. Wang, X. N. Yang, and Q. Y. Wu, *Study of the immobilization of 226Ra- Cement solidification of 226Ra waste.* Radioanalytical and nuclear chemistry, 1995. **198**(2): p. 281-285.
53. H. Taylor, *Cement chemistry*. 2 ed. 1990, London: Thomas Telford.
54. I. Odler, *Hydration, Setting and Hardening of Portland Cement*, in *Lea's Chemistry of Cement and Concrete*, P.C. Hewlett, Editor. 2001, Butterworth-Heinemann: Oxford. p. 241-298.
55. H. Pollmann, *Composition of cement phases*, in *Structure and performance of cements*, J.B.P. Barnes, Editor. 2002, Spon Press. p. 25-56.
56. H. Taylor, *Chapter 7: Hydration of Portland cement* in *Cement Chemistry*. 1990, Thomas Telford London. p. 187-226.
57. E. Gartner, J. Young, D. Damidot, and I. Jawed, *Chapter 3: Hydration of Portland cement*, in *Structure and performance of cements*, J.B. P. Barnes, Editor. 2002, Spon Press. p. 57-113.
58. I. G. Richardson, *Tobermorite/jennite- and tobermorite/calcium hydroxide-based models for the structure of C-S-H: applicability to hardened pastes of tricalcium silicate, β-dicalcium silicate, Portland cement, and blends of Portland cement with blast-furnace slag, metokaol.* Cement and Concrete Research, 2004. **34**: p. 1733-1777.
59. G. Bye, *Portland Cement*, ed. 2. 1999, London: Thomas Telford.

60. N. K. Katyal, S. C. Ahluwalia, and R. Parkash, *Effect of barium on the formation of tricalcium silicate.* Cement and Concrete Research, 1999. **29**: p. 1857-1862.
61. H. Taylor, *Chapter 11: High-pressure steam curing*, in *Cement chemistry*. 1990, Thomas Telford: London. p. 365-371.
62. C. H. Mattus and T. M. Gilliam, *A literature review of mixed waste components: sensitiv* 1994, U.S. department of energy, offic technology development: Washington, D.C. p. 118.
63. A.Setiadi, *Corrosion of metals in composite cement*, in *Department of Engineering Materials*. 2006, PhD thesis, University of Sheffield: Sheffield.
64. K. L. Scrivener, *Backscattered electron imaging of cement microstructures: understanding and quantification.* cement and Concrete Research, 2004. **26**(8): p. 935-945.
65. I. Odler, *Hydration, Setting and Hardening of Portland Cement*, in *Lea's Chemistry of Cement and Concrete* P.C. Hewlett, Editor. 2004, Butterworth-Heinemann: Oxford. p. 241-298.
66. E. M. Gartner, J. F. Young, D. A. Damidot, and I. Jawed, *Hydration of Portland cement*, in *Structure and performance of cements*, P.B. J. Bensted, Editor. 2002, Spon Press. p. 57-113.
67. C. Utton, *The encapsulation of a BaCO3 waste in composite cements*, in *Department of Engineering Materials*. 2006, PhD thesis, University of Sheffield: Sheffield.
68. N. Tsuyuki, R. Watanabe, K. Koizumi, Y. Umemura, and O. Machinaga, *Effects of barium salt on the fixation of chloride ions in hardened mortars.* Cement and Concrete Research 2000. **30**: p. 1435-1442.
69. M. Moranville-Regourd, *Chapter 11: Cements made from blastfurnace slag*, in *Lea's chemistry of cement and concrete*, P. Hewlett, Editor. 2004, Elsevier Science & Technology Books. p. 637-678.
70. R. David, *CRC Handbook of Chemistry and Physics*. 2005: Taylor and Francis Group.
71. R. B. Gallaher and A. S. Kitzes, *Summary report on Portland cement concretes for shielding*. ORNL-1414. 1953: Oak Ridge National Laboratory
72. M. A. Sharaf and G. M. Hassan, *Radiation induced radical in barium sulphate for ESR dosimetry: a preliminary study.* Nuclear Instruments and Methods in Physics Research B, 2004. **225**: p. 521-527.
73. I. Akkurt, H. Akyıldırım, B. Mavi, S. Kilincarslan, and C. Basyigit, *Photon attenuation coefficients of concrete includes barite in different rate.* Annals of Nuclear Energy, 2010. **37**: p. 910-914.
74. Y. Esen and B. Yilmazer, *An investigation of X-ray and radio isotope energy absorption of heavyweight concretes containing barite.* Bull. Mater. Sci, 2011. **34**: p. 169-175.
75. D. Mostofinejad, M. Reisi, and A. Shirani, *Mix design effective parameters on γ-ray attenuation coefficient and strength of normal and heavyweight concrete.* Construction and Building Materials, 2012. **28**: p. 224-229.
76. D. Dahiru, *Investigation of the compressive strength of heavy concrete made with loacally sourced Barite aggregates.* Research journal of applied sciences, 2008. **3**(6): p. 447-455.
77. S. Kilincarslan, I. Akkurt, and C. Basyigit, *The effect of barite rate on some physical and mechanical properties of concrete.* Material Science and Engineering, 2006. **424**(A): p. 83-86.
78. B. Khan. *Effects of high early temperatures on setting time and strength of cement paste and morters blended with baryte powder*. in *CBM-CI International Workshop*. 2007. Karachi, Pakistan.
79. I. B. Topcu, *Properties of heavyweight concrete produced with barite.* Cement and Concrete Research, 2003. **33**: p. 815-822.

80. B. B. Sabir, S. Wild, and J. Bai, *Metakaolin and calcined clays as pozzolans for concrete: a review.* Cement and Concrete Composites, 2001. **23**(6): p. 441-454.
81. H. Taylor, C. Famy, and K. Scrivener, *Delayed ettringite formation.* Cement and Concrete Research, 2001. **31**: p. 683-693.
82. R. Siddique and J. Klaus, *Influence of metakaolin on the properties of mortar and concrete: A review.* Applied Clay Science 2009. **43** p. 392–400.
83. J. M. Crennan, S. A. S. E.-. Hemaly, and H. F. W. Taylor, *Autoclaved lime-quartz materials. Some factores influncing strength.* Cement and concrete research, 1977. **7**: p. 493-502.
84. M. F. Rojas and M. I. S. n. d. Rojas, *Influence of metastable hydrated phases on the pore size distribution and degree of hydration of MK-blended cements cured at 60C.* Cement and Concrete Research, 2005. **35**: p. 1292– 1298.
85. D. S. Klimesch, A. Ray, and B. Sloane, *Autoclaved cement-quartz pastes: the effects on chemical and physical properties when using ground quartz with differnt surface areas. part 1:quartz of wide partical size distrbution* Cement and Concrete Research 1996. **26**(9): p. 1399-1408.
86. A. Alhozaimy, M. S. Jaafar, A. Al-Negheimish, A. Abdullah, Y. H. Taufiq-Yap, J. Noorzaei, and O. A. Alawad, *Properties of high strength concrete using white and dune sands under normal and autoclaved curing.* Construction and Building Materials 2012. **27**: p. 218–222.
87. F. G. F. Gibb, K. P. Travis, N. A. McTaggart, and D. Burley, *A model for heat flow in deep borehole disposals of high-level nuclear waste.* Journal of Geophysical Reaearch, 2008. **113**: p. B05201.
88. F. G. F. Gibb, N. A. McTaggart, K. P. Travis, D. Burley, and K. W. Hesketh, *High-density support matrices: Key to the deep borehole disposal of spent nuclear fuel.* Journal of Nuclear Materials 2008. **374** p. 370–377.
89. A. C. Jupe, A. P. Wilkinson, K. Luke, and G. P. Funkhouser, *Class H cement hydration at 180 °C and high pressure in the presence of added silica.* Cement and Concrete Research, 2008. **38**: p. 660–666.
90. G. W. Scherer, G. P. Funkhouser, and S. Peethamparan, *Effect of pressure on early hydration of class H and white cement.* Cement and Concrete Research, 2010. **40**: p. 845-850.
91. M. Michaux and C. Defosse, *Oil will cement slurries:microstructural approach of their rheology* Cement and Concrete Research, 1986. **16**: p. 23-30.
92. J. Zhang, E. A. Weissinger, S. Peethamparan, and G. W. Scherer, *Early hydration and setting of oil well cement.* Cement and Concrete Research, 2010. **40**( ): p. 1023–1033.
93. A. Saasen and P. A. Log, *The effect of ilmenite plant dusts on rheological properties of class G oil well cement slurries.* Cement and Concrete Research, 1996. **26**(5): p. 707-715.
94. J.Bensted, *Use of ferrophosphorus as a heavyweight additives for oil well cements.* Cement and Concrete Research, 1993. **23**: p. 988-990.
95. Y. T. Mihiretu, *Fundamentals of Segregation*, in *Civil and Environmental Engineering*. 2009, PhD thesis, University of Alberta. p. 49.
96. R. J. Flatt, *Interpartical forces and superplasticizers in cement suspensions*, in *Department of materials*. 1999, Lausanne: Lausanne. p. 330.
97. A. Papo, L. Piani, and R. Ricceri, *Rheological Properties of Very High-Strength Portland Cement Pastes: Influence of Very Effective Superplasticizers.* International Journal of Chemical Engineering, 2010. **2010**.
98. R. Shaughnessy and P. E. Clark, *The rheological behavior of fresh cement pastes.* Cement and Concrete Research, 1988. **18**: p. 327-341.

99. K. H. Khayat, M. Saric-Coric, and F. Liotta, *Influence of thixotropy on stability characteristics of cement grout and concrete.* ACI Materials Journal, 2002. **99**(3): p. 234-241.
100. Y. Shi, I. Matsui, and Y. Guo, *A study on the effect of fine mineral powders with distinct vitreous contents on the fluidity and rheological properties of concrete.* Cement and Concrete Research 2004. **34**: p. 1381–1387.
101. A. Hallal, E. H. Kadri, K. Ezziane, A. Kadri, and H. Khelafi, *Combined effect of mineral admixtures with superplasticizers on the fluidity of the blended cement paste.* Construction and Building Materials 2010. **24** p. 1418–1423.
102. C. K. Park, M. H. Noh, and T. H. Park, *Rheological properties of cementitious materials containing mineral admixtures.* Cement and Concrete Research, 2005. **35**: p. 842– 849.
103. A. Shahriar, *Investigation of rheology of oil well cement slurries*, in *Department of Civil and Environmental Engineering*. 2011, The University of Western Ontario: Ontario.
104. B. Felekoğlu, K. Tosun, B. Baradan, A. Altun, and B. Uyulgan, *The effect of fly ash and limestone fillers on the viscosity and compressive strength of self-compacting repair mortars.* Cement and Concrete Research, 2006. **36** p. 1719-172.
105. B. Lothenbach, F. Winnefeld, C. Alder, E. Wieland, and P. Lunk, *Effect of temperature on the pore solution, microstructure and hydration products of Portland cement pastes.* Cement and Concrete Research, 2007. **37**: p. 483-491.
106. B. Iverson and J. Maxson. *Strength retrogression in cement under high-temperature conditions*. in *Thirty-Fifth Workshop on Geothermal Reservoir Engineering*. 2010. Stanford, California: Stanford University.

# Chapter 3: Materials and methods

## 3.1 Introduction

This chapter provides the details of the experimental works undertaken in the present study. The chapter is divided into three sections. The first section characterises the raw materials used in experiments. The second section describes the sample preparation whereas the last section outlines the characterisation techniques used in the project.

## 3.2 Raw materials

### 3.2.1 Portland cement (PC)

The PC used in this project was a CEM I type, provided by Castle Cements product UK. The oxide composition of the PC is shown in Table 3.1 [1]. The cement has a fineness of 352 $m^2$/kg Blaine. Bogue analysis using the above oxide contents was performed and the percentage of the four major clinker phases in PC estimated in Table 3.2 [2]. Figure 3.1 shows the XRD trace of the anhydrous PC used in the present study. All of the four crystalline clinker phases $C_3S$, $C_2S$, $C_3A$ and $C_4AF$ can be identified. The calcium sulphate phase present is hemihydrate ($CaSO_4.½H_2O$) rather than gypsum ($CaSO_4.2H_2O$) indicating that the gypsum had been dehydrated probably during the grinding in production. A small peak of calcite is also identified.

Table 3.1: Composition of the raw materials

| Material | Component Wt% | | | | | | | | | | |
|---|---|---|---|---|---|---|---|---|---|---|---|
| | CaO | $SiO_2$ | $Al_2O_3$ | $Fe_2O_3$ | MgO | $SO_3$ | $K_2O$ | $Na_2O$ | Free Lime | Loss on ignition | Total |
| PC | 64.58 | 20.96 | 5.24 | 2.61 | 2.09 | 2.46 | 0.59 | 0.28 | 0.9 | 0.73 | 100 |
| MK | 0.02 | 54.8 | 41.2 | 0.57 | 0.31 | 0.3 | 2.27 | 0.04 | - | 1.0 | 99.54 |
| Q | 0.05 | 97.88 | 0.98 | 0.08 | 0.05 | 0.29 | 0.10 | 0.29 | - | - | 99.72 |

PC: Portland cement

MK: Metakaolin

Q: Quartz

Table 3.2 Bogue Analysis for the clinker phases in PC used in the present study [2]

| Compound | Chemical Formula | Name | Abbreviation | Bogue analysis wt% |
|---|---|---|---|---|
| Tricalcium silicate | $Ca_3SiO_5$ | alite | $C_3S$ | 53.2 |
| Dicalcium silicate | $Ca_2SiO_4$ | belite | $C_2S$ | 20.1 |
| Tricalcium aluminate | $Ca_3Al_2O_6$ | alumiate phase | $C_3A$ | 9.54 |
| Tetracalcium aluminoferrite | $Ca_4(Al,Fe)_2O_7$ | ferrite phase | $C_4AF$ | 8.60 |

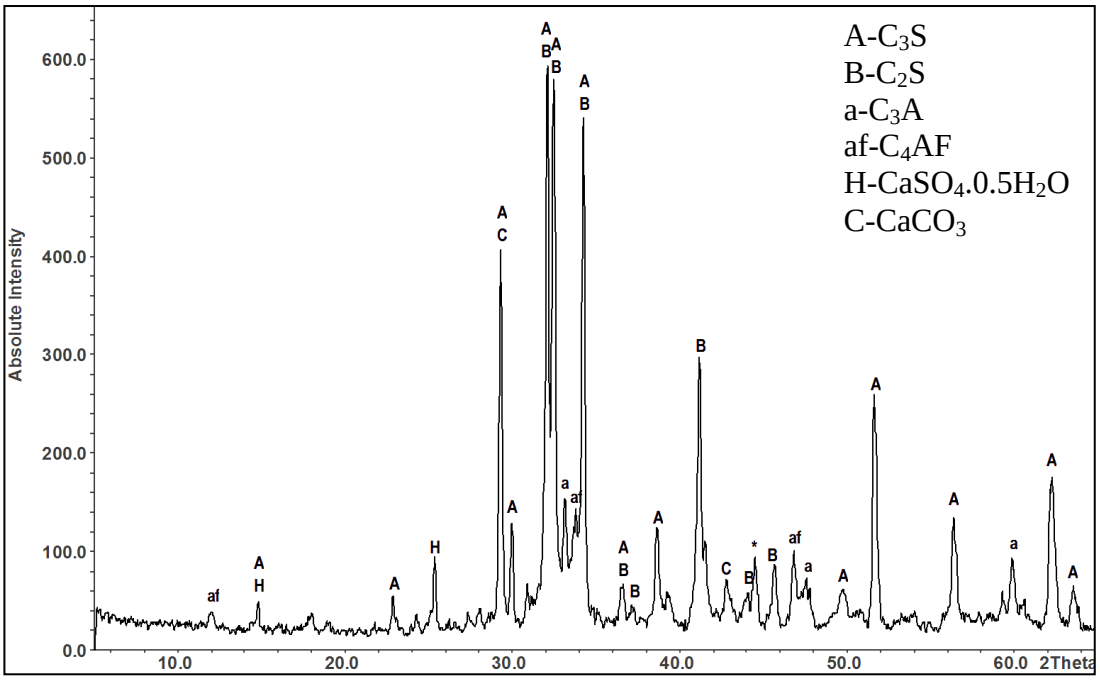


Figure 3.1 XRD trace of raw materials (PC) (*Al peak due to the sample holder)

### 3.2.2 $BaSO_4$

Three types of $BaSO_4$ were used in this project:

a) $BaSO_4$ powder - Analytical grade $BaSO_4$ of particle size less than 1 µm with 99.9% purity was used for the initial characterisation of PC-$BaSO_4$ system, and that with 98% purity for the rest of the project. Both were sourced from Acros organics. $BaSO_4$ has been known to be insoluble in acids and water, and is therefore considered to be chemically inert [3]. Figure 3.2 shows the XRD trace of the $BaSO_4$ powder which appears crystalline, indicated by the presence of clear peaks.

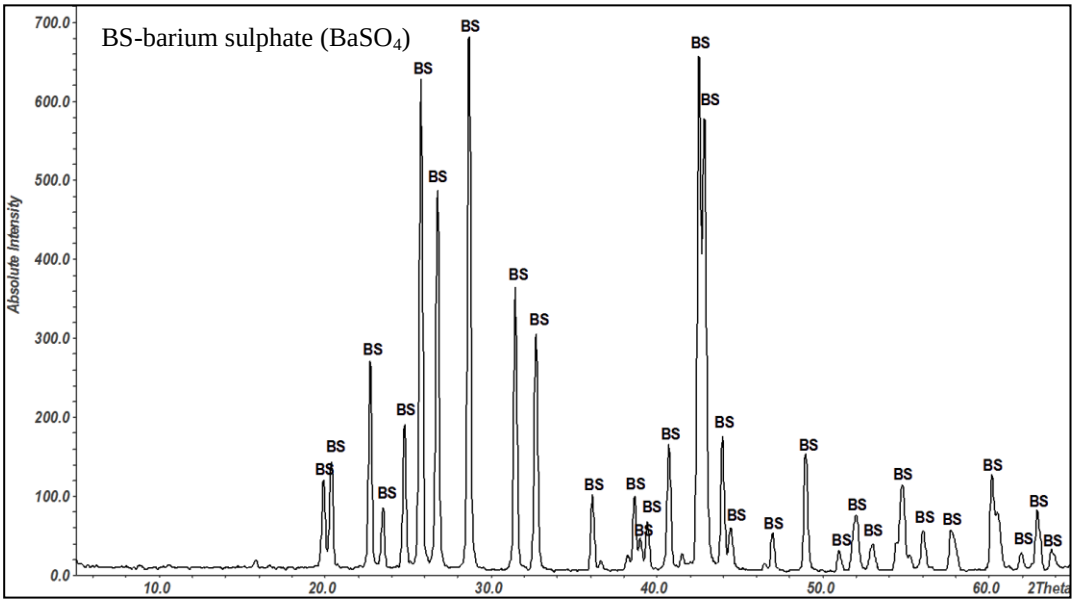


Figure 3.2 XRD trace of $BaSO_4$ powder

b) $BaSO_4$ granules were prepared using the $BaSO_4$ powder with particle size less than 1 µm, 98% purity sourced from Acros organics. The $BaSO_4$ powder was mixed with distilled water at the water to $BaSO_4$ ratio of 1 on mass basis, manually mixed using a spatula at room temperature for 2

minutes, dried in an oven at 90°C for 24 hours, then sintered in an Elite furnace in air at 1000°C for 24 hours. The final product was crushed to the size of between 0.6-5 mm to simulate scale products as shown in Figure 3.3. The XRD trace of the obtained $BaSO_4$ granules shown in Figure 3.4 confirms that the crystal structure did not change, suggesting that $BaSO_4$ is stable up to 1000°C.

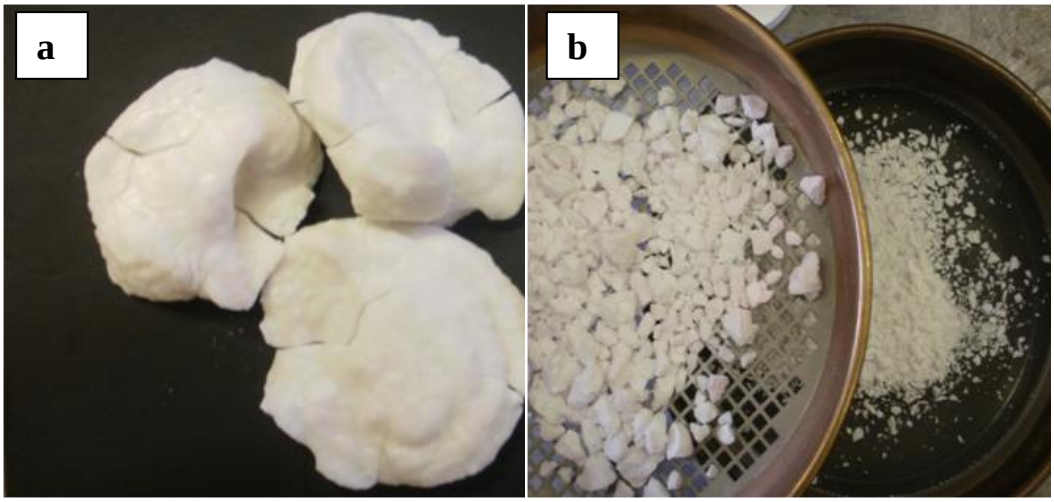


Figure 3.3: (a) the $BaSO_4$ scale simulant obtained after sintering, (b) $BaSO_4$ granules after sintering

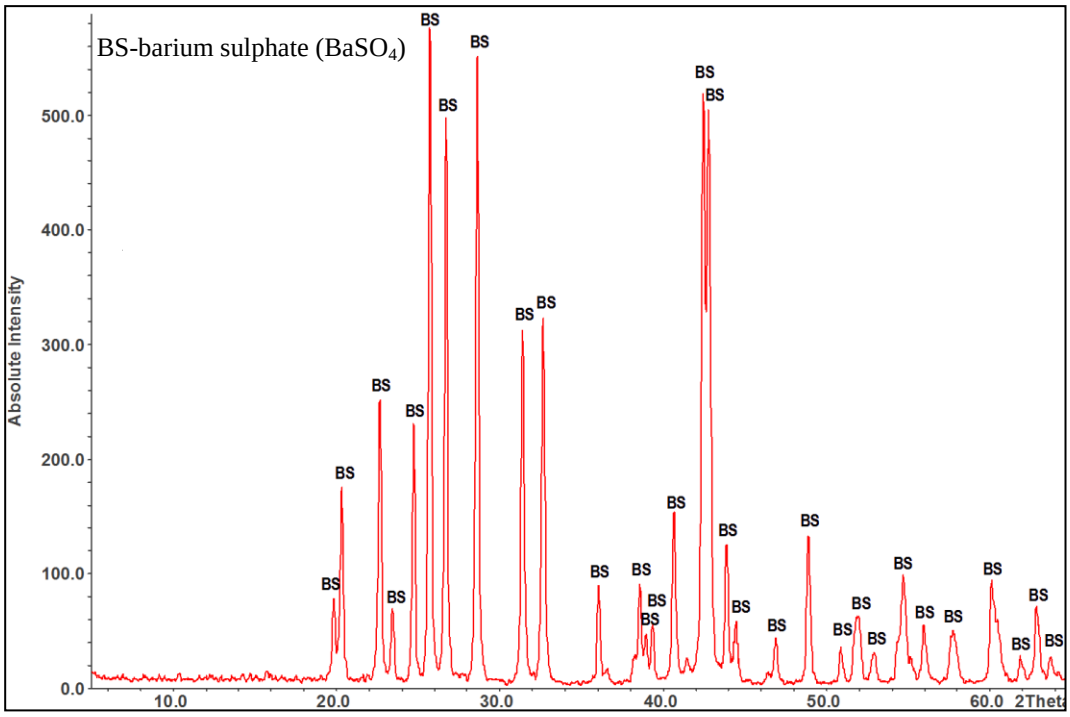


Figure 3.4 XRD trace of $BaSO_4$ granule

c) Barite, provided by Richard Baker Harrison Ltd SGS with the particle size of between 2-3 mm, was also used in the present study. Barite is the mineralogical name for barium sulphate. The barite was used when the setting time of the PC-$BaSO_4$ system was studied. Table 3.3 shows the chemical composition of barite [4].

Table 3.3: The composition of barite

| **Component** | **wt%** |
|---|---|
| $BaSO_4$ | 95 |
| CaO | 0.264 |
| $SiO_2$ | 3.02 |
| $Fe_2O_3$ | 1.51 |
| MgO | 0.206 |

### 3.2.3 Metakaolin

Commercial metakaolin (Imerys metastart 501) was used as a mineral admixture to study its effect on the setting time and rheological properties of cement paste as well as that on the microstructure of $BaSO_4$-containing cement wasteforms. The oxide composition of metakaolin is shown in Table 3.1. XRD trace of the metakaolin is shown in Figure 3.5. The glassy nature of this material is shown by the amorphous hump at approximately 15~35 ˚2θ, and the presence of a crystalline phase, quartz ($SiO_2$) is also detected.

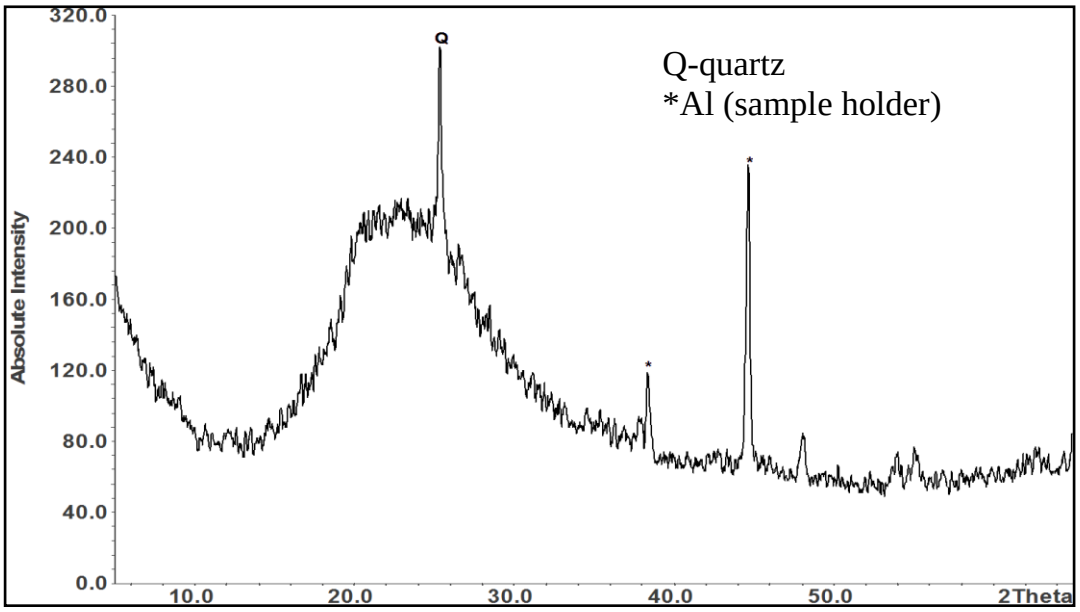


Figure 3.5: X-ray diffraction pattern of metakaolin and identified mineral phases

### 3.2.4 Quartz

Commercial fine quartz sand (CERAC, USA, 99.5% purity) with the average particle size of 44 μm was also used as a mineral admixture. The oxide composition of the quartz is given in Table 3.1.

## 3.3 Sample preparation

### 3.3.1 Mixing procedure

Table 3.4 outlines the sample formulations studied in the present project. The dry powders were firstly weighed to the correct proportions and dry mixed in plastic containers to have a total weight of 100g usually, and 200g for the setting time measurement. A desired amount of distilled water was weighed and poured into the pre-mixed powders in the plastic containers to form a paste. The paste was manually mixed for 2 minutes, for further 5 minutes using Whirh Mixer (UK) to remove air bubbles, then sealed and placed into environmental chamber. For the PC-$BaSO_4$ granule systems, samples were placed further on a rolling mixer for an additional 20 hours before stored in the same environmental chamber to avoid the sedimentation of coarse $BaSO_4$ particles. A minimum of 12 wt% and up to 60 wt% $BaSO_4$ was introduced because one of the key objectives for the present study was to increase the $BaSO_4$ loading. The maximum $BaSO_4$ loading previously reported in the literature is 14 wt%. The w/s=0.53 used in the initial stage of present study was based on the w/s ratio used in a previous study by Read et al. [5]. For comparison, w/c=0.53 was also used for some samples, which was later adopted as our base formulation throughout the rest of the study owing to its sufficient workability and better product properties found during the study. Higher water content was used for the metakaolin samples to assure sufficient workability, compared to the samples with $BaSO_4$ or quartz.

Table 3.4 Formulation of cement samples studied in the present project

| | Sample ID | PC (g) | $BaSO_4$ Powder (g) | Quartz (g) | Meta-kaolin (g) | $BaSO_4$ Granule (g) | Water (g) | w/c | w/s |
|---|---|---|---|---|---|---|---|---|---|
| Basic characterisation of PC-$BaSO_4$ system | PC | 100 | 0 | - | - | 0 | 53 | 0.53 | 0.53 |
| | CPC1 | 88 | 12 | - | - | 0 | 46.6 | 0.53 | 0.46 |
| | CPC2 | 64 | 36 | - | - | 0 | 33.9 | 0.53 | 0.34 |
| | CPC3 | 40 | 60 | - | - | 0 | 21.2 | 0.53 | 0.21 |
| | CPS1 | 88 | 12 | - | - | 0 | 53 | 0.60 | 0.53 |
| | CPS2 | 64 | 36 | - | - | 0 | 53 | 0.83 | 0.53 |
| | CPS3 | 40 | 60 | - | - | 0 | 53 | 1.33 | 0.53 |
| | CGC1 | 88 | 0 | - | - | 12 | 46.6 | 0.53 | 0.46 |
| | CGC2 | 64 | 0 | - | - | 36 | 33.9 | 0.53 | 0.34 |
| | CGC3 | 40 | 0 | - | - | 60 | 21.2 | 0.53 | 0.21 |
| | CGS1 | 88 | 0 | - | - | 12 | 53 | 0.60 | 0.53 |
| | CGS2 | 64 | 0 | - | - | 36 | 53 | 0.83 | 0.53 |
| | CGS3 | 40 | 0 | - | - | 60 | 53 | 1.33 | 0.53 |
| Setting time study of cement paste | C1 | 132 | 0 | - | 0 | 0 | 68 | 0.34 | 0.34 |
| | C2 | 120 | 0 | - | 0 | 0 | 80 | 0.4 | 0.4 |
| | C3 | 94 | 0 | - | 0 | 0 | 106 | 0.53 | 0.53 |
| | C4 | 80 | 0 | - | 0 | 0 | 120 | 0.60 | 0.60 |
| | CP1 | 140 | 60 | - | 0 | 0 | 74.2 | 0.53 | 0.37 |
| | CG1 | 140 | 0 | - | 0 | 60 | 74.2 | 0.53 | 0.37 |
| | CG2 | 80 | 0 | - | 0 | 120 | 74.2 | 0.53 | 0.37 |
| | CB1 | 180 | 0 | - | 0 | 20* | 95.4 | 0.53 | 0.47 |
| | CB2 | 160 | 0 | - | 0 | 40* | 84.8 | 0.53 | 0.42 |
| | CB3 | 140 | 0 | - | 0 | 60* | 74.2 | 0.53 | 0.37 |
| | CB4 | 120 | 0 | - | 0 | 80* | 63.6 | 0.53 | 0.31 |
| | CB6 | 80 | 0 | - | 0 | 120* | 42.4 | 0.53 | 0.21 |
| | CMK1 | 180 | 0 | - | 20 | 0 | 95.4 | 0.53 | 0.47 |
| | CMK2 | 160 | 0 | - | 40 | 0 | 84.8 | 0.53 | 0.42 |
| Development of wasteform formulation | 20P40G-A | 40 | 20 | 0 | 0 | 40 | 17.2 | 0.43 | 0.28** |
| | 20P40G | 40 | 20 | 0 | 0 | 40 | 21.2 | 0.53 | 0.35** |
| | 12P48G | 40 | 12 | 0 | 0 | 48 | 21.2 | 0.53 | 0.41** |
| | 12Q 48G | 40 | 0 | 12 | 0 | 48 | 21.2 | 0.53 | 0.41** |
| | 12MK48G | 40 | 0 | 0 | 12 | 48 | 34.8 | 0.87 | 0.67** |

*Barite (details in 3.3.1 $BaSO_4$) was used

**(water)/(matrix) ratio was calculated, where matrix is a mix of PC with either $BaSO_4$ powder, quartz or metakaolin.

### 3.3.2 Curing procedure (standard curing)

After the mixing process, the samples were placed into environmental chamber (Sayno Climatic Test Chamber) set at 40°C with a relative humidity (RH) of 95% for curing. After the curing period of 28 days, samples were de-moulded from the plastic container. Some of them were cut into a cylinder of 25mmØ×25mm for the immediate testing on compressive strength test, and the others were broken into smaller pieces and submerged in acetone for 3 days to arrest the hydration reactions for the other analysis. The broken samples were then dried and desiccated under vacuum to drive off the acetone, and stored in sealed containers prior to the analysis to avoid carbonation.

### 3.3.3 Heat-treatment

After the curing period of 28 days, some samples from the PC and CGC3 were further heat-treated in an Elite furnace in air to understand the behaviour of the hardened PC-$BaSO_4$ system at a high temperature. The heating and cooling rate were both 5°C/min, and the samples were heated at 300°C for 24 hours in air. It has been reported that the temperature of the DBGD environment can rise up to ~300$^{o}$C [6, 7]. After heating, the samples were left in the furnace, thus allowing the samples to cool slowly. After cooling, the samples were stored in sealed containers prior to analysis.

### 3.3.4 Hydrothermal curing

The cement pastes were prepared in accordance with the standard mixing procedure described in section 3.3.1. After mixing, the pastes were placed in a Teflon pot of 26 mm in diameter and 42 mm in height (Figure 3.6). The Teflon

pot containing the cement paste was placed in a stainless-steel vessel, of 35 mm in diameter and 58 mm in height (Figure 3.6). The steel vessel was sealed tightly with an allen/hex key. Once the vessels were sealed, they were placed in an oven previously heated at 180°C and left for 28 days under its autogenous pressure. After the required curing time, samples are left to cool down slowly to prevent the samples cracking. The samples were de-moulded, some of them were cut into a cylinder of 20mmØ×20mm for the immediate compressive strength test, and the others were broken into smaller pieces and submerged in acetone for 3 days to arrest hydration reactions for other analysis. The broken samples were then dried and desiccated under vacuum to drive off the acetone, and stored in sealed containers prior to analysis to avoid carbonation.

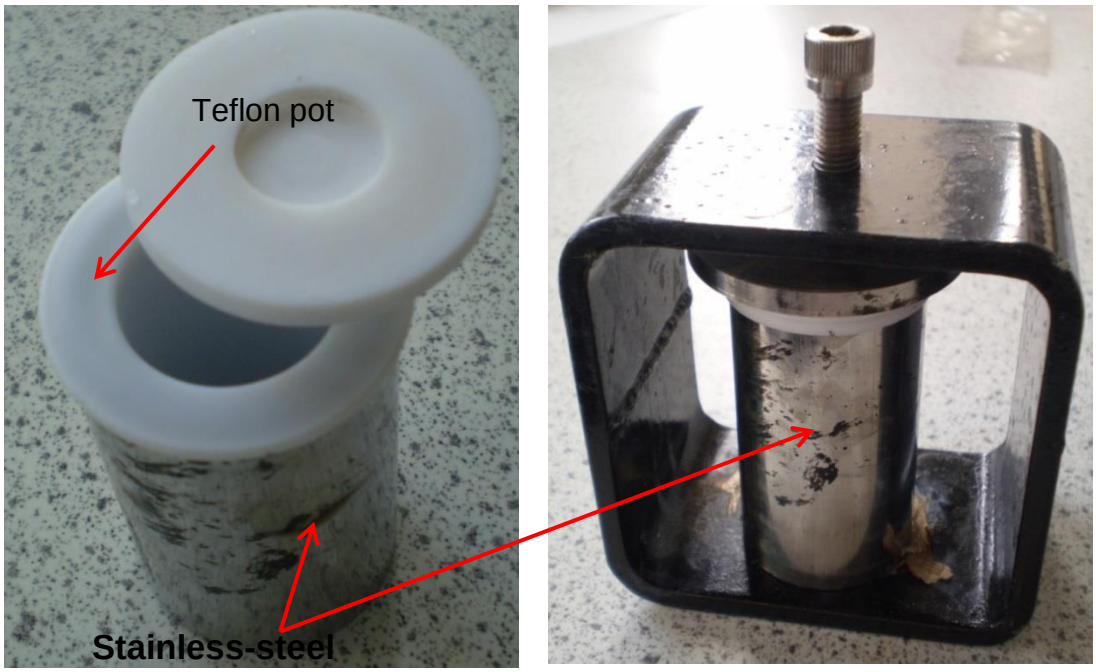


Figure 3.6 Stainless-steel cylinders for high temperature curing samples

## 3.4 Characterisation

### 3.4.1 X-ray diffraction (XRD)

**Principle**

An X-ray tube, the main part of an X-ray machine is schematically shown in Figure 3.7. The first component of the X-ray tube is the source of electrons (or cathode). Heated tungsten (or molybdenum) filament (1) connected to a generator of voltage (2), emits electrons (3). These are accelerated by applied high voltage (typically in the range of 30 to 60 kV) and collide with a metal target (or anode) (4) such as Cu, Co, Fe, and Cr. If the bombarding electrons have sufficiently high kinetic energy in comparison to the binding energy of the inner shell electrons in the atoms of the target metal, they can eject a core shell electron leaving behind a core hole (Figure 3.8). Then an electron from a higher energy level fills in the core hole. This is accompanied by an emission of X-ray photons giving rise of the characteristic radiation. They are passed out of the tube through beryllium windows (5). Beryllium is used because of its low atomic number (Z=4) and therefore low X-ray absorption. The X-ray tubes are highly inefficient as only 1% of the electron kinetic energy is radiated as X-rays. The heat generated at the anode is removed from the tube usually by water coolant.

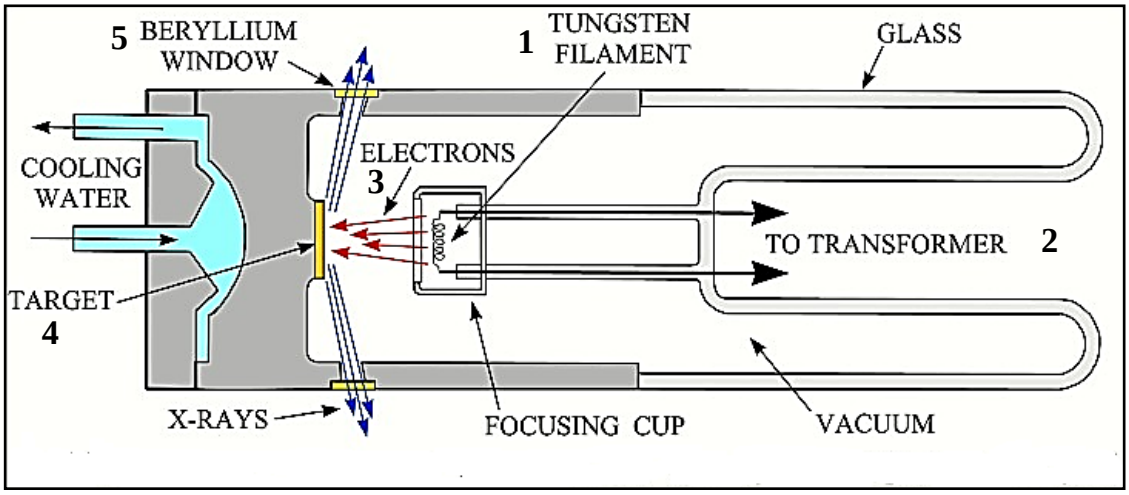


Figure 3.7 Schematic cross section of an X-Ray tube [8]

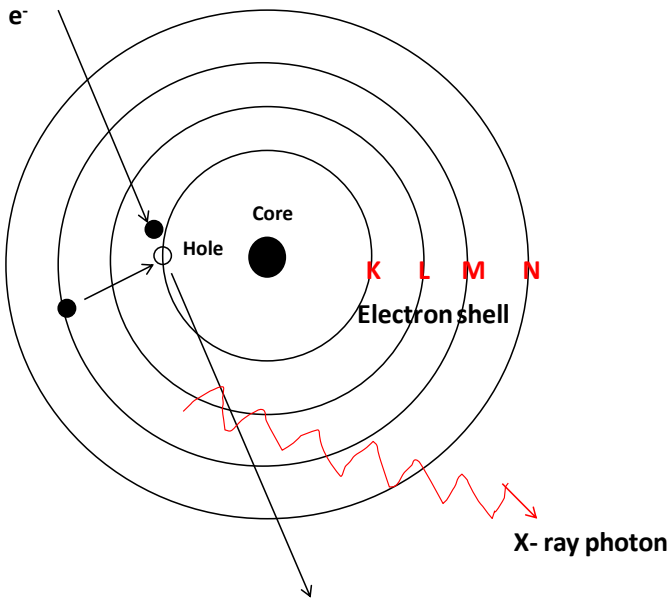


Figure 3.8: Schematic of X-ray photon generation

English physicists Sir W.H. Bragg and his son Sir W.L. Bragg introduced a relationship known as Bragg's Law in 1913 to explain why the cleavage faces of crystals appear to reflect X-ray beams at certain angles of incidence (theta, θ). Bragg's Law states:

$$n\lambda = 2d \sin\theta \qquad 3.1$$

The variable d is the difference between two lattice planes of the crystal, θ is the X-ray incidence angle (Bragg angle), and the variable lambda λ is the wavelength of the characteristic X-ray beam and n is an integer usually set equal to 1. The scattering of x-rays from a crystalline solid is shown schematically in Figure 3.9. The distance AB and BC is corresponding to d sin θ.

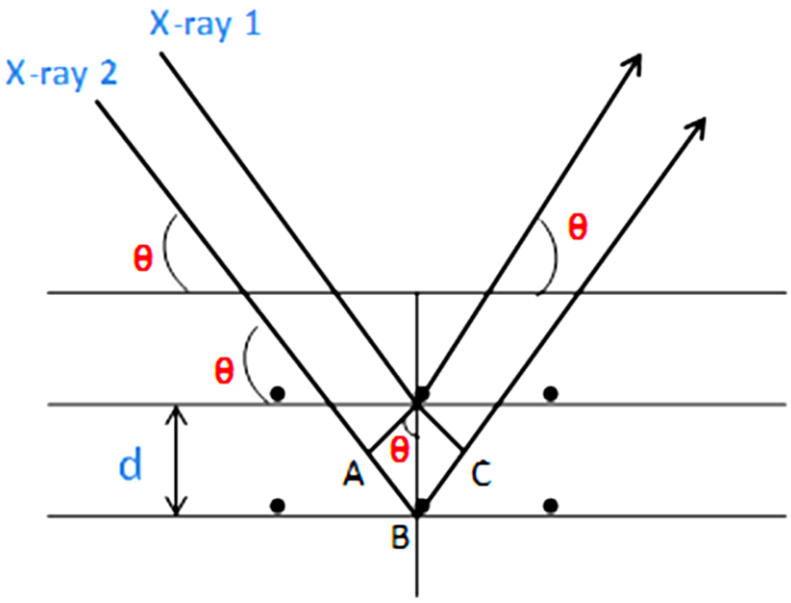


Figure 3.9 Schematic of the diffraction of X-rays

**XRD measurement**

XRD was used to identify the crystalline phases present in the samples. Two models of XRD machine were used in the present study; a Siemens D500 and a Philips PW1373. In both cases, an X-ray diffractometer with monochromatic Cu Kα radiation with a wavelength of 1.5405 Å was operated at voltage of 40 kV

and current of 30 mA .The 2θ scans were used to examine the samples over the range of 5-65$^{o}$ with a step size of 0.02$^{o}$ and scanning speed of 2$^{o}$ 2θ /min. The specimens were prepared by crushing samples using a percussion mortar then grinding using an agate mortar and a pestle, sieving with a brass sieve, to the particle size less than 63 µm and placed in an aluminium sample holder. The resulting traces were interpreted using the ICDD files in the standard JCPDF card on STOE WinXPOW software.

### 3.4.2 Thermogravimetric analysis (TGA)

This technique works by measuring the weight loss of the sample over time with a set temperature programme. TGA was used to identify the phases present in each sample based on their dehydration and decomposition up on heating**.** The TGA was carried out using a Perkin Elmer Pyris 1 TGA. Powder was obtained crushing specimens by an agate mortar and pestle. Samples were sieved to <63µm, and approximately 40 mg of sample was weighed and used in an alumina crucible. The samples were heated under flowing nitrogen. A uniform heating rate of 10°C per minute from room temperature up to 1000°C was selected. Temperature and weight measurements were taken every 0.1S. The data was analysed based on the information available in the literature [9, 10], a summary of which can be found in Table 3.5. Differential thermogravimetric (DTG) curves were also obtained from the TG data to clarify the temperature range of the observed thermal events.

Table 3.5 Temperatures of water loss and decomposition of cement phases [9, 10]

| Cement phases | Formula | Temperature($^{o}$C) |
|---|---|---|
| C-S-H | Amorphous calcium silicate hydrate | 110-120 |
| Ettringite | $Ca_6Al_2\ (OH)_{12}\ (SO_4)_3.26H_2O$ | 130-140 |
| Monosulphate | $Ca_4Al_2\ (OH)_{12}\ (SO_4).6H_2O$ | 180-210, 300 |
| Stratlingite | $Ca_2Al_2SiO_7.8H_2O$ | 220-230 |
| Hydrogarnet | $Ca_3Al_2\ (OH)_{12}$ | 380-400 |
| Portlandite | $Ca(OH)_2$ | 480-520 |
| Calcite | $CaCO_3$ | 600-700 |

### 3.4.3 Scanning electron microscopy (SEM)

**Principle**

In this technique, an electron gun is used to emit a beam of electrons (Figure 3.10). The electron source is usually a tungsten filament. The filament is heated until a steam of electron is produced. The electrons are accelerated to energy of between 1 and 30 keV, usually around 15 keV for powders and 20 keV for bulk samples. Before electron beam pass through aperture, a set of lenses are used to condense the stream of monochromatic electron to demagnify the beam. Then a set of coils scans the beam in a grid fashion, and the beam is focused by the objective lens onto the desired part of the specimen.

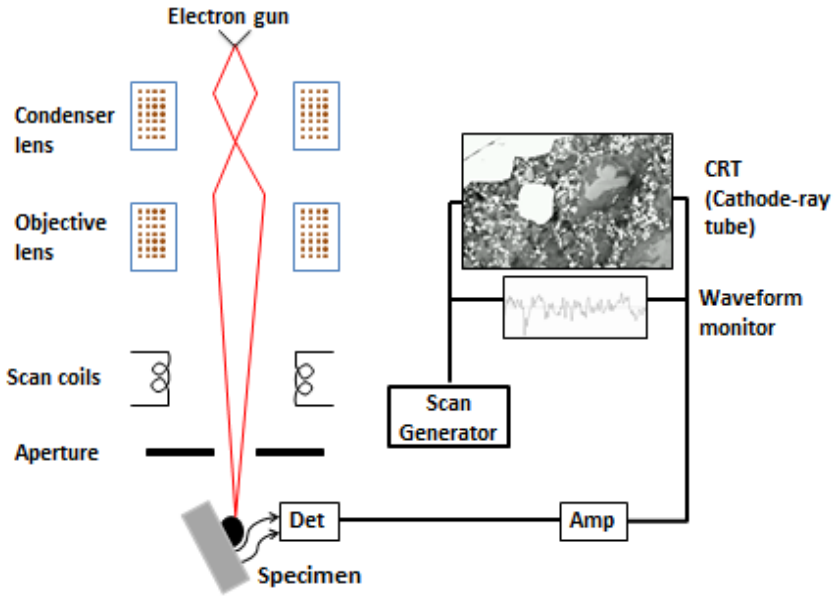


Figure 3.10 SEM Schematic [11]

The collision of a high energy electron beam with matter results in secondary electrons as well as backscattered electrons. With secondary electrons image (SEI), primary electrons generated escape from the specimen with low energies (<50eV) and have negligible element information. Because they have low energy they can provide information about the topographical layout of the surface of the sample. Backscattered electrons (BSE) are the result of the deflection of an electron by the electrons of an atom in the sample, causing the high energy electron to emerge at a wide angle scattering, approaching $180^{o}$, from the incident beam direction having lost little or none of its energy. These electrons are used for imaging and analysis because the intensity of the signal is proportional to the atomic number of the interacted elements. This shows the contrast of the elements, producing the image of varying shades of grey, e.g. a heavier element such as barium will appear much brighter than a lighter

element such as calcium. The porous areas of a sample are displayed as black. Electron specimen interactions are outlined in Figure 3.11.

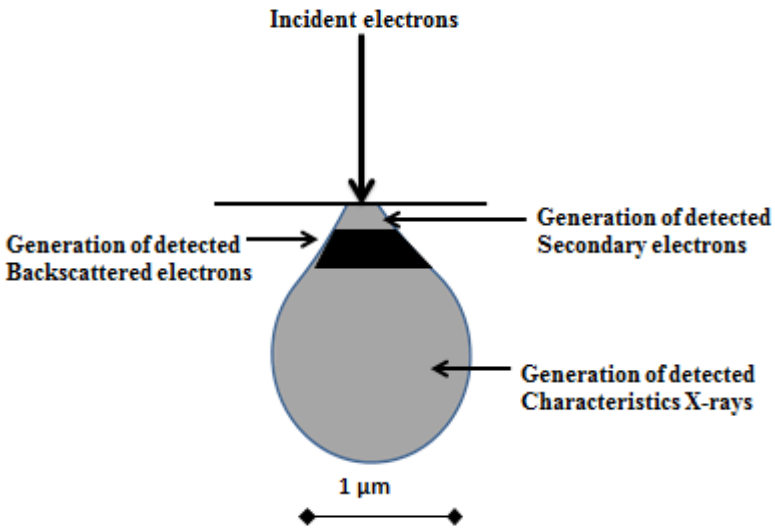


Figure 3.11 Secondary and backscattered electron sources and characteristic x-rays [12]

**Energy dispersive X-ray spectroscopy (EDS)**

EDS was used to determine the elements present in samples studied by SEM. With the same principle outlined in the X-ray photon generation (Figure 3.8), the collision of a high energy electron beam with matter ejects electron from an inner shell and a higher energy electron moves to fill this lower energy vacancy. The difference between the two energy shells is released as an electrical pulse in the form of an X-ray photon which has a characteristic energy unique to the element of origin. By measuring the energy released, it is possible to determine the elements present in the specimen. EDS generally provides the chemical analysis of the local area as shown in Figure 3.11.

**SEM measurement**

Scanning electron microscopy (SEM) is the main technique used to characterise the microstructure, morphology to gain information about the surface or near surface of the specimen. SEM images were taken by JEOL electron microscope; model JSM 6400 linked to EDS analyser. The acceleration voltage was 20 KeV with a spot size of 9. Most of the samples investigated with SEM were carried out in backscattered electron imaging mode (BSE), which shows the distribution of elements in different contrast. All samples for BSE analysis require a smooth, polished section representative of the whole sample. Samples were prepared by mounting a small solid portion of the specimen in a cold set epoxy resin using a cylindrical plastic mould. The epoxy resin was poured over the samples, and the mould was left under vacuum to fill as many pores as possible. The samples were removed from the vacuum after approximately 15 minutes and left for 24 hours to harden before grinding manually with grinding papers of 250, 400, 800 and 1200 grits. Samples were then polished with 6, 3, 1, and 1/4 μm diamond pastes, and finally coated with carbon using an Edwards 'speedivac' carbon coating unit and silver dagged to make them electrically conductive before being analysed in the microscope.

### 3.4.4 Mercury intrusion porosimetry (MIP)

**Principle**

With the assumption that pores are cylindrical and entirely and equally accessible to mercury, Washburn [13] showed that the pressure, *P,* required to force a non-wetting fluid into a circular cross section capillary of diameter, *d,* is given by.

$$P = 4\gamma \cos\frac{\theta}{d} \qquad 3.2$$

where, d is the equivalent pore diameter of the mercury filled pores, P is the applied pressure, ɣ is the surface tension of mercury and θ is the contact angle between mercury and solids.

The mercury porosity is defined as the ratio between the total injected mercury volume and the total volume of the sample. The intrusion pressure values can be converted into pore diameter, d, using the above equation. The pore size distribution of the samples can then be estimated in terms of the volume of pores intruded for a given radius. MIP is based on the assumption that the pores are cylindrical and the contact angle between mercury and solids is 130˚, and also mercury sometimes does not pass through the narrowest pores connecting the pore network. Therefore, Mercury porosimetry usually indicate smaller than actual porosity values, which is called “ink bottle” effect.

**MIP measurement**

The size of pores, pore size distribution and total porosity of the samples were studied using Mercury Intrusion Porosimetry (MIP) technique. The measurement was carried out using Micromeritics Pore Sizer 9320 porosimeter that can generate a maximum pressure of 414 MPa and can evaluate a theoretical pore diameter by assuming a contact angle of 130˚ and a mercury surface tension of $485\times10^{-3}$ N/m. Small piece of approximately 3 mm in diameter were taken from different regions from each sample, first dried to remove water from pores. The dried specimen were weighted and placed into

sample holder. The sample holder was evacuated, then mercury was introduced into the sample holder, and the sample was surrounded by mercury. The pressure on the mercury was gradually increased initially from about 7 to 345 kPa. The pressure was further increased from 345 kPa to 414 MPa. The mercury intrusion volumes and the corresponding applied pressures within a period of 8 hours were recorded at every pressure steps to provide the basic data for the analysis of pore structure. All tests were performed to achieve the manufacturer's recommendation of a mercury stem volume between 25% and 90%.

### 3.4.5 Compressive strength test

Compressive tests were carried out in accordance with the American Society for Testing and Materials (ASTM) C39-9620. The tests were performed on 25 mm Ø x 25 mm cylindrical specimens, two cylindrical samples of each formulation. Grinding papers of 250 grit were used to produce smooth parallel surfaces for measurement. The measurements were carried out using a HTE Hounsfield automatic compressive strength testing machine, shown in Figure 3.12, with the normal loading capacity of 50 KN and a displacement rate of 0.4 mm/ min. The maximum load reached prior to cement paste failure was taken as the maximum compressive resistive load during the compression test. The compressive strength was calculated based on the maximum compressive resistive load divided by the cross sectional area of the sample. An average compressive strength was then calculated from the two specimen tested for each formulation. As that the aspect ratio of the specimens tested was 1.0, a correction factor of 0.87 was applied to the measured data according to the

recommendation of the Standard test ASTM C39/ C39M-09a (*Compressive strength of cylindrical concrete specimens*).


Figure 3.12 HTE Hounsfield automatic compressive strength testing machine

### 3.4.6 Rheology test

In this technique, two parallel plates are used to characterise the rheology of cement pastes. The upper plate is usually rotated at a specified shear rate and the resulting torque is measured. From the measurement of the torque, the viscosity and the relation between shear stress $(\tau)$ and shear rate $(\dot{\gamma})$ are evaluated. Cement slurries are usually described by the Bingham model [14], and often characterised by two parameters, yield stress $(\tau_0)$ and plastic viscosity (η) as defined by the Bingham equation (Eq. 3.3).

$$\tau = \tau_0 + \eta\dot{\gamma} \quad (3.3)$$

where: $\tau$ is the shear stress (Pa) and $\dot{\gamma}$ is the shear strain rate ($s^{-1}$).

A rheometer RC 2000 flow test was used to measure rheological properties of cement pastes in the present study. Figure 3.13 shows the main components of the rheometer. The upper plate was a rotable plate attached to rotor and the lower was a fixed base plate (diameter = 40 mm). The upper plate had a standard cone geometry made from plastic (diameter = 40 mm, angle = $2^o$). Samples of approximately 25 g of selective formulation cement powder were mixed by hand for 1 minute. The cement pastes were prepared by adding the hand-mixed cement powder to the distilled water in a small plastic cup, and the total mixing time was about 3 minutes. The cement paste sample was put in between the cone and the fixed base plate. The strain rate was then increased gradually over 10 min to a final value of 200 $s^{-1}$. The gap between the upper plate and the fixed base plate 2 mm were kept constant during the measurements. The temperature of the specimen was kept constant during the test through a water circulation system inside the fixed base plate. Water trap was used to prevent evaporation from the tested cement paste sample by covering the parallel plates and top of the hollow cylinder. Continuous flow conditions tests were used and the shear rate, shear stress, and viscosity were recorded.


Figure 3.13 The rheometer used in the present study

### 3.4.7 Vicat setting test

Setting time tests were carried out in accordance with a British standard (BS EN 196-3: 1995) using Vicatronic automatic recording apparatus (vicat needle method) (Figure 3.14). This method is the most commonly used to identify the initial and final setting time for hydrating cementitious mixtures [15, 16]. A 200 g of paste was prepared for each measurement according to the mixing procedure described in the former section and placed in a wide-mouth polypropylene mould (height, 40 mm; diameter, 40mm). The repeated penetration of a 1.13 mm diameter needle forced by its own weight (300 g), on the surface of cement paste at different positions was monitored. The setting

time was measured from the instant when the cement was placed in the Vicat mould. Initial setting time was considered in the present study as the time when the needle penetration is 35 mm ±0.5 mm. The final setting time corresponds to less than 0.5 mm of penetration. The measurements were carried out at 20-23 $^{o}$C and 30-38% relative humidity.

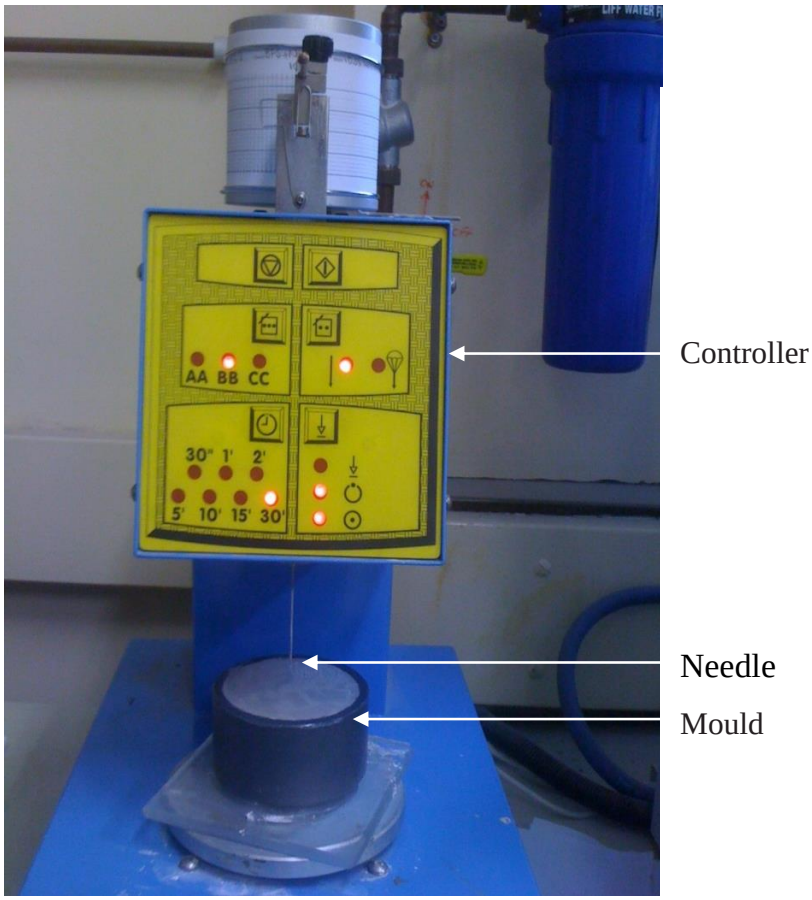


Figure 3.14 Vicat setting test machine

### 3.4.8 Leaching test

A series of static leaching test was performed to study the leaching of elements from the hardened cement samples. Distilled water was used as the leachant. For each sample, after the required curing time, a one disc with a diameter of 20 mm and 7 mm thickness was prepared (Figure 3.15) and placed in plastic container filled with distilled water (Figure 3.16) for 30 days at room temperature. The surface area of samples to the water volume (SA/V) ratio was set as 6.8 $m^{-1}$. At the end of leaching period, about 5 ml of the leachate was collected in a centrifuge tube and sent to the Department of Chemistry where the inductively coupled plasma optical emission spectroscopy (ICP/MS) was performed.

In the ICP, there is a flow of argon gas within a high energy field, in which argon plasma is created, causing intense heating as the gas is ionised. A nebulised mist from the leachate solution is injected into the centre of the argon plasma. Due to the high temperature, the chemical compounds of the mist dissociate into the component atoms. These atoms absorb the energy resulting in ionisation energy transitions which then produce spectral emission of the elements involved. The Ca, Si, Ba and S content were analysed in addition to Al, Na, Fe and Mg.

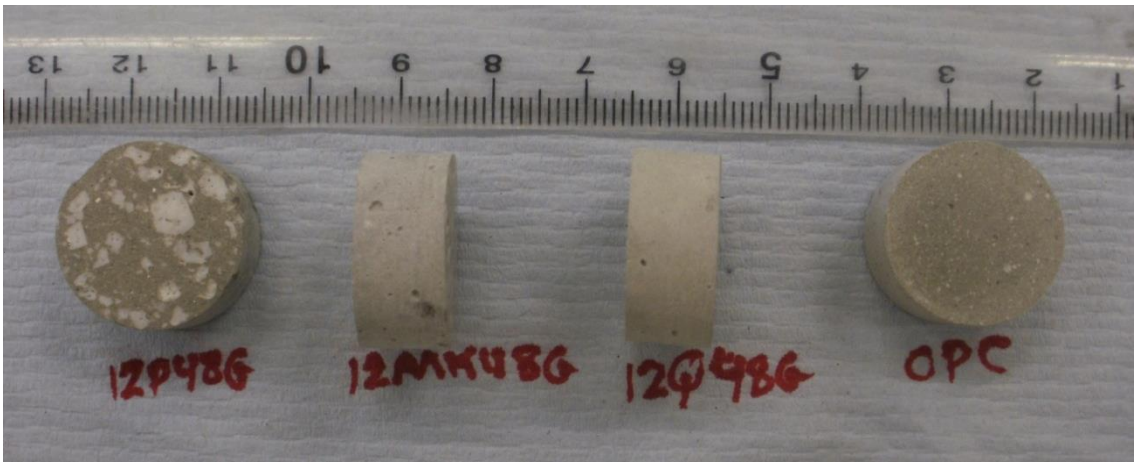


Figure 3.15 Leaching test samples

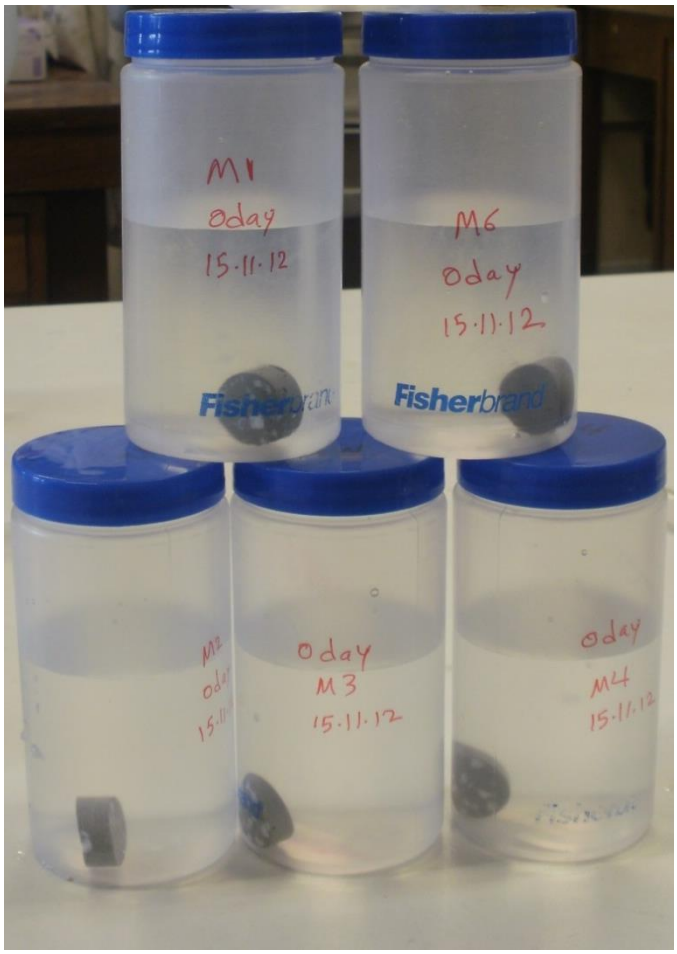


Figure 3.16 Typical leaching experiment container with samples submerged in water

## 3.5 References


1. C. Utton, E. Gallucci, J. Hill, and N.B. Milestone, *Interaction between BaCO3 and OPC/BFS composite cements at 20 °C and 60 °C.* Cement and Concrete Research, 2011. **41**: p. 236-243.
2. C. Utton, *The encapsulation of a BaCO3 waste in composite cements*, in *Department of Engineering Materials*. 2006, PhD thesis, University of Sheffield: Sheffield.
3. R. David, *CRC Handbook of Chemistry and Physics*. 2005: Taylor and Francis Group.
4. R. B. H. Ltd, *Barytes B2000*. 2013, Richard Baker Harrison
5. D. Read, B. Rabey, S. Black, F. P. Glasser, C. Grigg, and A. Street, *Implementation of a strategy for managing radioactive scale in the China clay industry.* Minerals Engineering, 2004. **17**: p. 293-304.
6. F. G. F. Gibb, N. A. McTaggart, K. P. Travis, D. Burley, and K. W. Hesketh, *High-density support matrices: Key to the deep borehole disposal of spent nuclear fuel.* Journal of Nuclear Materials 2008. **374** p. 370–377.
7. F. G. F. Gibb, *High-temperature, very deep, geological disposal: a safer alternative for high-level radioactive waste?* Waste Management, 1999. **19** p. 207-211.
8. U. S. G. Survey, *A Laboratory Manual for X-Ray Powder Diffraction*. 2013.
9. H. Taylor, *Cement chemistry*. 2 ed. 1990, London: Thomas Telford.
10. A.Setiadi, *Corrosion of metals in composite cement*, in *Department of Engineering Materials*. 2006, PhD thesis, University of Sheffield: Sheffield.
11. P. J. Goodhew, J. Humphreys, and R. Beanland, *Electron microscopy and analysis*. 3 ed. 1997, London: Taylor and Francis Inc.
12. K. L. Scrivener, *Backscattered electron imaging of cement microstructures: understanding and quantification.* cement and Concrete Research, 2004. **26**(8): p. 935-945.
13. E. W. Washburn, *Note on a Method of Determining the Distribution of Pore Sizes in a Porous Material.* Proceeding of National Academy Sciences of United States of America., 1921. **4**(7): p. 115-116.
14. R. Shaugnessy and P. E. Clark, *The Rheological Behaviour of Fresh Cement Pastes.* Cement and Concrete Research, 1988. **18**: p. 327-341.
15. H. Sleiman, A. Perrot, and S. Amziane, *A new look at the measurement of cementitious paste setting by Vicat test.* Cement and Concrete Research 2010. **40**: p. 681–686.
16. J. Zhang, E. A. Weissinger, S. Peethamparan, and G. W. Scherer, *Early hydration and setting of oil well cement.* Cement and Concrete Research, 2010. **40**( ): p. 1023–1033.

# Chapter 4: Characterisation of PC-$BaSO_4$

## 4.1 Introduction

In this chapter, basic characterisation of PC-$BaSO_4$ systems cured at 40$^oC$ is presented. A slightly high curing temperature of 40$^oC$ was used to represent the climate of the areas some oil wells are located. Such a curing temperature at this level is expected to lead to a faster initial progress of hydration resulting a higher early strength as well as a coarser porosity due to the heterogeneous distribution of the hydration products [1, 2].

The chapter has two sections. The first section presents the characterisation of neat PC system at early age of 28 days and after long curing at 360 days. The second section contains results for PC-$BaSO_4$ system. For each system, the phases formed in the products were analysed using XRD and TG. The microstructures of the products were studied using SEM and MIP, while the compressive strength was also measured. The labelling used in the XRD and TGA results is outlined in Table 4.1.

Table 4.1 Key to XRD and TGA labelling

| Labeling | Name | Cement nomenclature | Chemical formula | JCPDS card |
|---|---|---|---|---|
| A | Alite (tricalcium silicate) | $C_3S$ | $3CaO.SiO_2$ | 49-442 |
| B | Belite (dicalcium silicate) | $\beta$-$C_2S$ | $2CaO.SiO_2$ | 33-0302 |
| af | Tetracalcium aluminoferrite | $C_4AF$ | $4CaO.Al_2O_3.Fe_2O_3$ | 30-0226 |
| C | Calcite | $C\bar{C}$ | $CaCO_3$ | 05-0586 |
| P | Portlandite | CH | $Ca(OH)_2$ | 44-1481 |
| E | Ettringite (AFt) | $C_6A\bar{S}_3H_{32}$ | $Ca_6Al_2(OH)_{12}(SO4)_3.26H_2O$ | 41-1451 |
| MS | Monosulphate (AFm) | $C_4A\bar{S}_3H_{12}$ | $Ca_4Al_2(OH)_{12}(SO_4).6H_2O$ | 45-0158 |
| BS | Barium sulphate | $BaSO_4$ | $BaSO_4$ | 72-1390 |
| Hg | Hydrogarnet | $C_3AH_6$ | $Ca_3Al_2(OH)_{12}$ | 38-0368 |
| CSH | calcium silicate hydrate | C-S-H | - | Taylor [3] |

## 4.2 Neat PC

### 4.2.1 Phase analysis

Figure 4.1 shows XRD traces for the neat PC samples, hydrated at 40$^{o}$C for 28 and 360 days. For the PC cured for 28 days, the main crystalline hydrated phases detected are: portlandite ($Ca(OH)_2$, P), and calcium monosulphoaluminate (monosulphate, MS). Strong portlandite peaks illustrates the rapid reaction of clinker phases with water at 40$^{o}$C, but alite (A) and belite (B), associated with the unreacted cement in the system were also present, suggesting that the system had not completely hydrated. Crystalline or semicrystalline phase of monosulphate is often observed in the neat PC [3].

Calcium carbonate in its calcite form was also detected due to the reaction of portlandite and /or the C-S-H with $CO_2$ in atmosphere.

When the PC is cured for 360 days, the peaks attributed to portlandite became more prominent, with less intensity of peaks attributed to the alite and belite, indicating a greater degree of hydration. Usually, ettringite initially formed transforms to monosulphate as a consequence of the decrease in the $SO_4^{2-}$:$Al^{3+}$ ratio with the progressive hydration reaction of the $C_3A$ during the first few weeks of curing [3, 4]. Ettringite was not observed after 28 days of curing as expected. However, clear peaks for ettringite were observed in the XRD pattern of 360 days sample. This may imply that a delayed formation of ettringite was occurred. XRD pattern for 360 days sample also showed a further formation of monosulphate and the presence of a hydrogarnet-type phase. Taylor documented the formation of a cubic hydrate ($C_3AH_6$) in significant quantities from older Portland cements, but not as a major hydration product of typical

modern Portland cements under room temperature [3]. Calcium carbonate in its calcite form ($CaCO_3$) was also detected.

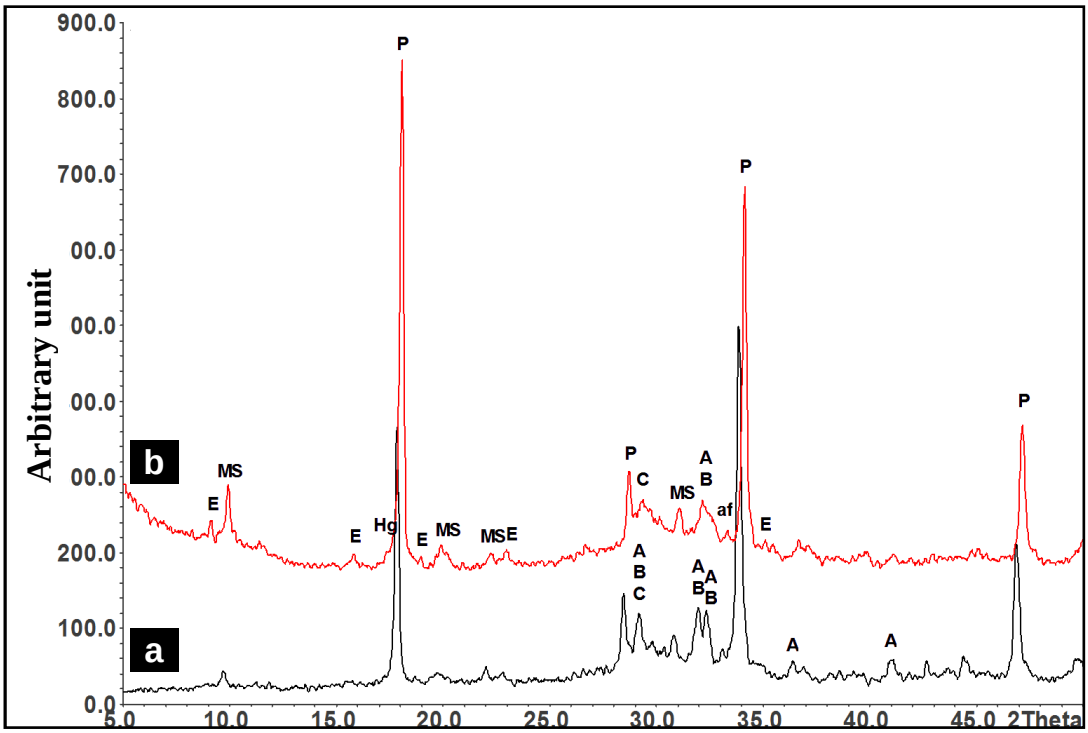


Figure 4.1 XRD traces for neat PC cured at 40°C: (a) for 28 days, (b) for 360 days

The TGA and DTG curves for the neat PC after 28 and 360 days hydration are presented in Figure 4.2. The curves after 28 days were similar to the data available in the literature [3]. The first mass loss identified at ~100°C in both samples is attributed to the elimination of evaporable water, along with the dehydration of the calcium silicate hydrate (C-S-H) gel. In PC systems, evaporable water is removed below 120°C [5]. The weight loss at around 180°C was the result of the dehydration of monosulphoaluminate hydrate (AFm) phases [5] while a small peak observed at about 380°C is assigned to the decomposition of poorly crystallined hydrogarnet ($C_3AH_6$) [3]. Hydrogarnet

phase was not observed in the XRD result for the 28 days sample, likely because it was present as a poorly crystalline phase or in a small quantity to be observed by XRD. The most significant weight loss at around 480 °C was due to the dehydroxylation and consequent decomposition of portlandite [5] to form calcium oxide. The gradual weight loss at 550-750°C could be due to the loss of $CO_2$ from $CaCO_3$.

A small mass losses around 120°C is assigned to the decomposition of ettringite phase [6], consistent with the XRD observations (Figure 4.1), suggesting that the raised curing temperature has delayed the formation of ettringite. Further weight losses at ~150ºC and ~280ºC were attributed to the decomposition of monosulphate, identified in the XRD results. In contrast with 28 days sample, PC cured for 360 days shows larger weight loss at 380-400ºC, which was thought to be from the decomposition of the hydrogarnet-type phase. The weight loss due to the decomposition of $Ca(OH)_2$ and $CaCO_3$ were also more significant in the sample cured for 360 days.

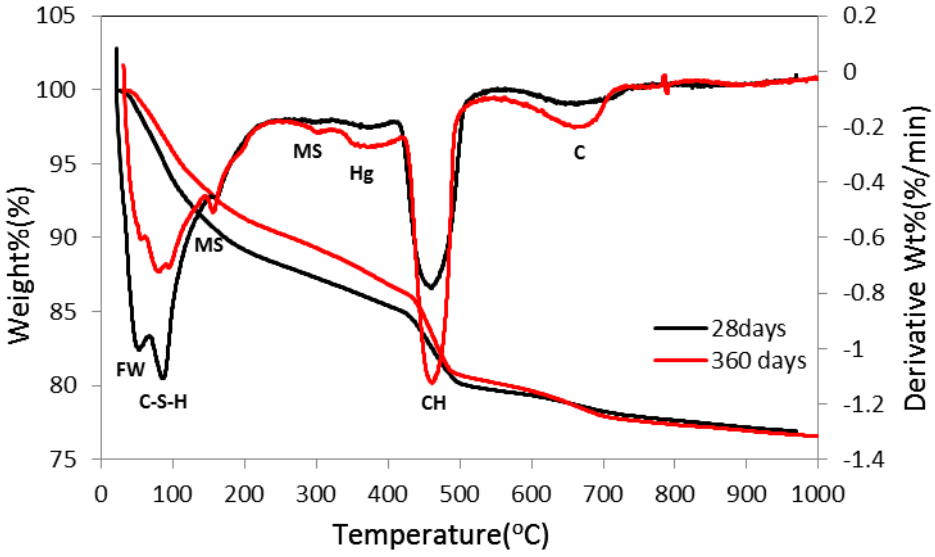


Figure 4.2 TG-DTG curves for PC cured at 40ºC for 28 and 360 days

### 4.2.2 Microstructural analysis

A backscattered electron (BSE) image of the neat PC after 28 days is shown in Figure 4.3. Based on the grey level scales, the microstructure of hydrated cement can be analysed [7]. The lighter grey particles are the anhydrous Portland cement, as the average elemental number in the unreacted clinker phases is expected to be higher than that in the hydration products. A grey rim forming around the unreacted PC particles is the formation of an ‘inner’ C-S-H type product, surrounded by darker ‘outer’ C-S-H type products. The differences in brightness between inner and outer C-S-H type products are associated with the differences in the Ca/Si ratio and in the microporosity products [8]. As the inner products form closer to the clinker phases, they likely to have higher Ca/Si ratio and a lower amount of fine pores than the outer product [8]. Dark grey areas for C–S–H gel in the outer product most likely also contain AFm phases as observed in XRD. However, is not possible to distinguish between these two phases on the grey level alone at this magnification. The light grey agglomerations forming near partially reacted PC particles are attributed to portlandite.

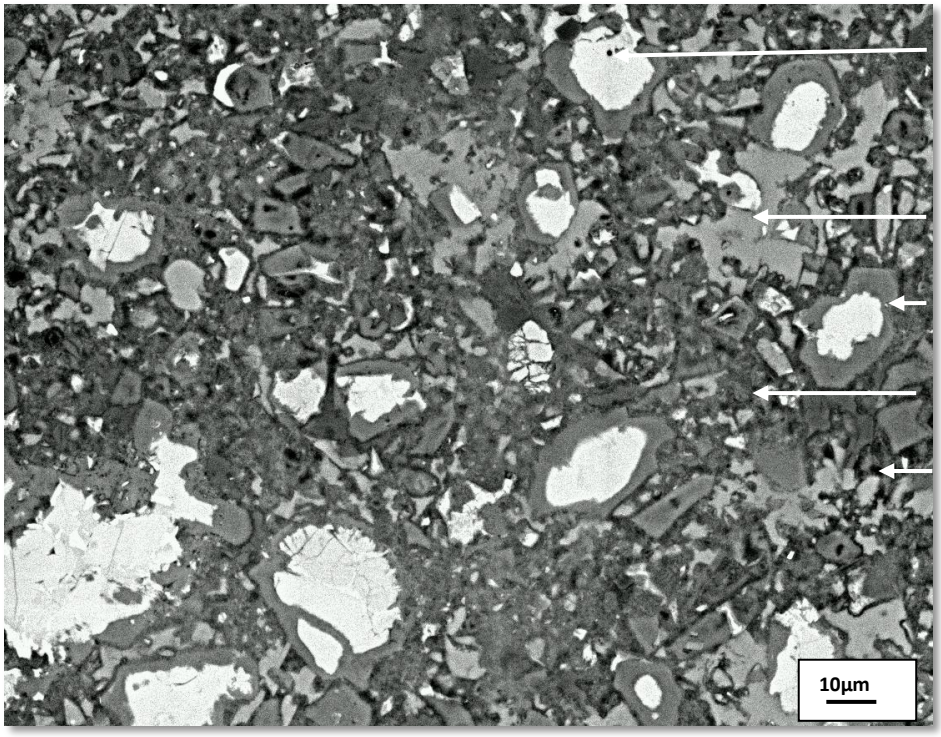


Figure 4.3 BSE image of PC after 28-days of curing

BSE image of the neat PC sample hydrated for 360 days at 40°C is shown in Figure 4.4. The basic features in the microstructure of the product were similar to that of the 28 days sample. However, it seems that anhydrous cement particles decreased after 360 days compared with that cured for 28 days. $Ca(OH)_2$ constituted a higher proportion of the microstructure alongside outer hydration products which is consistent with the TG results. Fewer pores were visually observed after 360 days compared to 28 days.

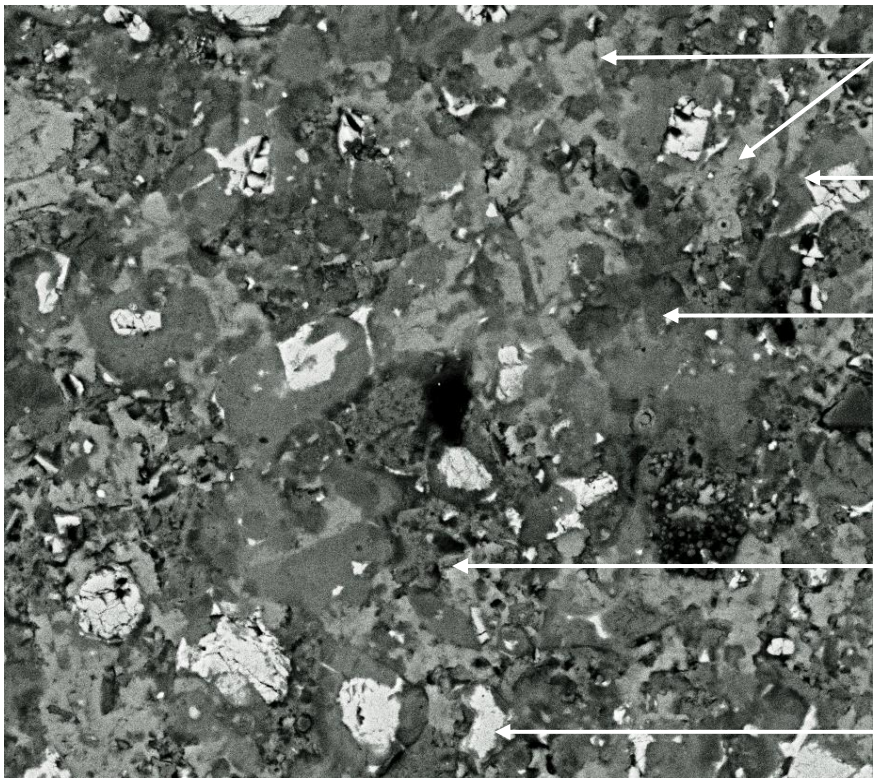


Figure 4.4 BSE images of PC cured at 40 $^{o}$C for 360 days.

## 4.3 PC-$BaSO_4$ systems

### 4.3.1 Phase analysis of PC-$BaSO_4$ systems

#### 4.3.1.1 Effect of $BaSO_4$ powder

Figure 4.5 (a) and (b) show XRD patterns of the PC-$BaSO_4$ powder samples (0, 12, 36, 60 wt% $BaSO_4$) cured at 40$^{o}$C for 28 days for w/c=0.53 and w/s=0.53 series, respectively. The main crystalline phases detected from the hydration of neat PC were calcium hydroxide (P) and monosulphate (MS). Some of unreacted alite (A) and belite (B) were also present in addition to calcium carbonate (C). In w/c=0.53 series, XRD results showed a gradual change in the peak intensity; those attributed to the cement clinker phases and hydration products decreased whereas those for $BaSO_4$ increased as $BaSO_4$ loading was increased. XRD patterns for w/s=0.53 series were very similar to those for

w/c=0.53 in general. However, the peaks attributed to calcium carbonate were prominent for w/s=0.53 series (e.g. at 29 $^{o}$ 2θ) when $BaSO_4$ was 36 and 60 wt%, which suggests extra amount of water in the system caused a significant carbonation in these systems. For both series, no obvious product from the reaction between $BaSO_4$ and PC was identified from the obtained XRD patterns. These results suggest that $BaSO_4$ was encapsulated without obvious reactions with the cement matrix.

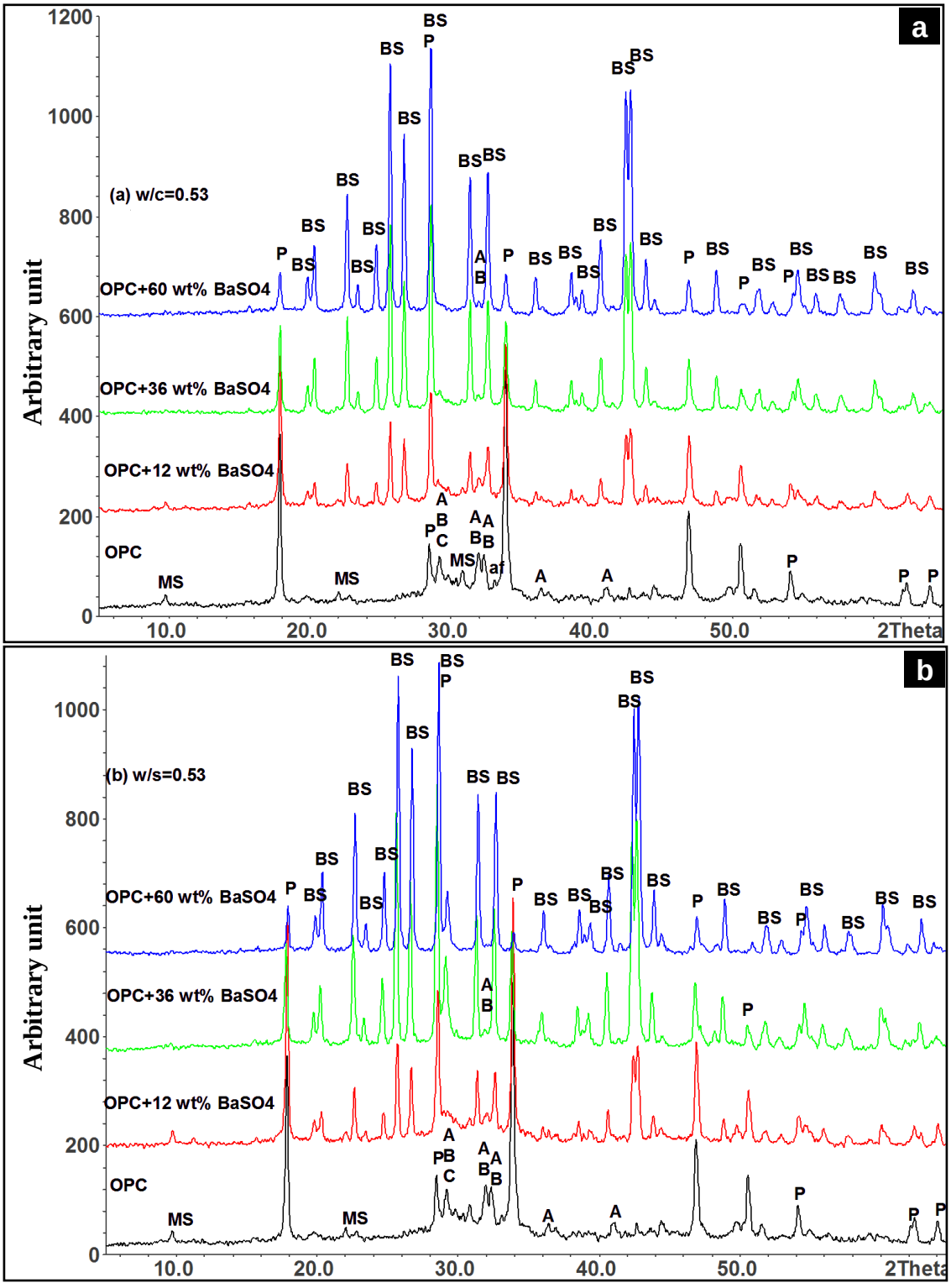


Figure 4.5 XRD patterns of PC-$BaSO_4$ powder samples: (a) w/c=0.53 and (b) w/s=0.53 series cured at 40 $^{o}$C for 28 days

Typical TG-DTG curves for w/c=0.53 and w/s=0.53 series are presented in Figures 4.6 and 4.7, respectively. These Figures also show the data for $BaSO_4$ used in the present study for comparison. The data for $BaSO_4$ did not show any significant features in TG and DTG curves due to its stability up to about 1100$^oC$ of decomposition temperature [9, 10]. The DTG curves for both series were similar at lower temperature, with comparable amounts of free water, C-S-H, and monosulphate. In w/c=0.53 series $Ca(OH)_2$ peak gradually decreased with $BaSO_4$ loading. $CaCO_3$ in this system increased when $BaSO_4$ was introduced into the system, suggesting that the introduction of fine $BaSO_4$ powder encouraged the formation of $CaCO_3$, probably by increasing the surface area for nucleation site and growth [11]. However, the amount of $CaCO_3$ decreased with the increase of $BaSO_4$ and corresponding to decrease of PC, showing the formation of $CaCO_3$ is also related to the amount of PC in the system. In the w/s =0.53 series, on the other hand, the $Ca(OH)_2$ dehydration peak did not change much at 12 wt% of $BaSO_4$ loading compared to that of the neat PC, most likely due to the extra amount of water in the system helped further hydration of PC in the system, but decreased at 36 and 60 wt% due to the significant reduction of PC in the system (64 and 40 wt%, respectively). Differing from the w/c=0.53 series, the peak associated with $CaCO_3$ decomposition in w/s=0.53 series generally increased with $BaSO_4$ loading, which corresponds the XRD results. These results suggest the excess water content in w/s=0.53 series had positive effects on the formation of $Ca(OH)_2$ and $CaCO_3$ in the PC-$BaSO_4$ powder system.

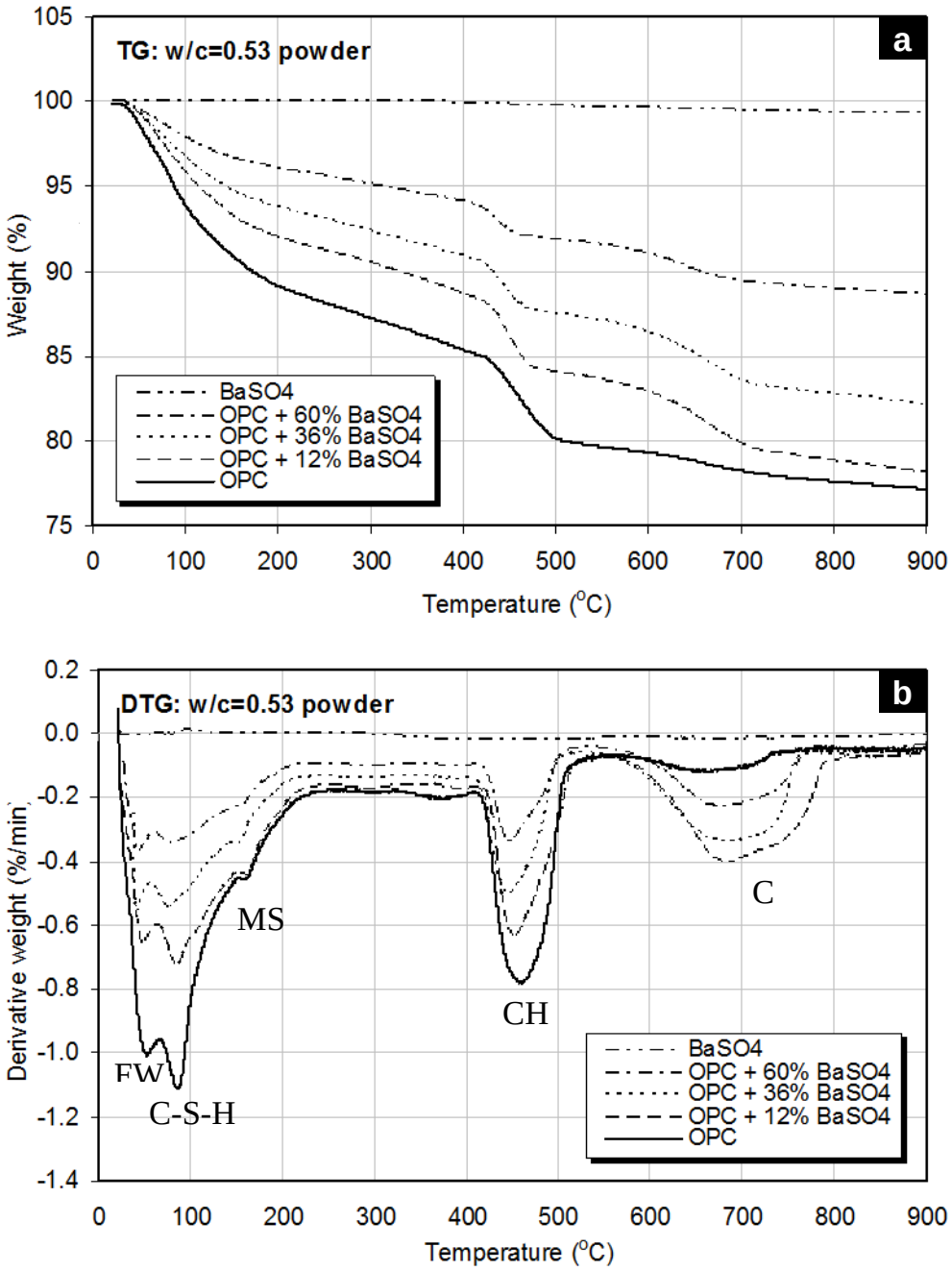


Figure 4.6 Typical TG data of cement samples for PC-$BaSO_4$ powder system with w/c=0.53: (a) TG data and (b) DTG data.

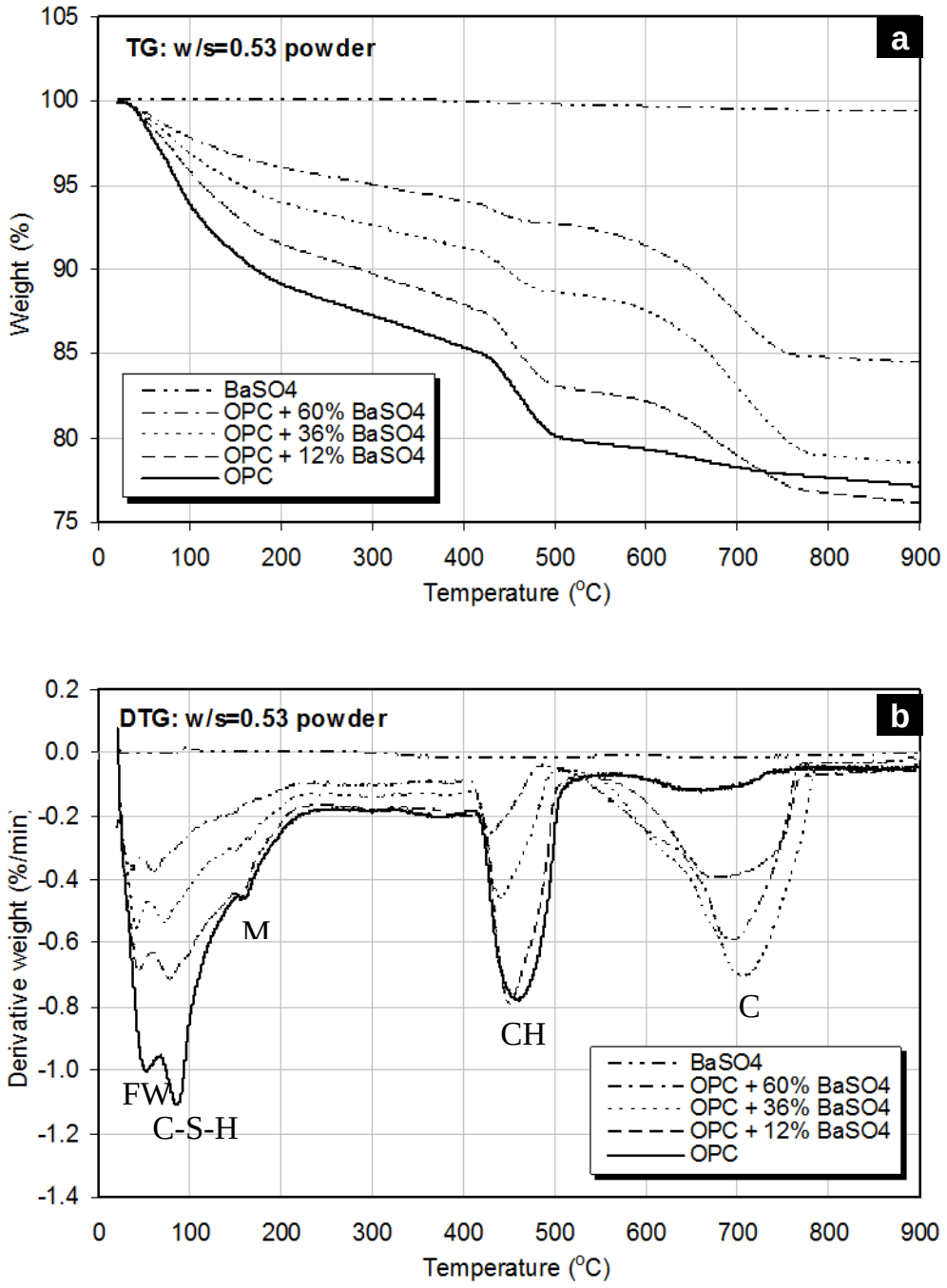


Figure 4.7 Typical TG data of cement samples for PC-$BaSO_4$ powder system with w/s=0.53: (a) TG data and (b) DTG data.

4.3.1.2 Effect of $BaSO_4$ granules

XRD results for the PC-$BaSO_4$ granule systems cured at 40$^oC$ for 28 days, both w/c=0.53 and w/s=0.53 series are shown in Figure 4.8. The feature of the results was very similar to those for the PC-$BaSO_4$ powder systems. Calcium hydroxide (P) and monosulphate (Ms) were identified as hydration phases in addition to the unreacted alite (A) and belite (B). A significant difference from the PC-$BaSO_4$ powder systems was the lack of the distinctive reflection peak at approximately 29 $^o2\theta$ in w/s=0.53 series. This suggests that excess water in the system did not lead to the large amount of $CaCO_3$ formation when $BaSO_4$ was introduced in the system as granules. Reflection peaks for ettringite were also observed in the w/s=0.53 systems and w/c=0.53 system with 12 wt% $BaSO_4$. The formation of ettringite may be related to the carbonation of monosulphate phase. The carbonation of monosulphate can result in the formation of hemi- and/or mono-carbonate phases, which usually leads to the formation of ettringite [12, 13]. The w/s=0.53 series indicate reflection peaks at 10-11 $^o$ 2$\theta$ which may be due to these phases.

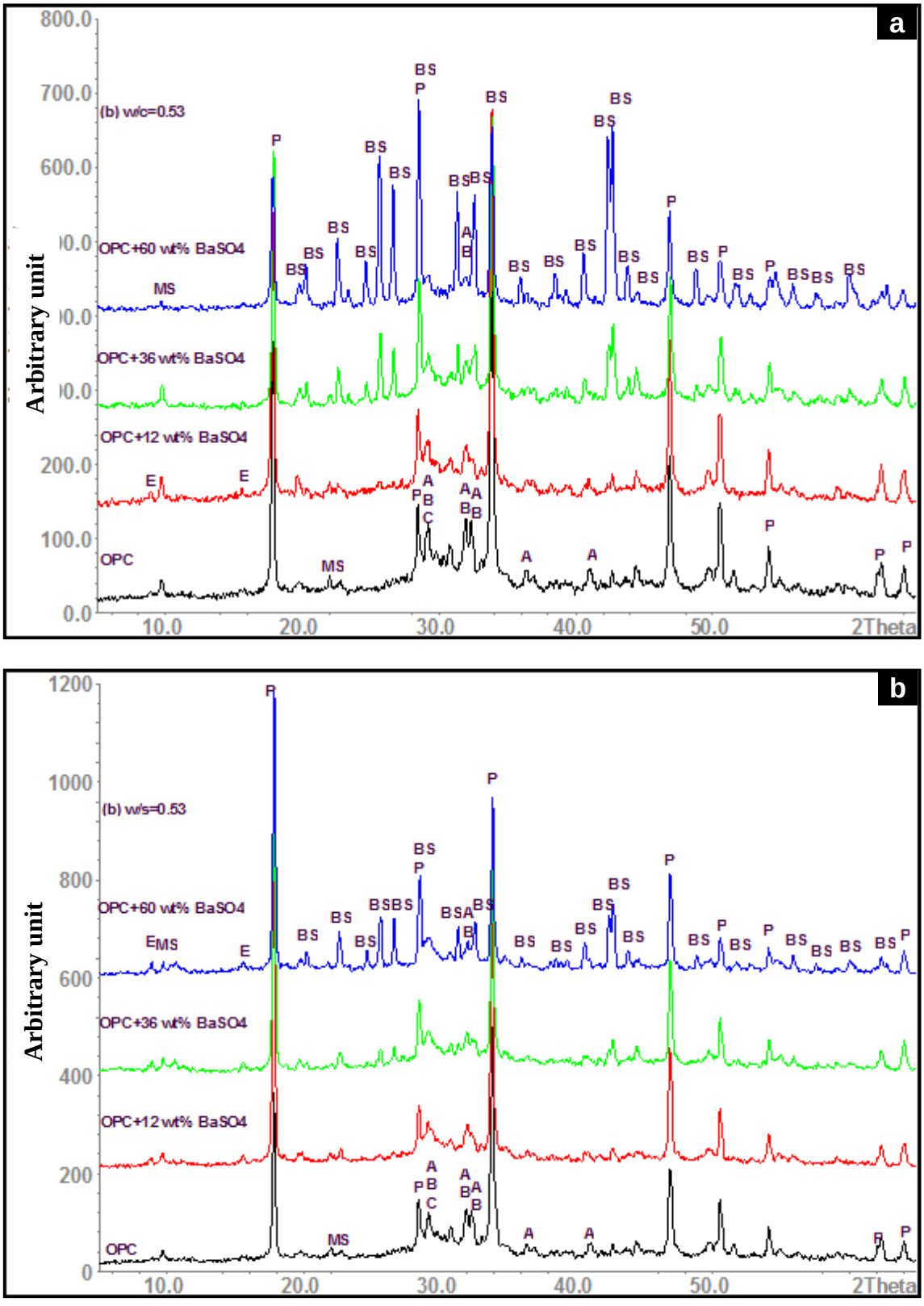


Figure 4.8 XRD patterns of PC-$BaSO_4$ granule samples: (a) w/c=0.53 and (b) w/s=0.53 series. (*Al peak due to the sample holder)

Typical TG-DTG curves of PC-$BaSO_4$ granule systems, w/c=0.53 series and w/s=0.53 series are presented in Figures 4.9 and 4.10, respectively. The TG curves indicated a gradual shift for both series, showing less weight loss when the $BaSO_4$ loading increased and the fraction of PC decreased. The DTG curves also showed similar trend. Although the basic feature of the results was similar to those of the PC-$BaSO_4$ powder system, the PC-$BaSO_4$ granule systems indicated much less weight loss associated with the decarbonation of $CaCO_3$ at 550-750 $^oC$, both in w/c=0.53 and w/s=0.53 series. It is evident that the surface area of $BaSO_4$ in the system is an important factor for $CaCO_3$ formation in the PC-$BaSO_4$ systems. Some of the PC-$BaSO_4$ granule system also appears to have a slightly less weight change than the PC-$BaSO_4$ powder system at the lower temperature region up to 250 $^oC$, suggesting that the granule system formed less C-S-H. It has been known that the C-S-H formation can be controlled both by homogeneous and heterogeneous nucleation [1, 14], thus less surface area available in the PC-$BaSO_4$ granule system may have contributed to the less C-S-H formation. Some of the data indicated broad shoulder in the DTG curves at ~150 $^oC$, which could be due to monocarbonate phase as well as ettringite identified in the XRD results.

.

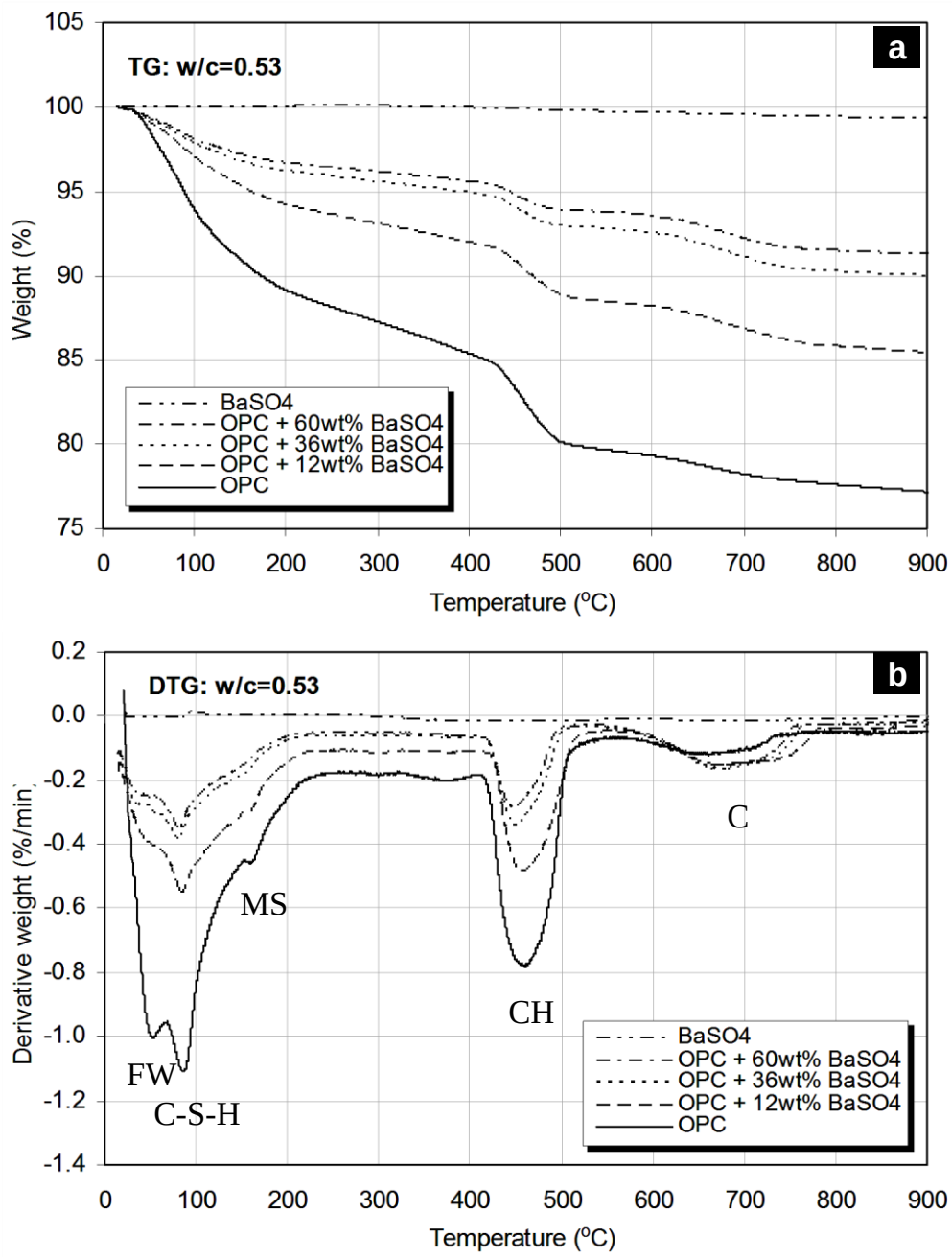


Figure 4.9 Typical TG data of cement samples for PC-$BaSO_4$ granule system with w/c=0.53 cured at 40 °C for 28 days: (a) TG data and (b) DTG data.

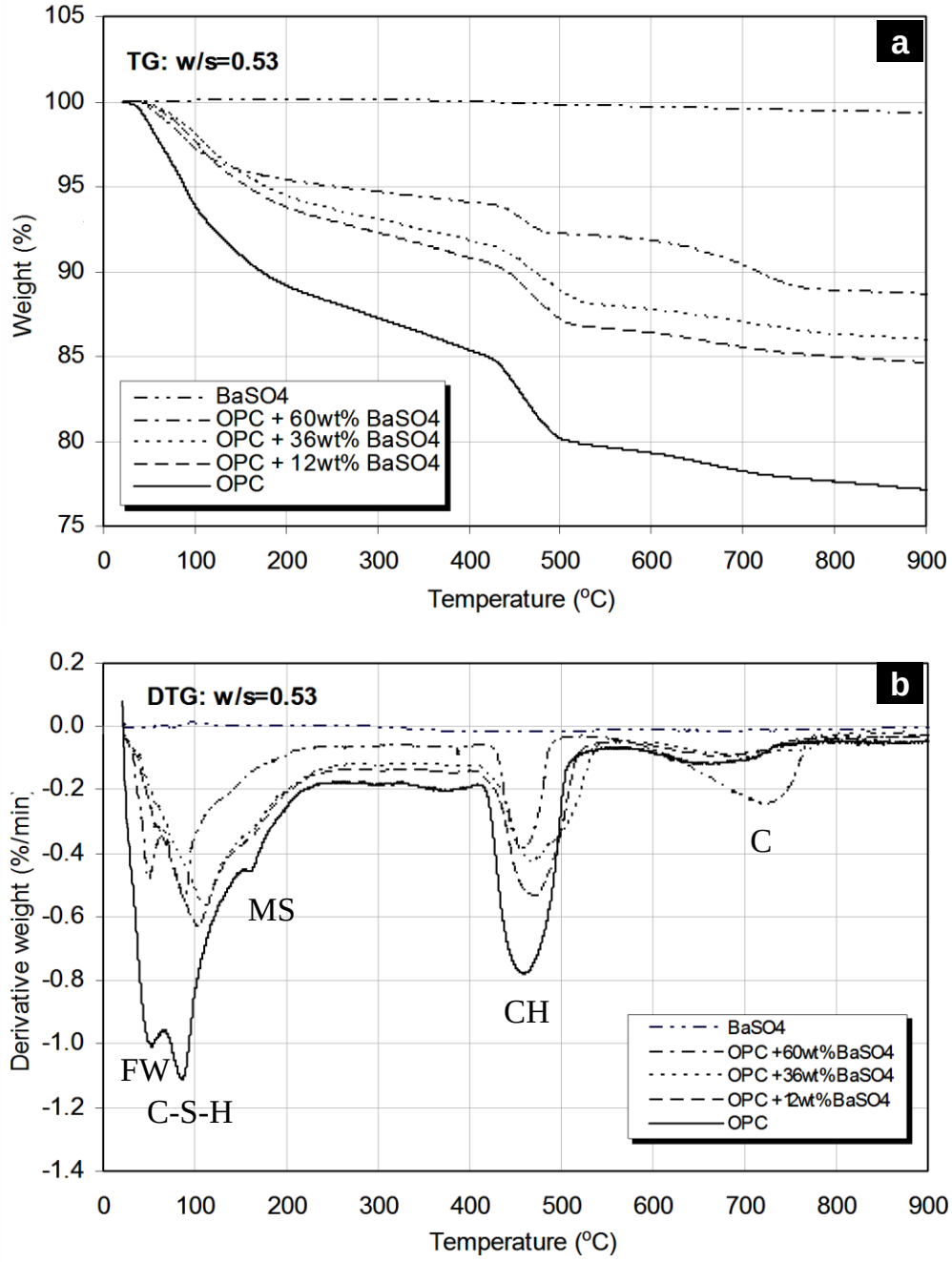


Figure 4.10 Typical TG data of cement samples for PC-$BaSO_4$ granule system with w/s=0.53 cured at 40 °C for 28 days: (a) TG data and (b) DTG data.

### 4.3.2 Microstructure of PC- $BaSO_4$ systems

#### 4.3.2.1 Effect of $BaSO_4$ powder

The BSE images of PC-$BaSO_4$ powder systems, w/s=0.53 and w/c=0.53 series are presented in Figures 4.11 and 4.12, respectively. The fine $BaSO_4$ particles are dispersed throughout the microstructure, which indicates that the $BaSO_4$ particles were incorporated well in the products. Both in w/s=0.53 and w/c=0.53 series, anhydrous cement particles seemed to decrease as the quantity of added $BaSO_4$ increased. The w/s=0.53 series appears more porous compared with w/c=0.53 series at all $BaSO_4$ loading probably due to the larger amount of water in the system. Hydration products were difficult to distinguish within the microstructure due to the brightness of the $BaSO_4$ particles in BSE.

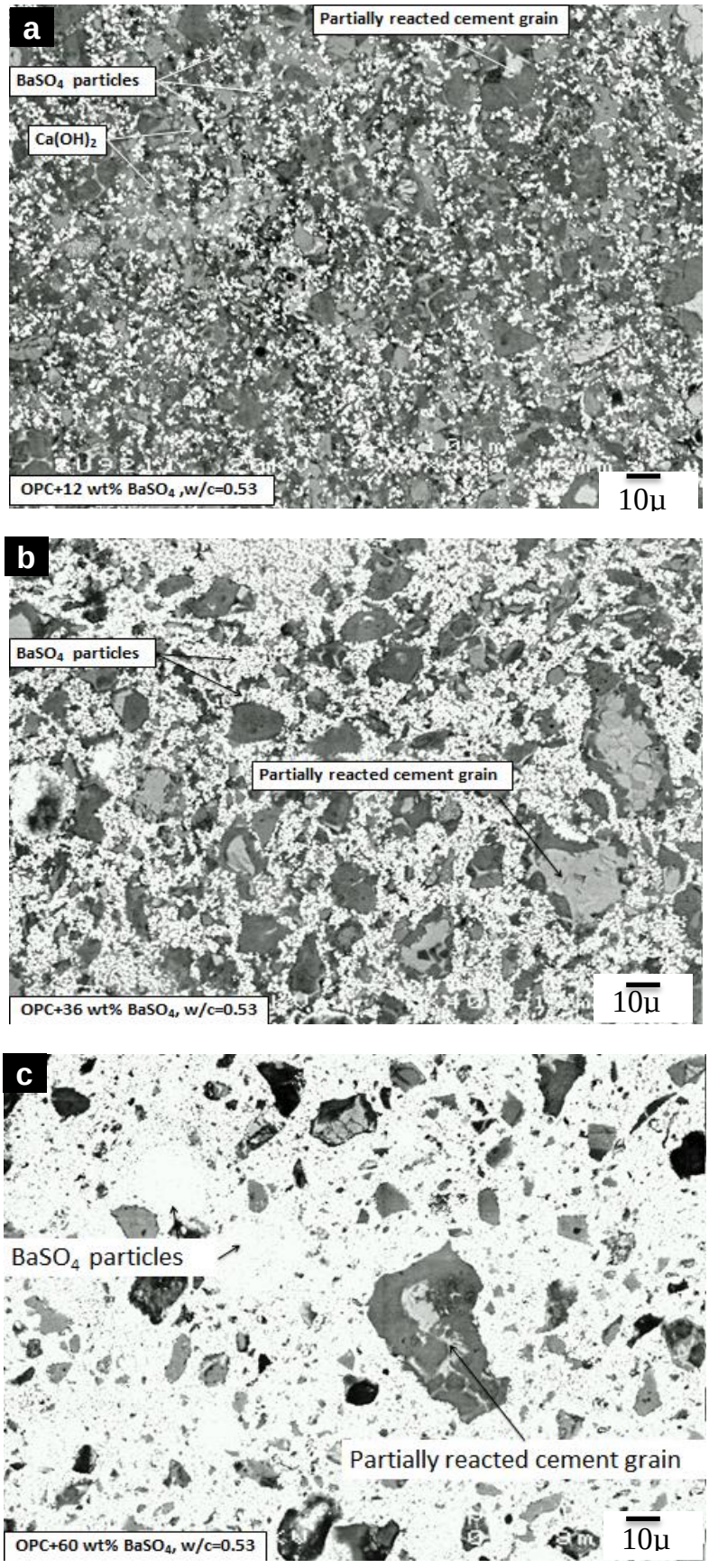


Figure 4.11 BSE images of PC-$BaSO_4$ powder system with w/c=0.53: ( a) 12 wt% $BaSO_4$, ( b) 36 wt% $BaSO_4$, (c) 60 wt% $BaSO_4$.

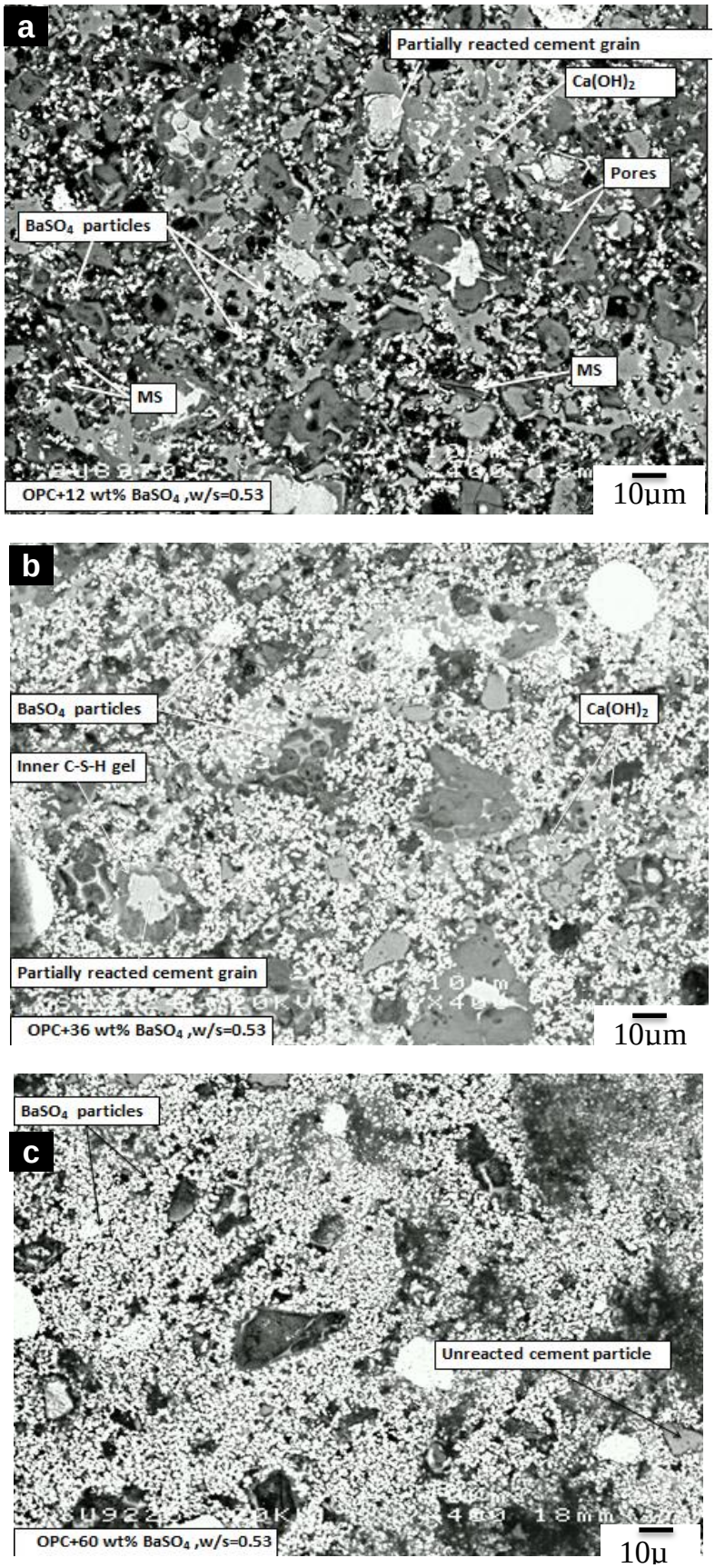


Figure 4.12 BSE images of PC-$BaSO_4$ powder system with w/s=0.53: ( a) 12 wt% $BaSO_4$, ( b) 36 wt% $BaSO_4$, (c) 60 wt% $BaSO_4$.

Figure 4.13 and 4.14 show cumulative pore volume obtained via MIP for w/c=0.53 and w/s=0.53 series respectively. It is important to note that the diameters shown in the MIP analysis may not directly represent the pore size of the real system. One of the limitations of MIP is that the larger voids and pore structures cannot be detected, resulting in a smaller average pore size [15].

In neat PC, the largest concentration of pores lies in the range of < 1.2 μm. $BaSO_4$ addition at 12 wt% in w/c=0.53 series (Fig. 4.13) increased the cumulative pore volume in the diameter range from 1 to 0.1 μm. The pores in this range appeared to decrease in the 36 wt% sample, and further additions of $BaSO_4$ up to 60 wt% caused a reduction in smaller pores approximately < 0.03 μm. In contrast, the cumulative pore volume was increased significantly in w/s=0.53 series due to the excess water in the system, since the w/c ratio in the w/s=0.53 series increases with the increase of $BaSO_4$. The excess water generates a large capillary porosity. This system also showed an increase of cumulative pore volume, when 12 wt% of $BaSO_4$ was introduced, in the diameter range from 1 to 0.1 μm.

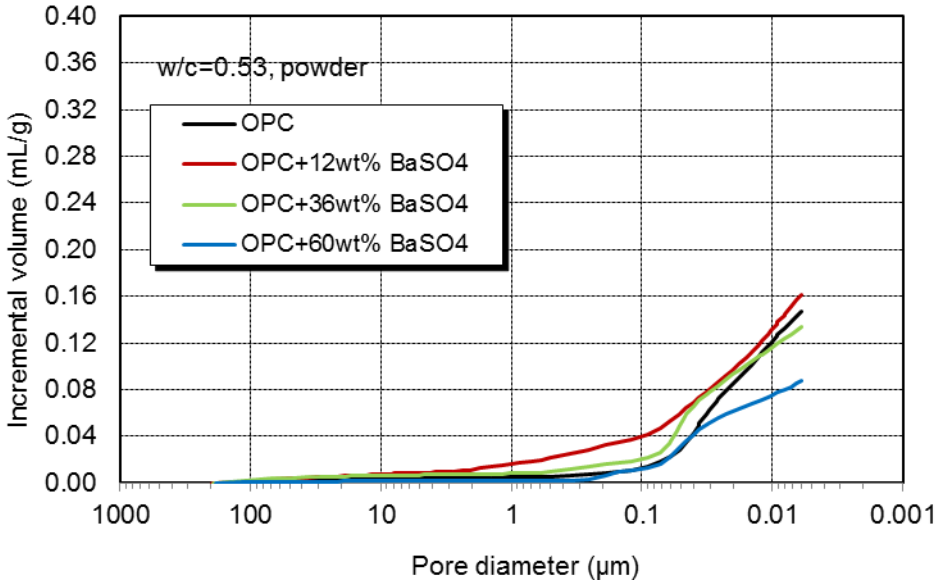


Figure 4.13 Typical pore size distribution of PC-$BaSO_4$ powder systems, w/c=0.53 series

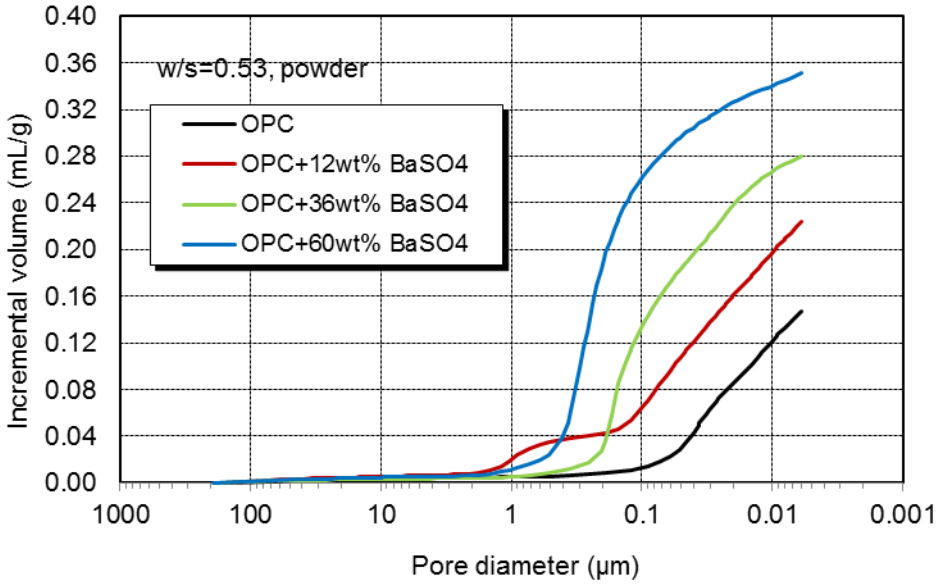


Figure 4.14 Typical pore size distribution of PC-$BaSO_4$ powder systems, w/s=0.53 series

Figure 4.15 illustrates the total porosity of samples obtained from MIP data using the following equation.

$$(Total\ porosity) = \frac{(total\ int\ volum)}{(sample\ volume)} \times 100 \qquad \% \qquad (4.1)$$

In w/s=0.53 series, the total porosity of the samples clearly increased with $BaSO_4$ loading whereas that in w/c=0.53 series slightly decreased at high $BaSO_4$ loading. The difference between these series accounts for the difference in the w/c ratio, which increases significantly in the w/s=0.53 series because of the reduction in the amount of PC due to the $BaSO_4$ loading. The w/c ratio was kept constant as 0.53 for the w/c=0.53 series, the slight decrease in total porosity in the w/c=0.53 series may suggest a gradual filling of large pores by $BaSO_4$. Similar results have also been reported elsewhere [16, 17]. These results also confirm the observation in BSE images. It is evident from MIP results that, for the same degree of $BaSO_4$ loading, the porosity of the products is higher in w/s=0.53 series than in w/c=0.53 series.

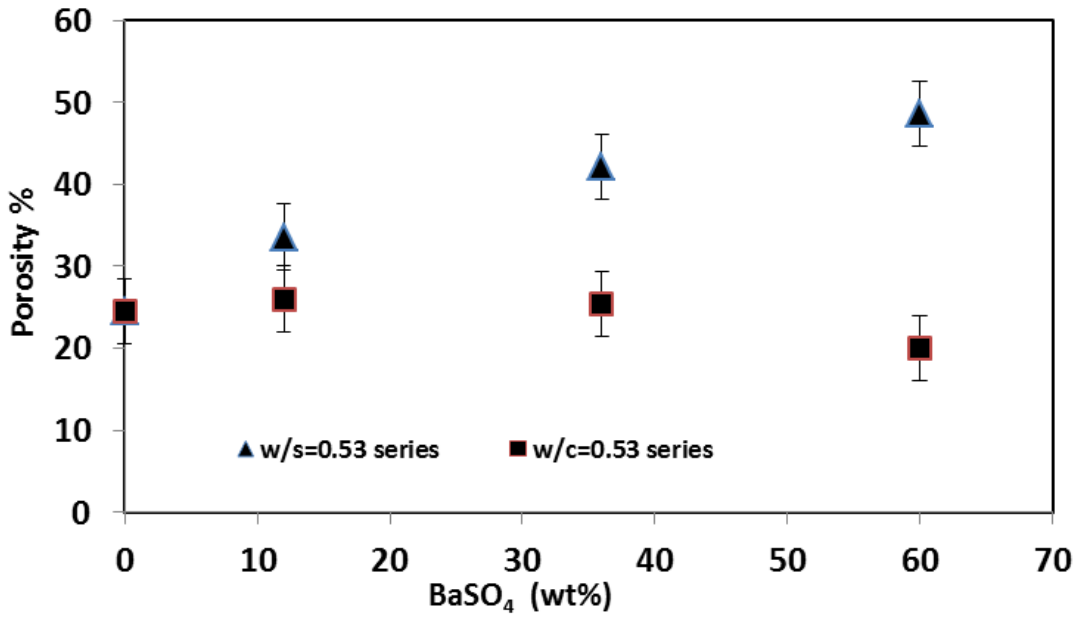


Figure 4.15: Total porosity of PC-$BaSO_4$ powder systems cured at 40 $^{o}$C for 28 days.

4.3.2.2 Effect of $BaSO_4$ granules

The BSE images of PC- $BaSO_4$ granule systems, w/s=0.53 and w/c=0.53 series are presented in Figs. 4.16 and 4.17, respectively. In both series, because of the localised distribution of $BaSO_4$ due to the larger size of granule, the microstructure of cement matrix appeared quite similar for all granule samples and resembles the neat PC more compared with the PC-$BaSO_4$ powder system. w/c=0.53 series has slightly more anhydrous cement particles than w/s=0.53 series, suggesting more hydration took place in w/s=0.53 series. This higher degree of hydration in w/s=0.53 series did not appear to result in the denser microstructure than that of w/c=0.53 series, which was also observed in the PC-$BaSO_4$ powder systems. Additionally, formation of a needle-like ettringite (AFt) phase was observed in w/s=0.53 series (Figure 4.17 (b) and (c)), in accordance with the XRD results. One of the microstructural features of the observed in the PC- $BaSO_4$ granule system (both in w/c=0.53 and w/s=0.53 series) is a porous region surrounding the $BaSO_4$ granules, filled with portlandite. Typical examples are shown in Figure 4.18, in which a higher amount of portlandite formation is easily observable around the $BaSO_4$ granules. This type of feature, often referred as interfacial transition zone is usually observed between aggregates and cement matrix in mortars and concretes [18, 19]. This suggests that $BaSO_4$ granules used in the present work acted in the same way as aggregates, leaving a more porous zone around the granules by disrupting the packing of cement particles [18, 19], and then portlandite was deposited in the porous region with the progress of hydration reaction.

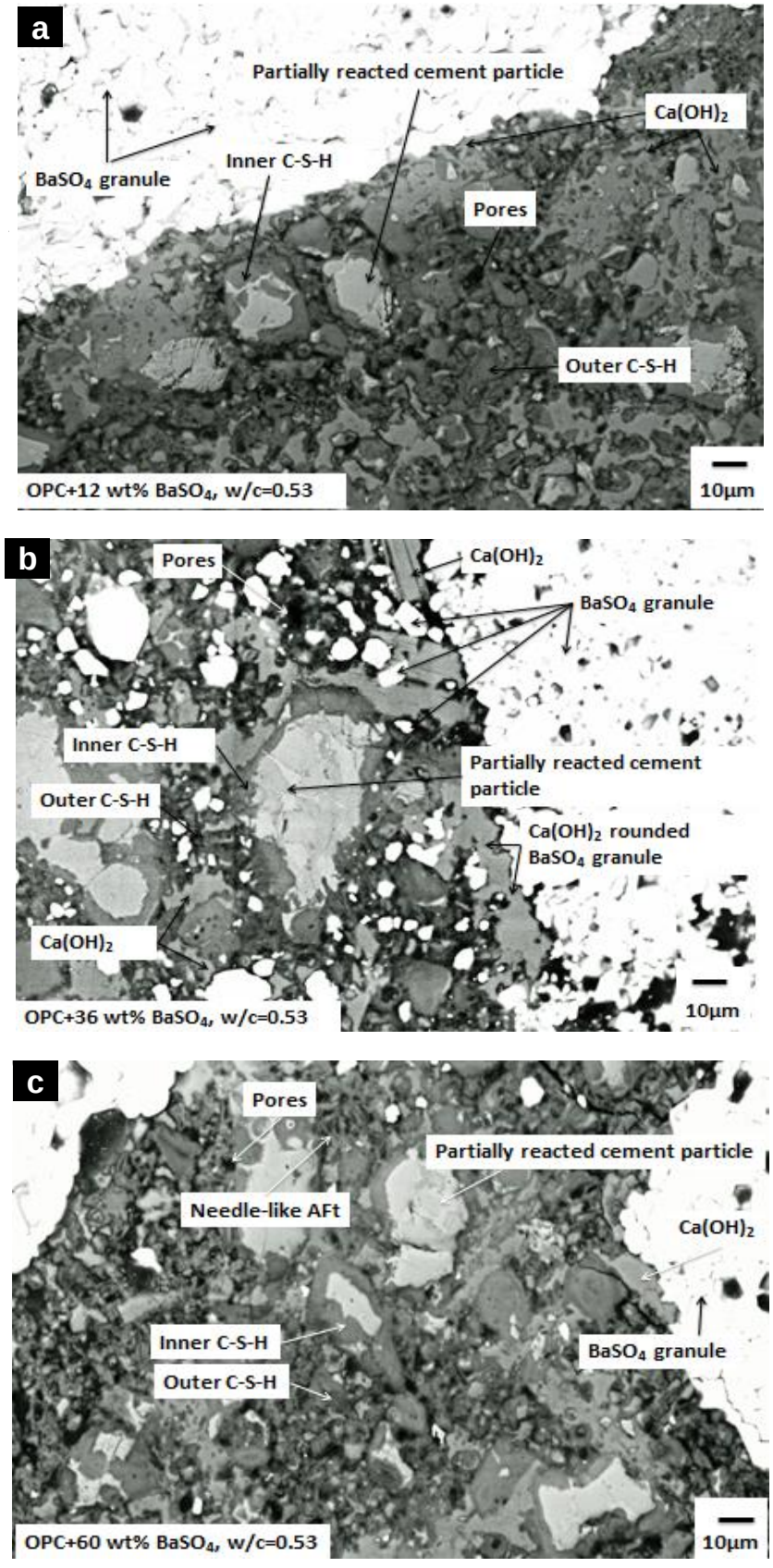


Figure 4.16 BSE images of PC-$BaSO_4$ granule system with w/c=0.53: ( a) 12 wt% $BaSO_4$, ( b) 36 wt% $BaSO_4$, (c) 60 wt% $BaSO_4$

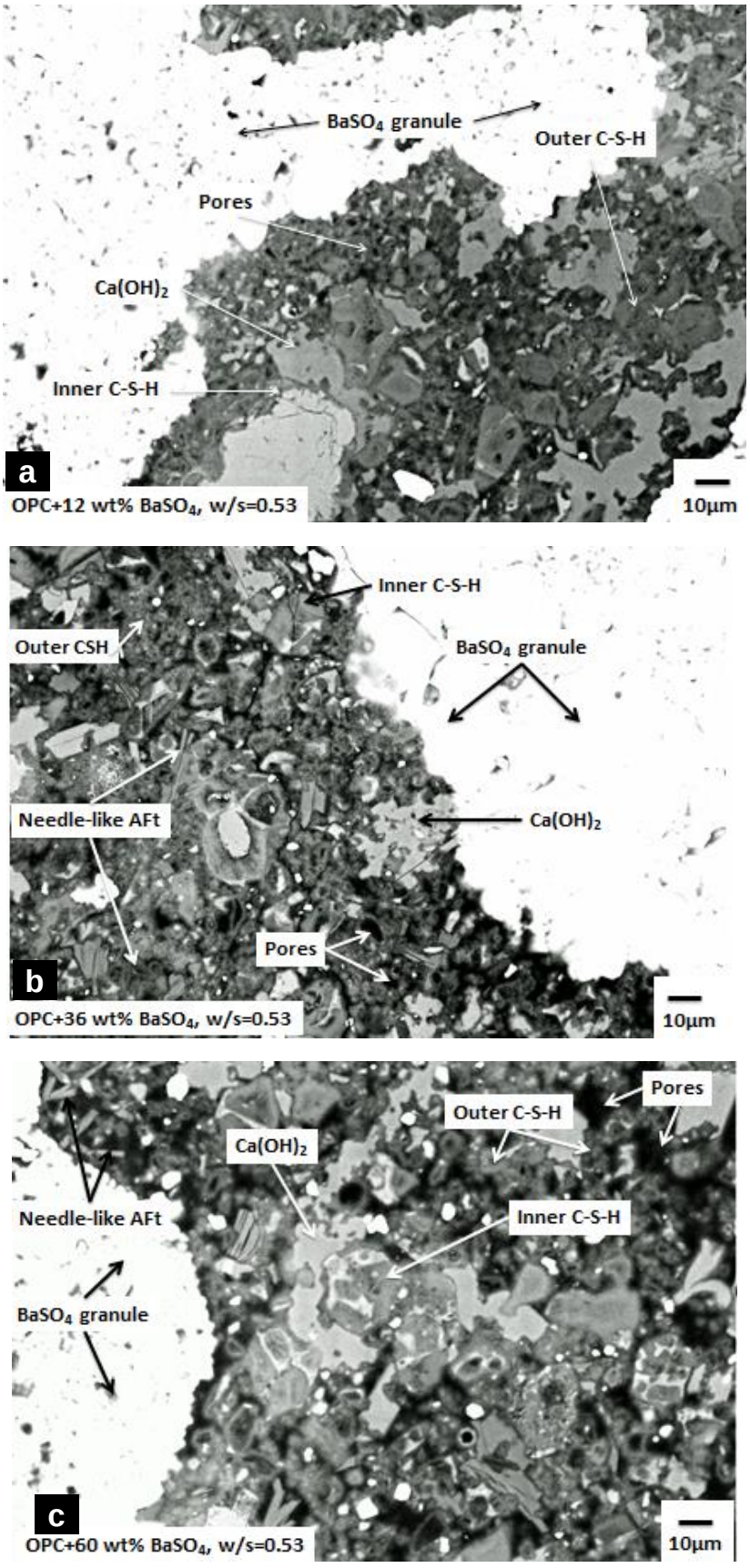


Figure 4.17 BSE images of PC-$BaSO_4$ granule system with w/s=0.53: ( a) 12 wt% $BaSO_4$, ( b) 36 wt% $BaSO_4$, (c) 60 wt% $BaSO_4$.

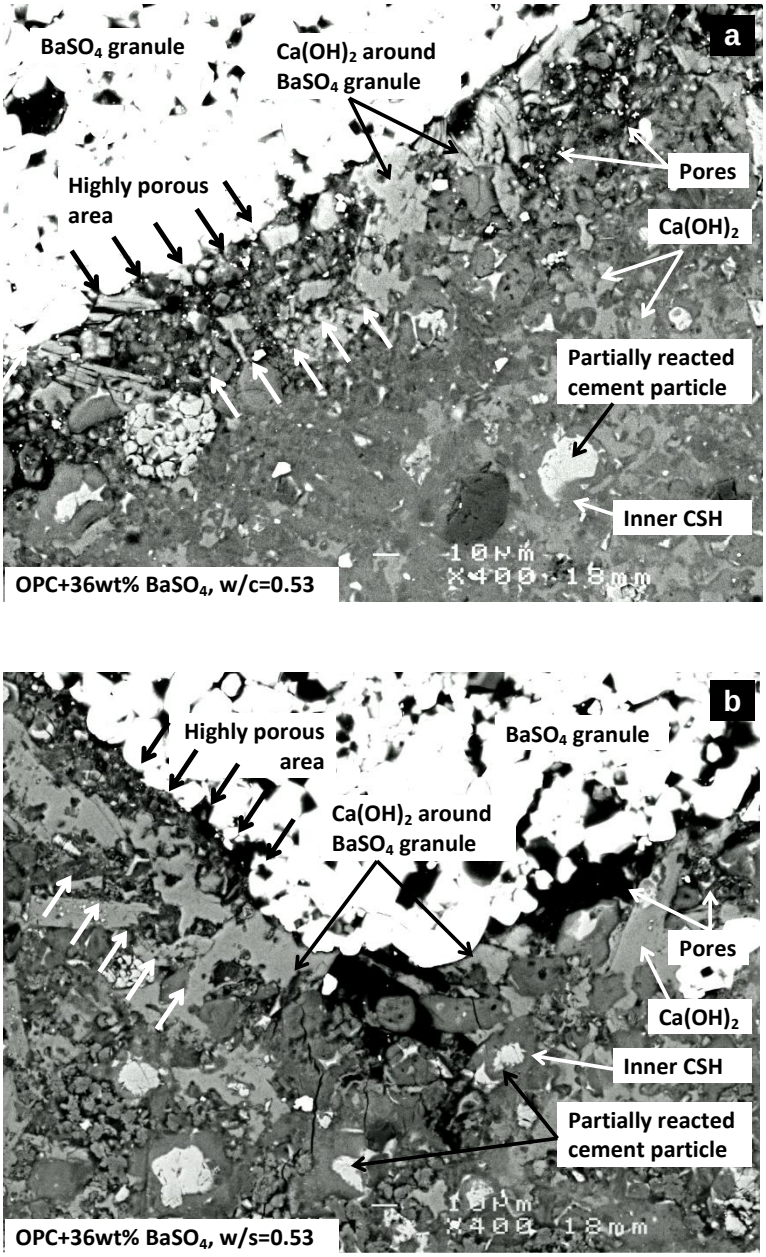


Figure 4.18 BSE image of 36 wt% $BaSO_4$ granule system: (a) w/c=0.53, (b) w/s=0.53, showing the formation of an interfacial transition zone.

The elemental mapping based on the EDS analysis over the area of an encapsulated $BaSO_4$ (Figure 4.19) suggests that the $BaSO_4$ did not react with cement hydration product. The barium was not detected over cement hydration products and was only detected on $BaSO_4$ granule in the entire sample

hydrated for 28 days. These results, suggest that the $BaSO_4$ granules when encapsulated without reacting with the cement hydration products.

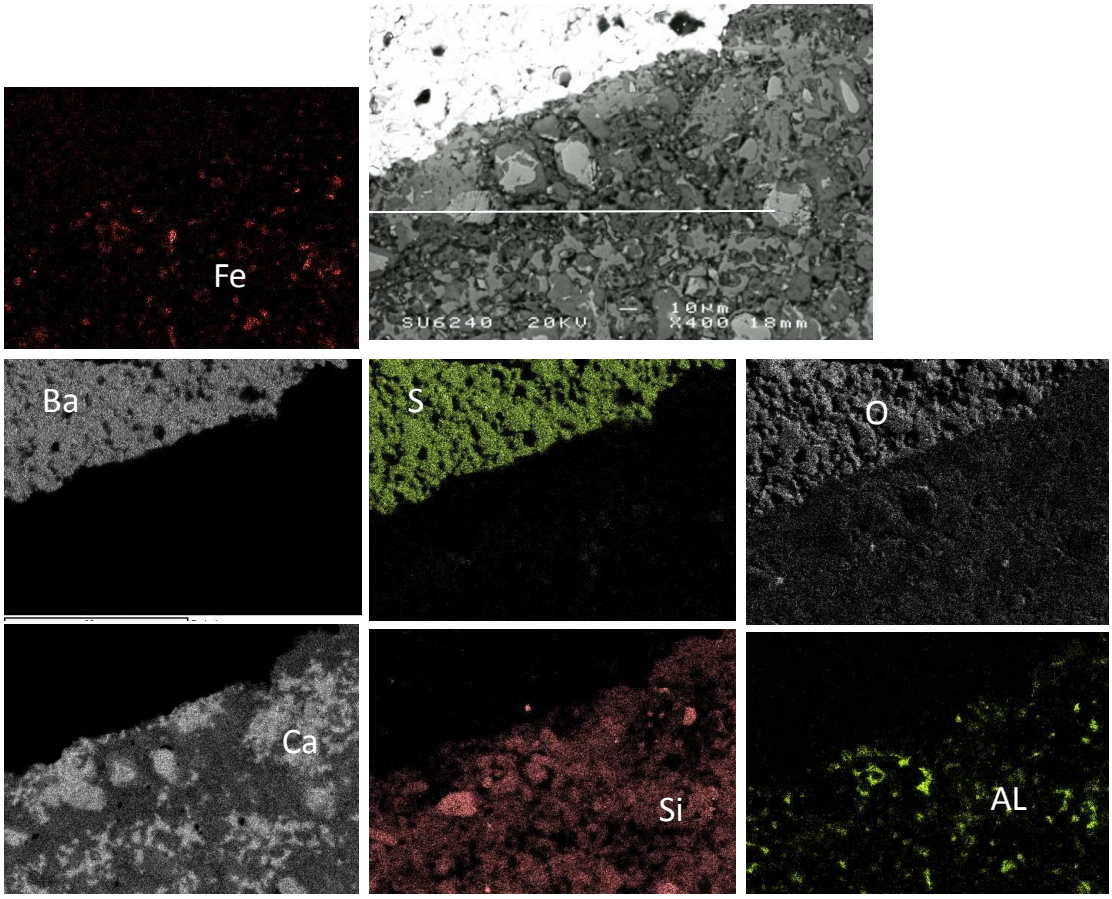


Figure 4.19 BSE image of PC+60 wt% $BaSO_4$, w/s 0.53 cured at 40ºC for 28 days and elemental maps

Figure 4.20 and 4.21 show cumulative pore volume obtained via MIP for w/c=0.53 and w/s=0.53 series respectively. The change in porosity was not very significant in the w/c=0.53 series whereas it indicated a general increase in the w/s=0.53 series. These trends are similar to the PC-$BaSO_4$ powder systems previously discussed. However, the increase in the pores in the diameter range from 1 to 0.1 μm, observed for the PC-$BaSO_4$ powder systems, was not

observed for the PC-$BaSO_4$ granule systems. It appears that this effect is specific for the addition of $BaSO_4$ powder. Based on the total intrusion volume, the total porosity was estimated as shown in Figure 4.22

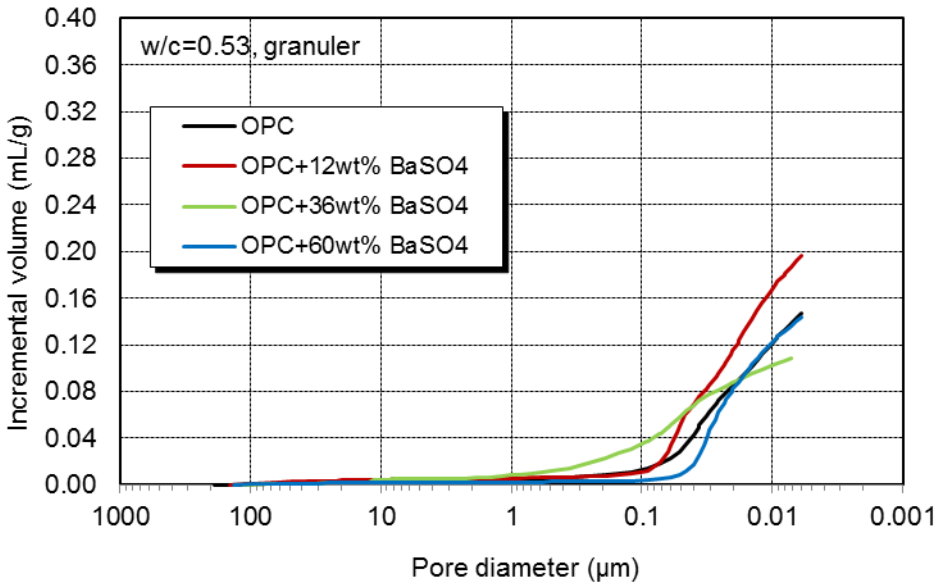


Figure 4.20 Typical pore size distribution of PC-$BaSO_4$ granule systems, w/c=0.53 series

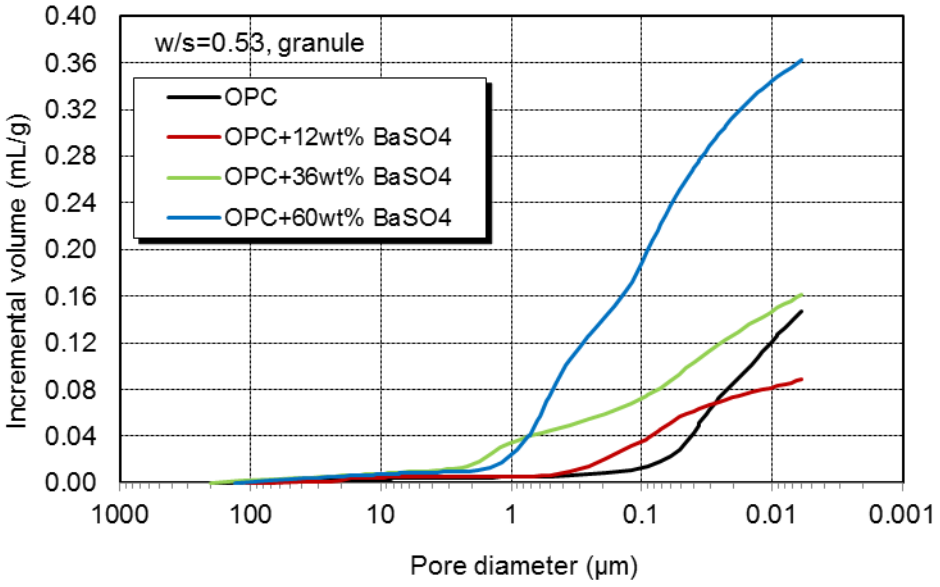


Figure 4.21 Typical pore size distribution of PC-$BaSO_4$ granule systems, w/s=0.53 series

Figure 4.22 illustrates the porosity data. The level of the total porosity was similar both in w/s=0.53 and w/c=0.53 series up to 36 wt% of $BaSO_4$ loading, and w/s=0.53 series become significantly more porous at 60 wt% of $BaSO_4$ loading. Similar to the PC-$BaSO_4$ powder system, w/c=0.53 series did not show a significant change in total porosity with $BaSO_4$ loading except a possible reduction at larger $BaSO_4$ granule contents. This suggests that the effect of $BaSO_4$ particle size on the total porosity is very small when the w/c is fixed as 0.53. In w/s=0.53 series, the porosity of the sample increased with $BaSO_4$ loading, which confirms the observation in BSE images. The increased amount of water in the w/s=0.53 series (w/c > 0.53) resulted in the higher porosity than in the w/c=0.53 series, but the extent of this effect appears to be different depending on the type of $BaSO_4$ in the system. With the $BaSO_4$ powder, the excess water in the system contributed to the increase of porosity at all level of $BaSO_4$ loading whereas its contribution did not become clear with the $BaSO_4$ granule until the $BaSO_4$ loading exceeds 12 wt%. The amount of water directly contributing to increase porosity must have been less in the PC-$BaSO_4$ granule system. This could be related to the formation of the interfacial transition zone. It has been reported that the effective w/c ratio of the bulk paste becomes lower than overall w/c ratio due to the locally increased w/c ratio in the interfacial transition zone [19].

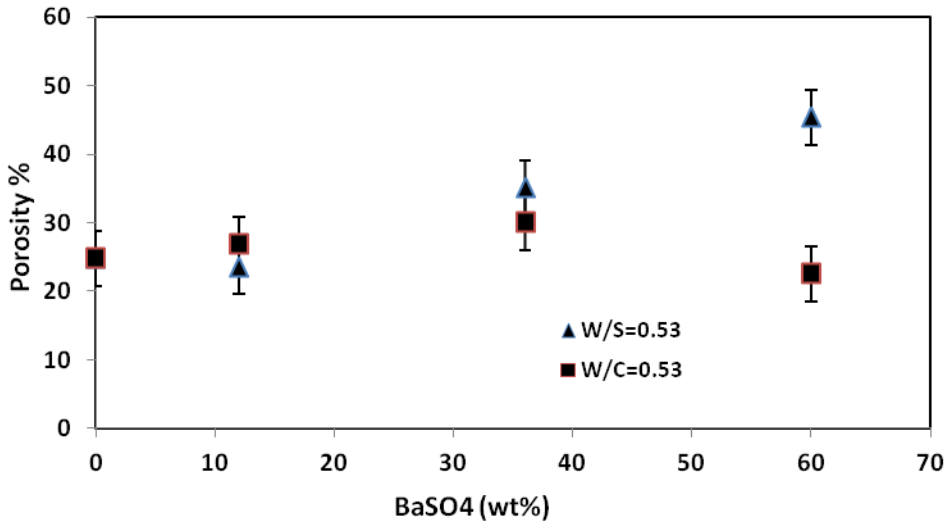


Figure 4.22: Total porosity of cement samples with different amount of $BaSO_4$ loading for PC-$BaSO_4$ granules systems cured at 40 $^oC$ for 28 days.

### 4.3.3 Compressive strength of PC-$BaSO_4$ systems

#### 4.3.3.1 Effect of $BaSO_4$ powder

Figure 4.23 show the compressive strength data obtained for PC-$BaSO_4$ powder system. All formulation except $BaSO_4$ 60 wt% sample of w/s=0.53 series satisfied the minimum compressive strength of 7 MPa required for the radioactive wasteform [20, 21], which is indicated as a dotted line in Figure 4.23. The general decrease in strength can be observed in both series with the increase in $BaSO_4$ loading due to the decrease in the binding PC matrix.

In the w/c=0.53 series, the compressive strength of the samples slightly increased at 12 wt% of $BaSO_4$ loading and gradually decreased at higher $BaSO_4$ loading. The strength of hardened cement is generally described based on the effect of porosity, the amount (volume) of hydrated cement[22, 23]. In the case of w/c=0.53 series, because the porosity of the products showed no significant change with $BaSO_4$ loading, the physical filling effect of pore by the

fine $BaSO_4$ powders is expected to be minimal.. Cyr et al. [23] explained, for the similar increase in strength of cement systems caused by the addition of inert powder, it was mainly because of the enhanced hydration of the system owing to the larger surface area available for nucleation. These aspects can be examined using the average values of the weight loss associated with different phases observed in the TG data (examples shown in Figures 4.6 and 4.7) presented in Figure 4.24 (a1), (b1) and (c1). These weight losses are due to dehydration of C-S-H, dehydroxylation of $Ca(OH)_2$ and decarbonation of $CaCO_3$, respectively, and thus directly related to the amount of the corresponding phases; the more weight loss is observed, the more the phase exists. It should be noted that the weight losses at lower temperature region associated with C-S-H also contains that with monosulphate (and possibly ettringite and monocarbonate) due to the difficulty in separation of peaks in the data, which may be due to the heating rate of 10 $^{o}$C/min used for the TGA in the present study. As expected, the amount of hydration products, C-S-H and $Ca(OH)_2$ decreased with the replacement of PC with $BaSO_4$ powder. On the other hand, the amount of $CaCO_3$ in the w/c=0.53 series increased when $BaSO_4$ was introduced, with the maximum $CaCO_3$ formed at 12 wt% $BaSO_4$. These results suggest that the solid products in the system, including calcite formed in the system contributed to the compressive strength of the products and that the calcite formation was a likely reason for the increase in compressive strength of the product at 12 wt% $BaSO_4$ loading. The weight loss shown Figure 4.24 (a1), (b1) and (c1) were normalised by the amount of the PC (divided by the wt% of PC) in the system and shown in Figure 4.24 (a2), (b2) and (c2) to estimate amount of hydration products per unit PC. Although the

increase in $CaCO_3$ is evident, no significant change was observed for the C-S-H and $Ca(OH)_2$.

In the w/s=0.53 series, although the compressive strength of the products generally decreased with the amount $BaSO_4$ powder in the system, the effect was more significant compared with the w/c=0.53 series. This corresponds to the more porous microstructures in w/s=0.53 series due to the increased w/c ratio in this series as discussed in former section. It is also clear based on the data shown in Figure 4.24 (a1), (b1) and (c1) that the amount of solid products including calcite is contributing to the strength of the products also in the w/s=0.53 series.

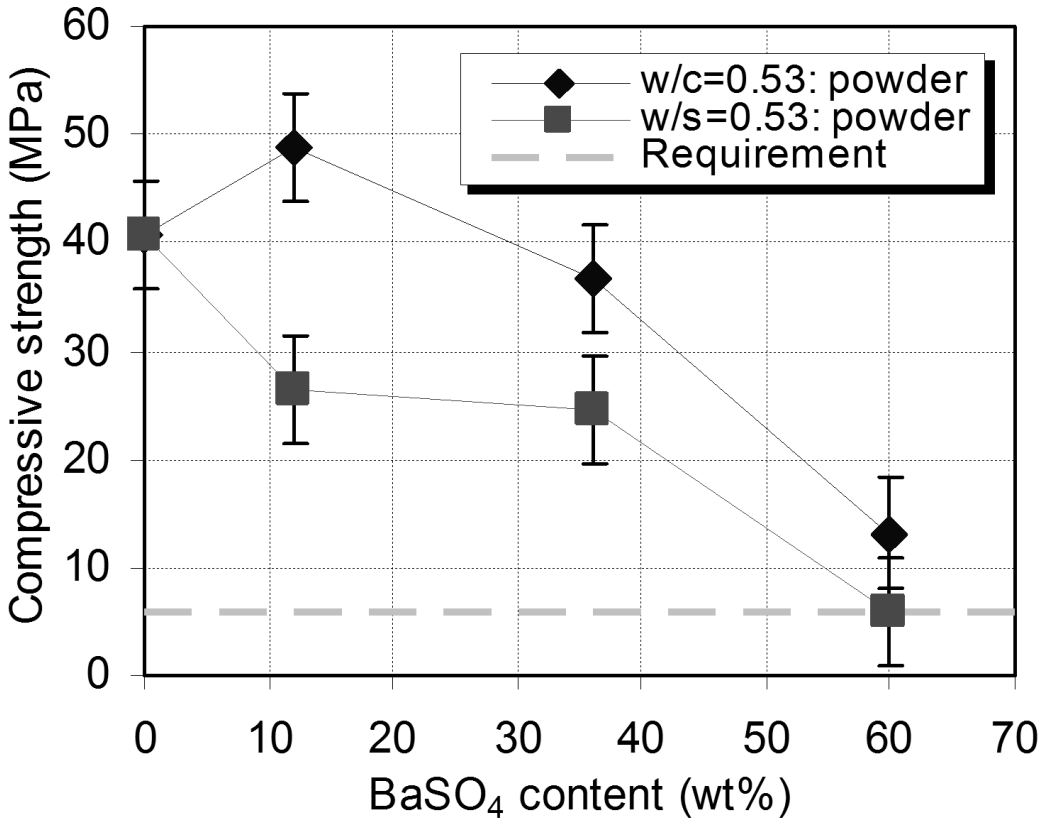


Figure 4.23: Compressive strength of cement samples with different amount of $BaSO_4$ loading for PC-$BaSO_4$ powder systems cured at 40 $^oC$ for 28 days.

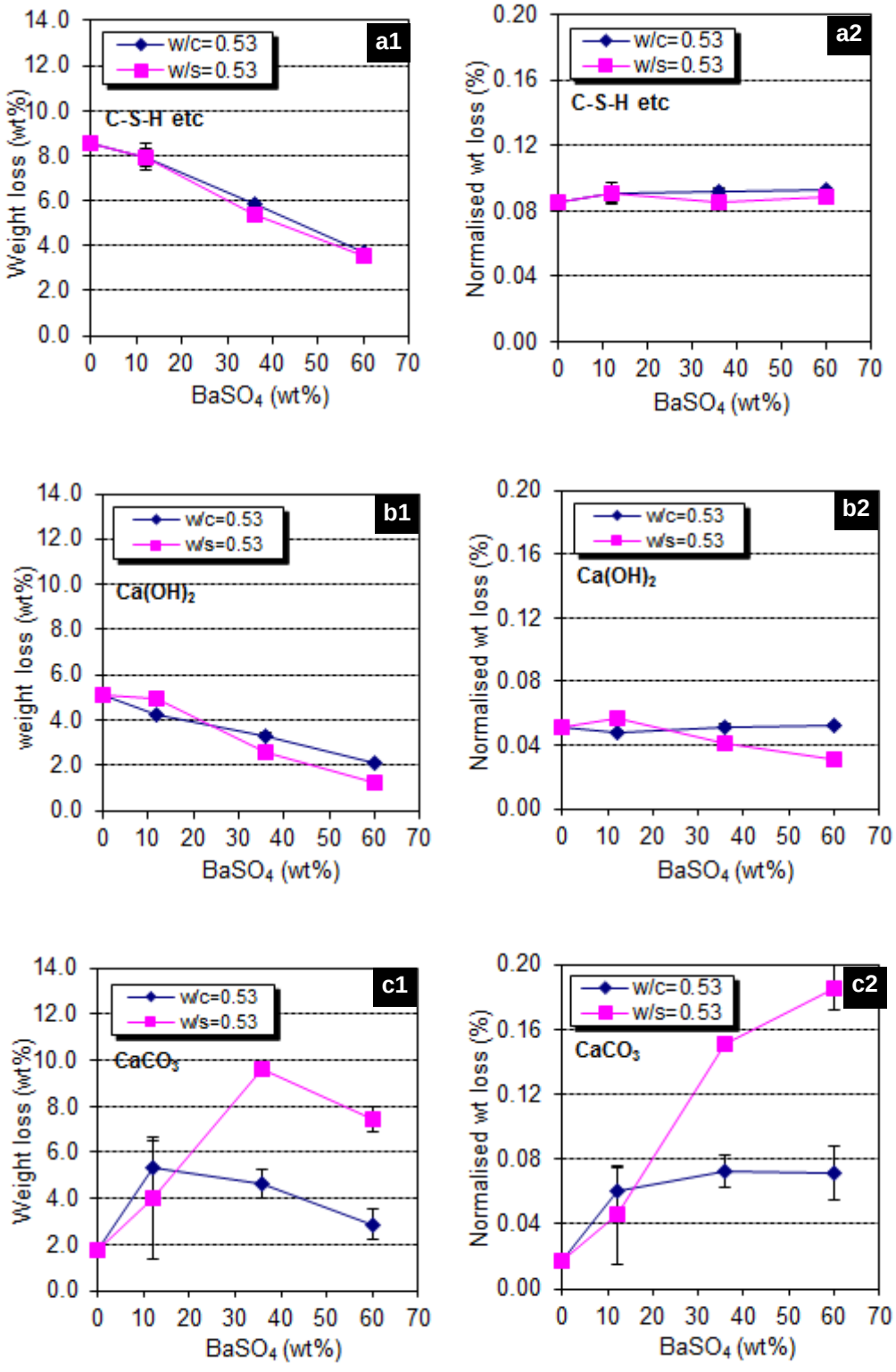


Figure 4.24: PC-$BaSO_4$ powder systems: (a1) C-S-H and other phases, (b1) $Ca(OH)_2$, (c1) $CaCO_3$. The (a2), (b2) and (c2) show the corresponding values normalised by the amount of the PC (wt% of PC) in the system.

4.3.3.2 Effect of $BaSO_4$ granules

Figure 4.25 shows the compressive strength data obtained for PC-$BaSO_4$ granule systems. Although these systems also showed a general decrease in strength in both series with the increase in $BaSO_4$ loading due to the decrease in the binding PC matrix, the trends are different from those for PC-$BaSO_4$ powder systems shown in Figure 4.23. When $BaSO_4$ was added in the form of granules to PC, the compressive strength decreased to approximately 20 MPa for w/c=0.53 series, and approximately 14 MPa for w/s=0.53 series, and did not change significantly with increase in the replacement level of $BaSO_4$.

The results for the w/c=0.53 series can be analysed based on the amount of solid phases in the products, as the porosity of this system showed no significant change with $BaSO_4$ loading similar to the PC-$BaSO_4$ powder systems as already discussed (Figure 4.24). Figure 4.26 show the average values of the weight loss associated with different phases observed in the TG data (examples shown in Figures 4.9 and 4.10) for PC-$BaSO_4$ granule systems and their normalised values by the amount of the PC in the system. These data show significantly large deviations compared with those for the PC-$BaSO_4$ powder system due to the general inhomogeneity of the samples associated with the large $BaSO_4$ particle size. It is difficult to draw a clear conclusion for the weight loss at the lower temperature associated with C-S-H (and other phase) because of the large deviation, but the weight losses associated with $Ca(OH)_2$ show a general decrease resembling the decrease in the compressible strength. It is also noticeable that $CaCO_3$ did not form in this system to the extent of the PC-$BaSO_4$ powder system.

The results for the w/s=0.53 series indicated the similar trend. More hydration product appeared to be present, which seems to be the main effect of increased water in the w/s=0.53 series. Similar to the PC-$BaSO_4$ powder system, the PC-$BaSO_4$ granule system indicated less compressive strength in the w/s=0.53 series compared with w/c=0.53 series due to the higher porosity originated from the increased w/c ratio in this series.

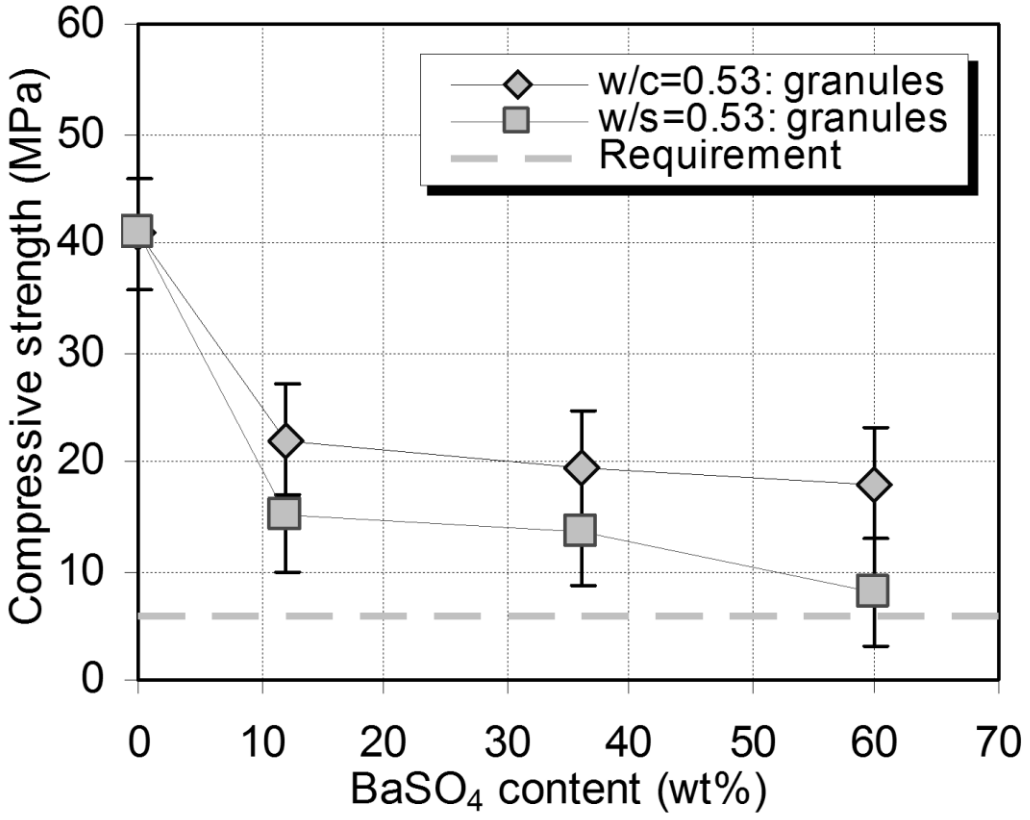


Figure 4.25 Compressive strength of cement samples with different amount of $BaSO_4$ loading for PC-$BaSO_4$ granule systems cured at 40 $^{o}$C for 28 days

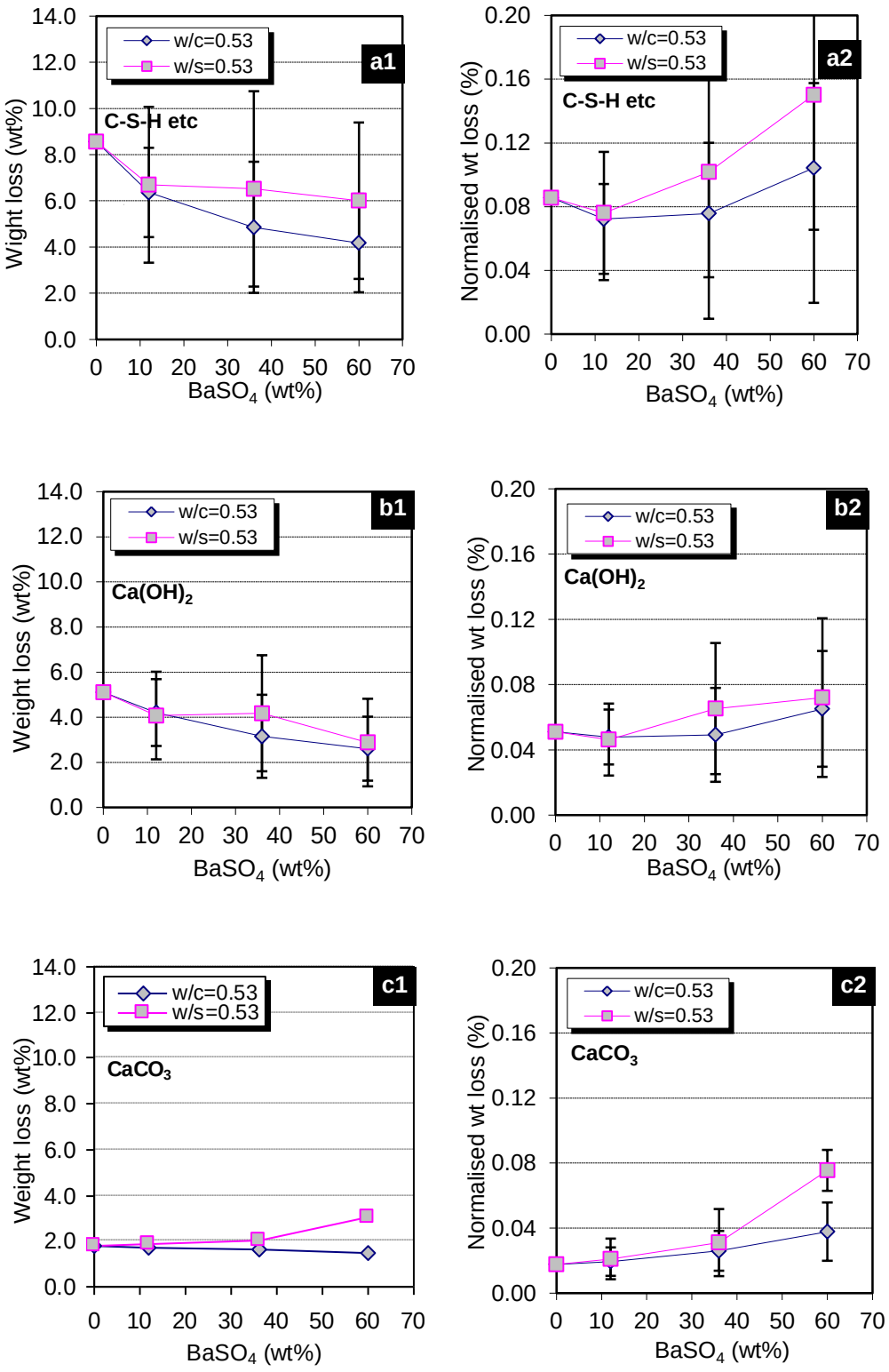


Figure 4.26 Weight loss associated with different phases observed in the TG data for PC-$BaSO_4$ granule systems: (a1) C-S-H and other phases, (b1) $Ca(OH)_2$, (c1) $CaCO_3$. The (a2), (b2) and (c2) show the corresponding values normalised by the amount of the PC (wt% of PC) in the system.

### 4.3.4 Effect of $BaSO_4$ powder and water on $CaCO_3$ formation

Increased carbonation was observed in the PC-$BaSO_4$ powder system. Carbonation of cement samples can occur either as an intrinsic reaction during the hydration and curing process or as an extrinsic reaction during the sample preparation for different testing. Because such an increase in carbonation was not observed in the PC-$BaSO_4$ granule samples, despite the fact that they were handled in the same manner as the PC-$BaSO_4$ powder samples for the preparation of samples for testing, the increased carbonation in the PC-$BaSO_4$ powder systems is considered to be intrinsic.

The significant increase in $CaCO_3$ formation caused by the introduction of fine $BaSO_4$ powder, as shown in Figure 4.24 (c1), was most likely by increasing the surface area for nucleation site and growth. The surface area available for nucleation is one of the key factors influencing the precipitation kinetics of $CaCO_3$ in high pH solution [11, 24]. The effect of the increased surface area can be confirmed by the weight loss associated with $CaCO_3$ normalised by amount of $CaCO_3$-PC (divided by the wt% of PC) represented in Figure 4.24 (c2). The Figure also shows that in the PC-$BaSO_4$ powder system, the amount of water available is another important for $CaCO_3$ formation. The formation of $CaCO_3$ per unit PC increases with replacement level of $BaSO_4$ in the w/s=0.53 series whereas it remains at a constant level in the w/c=0.53 series. As shown in Figure 4.27, the amount of water in the system available for PC (w/c ratio) increases with replacement level of $BaSO_4$ in the w/s=0.53 series whereas it is constantly 0.53 in the w/c=0.53 series. It appears that a minimum amount of water is required for the increased surface area to work as nucleation site for the enhanced $CaCO_3$ formation. The water in the system could also influence

carbonation either directly increasing the amount of $Ca^{2+}$ and $CO_3^{2-}$ ions in the system for $CaCO_3$ formation through the reaction with $CO_2$ in the atmosphere or increasing porosity of the hardened products allowing easier ingress of $CO_2$. The alkalinity of the system would decrease due to the increase in the w/c ratio with replacement level of $BaSO_4$, which may decrease the formation of $CaCO_3$. The obtained results suggest that the influence of surface area, water and porosity was greater than that of the decreased alkalinity in the condition in the present work.

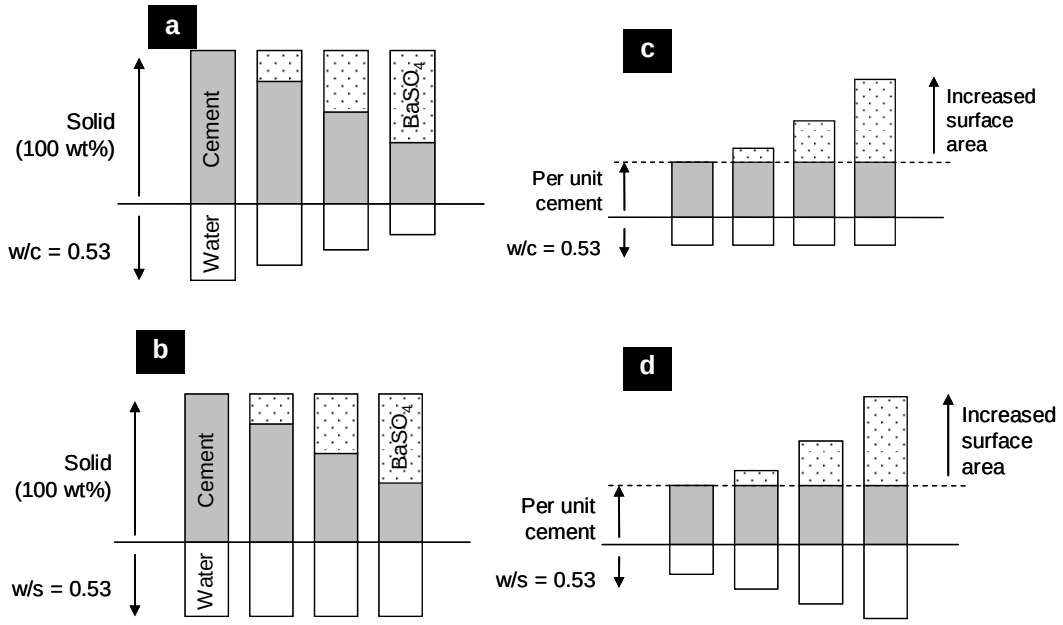


Figure 4.27 Schematic diagrams of formulations: (a) w/c=0.53 series, (b) w/s=0.53 series, (c) w/c=0.53 series per unit cement, (b) w/s=0.53 series per unit cement. The amount of $BaSO_4$ corresponds to the increase in surface area, which is significant in PC- $BaSO_4$ powder system.

## 4.5 Summary

Both in PC–$BaSO_4$ powder and PC–$BaSO_4$ granule systems, it was possible to produce solid products with high $BaSO_4$ loading which satisfies the minimum compressive strength of 7 MPa required for the radioactive wasteforms. Introduction of fine $BaSO_4$ powder resulted in an increased formation of $CaCO_3$, which appeared to contribute to the compressive strength of the products. Although the strength decreased with the introduction of $BaSO_4$ granules, it was maintained at approximately 20 MPa for w/c=0.53 series and around 10 MPa for w/s=0.53 series, and did not change significantly with an increase in the replacement level of $BaSO_4$. Increase in water in the system resulted in the increase in porosity of products, which was more significant in the PC–$BaSO_4$ powder system than in the PC–$BaSO_4$ granule system. There was no significant difference in porosity between $BaSO_4$ powder and $BaSO_4$ granule systems when w/c was 0.53. Maintaining the w/c ratio at this level would be beneficial to maintain a low porosity of the products. Based on the obtained results, it is concluded that it is possible to achieve high $BaSO_4$ loadings whilst retaining the initial integrity of the wasteform products. It would be beneficial to incorporate small amount of fine $BaSO_4$ powder of about 12 wt% to maximise the strength of the product if the formation of $CaCO_3$ in the product is not an issue. $BaSO_4$ may be further incorporated, in the form of coarse granules to give a total of 60 wt% without reducing the strength of the product below 7 MPa. It is important to maintain w/c ratio at around 0.53 to keep the level of porosity in the final waste product around 25 % similar to the reference PC system.

## 4.6 References


1. B. Lothenbach, F. Winnefeld, C. Alder, E. Wieland, and P. Lunk, *Effect of temperature on the pore solution, microstructure and hydration products of Portland cement pastes.* Cement and Concrete Research, 2007. **37**: p. 483-491.
2. M. F. Rojas and J. Cabrera, *Pore size distribution and degree of hydration of metakaolin-cement pastes.* Cement and Concrete Research, 2000. **30** p. 561-569.
3. H. Taylor, *Chapter 7: Hydration of Portland cement* in *Cement Chemistry*. 1990, Thomas Telford London. p. 187-226.
4. I. Odler, *Hydration, Setting and Hardening of Portland Cement*, in *Lea's Chemistry of Cement and Concrete*, P.C. Hewlett, Editor. 2001, Butterworth-Heinemann: Oxford. p. 241-298.
5. L. Alarcon-Ruíz, G. Platret, E. Massieu, and A. Ehrlacher, *The use of thermal analysis in assessing the effect of temperature on a cement paste. .* Cement and Concrete Research, 2005. **35**(3): p. 609-613.
6. C. Hall, P. Barnes, A. D. Billimore, A. C. Jupe, and X. Turrillas, *Thermal decomposition of ettringite $Ca_6[Al(OH)_6]_2(SO_4)_3.26H_2O$.* Journal of the Chemical Society, Faraday Transactions, 1996. **92**(12): p. 2125-2129.
7. K. L. Scrivener, *Backscattered electron imaging of cement microstructures: understanding and quantification.* cement and Concrete Research, 2004. **26**(8): p. 935-945.
8. C. Famy, K. L. Scrivener, and A. K. Crumbie, *What causes differences of C-S-H gel grey levels in backscattered electron images?* Cement and Concrete Research, 2002. **32**(9): p. 1465-1471.
9. J. Aguilar-Santillan, *Wetting of Al2O3 by Molten Aluminum: The Influence of BaSO4 Additions.* Journal of Nanomaterials, 2008.
10. B. V. L'vov and V. L. Ugolkov, *Kinetics of free-surface decomposition of magnesium and barium sulfates analyzed thermogravimetrically by the third-law method.* Thermochimica Acta, 2004. **411**: p. 73–79.
11. I. Lebron and D. L. Suarez, *Calcite nucleation and precipitation kinetics as affected by dissolved organic matter at 25°C and pH > 7.5.* Geochimica et Cosmochimica Acta, 1996. **60**(15): p. 2765-2776.
12. T. Matschei, B. Lothenbach, and F. P. Glasser, *The role of calcium carbonate in cement hydration.* Cement and Concrete Research, 2007. **37**: p. 551-558.
13. B. Lothenbach, G. L. Saout, E. Gallucci, and K. Scrivener, *Influence of limestone on the hydration of Portland cements.* Cement and Concrete Research, 2008. **38**( ): p. 848–860.
14. S. Garrault-Gauffinet and A. Nonat, *Experimental investigation of calcium silicate hydrate (C-S-H) nucleation.* Journal of Crystal Growth, 1999. **200**: p. 565-574.
15. S. Diamond, *Mercury porosimetry -An inappropriate method for the measurement of pore size distributions in cement-based materials.* Cement and Concrete Research 2000. **30**: p. 1517-1525.
16. P. Lawrence, M. Cyr, and E. Ringot, *Mineral admixtures in mortars – Effect of inert materials on short-term hydration.* Cement and Concrete Research, 2003. **33**: p. 1939-1947.
17. M. Cyr, P. Lawrence, and E. Ringot, *Efficiency of mineral admixtures in mortars: Quantification of the physical and chemical effects of fine admixtures in relation with compressive strength.* Cement and Concrete Research 2006. **36** p. 264 - 277.

18. J. P. Ollivier, J. C. Maso, and B. Bourdette, *Interfacial transition zone in concrete.* Advanced Cement Based Materials, 1995. **2**(1): p. 30-38.
19. K. L. Scrivener, A. K. Crumbie, and P. Laugesen, *The interfacial transition zone (ITZ) between cement paste and aggregate in concrete.* Interface science, 2004. **12**: p. 411 - 421.
20. N. B. Milestone, T. Sugama, L. E. Kukacka, and N. Carclello, *Carbonation of geothermal grouts-part 2: CO2 attack at 250°C.* Cement and Concrete Research, 1987. **17**: p. 37-46.
21. M. I. Ojovan and W. E. Lee, *An introduction to nuclear waste immobilisation*. 2005, London: Elsevier Ltd.
22. J. J. Beaudoin, R. F. Feldman, and P. J. Tumidajski, *Pore structure of hardened Portland cement pastes and its influence on Properties.* Advn. Cem. Bas. Mat, 1994. **1**: p. 224-236.
23. M. Cyr, P. Lawrence, and E. Ringot, *Mineral admixtures in mortars - Quantification of the physical effects of inert materials on short-term hydration.* Cement and Concrete Research, 2005. **35**: p. 719-730.
24. W. P. Inskeep and P. R. Bloom, *An evaluation of rate equations for calcite precipitation kinetics at p CO2 less than 0.01 atm and pH greater than 8.* Geochimica et Cosmochimica Acta, 1985. **49**: p. 2165-2180.

# Chapter 5: Development of cement formulation for $BaSO_4$ NORM scale encapsulation

## 5.1 Introduction

The previous chapter provided a few important information associated with the size of $BaSO_4$ particles. Fine powders were effective to maintain the homogenous microstructure and sufficient strength of the product, but appeared to enhance the carbonation under tested curing condition. Coarse granules were able to suppress the carbonation of the product, but caused the formation of highly porous interfacial transition zone, resulting in the significant reduction in the strength.

Another issue noted during the preparation of PC-$BaSO_4$ granule systems was the sedimentation of coarse $BaSO_4$ granule occurred before the initial setting of the cement paste. The $BaSO_4$ particles are much denser (4.48 g/cm$^3$) [1] than the cement slurry (1.8 g/cm$^3$), and the coarse particles can separate out or settle down from the rest of the cement matrix. The specific surface of these particles is much lower than the cement particles, and consequently the surface forces between particles are of very much less significance than those of the cement particles.

In this chapter, wasteform formulations were developed to encapsulate coarse $BaSO_4$ granules. The sedimentation of $BaSO_4$ particle and the rheological behaviour of cement pastes were investigated with or without incorporation of $BaSO_4$ powder or mineral admixtures such as quartz or metakaolin. The chemical and physical effects of these mineral admixtures in the developed wasteform formulations were also studied through the microstructure development, mechanical strength, and chemical durability. The labelling used for XRD and TGA graphs in the following chapter is outlined in Table 5.1.

Table 5.1 Key to XRD and TGA labelling

| Labelling | Chemical name | Cement nomenclature | Chemical formula | JCPDS card |
|---|---|---|---|---|
| A | Alite (tricalcium silicate) | $C_3S$ | $3CaO.SiO_2$ | 49-442 |
| B | Belite (dicalcium silicate) | $\beta$-$C_2S$ | $2CaO.SiO_2$ | 33-0302 |
| af | Tetracalcium aluminoferrite | $C_4AF$ | $4CaO.Al_2O_3.Fe_2O_3$ | 30-0226 |
| C | Calcite | $C\bar{C}$ | $CaCO_3$ | 05-0586 |
| P | Portlandite | CH | $Ca(OH)_2$ | 44-1481 |
| E | Ettringite (AFt) | $C_6A\bar{S}_3H_{32}$ | $Ca_6Al_2(OH)_{12}(SO4)_3.26H_2O$ | 41-1451 |
| MS | Monosulphate (AFm) | $C_4A\bar{S}_3H_{12}$ | $Ca_4Al_2(OH)_{12}(SO_4).6H_2O$ | 45-0158 |
| BS | Barium sulphate | $BaSO_4$ | $BaSO_4$ | 72-1390 |
| St | Stratlingite | $C_2ASH_8$ | $Ca_2Al_2SiO_7.8H_2O$ | 29-0285 |
| Hg | Hydrogarnet | $C_3AH_6$ | $Ca_3Al_2(OH)_{12}$ | 38-0368 |
| CSH | calcium silicate hydrate | C-S-H | - | Taylor [2] |
| Q | Quartz | | $SiO_2$ | 46-1045 |

## 5.2 Sedimentation of $BaSO_4$ particles

### 5.2.1 Static curing

A clear sedimentation of $BaSO_4$ particles within the products was observed in the PC-$BaSO_4$ granule systems when they were cured directly after the manual mixing. The sedimentation is thought to occur when the mixtures are placed in the environmental chamber statically before the cement develops a sufficient viscosity. Figure 5.1 shows the cross section of PC+36 wt% $BaSO_4$ granule sample. The upper part of the sample is mainly cement matrix with little amount of $BaSO_4$ whereas the lower part contains most of the $BaSO_4$ granules. This visual observation was confirmed by XRD results shown in Figure 5.2. The XRD pattern of the lower part showed predominantly the reflection peaks for $BaSO_4$ whereas that of the upper part indicated the peaks for $BaSO_4$ in much lower

intensity. The clear peaks of $Ca(OH)_2$, as well as small peaks attributed to monosulphate, alite, belite and calcite suggest that the upper part is composed of mainly hydrated cement.

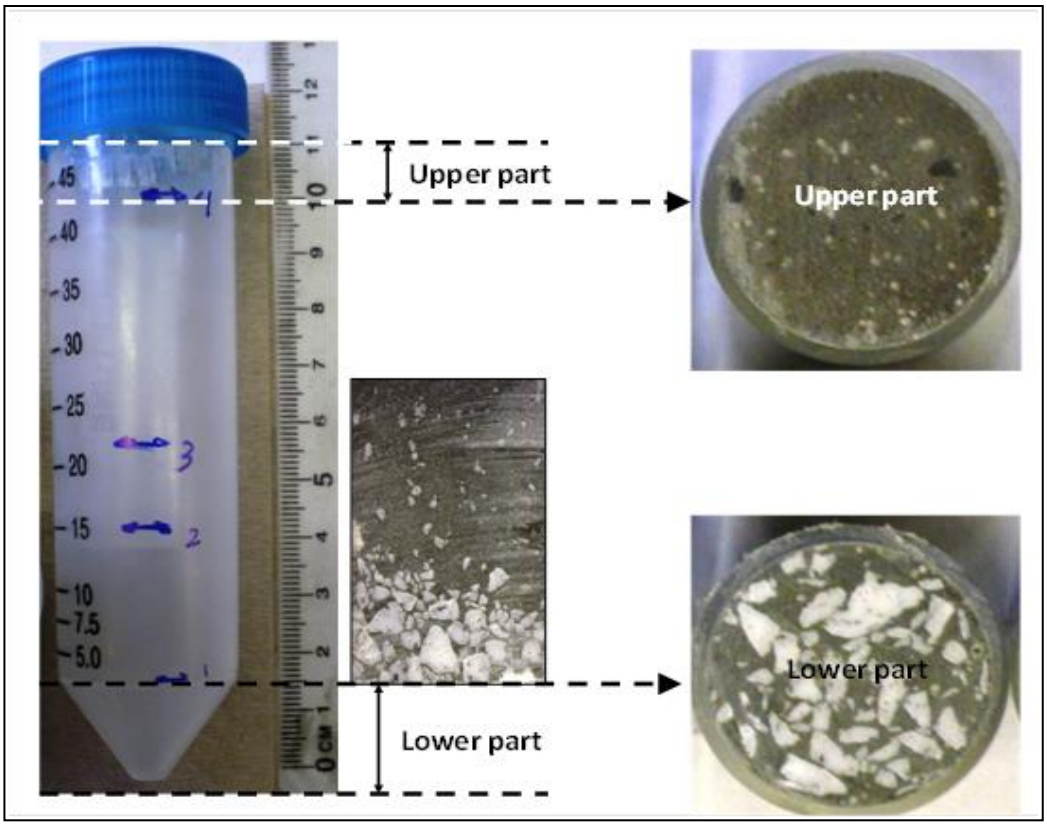


Figure 5.1 PC+36 wt%$BaSO_4$ granules, w/c=0.53

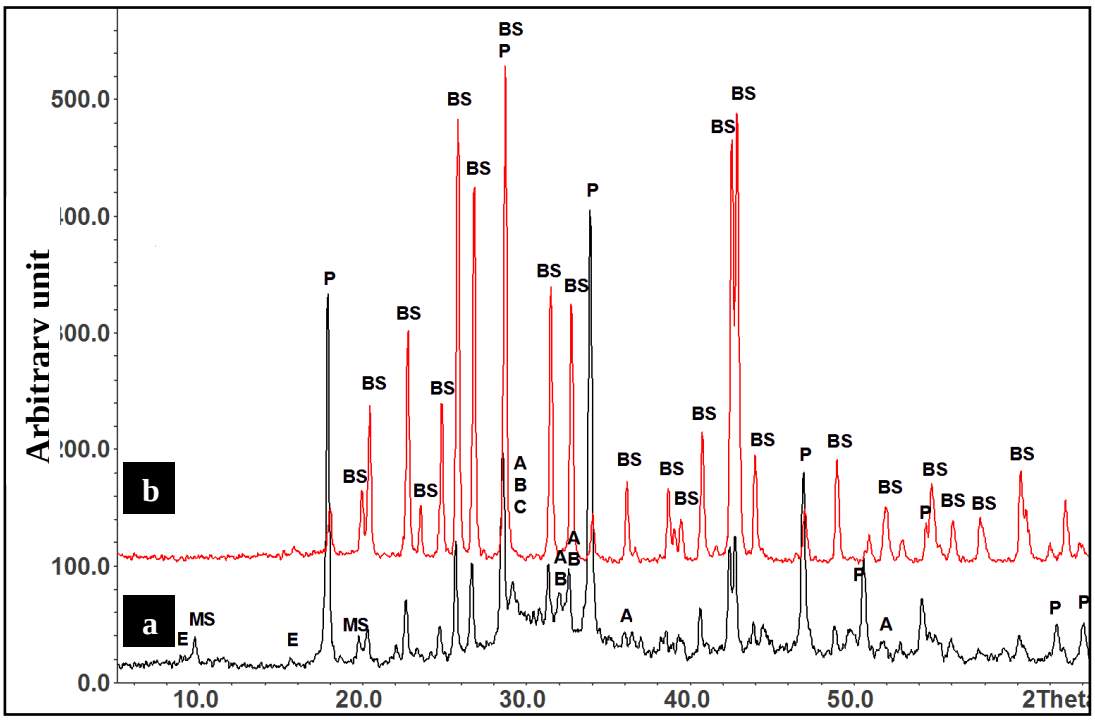


Figure 5.2 XRD traces for the PC+36 wt% $BaSO_4$ granule sample, w/c=0.53 statically cured for 28 days: (a) upper part, (b) lower part statically cured for 28 days

In contrast, the visual observations of PC-$BaSO_4$ powder systems, suggested a homogenous dispersion of $BaSO_4$ powder, showing no apparent sign of sedimentation. The XRD results for PC+36 wt% $BaSO_4$ powder sample also support these observations by showing no obvious difference between upper and lower parts of samples (Figure 5.3), confirming that the sedimentation of $BaSO_4$ did not occur in the PC-$BaSO_4$ powder samples.

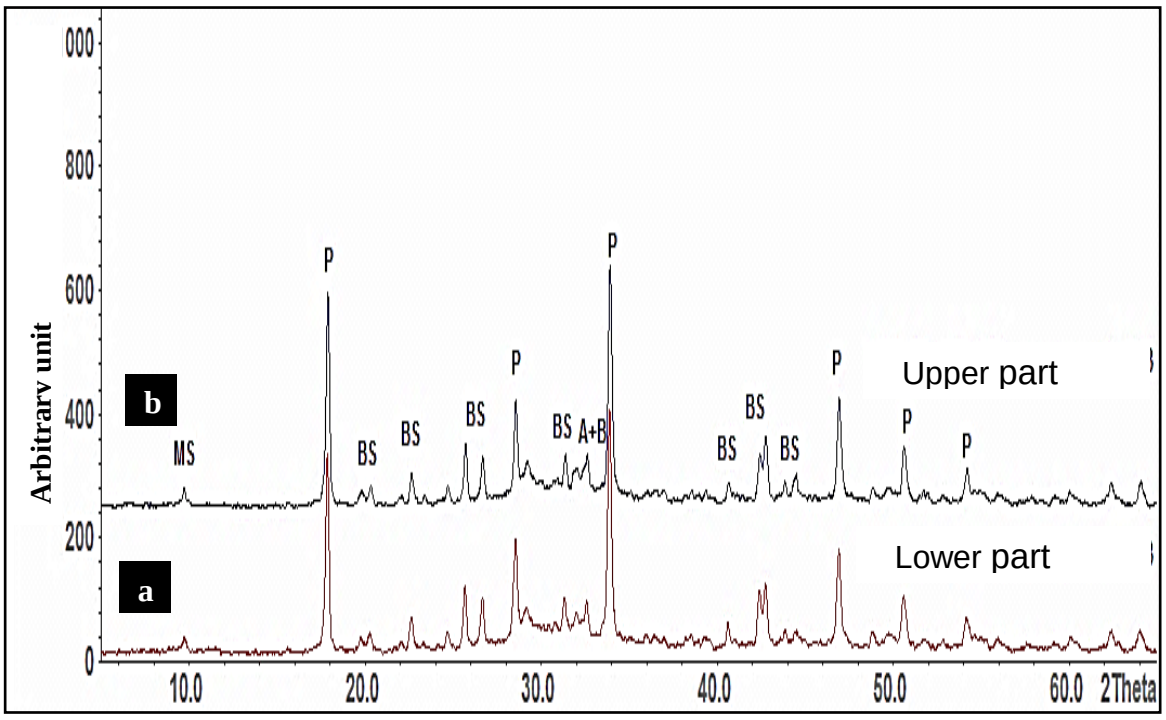


Figure 5.3 XRD traces for the PC+36 wt% $BaSO_4$ powder samples, w/c=0.53: (a) lower part, (b) upper part

5.2.2 Rolling mix curing

In order to avoid the sedimentation of $BaSO_4$ granule an additional mixing procedure for all PC-$BaSO_4$ granule samples were tested by rotating the pastes continuously for up to 20 hours using a rolling mixer. The visual observations of PC+36 wt% $BaSO_4$ granule sample rolled for 20 hours did not show any sign of sedimentation as shown in Figure 5.4, suggesting that the rolling procedure up to 20 hours was a good method to avoid the sedimentation of $BaSO_4$ granule. However, for industrial application, this procedure may be not best option to avoid the sedimentation as rolling a large amount of cement slurry for a long time requires a significant amount of energy input.

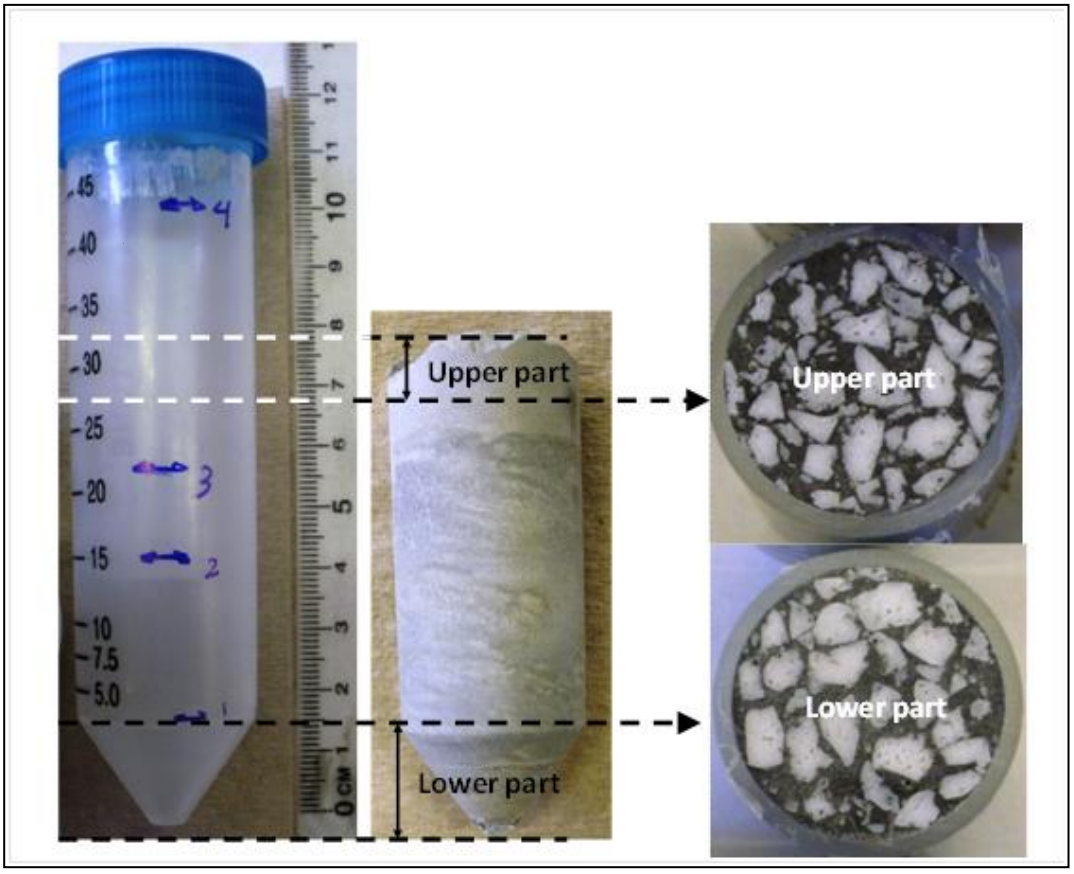


Figure 5.4 PC+36 wt% $BaSO_4$ granule, w/c=0.53, rolled 20 hours

## 5.3 Setting property

5.3.1 Effect of water

The initial and final setting time of neat PC pastes at different w/c ratios are shown in Figure 5.5. Both the initial and final setting times of Portland cement generally increased when the w/c ratio increased: from 3 to 7.5 hours for the initial set and from 8 to 15 hours for the final set. Similar results have been obtained by Stefanou et al. [3]. Detailed reviews and discussion on setting time have been previously published in the literature [2, 4-6]. Bogue [6] outlined the hydration and crystallisation of the calcium aluminate $C_3A$ and or $C_3S$ phases which are the main phases responsible for the initial set. At a lower w/c,

because of the higher possibility of the cement particles contacting each other, the hydration products bind the particles more efficiently. A fully connected solid frame and solid phase might be higher in this case. Consequently, the system with lower w/c needs a smaller volume of hydration products to form a stress-resisting network. On the other hand, the solid to solid space in the higher w/c ratio samples is greater than that in the lower w/c ratio samples. Therefore, more hydration product is needed to form a stress-resisting network.

More recently, Barnes et al. [7] pointed out that setting time is not always well defined and depends on w/c ratio. They described that the setting time increases with increasing amount of water in the system due to the reduction in the density of the cement hydrates and the delayed consolidation stage of the system. For general applications, according to the British Standard (BS12), the initial setting time should not be less than 45 min, and the final setting time not greater than 10 hours [2, 7]. The tested w/c ratio satisfied the initial setting requirement, but the final setting time for w/c=0.53 and 0.6 exceeds the maximum of the required final set.

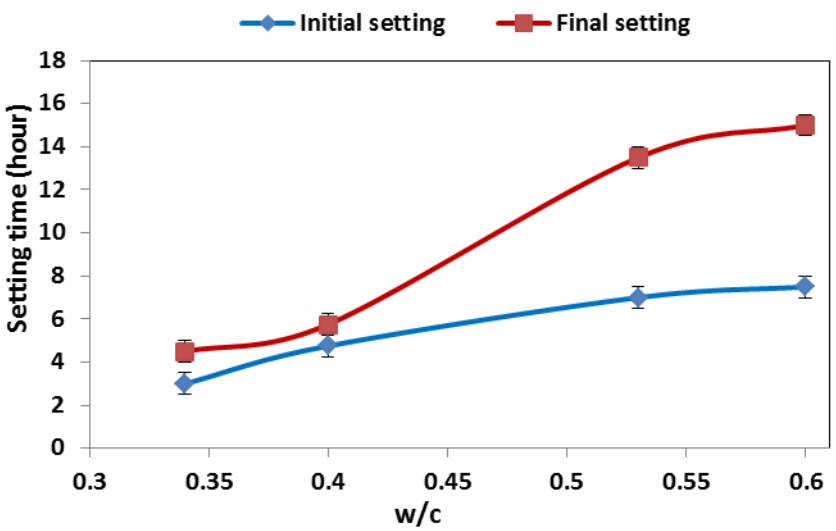


Figure 5.5 Setting times of neat PC cement pastes

### 5.3.2 Effect of $BaSO_4$

Figure 5.6 shows the initial and final setting time of PC-Barite system with different barite loading (10, 20, 30, 40, 60 wt%) for w/c=0.53. The Figure also shows the setting times for the chemical grade $BaSO_4$ powder and granule samples for comparison. Barite used in this test contains impurity which is no more than 5% whereas the chemical grade was 98% purity. The result shows that the introduction of barite generally reduced both the initial and final setting times. The initial setting time did not very differ from the typical values found in Portland cements at low barite loading, and gradually decreased with at higher barite loading. The final setting time also tended to decrease as the barite loading increased. The reduction of the initial and final setting times suggests that the barite may increase the initial rate of hardening. Since $BaSO_4$ is chemically inert, this must be a physical effect caused by the introduction of barite/ $BaSO_4$. Hewlett [8] pointed out that the surface area and the particle size distribution of inert additives have a major effect on setting behaviour and in

particular on water demand in the cement paste. Small amounts of silica (5 %) have been reported to increase the reactivity of the $C_3A$, leading to a faster setting [8]. Our results confirms the effect of surface area and the particle size as the fine $BaSO_4$ powder (<1µm) reduced the setting time more significantly than larger barite (<2µm) or the coarse granule (3-5mm).

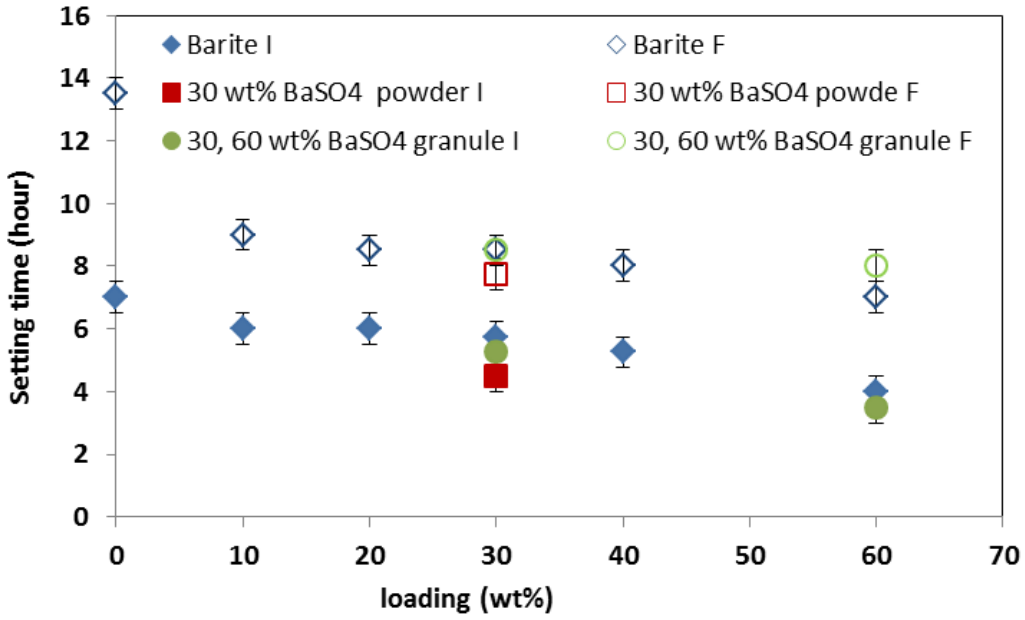


Figure 5.6 Initial setting and final setting times of PC-Barite and PC-$BaSO_4$ pastes. I- Initial, F- Final

### 5.3.3 Effect of metakaolin

The test results for initial and final setting times of PC-MK cement pastes at 10 and 20 wt% MK loading are shown in Figure 5.7. The results reveal that the metakaolin reduces the initial and final setting times of cement paste with increasing replacement level of PC by MK slightly more than barite. A similar trend has been reported with the PC replaced by up to 30% of MK [9]**.** Zhang and Malhotra reported that a 10% MK concrete showed a final setting time of

4.24 hours, compared with 5.12 hours for the control concrete with the water/binder ratio of 0.40 [10]. The effect of MK can be explained by the pozzolanic reactivity in addition to the increase in the surface area explained for the inert additives. MK as pozzolanic materials reacts with cement hydration product calcium hydroxide to form C-S-H gel. Metakaolin has a higher water demand compared to barite. Therefore it was difficult to prepare a sample with 30 wt% MK using the same w/c=0.53 ratio due to the higher water demand and flash set.

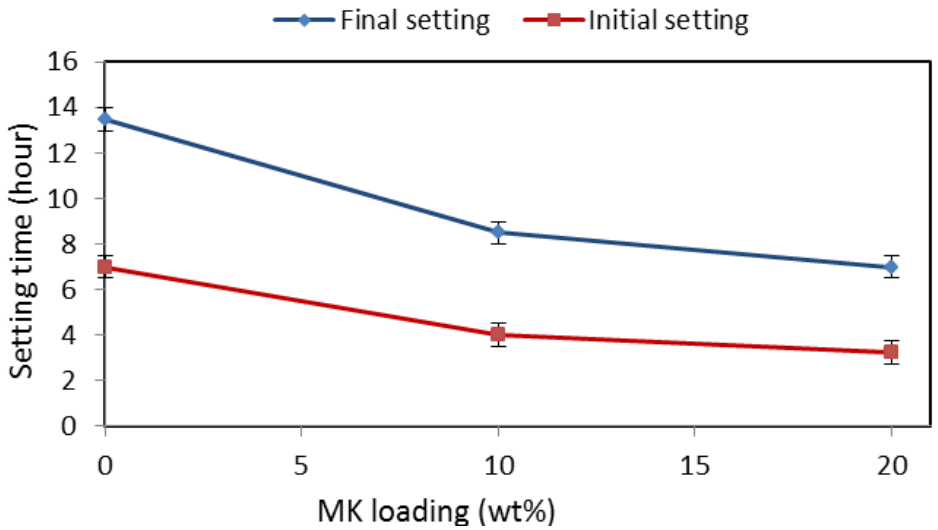


Figure 5.7 Setting times of PC-MK pastes

## 5.4 Rheological characteristics

### 5.4.1 Introduction

The rheological characteristics are one of the most important factors in workability of the cement slurry [11]. This is practically important for PC-$BaSO_4$ system because the sedimentation of the coarse $BaSO_4$ granules can occur due to its higher density compared with the cement slurry as mentioned before.

Development of cement formulation for $BaSO_4$ NORM scale encapsulation

Establishing knowledge in the rheological characteristics of cement slurry would help to understand the behaviour of cementing systems containing coarse $BaSO_4$ granules and avoid their sedimentation, maintaining a homogenous suspension.

Five cement slurries, candidate cementing matrices for the coarse $BaSO_4$ granules, were examined in comparison with neat PC system to establish their ability to sustain the coarse $BaSO_4$ granules in the suspension without their sedimentation. Mineral admixtures are introduced to enhance the viscosity of the slurry, and their rheological characteristics were studied in terms of viscosity and yield stress. Table 5.2 shows the formulation of cement samples used. The best formulation was identified in chapter 4; the incorporation of 12 wt% $BaSO_4$ powder maximises the compressive strength, and the use of w/c ratio of 0.53 maintains the porosity of PC- $BaSO_4$ cement system minimum. Based on this best formulation, a slight increase in $BaSO_4$ loading to 20 wt% and slight reduction of water to w/c=0.43 were tested. The effects of mineral admixtures were also studied at the same loading level of 12 wt%. The w/c ratio for the MK containing system was determined through try-and-error to workable consistency. The w/c ration of this level has been used to study PC-MK system [12].

Table 5.2 Formulation of the cement samples

| Formulation | w/c | Notation |
|---|---|---|
| PC | 0.53 | PC |
| PC+20wt% $BaSO_4$ (powder) | 0.43 | 20P 0.43 |
| PC+20wt% $BaSO_4$ (powder) | 0.53 | 20P 0.53 |
| PC+12 wt% $BaSO_4$ (powder) | 0.53 | 12P 0.53 |
| PC+12 wt% MK | 0.87 | 12MK 0.87 |
| PC+12 wt% quartz | 0.53 | 12Q 0.53 |

5.4.2 Bingham plastic behaviour of slurries

Figure 5.8 shows the correlation between shear stress $(\tau)$ and shear rate$(\gamma^{\cdot})$ for Newtonian fluid and that for non-Newtonian fluid expressed by Bingham plastic model. The simplest liquid behaviour is that of the Newtonian fluid whose shear stress linearly increases with shear rate as expressed by Equation 5.1 and pass through the origin as shown in Figure 5.8. The ratio of shear stress to shear rate is the viscosity$(\eta)$.

$$\tau = \eta\gamma \qquad (5.1)$$

The behaviour of cement slurry is more complex. Cement paste usually does not flow until the shear stress reaches a certain minimum value [13] called yield stress ( $\tau_0$ ). The yield stress must be applied to a fluid in order to change its behaviour from that of a solid to a liquid [14]. This behaviour of cement slurry is described by the Bingham plastic model given in equation 5.2 and shown in the Figure 5.8 [15, 16].

$$\tau = \tau_0 + \eta\gamma \qquad (5.2)$$

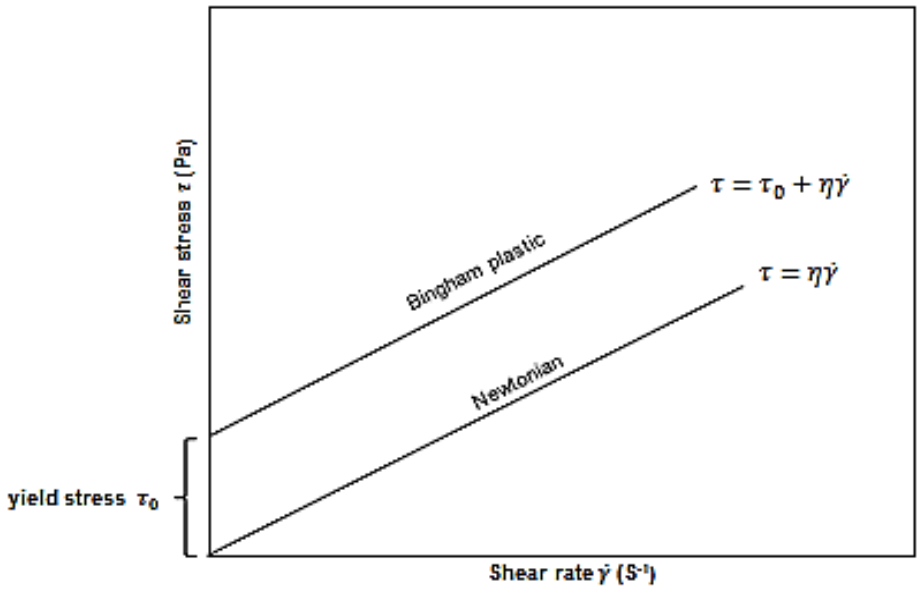


Figure 5.8 Bingham plastic model of non-Newtonian fluids

Figure 5.9 shows the shear rate - shear stress curves for the tested cement slurry. The Figure also shows the linear fitting for each data set based on Bingham plastic model. Because of the differences in their compositions, cement slurries incorporating fine powder of $BaSO_4$, quartz, and MK exhibited different rheological behaviour compared to the neat PC.

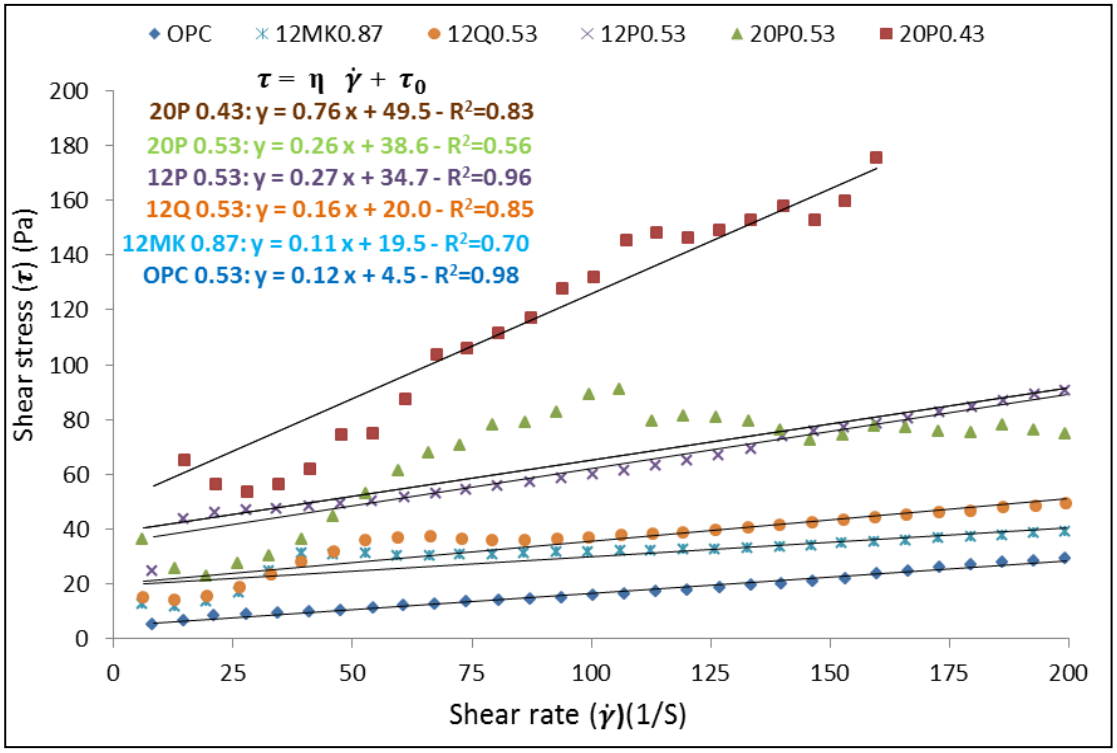


Figure 5.9 cement slurry shear rate - shear stress curves for different formulation based on Bingham model

The neat PC tested in the present study showed a linear correlation between shear stress and shear rate, indicating an ideal Bingham plastic behaviour. When fine $BaSO_4$ powder of 12 wt% was introduced, the yield stress appears to have increased. Overall, the slurry shows Bingham plastic behaviour. As the amount of $BaSO_4$ powder increased to 20 wt%, the deviation from the ideal Bingham plastic model became larger. But the average behaviour of this slurry appears to be similar to that of 12 wt% $BaSO_4$ system. When the amount of water in the system is reduced (20 wt% $BaSO_4$, w/c=0.43), the behaviour of the slurry was significantly different, indicating a strong influence of water content on the slurry. The introduction of quartz and metakaolin both resulted in a

similar result, indicating a small deviation from the ideal Bingham plastic model, with the average behaviour between the neat PC and the 12 wt% $BaSO_4$ (or 20 wt% $BaSO_4$, w/c=0.53). The average particle size of quartz is 44 µm which is less than the cement particle and greater than the $BaSO_4$ powder. The particle size of metakaolin was similar to that of the $BaSO_4$ powder, but the effect of metakaolin was less significant compared to the $BaSO_4$ powder, this result shows the importance of water content in the PC-metakaolin system. This slurry had a much higher water content of 0.87.

### 5.4.3 Viscosity

The plastic viscosity obtained as the gradient of the linear fitting of the shear stress - shear rate curves in Figure 5.9 for each slurry are shown in Figure 5.10. The viscosity of the cement slurry increased from 0.12 Pa.s to 0.27 and 0.26 Pa.s when fine $BaSO_4$ powder were introduced at 12 and 20 wt%, respectively.

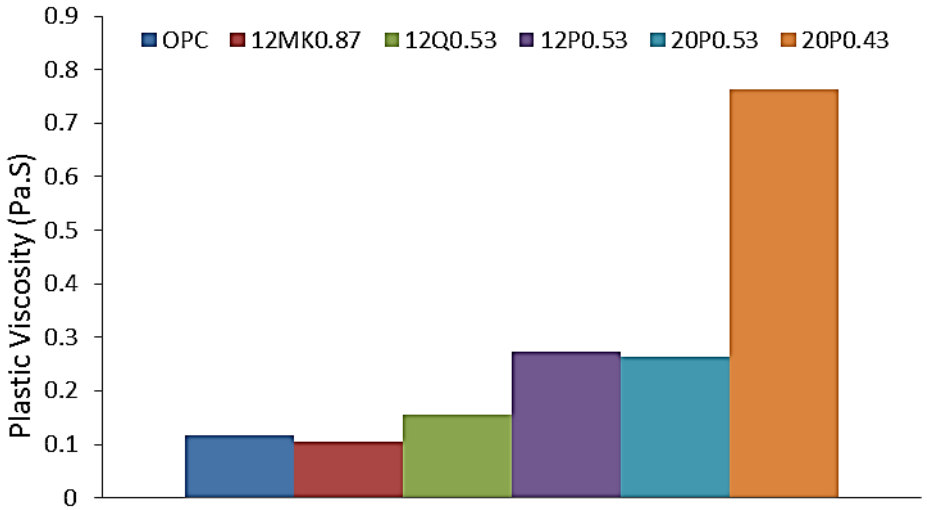


Figure 5.10 the plastic viscosity obtained from shear stress-shear rate curves for each formulation

The important factors for the rheological behaviour of the cement slurry include the specific surface area and chemical composition of cement, alkalis content, presence of additives, and w/c of the mixture [17]. Shaughnessy et al. reported that the hydration time, mixing procedures and curing temperature can also affect the rheological properties of fresh cement pastes [18]. Because $BaSO_4$ powder is considered to be chemically inert, these results suggest a physical effect of $BaSO_4$ powder on the viscosity of the slurry, most likely the large surface area. However, the difference between 12 wt% and 20 wt% was not significant in terms of the viscosity. On the other hand, when w/c ratio was decreased to 0.43, the viscosity of the 20 wt% $BaSO_4$ slurry increased from 0.26 to 0.76 Pa.s. Hence the effect of water content is significant. A higher value of viscosity may be advantage to avoid the sedimentation of larger $BaSO_4$ particles, but it may have a negative impact on the workability of the cement slurry. It is important to maintain the viscosity low enough for the industrial application such as 1.005 Pa.s for oilwell cement slurry [19]. The slurries containing quartz and metakaolin both indicated a similar level of viscosity to the neat PC system. Because of the relatively short duration of the measurement, the effect of these admixtures must be also the physical effect neither than the chemical effect associated with the pozzolanic reaction. Metakaolin requires large amount of water to maintain a similar level of viscosity as PC slurry to assure a sufficient workability.

### 5.4.4 Yield stress

Figure 5.11 shows the yield stress obtained as the intercept of the linear fitting of the shear stress - shear rate curves (Figure 5.9) for each slurry. The increase

of the yield stress induced by the incorporation of additives agrees with published studies which suggest that fine powder increases the yield stress and viscosity of cement slurry [20, 21]. The general trend of the yield stress is similar to that of the viscosity; the higher the viscosity, the higher the yield stress. The higher yield stress value of the slurry prepared with fine $BaSO_4$ powder may be due to the following reasons [15]:

- Physical effects: increased the thickening of cement slurry by occupying a significant volume in the liquid phase due to the Blaine fineness (large specific surface) of $BaSO_4$ powder.
- Physico-chemical effects: a higher percentage of smaller particles, making the interaction forces between them stronger (modification of interparticle forces)

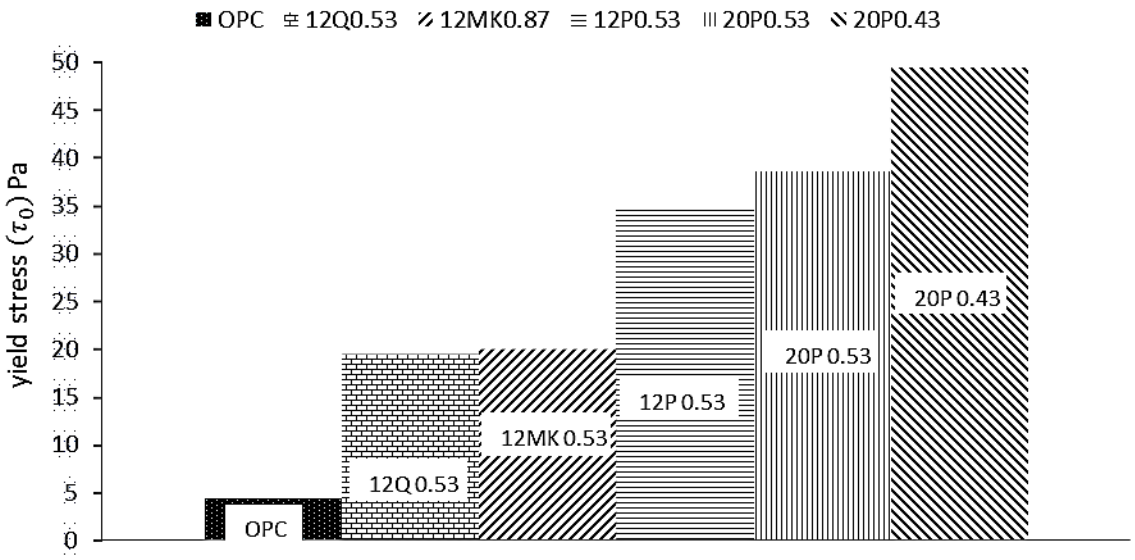


Figure 5.11 the yield stress obtained from shear stress-shear rate curves for each formulation

These values were used to estimate the maximum particle size of $BaSO_4$ which can be sustained in each slurry without sedimentation. $BaSO_4$ particles in cement slurry would receive the forces due to the gravity (Fg) and yield stress ($F_y$) as shown in Figure 5.12

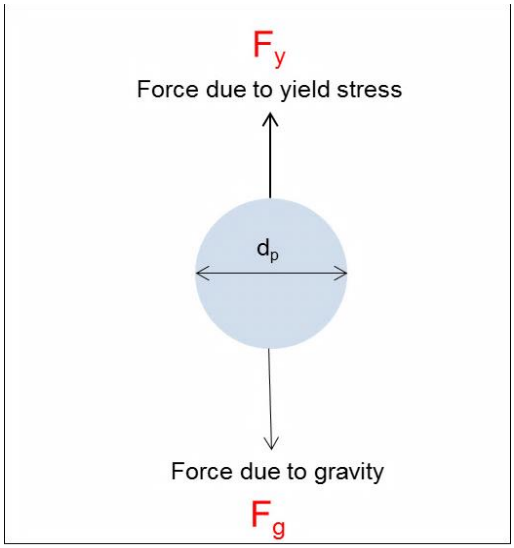


Figure 5.12 forces acting on $BaSO_4$ particles in cement slurry

Dimensionless factor *Y*, proportional to the ratio of these two forces, is often used to discuss the sedimentation of particles [22]. By supposing a spherical particle, they are expressed as Eqs. 5.3- 5.5.

$$Y \propto \frac{F_y}{F_g} \tag{5.3}$$

$$F_y = \tau_0 \pi \left(\frac{d_p}{2}\right)^2 \tag{5.4}$$

$$F_g = \frac{g\left(\rho_p - \rho_s\right)4}{3} \pi \left(\frac{d_p}{2}\right)^3 \tag{5.5}$$

where $g$ is gravity constant (9.8 m/s$^2$), $\rho_p$ and $\rho_s$ are the densities of $BaSO_4$ granule and cement slurry respectively. Therefore, the simplest definition of Y is:

$$Y = \frac{3}{2}\frac{\tau_0}{g d_p(\rho_p - \rho_s)} \qquad (5.6)$$

It has been suggested, by Chhabra and Richardson that the value of Y between 0.048-0.088 can be used to calculate the minimum diameter of spherical particles which can suspend in the cement slurry [22]. A more conservative value of Y =0.212 has also been mentioned [22]. When Y is larger than these values, $BaSO_4$ particles will stay in suspension, but if Y is smaller than these values, $BaSO_4$ particles will sediment.

Table 5.3 summarises the maximum $BaSO_4$ particle diameter which will be sustained in each cement slurry without sedimentation, obtained from Eq. 5.6 using three different values of Y. The result shows that the PC cement slurry with w/c=0.53 is capable of suspending $BaSO_4$ particle with diameter no more than 1.6 mm when Y=0.212. Because, the diameter of the $BaSO_4$ granules used in this project is 0.6-5 mm, and thus sedimentation of the coarse $BaSO_4$ granules can occur. On the other hand, diameter of $BaSO_4$ powder is less than 1μm, and the sedimentation does not occur in this system.

When fine $BaSO_4$ powder is introduced to the slurry at 12 wt%, the slurry will be able to sustain the coarse $BaSO_4$ particles of 13.9 mm in diameter. Introduction of the fine $BaSO_4$ powder is a good way to reduce the possible sedimentation of the coarse $BaSO_4$ particles. The increase in fine $BaSO_4$ powder up to 20 wt%

can further increase the yield stress, and the slurry is able to suspend up to 15.4 mm of $BaSO_4$ particles. The reduction of water showed a similar result, an increase in yield stress and the increase in the maximum diameter of the particle which can be suspended in the slurry.

The slurries containing quartz and metakaolin showed a milder increase in the yield stress and are estimated to be able to suspend the $BaSO_4$ particles up to 8.0 and 7.4 mm in diameter, respectively. The effect of quartz was less than that of $BaSO_4$ powder because of the less specific surface area. The mild effect of metakaolin must be attributed to the increased amount of water in the system.

Table 5.3 the $BaSO_4$ particle diameter

| | *$\rho_p$ ($kg/m^3$) | **$\rho_s$ ($kg/m^3$) | $\tau_0$ (Pa) | $d_p$ (mm) | | |
|---|---|---|---|---|---|---|
| | | | | Y=0.048 | Y=0.088 | Y=0.212 |
| PC | 3800 | 1800 | 4.53 | 7.2 | 3.9 | 1.6 |
| 12P 0.53 | | 2000 | 34.68 | 61.3 | 33.4 | 13.9 |
| 20P 0.53 | | 2000 | 38.60 | 68.4 | 37.3 | 15.4 |
| 20P 0.43 | | 2000 | 49.48 | 87.6 | 47.8 | 19.8 |
| 12Q 0.53 | | 2000 | 20.01 | 35.4 | 19.3 | 8.0 |
| 12MK 0.87 | | 1900 | 19.52 | 34.5 | 17.8 | 7.4 |

*$\tilde{n}_{p=}$ 3800 $kg/m^3$

**The density of slurry, ($\rho_s$) for each mixes determined from the weight and volume measurements after mixing for 10 minutes at ambient condition.

## 5.5 Development of wasteform formulation

### 5.5.1 Introduction

The results of setting time and the rheological performance of $BaSO_4$-including mineral admixtures pointed out that the sedimentation problems can be

overcome by including a moderate content of powdered $BaSO_4$ into the system or, incorporation of mineral admixtures such as quartz and metakaolin, without impacting the workability of the cement pastes. Based on these results, potential wasteform formulations were further investigated. The structural changes induced by the inclusion of mineral admixtures such as fine $BaSO_4$ powder, metakaolin and quartz in the $BaSO_4$-containing cement system were investigated through XRD, DTG analysis and SEM. A series of leaching test was also conducted.

### 5.5.2 Phase analysis

The formulations used in the rheological study (Table 5.2 except 20P0.43) were applied to encapsulate coarse $BaSO_4$ granules. Figure 5.13 shows XRD patterns for the cement samples cured for 28 days. The major crystalline phases identified in sample containing 20 wt% $BaSO_4$ powder (Figure 5.13 b) were CH and AFm. The initially-formed AFt transforms to AFm as a consequence of the decrease in the $SO_4^{2-}$:$Al^{3+}$ ratio with the progressive hydration reaction of the $C_3A$ during the first few weeks of curing [2, 23]. Calcium carbonate in its calcite form was also detected. Sharp reflection peaks for $BaSO_4$ were detected, suggesting that this material did not reacting to a major extent with the cement paste. In samples containing 12 wt% $BaSO_4$ powder (Figure 5.13 c), similar reaction products to those observed in the specimen with 20 wt% $BaSO_4$ powder were identified, along with the formation of hydrogarnet ($C_3AH_6$). Also, a substantial increment in the intensity of the main peak assigned to AFm (9.89° 2θ) was identified. It should be noted that the peaks for CH were significantly reduced in this sample.

The replacement of the 12 wt% $BaSO_4$ powder by MK in the cement wasteform (Figure 5.13 d) led to a dramatic decrease in the intensity of the peaks assigned to CH, as a consequence of pozzolanic reaction taking place between MK and this phase. Amorphous silica produced from MK usually reacts with the CH generated by the cement hydration reaction, resulting in extra C-S-H phase [24, 25]. In this specimen hydrogarnet was not identified as a reaction product, instead stratlingite ($C_2ASH_8$) was formed. Figure 5.14 shows the lower angle region (5.6-17° 2θ) of these XRD traces. The formation of stratlingite might be related to the hydration of $C_3A$. The hydration of $C_3A$ can form metastable $C_2AH_8$ and $C_4AH_{13}$, which later transform into the thermodynamically stable hydrogarnet [8] as observed in the blended systems based on high-alumina cements [26] and in aged Portland cements [2]. In a silicate-rich environment (with the presence of MK), it is possible that a part of the metastable $C_2AH_8$ transforms to stratlingite [27, 28]. The reduced portlandite content in the sample with MK also favours stratlingite formation, as it has been reported that stratlingite is unstable in the presence of calcium hydroxide and usually converts into hydrogarnet [29]. The inclusion of MK (5.14 d) also leads to the reductions in the intensities of the peaks assigned to AFm compared with specimens including 12 wt% $BaSO_4$ powder. It has been reported [25] that in $Al_2O_3$-saturated systems, such as when MK is added as a supplementary Al source, the formation of ettringite can be hindered, and only monosulphate will be formed.

The substitution of 12 wt% $BaSO_4$ powder by quartz (Figure 5.13 e) did not seem to cause a significant interaction either with the granulated $BaSO_4$ or with the cement paste on the XRD result, as comparable phases to those identified

in the PC-$BaSO_4$ systems were observed. In this system, monosulphate and hydrogarnet were not identified as reaction products. Ettringite is identified as the sole sulphate-rich hydrate phase in this cement. High intensity peaks of quartz ($SiO_2$) were also identified due to the addition of this less reactive material, along with clear peaks of portlandite in the absence of a pozzolanic additive.

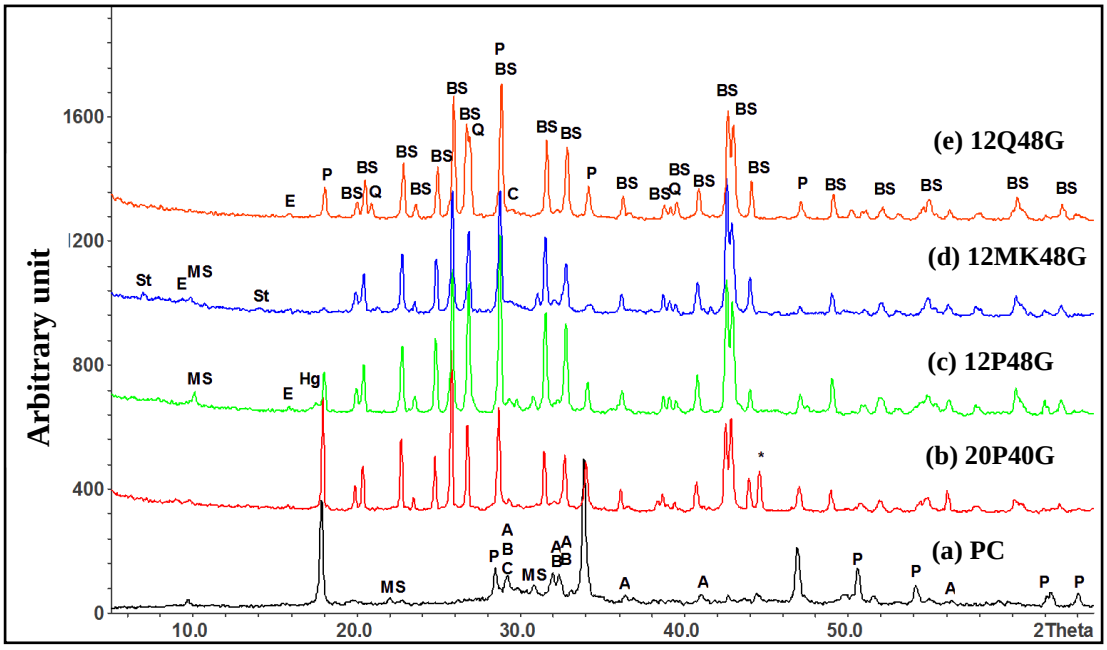


Figure 5.13 X-ray traces of wasteform formulation. Refer to Table 5.2 for notations. The peak marked with an asterisk is due to the Al sample holder used in XRD analysis.

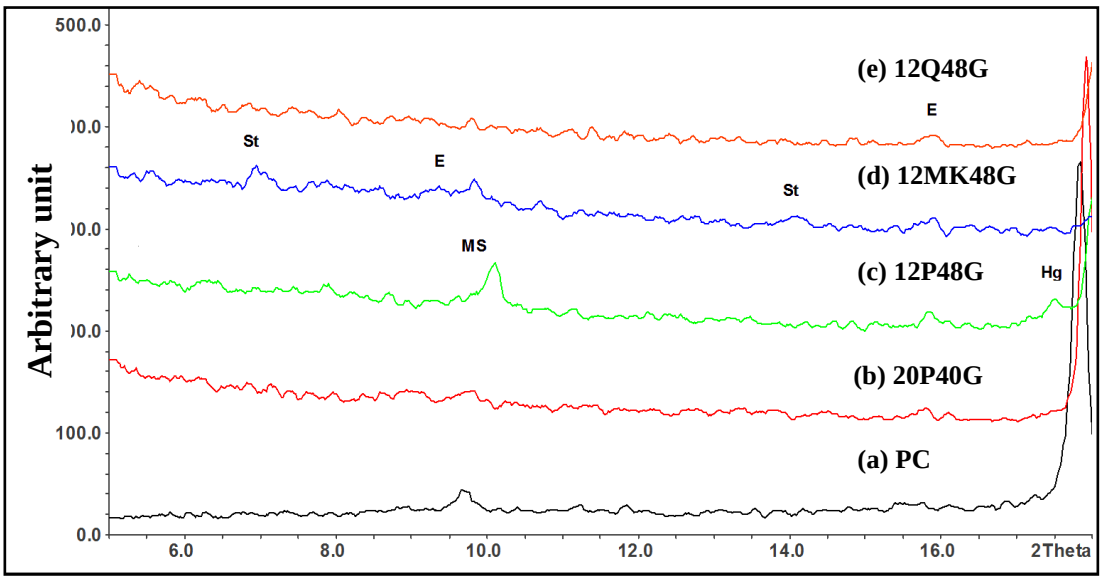


Figure 5.14 X-ray traces of wasteform formulation: the lower angle region (5.6-17° 2θ). Refer to Table 5.2 for notations.

The TG and DTG curves for the cements systems after 28 days are shown in Figure 5.15. The first mass loss identified at ~60°C (Figure 5.15) in all the samples is attributed to the elimination of evaporable water, along with the dehydration of the calcium silicate hydrate (C-S-H) gel around 100°C. In PC systems, evaporable water is removed below 120°C [30]. The mass losses between 100°C and 200°C are assigned to the decomposition of AFt (E) [31] and AFm (MS) [30] phases.

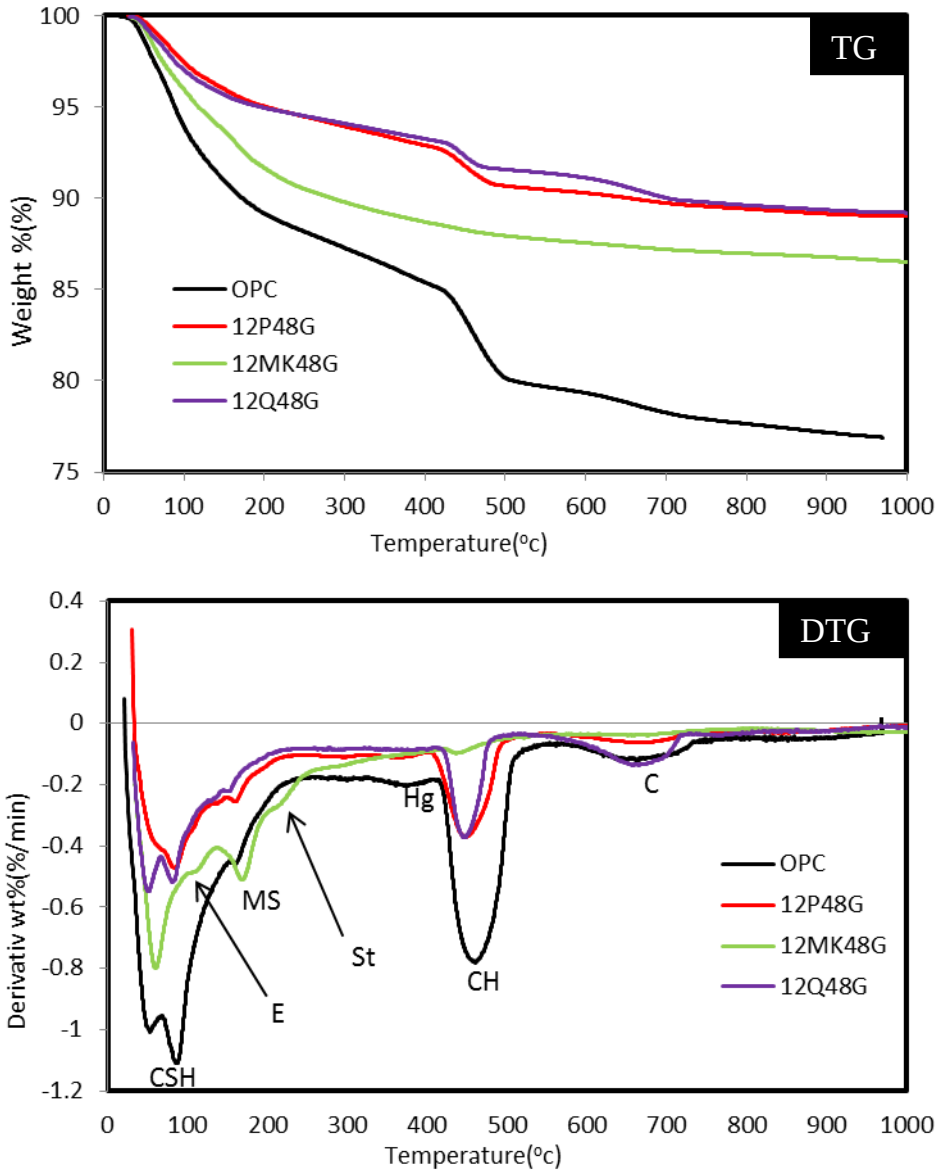


Figure 5.15 TG and DTG curves for cement systems

A peak at 250°C is attributed to the decomposition of stratlingite [32]. A significant mass loss is identified between 425°C and 550°C, especially in the neat PC, associated with the dehydroxylation and consequent decomposition of portlandite [30]. The peak for the decomposition of calcium carbonates between 600°C and 750°C is notably smaller compared in the PC-$BaSO_4$ powder system investigated in the former section.

In the paste with 20 wt% of powdered $BaSO_4$, it is possible to observe a low intensity peak assigned to the formation of AFm (MS), which was not identifiable through XRD probably due to the low concentration and/or crystallinity of this phase presented in the sample. A reduction of the content of powdered $BaSO_4$ to 12 wt% led to a similar result.

In the 12 wt% MK sample, the dehydration and decomposition of the C-S-H product was observed as a broad peak at temperatures up to 300°C, differing from PC-$BaSO_4$ system in which the dehydration of C-S-H was observed in a narrow temperature range. The C-S-H formed in MK-blended cement usually shows incorporation of aluminium into its structure [33], leading to the formation of a binding phase with a higher degree of crosslinking and therefore with water more tightly bonded. In this specimen, mass loss peaks attributed to the decomposition of ettringite, monosulphate and stratlingite are observed, consistent with the XRD results. A significant reduction in the peak intensity assigned to the dehydroxylation of portlandite is observed, as a consequence of the pozzolanic reaction as discussed above.

The DTG curve for the 12 wt% quartz sample shows the same features identified in the PC-$BaSO_4$ system. In this case, the peak assigned to the dehydroxylation of portlandite is sharper than that in the other samples, which could be attributed to the development of more crystalline portlandite [34].

### 5.5.3 Microstructural analysis

The BSE image of the 20 wt% powdered $BaSO_4$ (Figure 5.16) shows the bright colour (almost white) particles corresponding to the $BaSO_4$. These particles are brighter than Ca-containing compounds as Ba has a higher elemental number.

A highly dispersed powdered $BaSO_4$ is observed throughout the cement matrix. It is possible to identify the rims of inner C-S-H products forming around PC particles. The identification of other reaction products is quite difficult, as grey-scale differences within the matrix containing powdered $BaSO_4$ are not easily observable at this magnification.

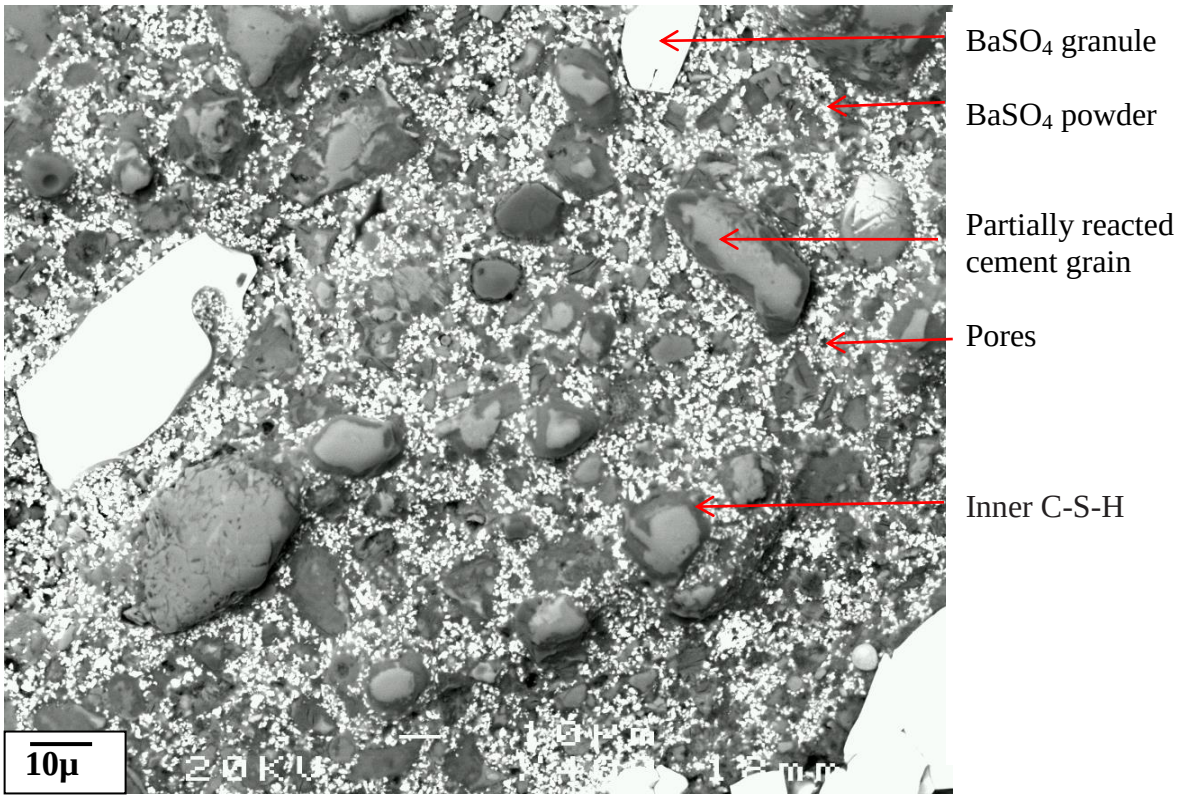


Figure 5.16 BSE image of 20wt% powder / 40wt% granulated $BaSO_4$ sample

In the specimens with a lower content of powdered $BaSO_4$ (12 wt%) (Figure 5.17), similar features are identified. Distinct particles of monosulphate are visible in this specimen, as observed in XRD. The important feature of these systems with $BaSO_4$ powders (both 12 and 20 wt%) is that the highly porous

interfacial zone previously observed in the PC-$BaSO_4$ granule system is less significant.

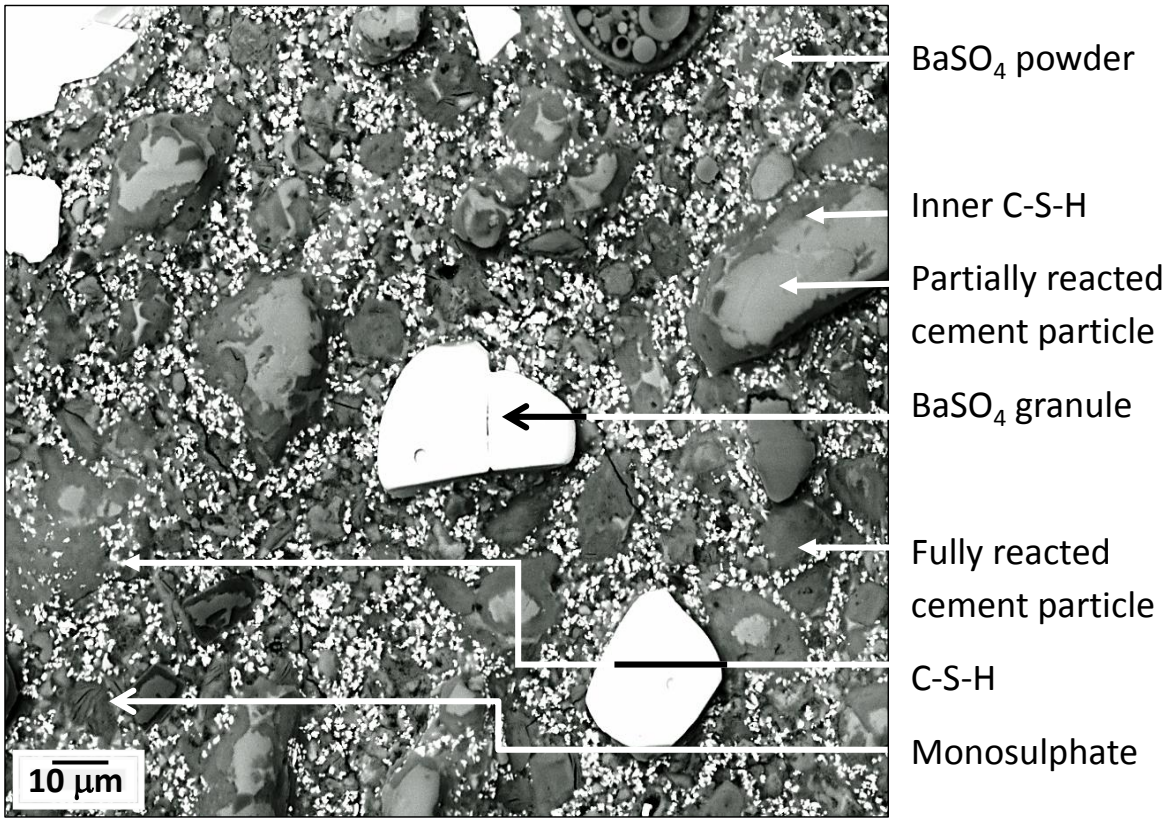


Figure 5.17 BSE image of 12 wt% powder / 48 wt% granulated $BaSO_4$ sample

A higher magnification of BSE image for this system (Figure 5.18) reveals that powdered $BaSO_4$ particles, filling the interfacial transition zone between the $BaSO_4$ granule and the cement matrix. As discussed in the former section, large $BaSO_4$ particles can disrupt the packing of the cement particles, leaving a more porous zone around aggregates [34, 35], and then with the progress of the hydration reaction, portlandite is deposited in the pores in this region together with the fine $BaSO_4$ particles.

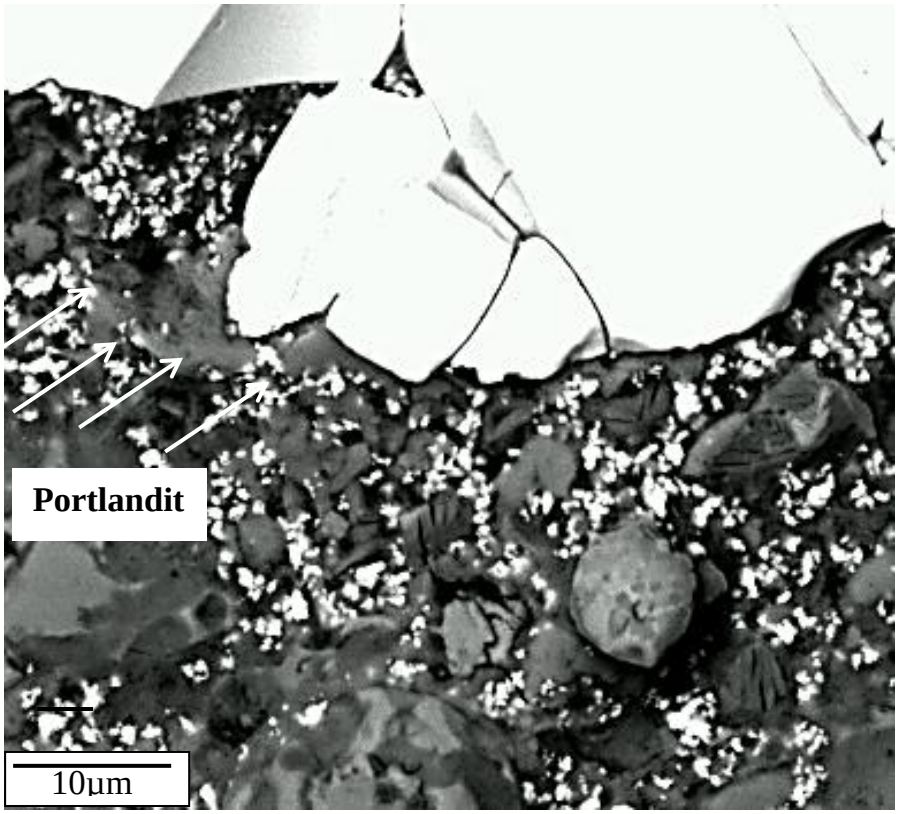


Figure 5.18 BSE image of 12 wt% powder / 48 wt% granulated $BaSO_4$ blended paste, showing the formation of portlandite around the $BaSO_4$ granule.

In the cement system including 12 wt% MK (Figure 5.19), the region around the $BaSO_4$ granule seems to be less porous compared with that further away from the $BaSO_4$ granules. It is likely that the pozzolanic reaction took place to a higher extent in that region, as a higher content of portlandite is expected to form in the areas close to $BaSO_4$ particles favouring the densification of the interfacial zone. In this system, formation of distinctive monosulphate morphology was again observed in a region (A) due to the increased concentrations of aluminium in the system as discussed in the former section. Additionally, formation of a needle-like phase (B) is observed in this specimen. As the content of aluminium is high as shown in EDS, it is likely that C-A-S-H

type gel and AFt type products are coexisting in this region, consistent with the presence of sulphates identified through EDS analysis.

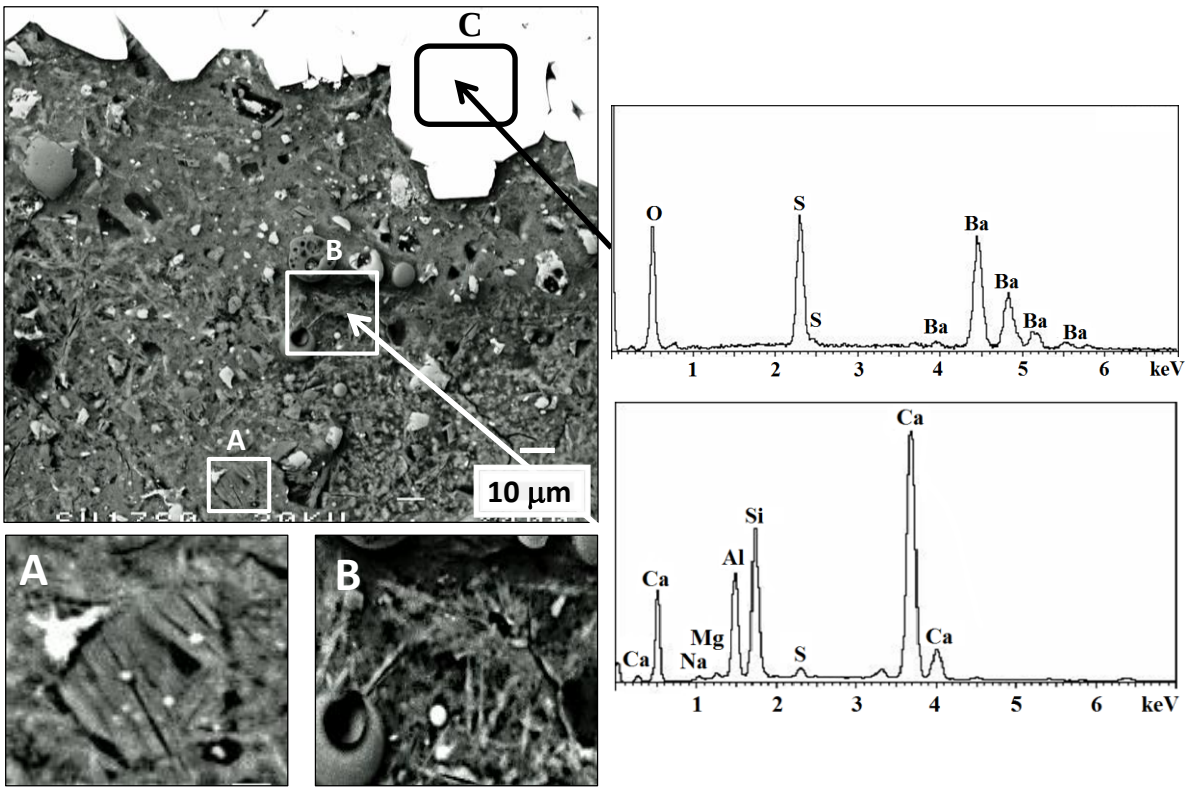


Figure 5.19 BSE image of 12 wt.% MK / 48 wt.% granulated $BaSO_4$ blended paste showing: A – a monosulphate particle, and B – formation of needle-like phases, probably a C-S-H product. EDS for B and C are also shown.

The substitution of MK by quartz has a different effect on the structure of the cement wasteform. In this case (Figure 5.20), the region around the $BaSO_4$ granule appeared slightly more porous than that far away from these particles, consistent with the formation of the ITZ zone as previously observed in specimens including powdered and granulated $BaSO_4$. As the XRD and TG results revealed, quartz particles were not participating to a major extent in the hydration reaction of the PC, but rather acting as inert filler in the system similar to the $BaSO_4$ powder.

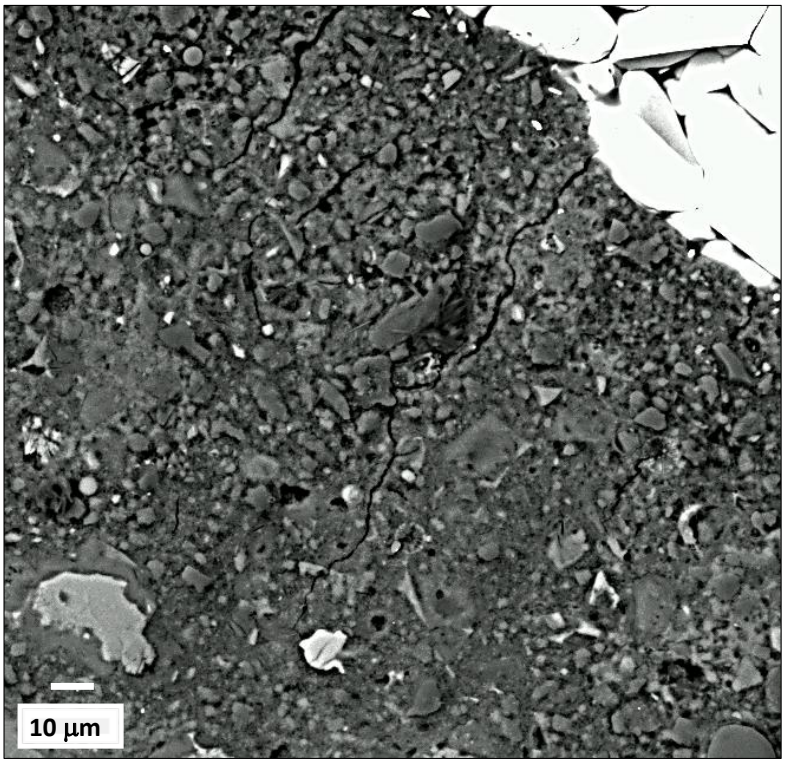


Figure 5.20 BSE image of 12 wt.% quartz / 48 wt.% granulated $BaSO_4$ blended paste sample, showing a highly porous interfacial transition zone between the $BaSO_4$ granule (top right) and the cement matrix

The total porosity of the cement systems studied is presented in Figure 5.21. The total porosity clearly decreased in the sample with 12 wt% and 20 wt% $BaSO_4$ powder, suggesting that this content of powdered $BaSO_4$ favours good particle-packing. These results confirm the observation in BSE images where the $BaSO_4$ powder fills the pore and decreases the highly interfacial transition zone. A similar result was obtained with the quartz, which appeared to be performing as a fine aggregate in the specimen. The total porosity in the metakaolin sample did not increase very much compared with neat PC even at a high w/c=0.87 ratio, which is known as the main reason to increase the porosity of cement paste. This is a well-known effect that has been previously

reported in MK blended cements [24], and is not notably disrupted by the presence of the $BaSO_4$ granule.

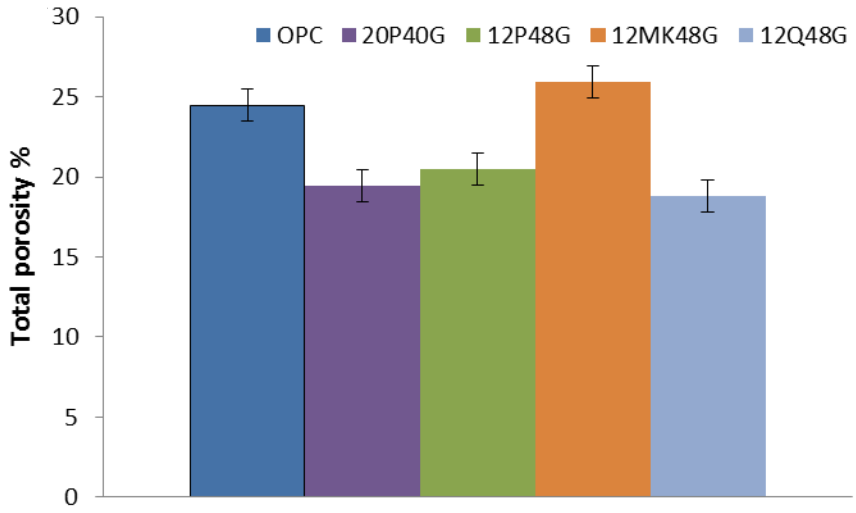


Figure 5.21 the total porosity of cement systems after 28 days

### 5.5.4 Compressive strength

The compressive strengths of the cement systems studied are presented in Figure 5.22. Even with 60 wt% PC replacement with other materials, the mechanical strengths of all of the systems are comparable to the reference PC sample. In the systems solely including powdered and granulated $BaSO_4$, the mechanical strength retention after replacing the PC in the system is attributed to the particle reinforcing effect where $BaSO_4$ is acting as an aggregate reinforcing the cement matrix. The slight reduction in the mechanical strength of the specimens with quartz suggests that this effect in this sample is slightly less. The quartz particle may have reduced the highly porous interfacial transition zone to a less extent than the powders due to the slightly larger particle size.

In the case of the cement a system including MK, the mechanical strength retention was probably not simply due to a physical effect. It was also a consequence of the pozzolanic reaction taking place between MK and portlandite, favouring the formation of C-S-H type gels that enhance the mechanical performance of the systems, and contributing to the densification of the system, even at a high w/c ratio.

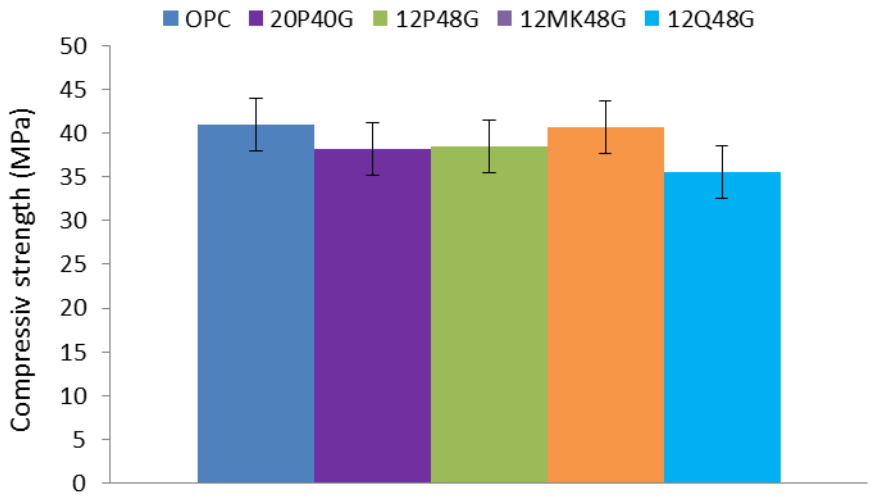


Figure 5.22 Compressive strength of cement systems after 28 days

### 5.5.5 Leaching test

Table 5.4 and 5.5 show the concentration of the major elements in the leachate after 30 and 180 days of leaching periods, respectively. The results of key elements for each wasteform formulation are summarised in Figure 5.23.

Table 5.4: Summary of leach tests for 30 days

| **Sample ID** | **Elements concentration** mg/L | | | | | | | |
|---|---|---|---|---|---|---|---|---|
| | Ca | Si | Ba | S | Al | Fe | Na | Mg |
| PC | 251 | 0.90 | 1.68 | 0.52 | 1.04 | 0.015 | 38.2 | 0.011 |
| 20 wt% P / 40 wt% G $BaSO_4$ | 91.30 | 2.16 | 1.92 | 0.63 | 1.88 | 0.005 | 60.3 | 0.018 |
| 12 wt% P / 48 wt% G $BaSO_4$ | 12.4 | 5.87 | 0.64 | 1.06 | 2.24 | 0.009 | 56.7 | 0.029 |
| 12 wt% MK / 48 wt% G $BaSO_4$ | 4.18 | 6.55 | 0.076 | 4.41 | 4.27 | 0.008 | 28.3 | 0.038 |
| 12 wt% Q / 48 wt% G $BaSO_4$ | 11.5 | 6.25 | 0.40 | 1.43 | 2.49 | 0.009 | 50.9 | 0.021 |

Table 5.5: Summary of leach tests for 180 days

| **Sample ID** | **Elements concentration** mg/L | | | | | | | |
|---|---|---|---|---|---|---|---|---|
| | Ca | Si | Ba | S | Al | Fe | Na | Mg |
| PC | 142 | 2.57 | 2.37 | <0.1 | 1.52 | 0.047 | 42.1 | <0.1 |
| 20 wt% P / 40 wt% G $BaSO_4$ | 62.4 | 1.73 | 2.36 | 0.21 | 2.53 | 0.22 | 59.1 | 0.16 |
| 12 wt% P / 48 wt% G $BaSO_4$ | 6.36 | 9.93 | 0.43 | 1.77 | 2.47 | 0.13 | 57.8 | 0.39 |
| 12 wt% MK / 48 wt% G $BaSO_4$ | 4.33 | 5.92 | 0.12 | 9.65 | 4.43 | 0.14 | 40.2 | 0.29 |
| 12 wt% Q / 48 wt% G $BaSO_4$ | 3.14 | 13.4 | 0.28 | 3.61 | 2.37 | 0.048 | 56.7 | 0.29 |

The neat PC sample showed a significantly large amount of Ca release within 30 days resulting in a high concentration of Ca in the solution. This should be attributed to the higher initial Portlandite (CH) content in this sample. It is known that the portlandite is usually the first cement phase to leach out [36]. The reduction in the concentration of Ca after 180 days could be due to the reaction of Ca ions with $CO_2$ in the atmosphere to form $CaCO_3$. For the 20P48G sample, the amount of leached Ca was lower, reflecting the less amount of CH. Since the wasteform formulations contain only 40 wt% of PC in solid mass basis, if they behave same as the PC sample, the level of Ca leaching and thus

concentration should be approximately 40% of that for PC sample (indicated in the Figure 5.23 by dotted line). The 20P40G sample indicated the predicted level of Ca concentration. The level of Ca leaching appeared to be much less for the other wasteform formulations, suggesting a reduced amount of CH available to leach. The XRD (Figure 5.13) and TG (Figure 5.15) data indicated that these samples had a less CH compare with the 20P40G sample.

Interestingly, the Si leaching and concentration showed an opposite trend, indicating the level of Si concentration higher than expected. It is known that the dissolution of C-S-H phase is the main source of Si leaching, which usually takes place after CH has leached [36]. Therefore, the C-S-H leaching at the early stage can occur in the system containing less CH. For the neat PC sample, the concentration of Si in the leachate was very little in 30 days, suggesting that the system still had enough CH at this stage to minimise the dissolution of C-S-H. Similar results were obtained for 20P48G, corresponding to the less amount of CH in the sample. The other wasteform formulation showed increased amount of Si leaching, corresponding to the reduced amount of CH. After 180 days, the 12MK48G sample indicated less amount of Si leached out compared with the 12P48G and 12Q48G samples. This may be attributed to the different types of C-S-H gel in the system. As already discussed in the former section, the C-S-H in this sample may have a significant amount of aluminium with more cross-linking structure. It has been also reported that the solubility of the C–S–H gel is a function of Ca/Si ratio of the gel [37, 38].

The concentration of S in the leaching solution was detected in all formulation but was more significant in the sample containing metakaolin. This must be due

to the significant amount of the sulphate-related phases (AFt and AFm) observed in this particular sample. It is not clear whether this S is from the cement or $BaSO_4$. Although the level of S concentration exceeded the expected level, this may be due to the increased dissolution of other phases such as AFt or AFm phases.

The behaviour of Ba was somewhat similar to that of Ca. As the neat PC sample does not contain any $BaSO_4$, the Ba concentration at this level is considered to be the impurity in the cement. However, the 20P40G sample showed a Ba concentration higher than expected, which may suggest that some of Ba is originated from $BaSO_4$. Further investigation is required to appreciate whether the Ba was released from $BaSO_4$ or from the impurity of the cement matrix. For the 12P48G, 12MK48G, and 12Q48G samples, the concentration of Ba did not exceed the expected level. The slight reduction in the concentration of Ba after 180 days may be due to the carbonation of Ba ions, possible incorporation of Ba in other phases or measurement error. The concentration of the leached Ba from these wasteform formulations was less than in some of the standardised leaching test for the stabilised toxic wastes [39]. The low concentration of Ba shows a good potential of these wasteform formulations.

Based on the concentration of the elements, normalised elemental mass loss (NL) was calculated using Equation 5.7.

$$NL_i = \frac{M_i \cdot V_W}{F_i \cdot SA} \qquad (5.7)$$

The $NL_i$ is the normalised elemental mass loss of element $i$ (g/cm$^2$), $M_i$ is the concentration of element $i$ in the leachate (g), $F_i$ is the fraction of element $i$ in

the cement sample (unitless) before leaching, and *SA* is the surface area ($cm^2$) of the sample. Because the $NL_i$ is normalised by the fraction of elements, when the elements dissolve congruently with the reacted cement mass, all of $NL_i$ must indicate the same value. In the present calculation, the mass fractions of elements in the fresh cement pastes for each formulation were used.

Figure 5.24 shows the normalised elemental mass loss of key elements for each formulation, in comparison to a literature data by Banba et al. [40]. In general, the normalised elemental mass loss is obtained in the present study is less by maximum of approximately one order compared with the literature data. This is probably attributed to the experimental condition. Banba et al. used the (Surface area) / (water volume) ratio of 0.12 $cm^{-1}$ [40] whereas it was much less value of 6.8 $m^{-1}$ (0.068 $cm^{-1}$) was used in the present study. Less surface area should provide less leaching of elements. The general trend of the results agrees with their data. Na indicated significantly higher mass loss compared with other elements, indicating its high mobility in cement matrix. The behaviour of Ca and Ba are very similar in all formulations, which may confirm that the Ba found in the leachate was an impurity in the cement matrix. The behaviour of Si and Al also appear to be similar. This may be related to their interaction via C-S-H phase. The behaviour of S is in general similar to those of Si and Al, except the sample containing metakaolin. The increased mass loss of S in this particular sample must be related to the sulphate related phases such as AFt and AFm as already discussed. The relation of the leaching behaviour of different elements can be further analysed in Figure 5.25. When elements are dissolving congruently, their data should be on the same straight line. A weak correlation between Ca and Ba can be observed. There could also be a

correlation between Si and S. However, a further investigation is required to draw a clear conclusion.

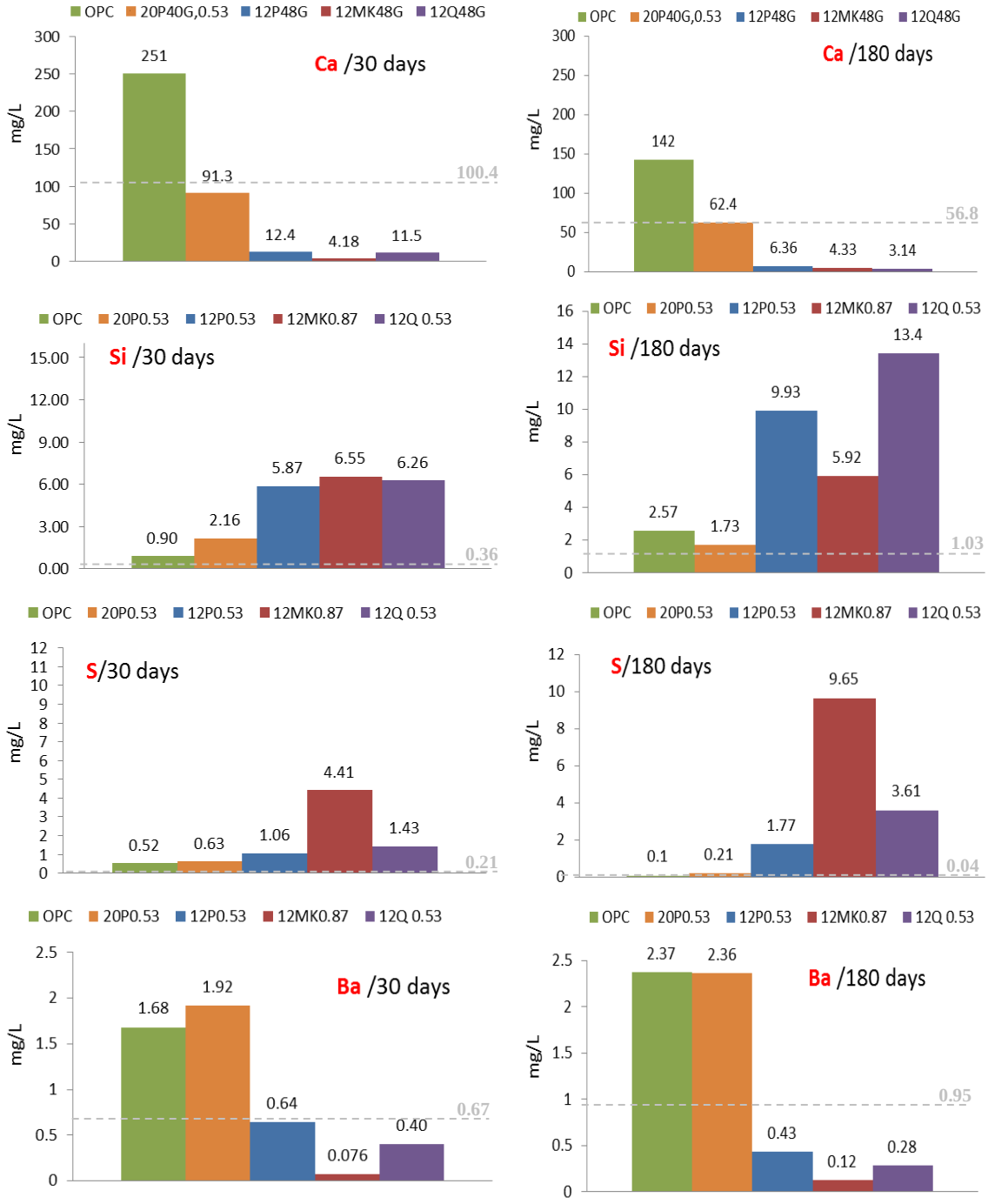


Figure 5.23 Total concentration of Ca, Si, Ba, and S in solution after: 30 days and after 180 days for each cement formulation

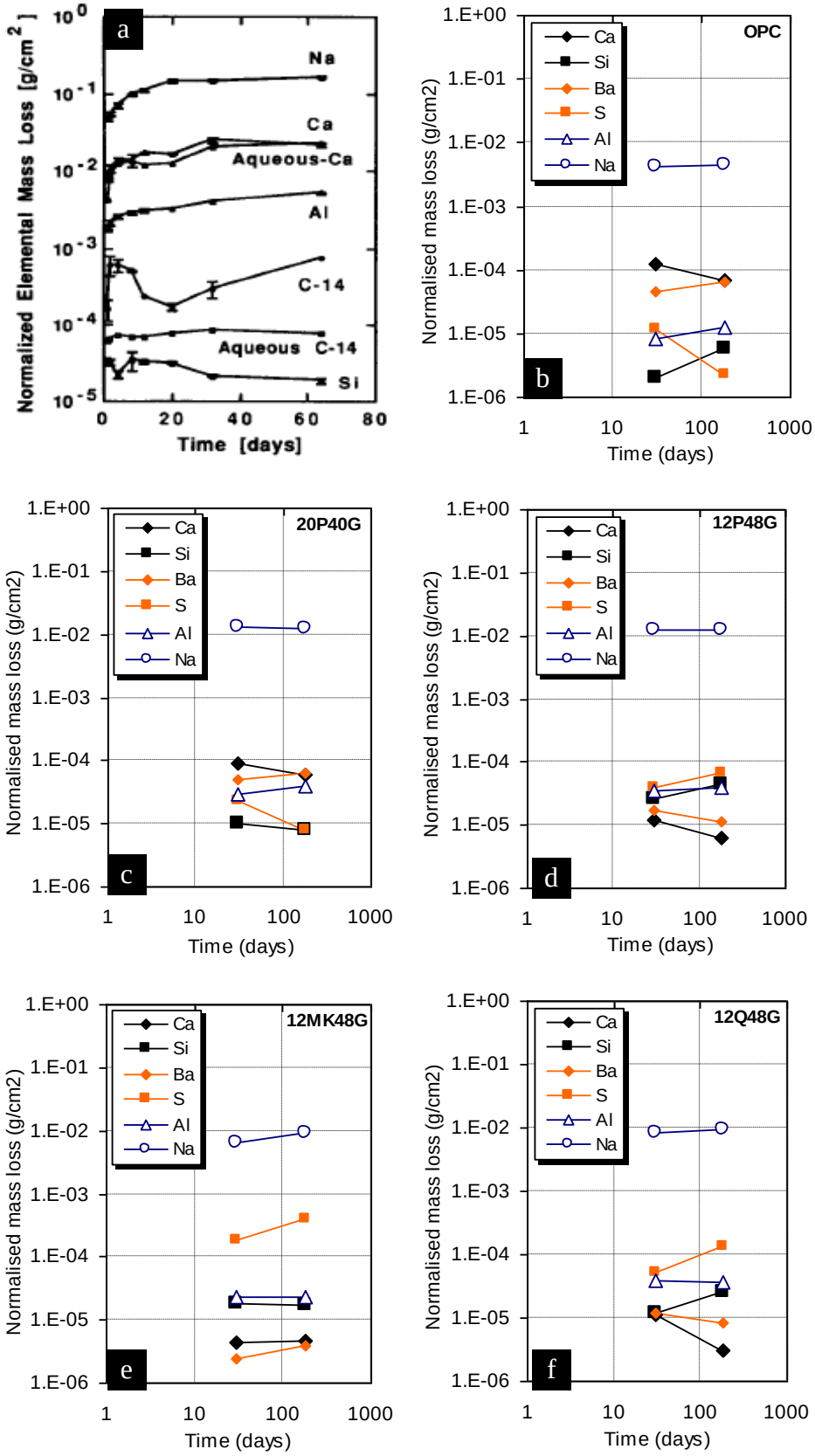


Figure 5.24 Normalised elemental mass loss from a cement wasteform: (a) literature data [5], (b) PC sample, (C) 20P40G sample, (d) 12P48G sample, (e) 12MK48G sample and (f) 12Q48G sample.

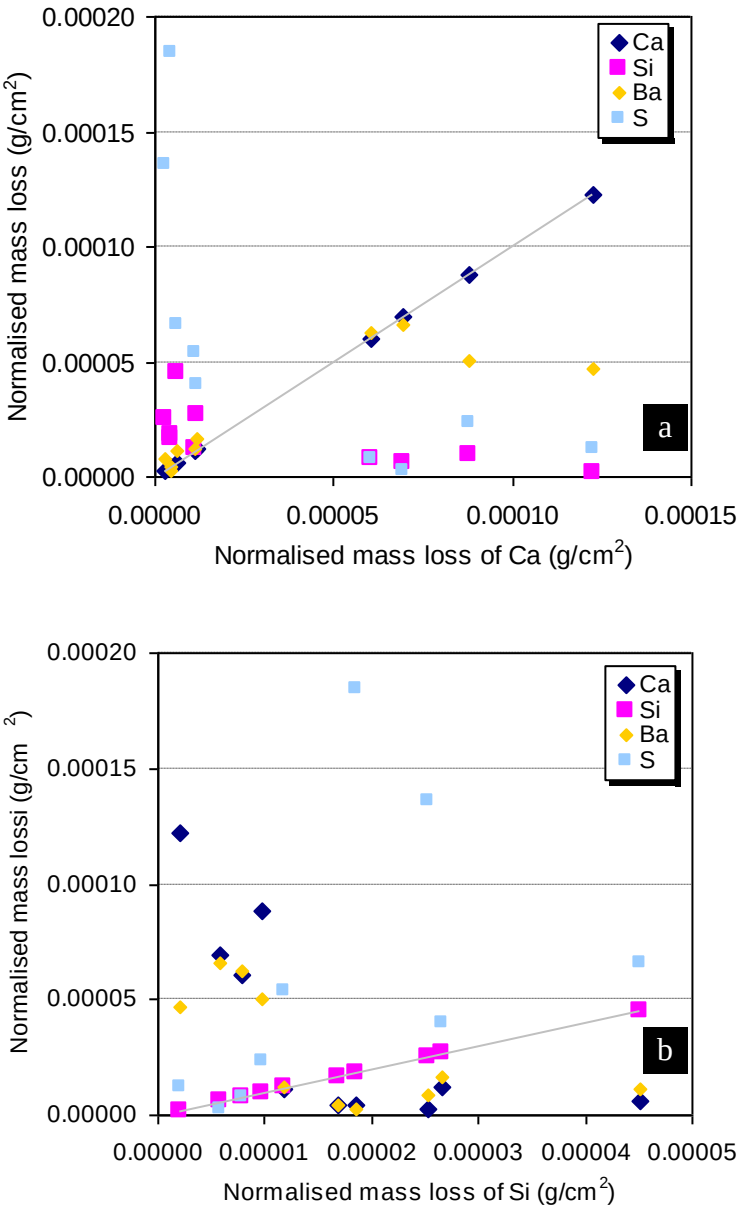


Figure 5.25 Normalised elemental mass loss from a cement wasteform: (a) plotted against the data for Ca, (b) plotted against the data of Si.

## 5.6 Summary

Sedimentation of $BaSO_4$ particles can occur in the cement paste due to its high density. Careful control of the setting time and the viscosity of cement slurry were necessary in order to avoid the sedimentation of $BaSO_4$ granules and obtain homogenous products.

The study on the rheological properties revealed that the neat PC cement slurry with w/c=0.53 is capable of suspending the $BaSO_4$ granules only with diameters less than 1.6 mm. Introduction of fine $BaSO_4$ powder was effective in improving the rheological properties of the cement paste. 12 wt% of $BaSO_4$ introduction was found sufficient to increase the viscosity and yield stress of the cement paste which can suspend the $BaSO_4$ granule of 13.9 mm in diameter. The same amount of metakaolin or quartz was also found to be effective to suspend coarse $BaSO_4$ granules without sedimentation.

Based on the information gained, the wasteform formulations were developed. Using both fine $BaSO_4$ powder and coarse $BaSO_4$ granules, it was possible to reduce the amount of highly porous interfacial zone around the coarse $BaSO_4$ granules, which resulted in the reduction of porosity, suppression of carbonation and improvement in the compressive strength. Replacing the fine $BaSO_4$ powder with metakaolin or quartz was also found effective in improving the microstructure of the wasteform. Although the metakaolin required more water, the pozzolanic reaction of metakaolin helped to maintain the strength of the product at a similar level as other formulations.

The results of leaching tests were comparable with the literature data for nuclear wasteforms, suggesting that the developed formulation had sufficient durability. The amounts of Portlandite and C-S-H in the system have a

significant effect on the leaching behaviour. The behaviour of Ba and S indicated a possible correlation with those of Ca and Si, respectively. Most of the Ba found in the leachant was considered to be from the cement matrix, although this was not conclusive.

## 5.7 References


1. R. David, *CRC Handbook of Chemistry and Physics*. 2005: Taylor and Francis Group.
2. H. Taylor, *Chapter 7: Hydration of Portland cement* in *Cement Chemistry*. 1990, Thomas Telford London. p. 187-226.
3. G. D. Stefanou and C. Larsinos, *Influence of Mixing Water on the Setting Time of Concrete.* Cement Composites and Lightweight Concrete, 1981. **3**: p. 45-48.
4. G. Bye, *Portland cement*, ed. 2. 1999: Thomas Telford.
5. R. Nurse, *Slag cements*, in *The chemistry of cement*, H. Taylor, Editor. 1964, Academic Press. p. 460.
6. R. Bogue, *The setting of cement paste*, in *The chemistry of portland cement*. 1955, Reinhod: New York.
7. J. Bensted and P. Barnes, *Structure and Performance of Cements*. 2002 Taylor & Francis. 565.
8. P. C. Hewlett, *Lea's Chemistry of Cement and Concrete*, ed. 4. 2004, Oxford, UK: Elsevier Science & Technology. 1057.
9. J. Ambroise, S. Maximilien, and J. Pera, *Properties of Metakaolin blended cements.* Advanced Cement Based Materials, 1994. **1**: p. 161-168.
10. M. H. Zhang and V. M. Malhotra, *Characteristics of a thermally activated alumino-silicate pozzolanic and its use in concrete.* Cement and Concrete Research, 1995. **25**: p. 1713-1725.
11. Z. Sun, T. Voigt, and S. P. Shah, *Rheometric and ultrasonic investigations of viscoelastic properties of fresh Portland cement pastes.* Cement and Concrete Research, 2006. **36**( (2006) ).
12. A. H. Asbridge, C. L. Page, and M. M. Page, *Effects of metakaolin, water/binder ratio and interfacial transition zones on the microhardness of cement mortars.* Cement and Concrete Research, 2002. **32**: p. 1365-1369.
13. M. Rhodes, *Slurry Transport*, in *Introduction to Particle Technology*. 2008, John Wiley & Sons: England. p. 99.
14. R. J. Flatt, *Interpartical forces and superplasticizers in cement suspensions*, in *Department of materials*. 1999, Lausanne: Lausanne. p. 330.
15. Y. T. Mihiretu, *Fundamentals of Segregation*, in *Civil and Environmental Engineering*. 2009, PhD thesis, University of Alberta. p. 49.
16. G. Sant, C. F. Ferraris, and J. Weiss, *Rheological properties of cement pastes: A discussion of structure formation and mechanical property development.* Cement and Concrete Research, 2008. **38**: p. 1286–1296.
17. A. Papo, L. Piani, and R. Ricceri, *Rheological Properties of Very High-Strength Portland Cement Pastes: Influence of Very Effective Superplasticizers.* International Journal of Chemical Engineering, 2010. **2010**.
18. R. Shaugnessy and P. E. Clark, *The Rheological Behaviour of Fresh Cement Pastes.* Cement and Concrete Research, 1988. **18**: p. 327-341.
19. J.Bensted, *Use of ferrophosphorus as a heavyweight additives for oil well cements.* Cement and Concrete Research, 1993. **23**: p. 988-990.
20. C. K. Park, M. H. Noh, and T. H. Park, *Rheological properties of cementitious materials containing mineral admixtures.* Cement and Concrete Research, 2005. **35**: p. 842– 849.
21. C. Liu, H. Shao, F. Chen, and H. Zheng, *Rheological properties of concentrated aqueous injectable calcium phosphate cement slurry.* Biomaterials, 2006. **27**: p. 5003–5013.
22. R. P. Chhabra and J. F. Richardson, *Non-Newtonian flow and applied rheology*. 2008, burlington: Elsevier.

23. I. Odler, *Hydration, Setting and Hardening of Portland Cement*, in *Lea's Chemistry of Cement and Concrete*, P.C. Hewlett, Editor. 2001, Butterworth-Heinemann: Oxford. p. 241-298.
24. B. B. Sabir, S. Wild, and J. Bai, *Metakaolin and calcined clays as pozzolans for concrete: a review.* Cement and Concrete Composites, 2001. **23**(6): p. 441-454.
25. H. Taylor, C. Famy, and K. Scrivener, *Delayed ettringite formation.* Cement and Concrete Research, 2001. **31**: p. 683-693.
26. H. G. Midgley and P. B. Rao, *Formation of strätlingite, $2CaO.SiO_2.Al_2O_3.8H_2O$, in relation to the hydration of high alumina cement.* Cement and Concrete Research, 1978. **8**: p. 169-172.
27. G. K. Sun, J. F. Young, and R. J. Kirkpatrick, *The role of Al in C-S-H: NMR, XRD, and compositional results for precipitated samples.* Cement and Concrete Research, 2006. **36**(1): p. 18-29.
28. I. G. Lodeiro, A. Fernández-Jimenez, A. Palomo, and D. E. Macphee, *Effect on fresh C-S-H gels of the simultaneous addition of alkali and aluminium.* Cement and Concrete Research, 2010. **40**(1): p. 27-32.
29. F. W. Locher, *Stoichiometry of tricalcium silicate hydration*. 1966: Washington. p. 300-308.
30. L. Alarcon-Ruíz, G. Platret, E. Massieu, and A. Ehrlacher, *The use of thermal analysis in assessing the effect of temperature on a cement paste. .* Cement and Concrete Research, 2005. **35**(3): p. 609-613.
31. C. Hall, P. Barnes, A. D. Billimore, A. C. Jupe, and X. Turrillas, *Thermal decomposition of ettringite $Ca_6[Al(OH)_6]_2(SO_4)_3.26H_2O$.* Journal of the Chemical Society, Faraday Transactions, 1996. **92**(12): p. 2125-2129.
32. S. Kwan, J. LaRosa, and M. W. Grutzeck, *$^{29}Si$ and $^{27}Al$ MASNMR study of strätlingite.* Journal of the American Ceramic Society, 1995. **78**(7): p. 1921-1926.
33. N. J. Coleman and W. R. McWhinnie, *The solid state chemistry of metakaolin-blended ordinary Portland cement.* Journal of Materials Science, 2000. **35**(11): p. 2701-2710.
34. K. L. Scrivener, A. K. Crumbie, and P. Laugesen, *The interfacial transition zone (ITZ) between cement paste and aggregate in concrete.* Interface science, 2004. **12**: p. 411 - 421.
35. J. P. Ollivier, J. C. Maso, and B. Bourdette, *Interfacial transition zone in concrete.* Advanced Cement Based Materials, 1995. **2**(1): p. 30-38.
36. H. Taylor, *Cement chemistry*. 2 ed. 1990, London: Thomas Telford.
37. X. Gaona, D. A. Kulik, and E. Wieland, *Aqueous-solid solution thermodynamic model of U(VI) uptake in C-S-H phases.* Applied Geochemistry 2012. **27**: p. 81-95.
38. M. Kersten, *Aqueous Solubility Diagrams for Cementitious Waste Stabilization Systems. 1. The C-S -H Solid-Solution System.* Environmental Science and Technology, 1996. **30**(7): p. 2286–2293.
39. S. Balzamo and A. Marchetti, *A New Standardized Leaching Test on Stabilized Wastes.* Mikrochim. Acta 1996. **123**: p. 145-150.
40. T. Banba, J. Matsumoto, and S. Muromura, *Leaching behavior of carbon-14 contained in Portland cement.* Cement and Concrete Research, 1992. **22**(2-3): p. 381-386.

# Chapter 6: Behaviour of PC-$BaSO_4$ system in high temperature environment

## 6.1 Introduction

Considering the sufficient mechanical strength of the $BaSO_4$-contaning cement systems shown in the former section together with the high thermal stability of $BaSO_4$, and the reduced radiation permeability of $BaSO_4$-containg cement [1], it may be possible to apply this system as a support matrix for the deep borehole geological disposal (DBGD) of high level radioactive wastes (HLRW). The support matrix for the DBGD needs to withstand the high temperature and pressure environment [2]. It has been known that the cementitious materials changes their microstructure and mechanical behaviour when subjected to high service temperatures [3]. This chapter studies the stability of $BaSO_4$-containing cement formulations studied as wasteforms in the former section under elevated temperatures. Firstly, hardened PC-$BaSO_4$ system was subjected to 300ºC in air to understand the basic responses of the material at a high temperature. It has been reported that the temperature of the DBGD environment can rise up to ~300$^{o}$C [2, 4]. Secondly, in order to evaluate the feasibility for the deep borehole disposal concept, PC-$BaSO_4$ pastes with different admixtures were subjected to a hydrothermal condition, which can affect the hydration process of cementitious material, and the properties of the products. The structural changes caused by the condition and the effects of mineral admixtures such as metakaolin and quartz were investigated using XRD, TGA, SEM, MIP, and mechanical strength. The labelling used for XRD and TGA graphs in the following chapter is outlined in Table 6.1.

Table 6.1: Key to XRD and TGA labelling

| Labelling | Chemical name | Cement nomenclature | Chemical formula | ICDD Card No |
|---|---|---|---|---|
| A | Alite (tricalcium silicate) | $C_3S$ | $3CaO.SiO_2$ | 49-442 |
| B | Belite (dicalcium silicate) | $\beta$-$C_2S$ | $2CaO.SiO_2$ | 33-0302 |
| af | Tetracalcium aluminoferrite | $C_4AF$ | $4CaO.Al_2O_3.Fe_2O_3$ | 30-0226 |
| C | Calcite | $C\bar{C}$ | $CaCO_3$ | 05-0586 |
| P | Portlandite | CH | $Ca(OH)_2$ | 44-1481 |
| E | Ettringite (AFt) | $C_6A\bar{S}_3H_{32}$ | $Ca_6Al_2(OH)_{12}(SO4)_3.26H_2O$ | 41-1451 |
| MS | Monosulphate (AFm) | $C_4A\bar{S}_3H_{12}$ | $Ca_4Al_2(OH)_{12}(SO_4).6H_2O$ | 45-0158 |
| BS | Barium sulphate | $BaSO_4$ | $BaSO_4$ | 72-1390 |
| St | Stratlingite | $C_2ASH_8$ | $Ca_2Al_2SiO_7.8H_2O$ | 29-0285 |
| Hg | Hydrogarnet | $C_3AH_6$ | $Ca_3Al_2(OH)_{12}$ | 38-0368 |
| CSH | calcium silicate hydrate | C-S-H | - | Taylor [5] |
| J | Jaffeite (tricalcium silicate hydrate) | $C_6S_2H_3$ | $Ca_6(Si_2O_7)(OH)_6$ | 77-0960 29-375 |
| Z | α-dicalcium silicate hydrate | α- $C_2SH$ | $Ca_2(SiO_3)(OH)_2$ | 29-0373 15-641 |
| R | Reinhardbraunsite | $C_5S_2H$ | $Ca_5(SiO_4)_2(OH)_2$ | 29-0380 |
| T | 11A° Tobermorite [6] | $C_5S_6H_5$ | | 45-1480 |
| Q | Quartz | | $SiO_2$ | 46-1045 |

## 6.2 Heat treatment at 300°C

### 6.2.1 Visual observation

Figure 6.1 shows the neat PC sample and PC with 60 wt% $BaSO_4$ granules after the heat treatment. A significant change in color occurred in both of them. The effect of the heat treatment were considerably severe for the neat PC which appeared to suffer from cracking due to the shrinking upon heating [7] and became fragile as shown in Figure 6.1. It has been reported that PC cement paste tend to lose their strength at such high temperatures due to the change in the main binding phase, C-S-H, as a result of the loss of capillary and

chemically bound water and that in other cement hydration phases such as ettringite, monosulphate [7, 8].

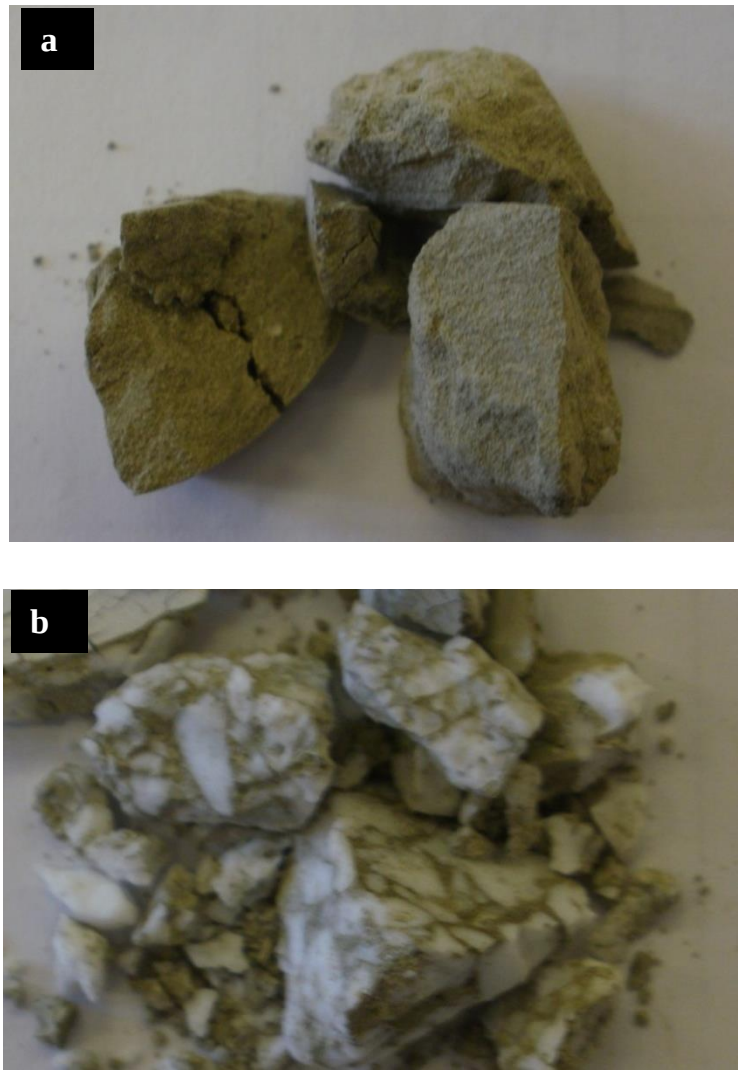


Figure 6.1 PC-$BaSO_4$ after heat treatment. (a) Neat PC, (b) PC+ 60 wt% $BaSO_4$ granule

### 6.2.2 Neat PC

Figure 6.2 shows the XRD patterns for the hydrated neat PC system before and after the heat-treatment at 300°C. The reflection peaks for monosulphate (AFm) disappeared after the heat treatment, suggesting that AFm phase had

dehydrated [9, 10]. It has been reported that AFm and C-S-H phases are readily destroyed, with loss of water, by heating in air at 300°C [7, 11]. The reflection peaks attributed to $Ca(OH)_2$, the main crystalline phase of cement hydration, are still clearly observed. This was expected as the dehydroxylation of $Ca(OH)_2$ occurs at higher temperature about 450°C. In addition, clear peaks attributed to $CaCO_3$ phases were also observed. Lee et al. [12] summarised the processes of decomposition of cement hydration phases in the different heating regime as shown in Table 6.2.

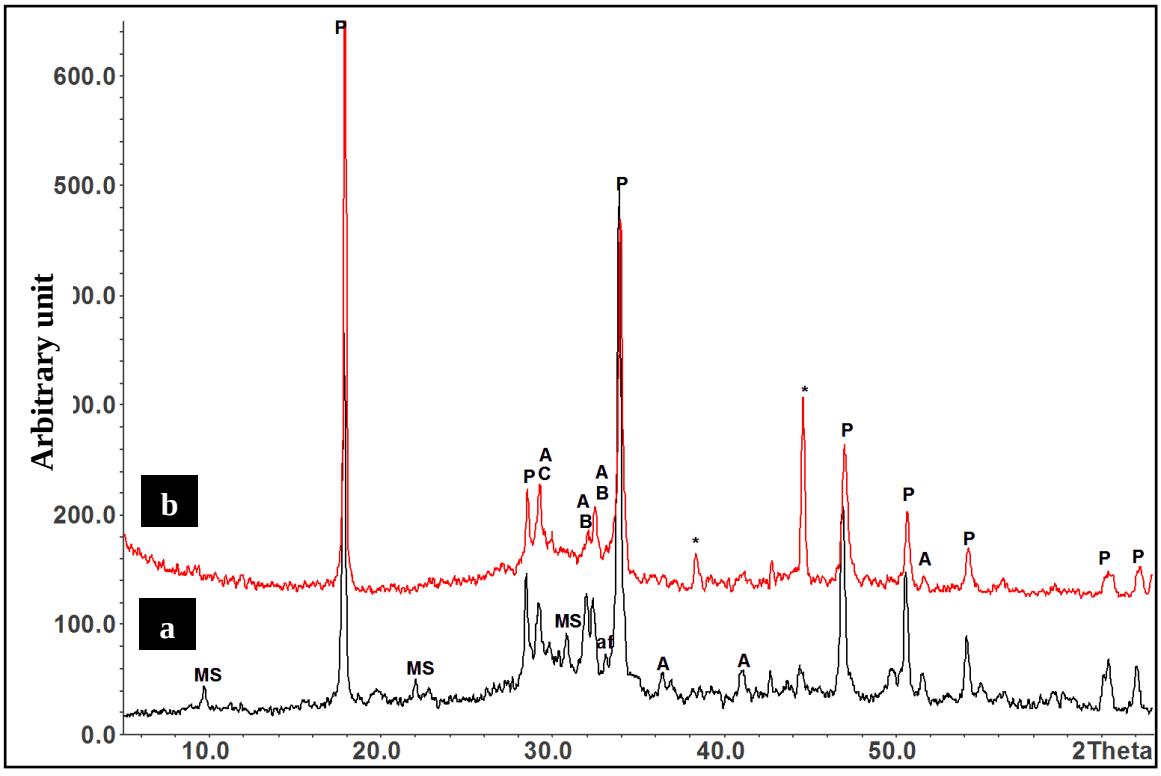


Figure 6.2 XRD patterns for hydrated PC: (a) before and (b) after heat treatment at 300°C, (*peak due to the Al sample holder)

Table 6.2 Processes of decomposition depending on the heating regime [12]

| Temperature | Decomposition |
|---|---|
| 20–120 °C | Evaporation of free water, dehydration of C-S-H and ettringite |
| 120–400 °C | Dehydration of C-S-H |
| 400–530 °C | Dehydration of C-S-H, dehydroxylation of CH |
| 530–640 °C | Dehydration of C-S-H, decomposition of poorly crystallized $CaCO_3$ |
| 640–800 °C | Dehydration of C-S-H, decomposition of $CaCO_3$ |

TG-DTG curves for neat PC system before and after heat-treatment at 300°C are presented in Fig 6.3. The total weight loss of the heat-treatment sample up to 300°C during TG measurement were decreased compared to that without the heat-treatment, indicating that the heat-treated samples contained less water in the system. Corresponding DTG curves (Figure 6.3 b) show the significant decrease in the peaks around 100-200$^oC$ associated with the water loss of C-S-H and AFm phases which are typically observed in the PC cement paste. Some C-S-H could remain, since DTG analysis show that the broad peak between 60°C and 180°C due to the dehydration of C-S-H and AFm. This confirms that the amount of water in the C-S-H structure was decreased due to heat-treatment [7]. The DTG curve shows the clear evidence of $Ca(OH)_2$ phase. The weight loss from this phase is slightly increased after heat treatment. The peak associated with $CaCO_3$ was more significant in the heat-treatment sample.

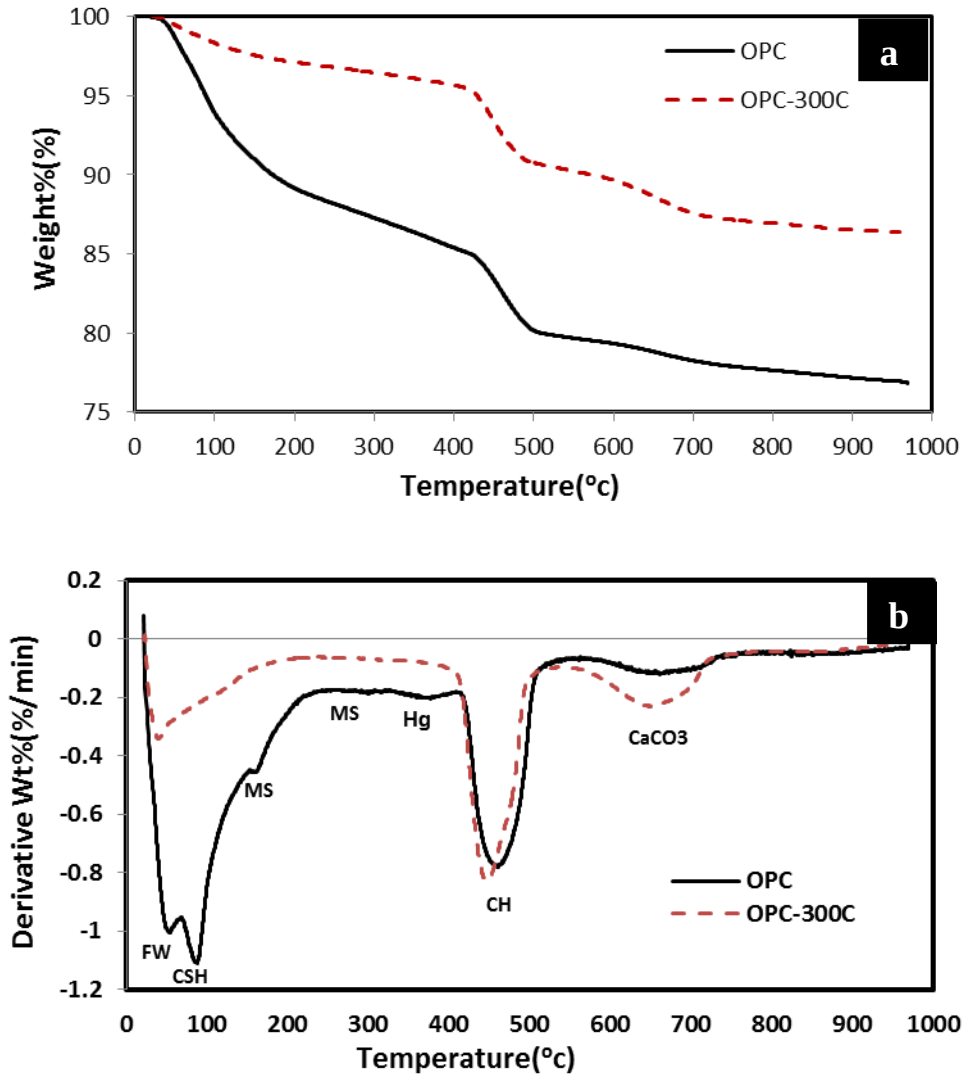


Figure 6.3 (a) TG and (b) DTG for PC before and after heat treatment at 300°C

BSE images of the sample are shown in Figure 6.4. The microstructure of PC was clearly affected by heating, and the heated sample appeared to be more porous. This is confirmed by the total porosity measured by MIP, which increased from 25% to 30% after the heat treatment. The increase in porosity is mainly associated with the loss of chemically bound water from C-S-H gel induced by the high temperatures, resulting in the decrease in the volume of the

C-S-H phase. Similar consequences have been reported for the PC cement paste [7]. The shade of grey level for the inner C-S-H became lighter after heating, confirming the increase in density of this phase due to loss of water. It is now difficult to distinguish from $Ca(OH)_2$ which is supposed to be the majority of the remaining original hydrated phase.

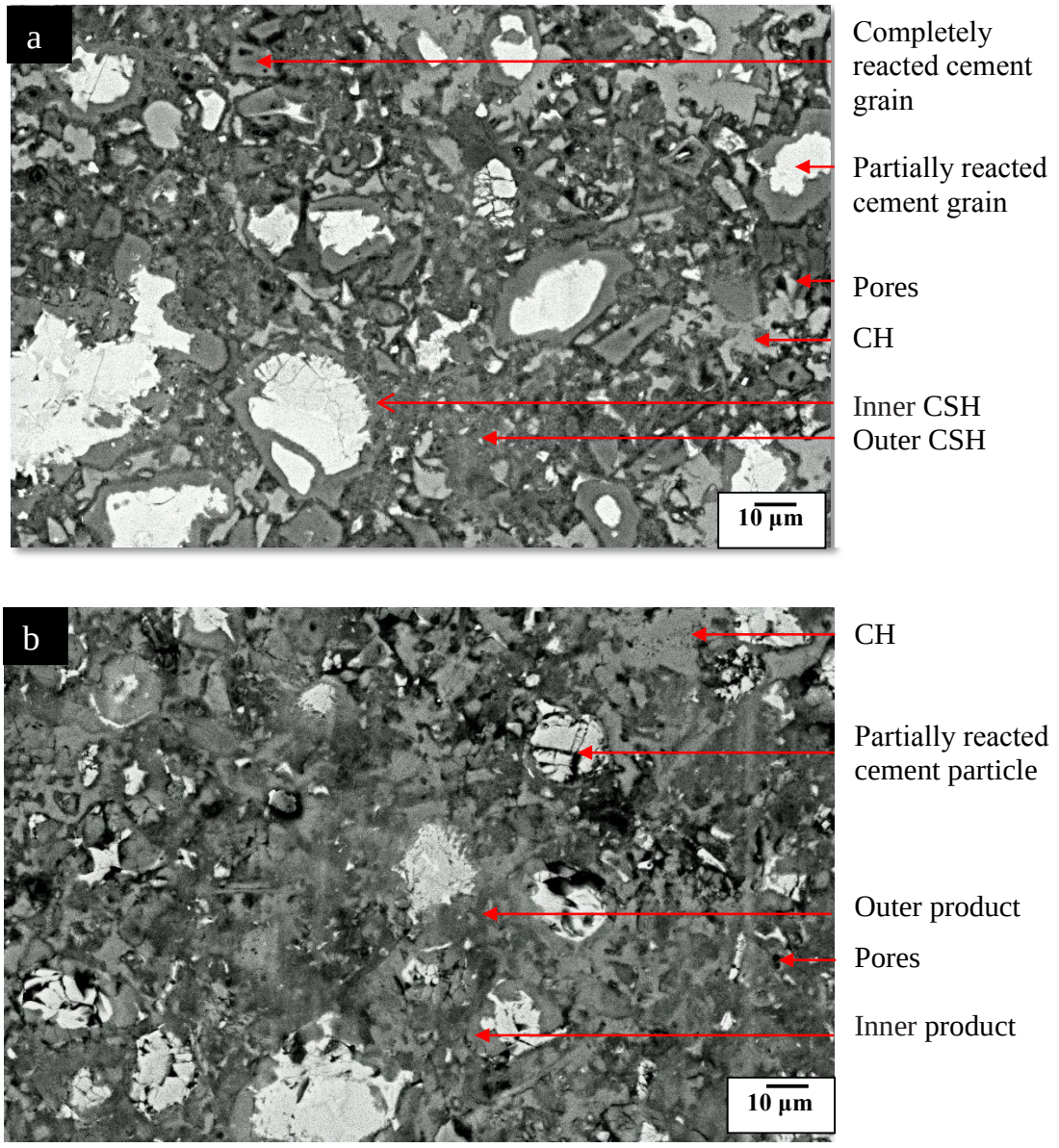


Figure 6.4 BSE of PC: (a) before heat -treatment, (b) after heat -treatment

### 6.2.3 PC-$BaSO_4$ granule system

Figure 6.5 shows the XRD patterns of the PC with 60 wt% $BaSO_4$ granule sample before and after heat-treatment at 300°C. As was the case for pure PC system, the XRD pattern of PC-$BaSO_4$ granule sample showed a slight alteration after heating. No peaks for AFm, and smaller peaks for $CaCO_3$ were detected in the samples after heat treatment. Clear peaks for $Ca(OH)_2$ were observed, but it is difficult to identify other cement hydration products due to the high intensity peaks for $BaSO_4$.

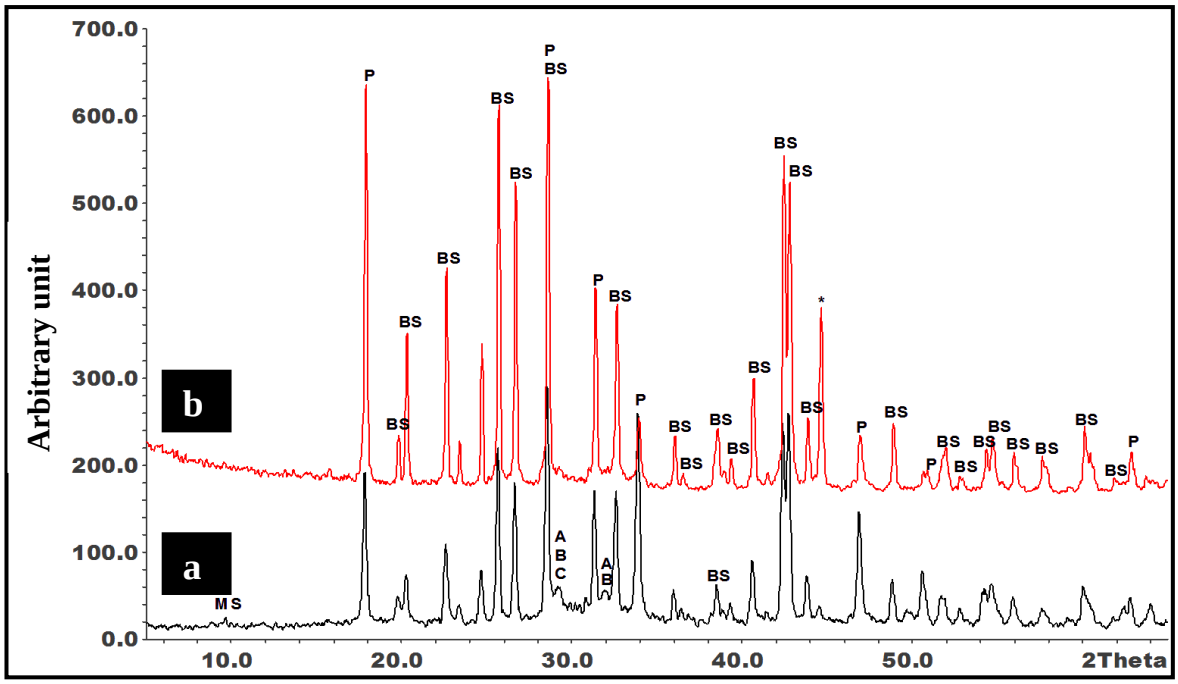


Figure 6.5 XRD patterns for PC with 60 wt% $BaSO_4$ granule: (a) before and (b) after heat treatment at 300°C. (*Al peak due to sample holder)

TG-DTG curves for the sample before and after the heat treatment at 300°C are presented in Figure 6.6. Similar to the neat PC system, the weight loss of the

granule samples up to 300$^{o}$C during TG measurement was significantly less compared to that before the heat treatment. The broad peak on DTG curve between 50°C and 150°C was thought to be due to the dehydration of remaining C-S-H and AFm [7, 13]. $Ca(OH)_2$ did not show any significant change. The amount of weight loss due to $CaCO_3$ between 600°C and 750°C was more significant in the heat-treated sample. Since XRD results did not show this phase clearly, thus it might be either poorly crystallined or from the carbonation by the exposure to the air during cooling and storage [14].

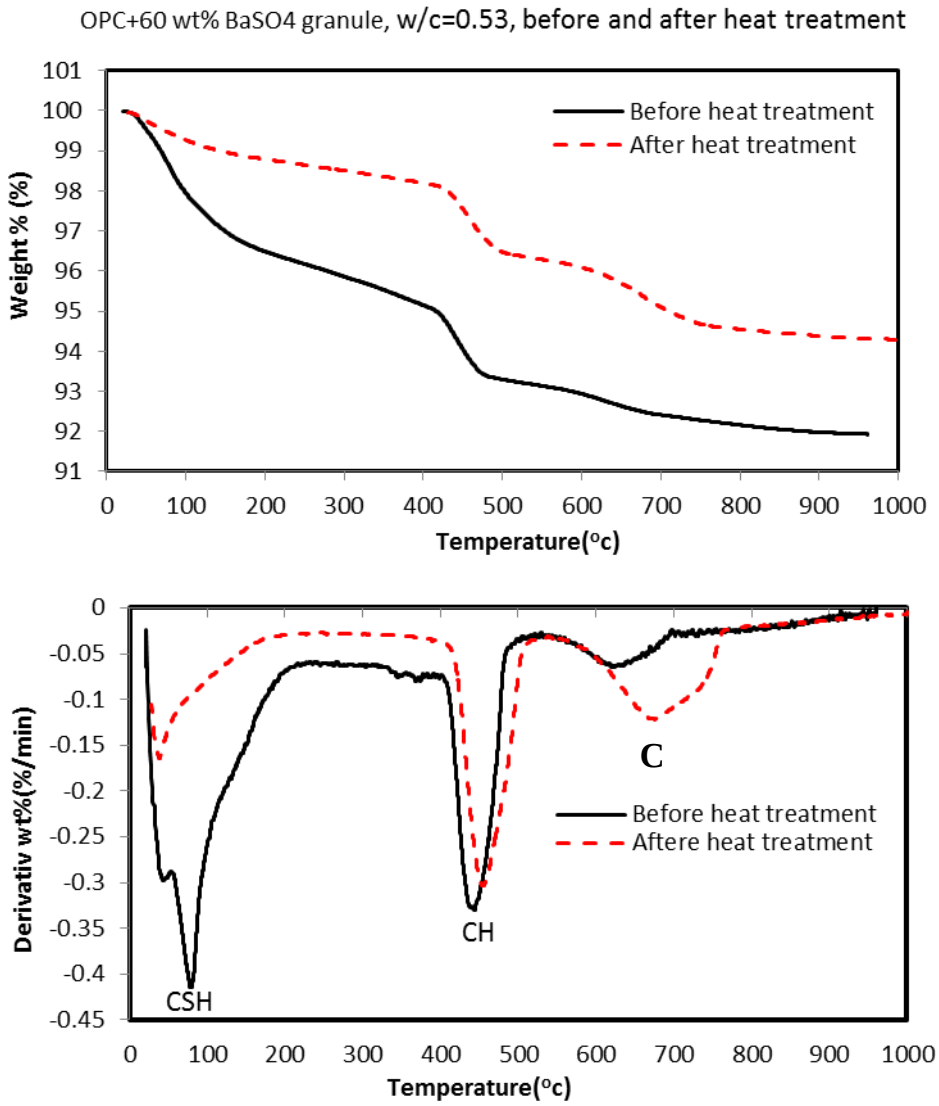


Figure 6.6 TG and DTG curves of PC with 60 wt% $BaSO_4$ granule before and after heat-treatment at 300°C, w/c=0.53

BSE images of those specimens are shown in Figure 6.7. The heated PC-$BaSO_4$ granule sample shows more pores, suggesting that the loss of water from the binding phase, C-S-H, increased the porosity of the cement matrix. A distinctive white rim was observed in the interface of inner C-S-H and anhydrited cement particle, the reasons of which are unclear.

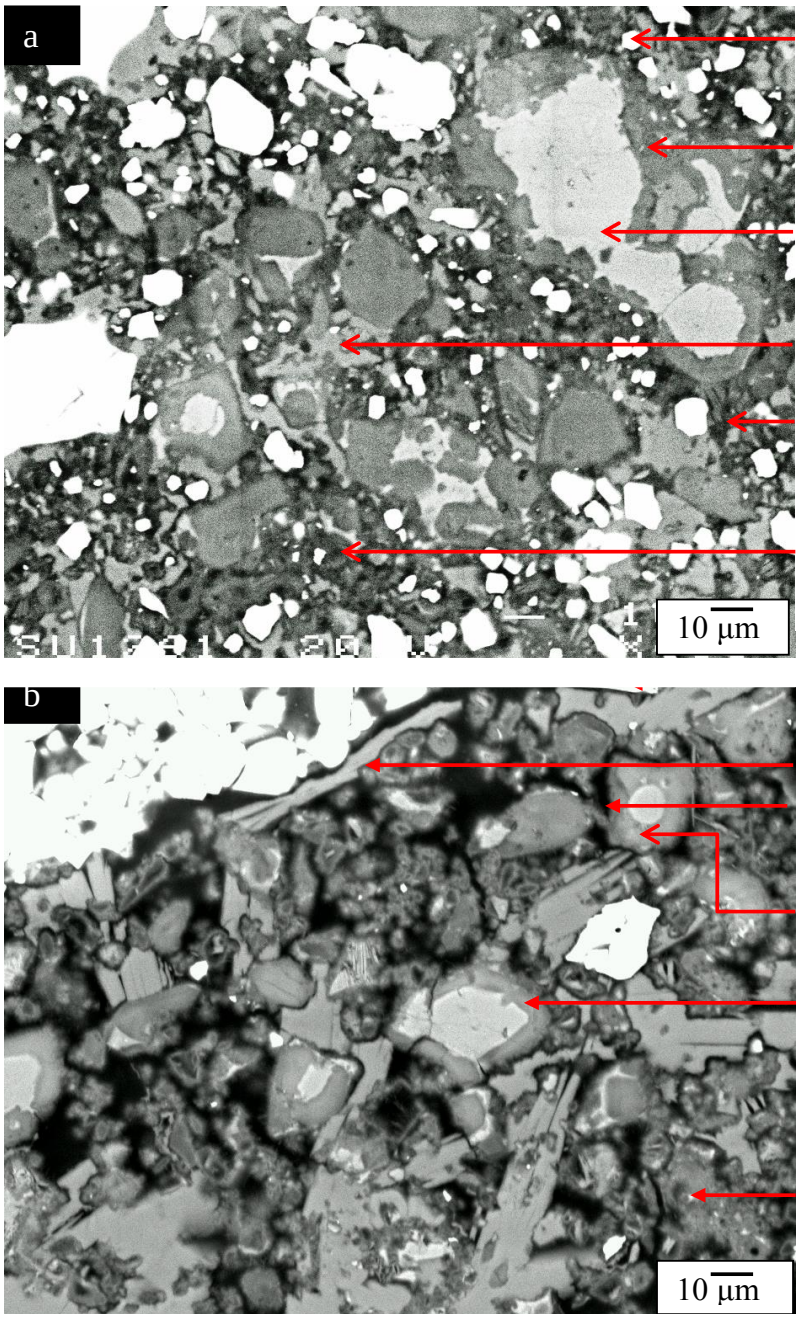


Figure 6.7 BSE images of PC with 60 wt% $BaSO_4$ granule: (a) before heat treatment, (b) after heat treatment at 300°C

Table 6.3 illustrates the total porosity of the samples before and after heat treatment. The total porosity of the neat PC and the PC-$BaSO_4$ granule samples has changed after the heat treatment, which confirms the observation in BSE images. The PC-$BaSO_4$ granule sample was slightly more porous than neat PC after the heat treatment.

Table 6.3 the total porosity of the samples before and after heat treatment

| Formulation | Total porosity % | |
|---|---|---|
| | before | after |
| PC | 24.47 | 30.25 |
| PC with 60 wt% $BaSO_4$ granule | 22.53 | 33.06 |

Figure 6.8 illustrates the pore size distribution of PC and PC-$BaSO_4$ granule samples before and after heat treatment. In both samples the most pores distribute at the diameter ranging from 0.1-0.01 μm before heat treatment. After the heat-treatment, the neat PC increased its porosity ranging from 1 to 0.01 μm. The sample containing $BaSO_4$ granules also showed an increase in the porosity, especially pores ranging from 10 to 0.01 μm.

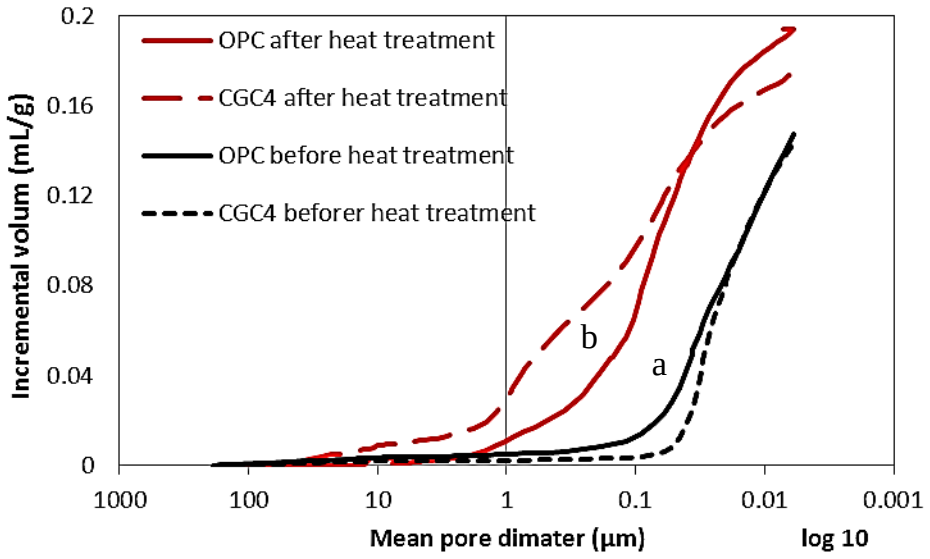


Figure 6.8 pore size distributions of PC and PC-$BaSO_4$ granule samples: (a) before and (b) after heat treatment

## 6.3 Hydrothermal curing at 180$^oC$

### 6.3.1 Neat PC

Figure 6.9 shows the XRD trace of the hardened PC after 28 days cured in the hydrothermal condition. The figure also shows the XRD trace of the PC cured at 40$^oC$ for comparison. Increasing the curing temperature resulted in more complex hydration phases. The major crystalline phases identified in the sample cured in the hydrothermal condition (Figure 6.9 b) are unhydrated alite and belite, along with the hydrated phases, being portlandite and hydrogarnet. The formation of hydrogarnet has been observed in PC samples cured at a higher temperature, 85 $^oC$ for up to 8.4 years [15]. Calcium carbonate in its calcite form ($CaCO_3$) was also detected. In this specimen monosulphate was not identified as a reaction product. Formation of lime-rich phases, Jaffeite ($C_6S_2H_3$), reinhardbraunsite ($C_5S_2H$), and α-dicalcium silicate hydrate (α- $C_2SH$) must be related to the decomposition/dehydration of C-S-H. It has been reported that C-S-H is not stable at high temperatures and often replaced by such crystalline phases with a high Ca/Si ratios [16-19]. The formation of Jaffeite and reinhardbraunsite agrees with published data[19, 20]. Sarp reported that Jaffeit can form between 175 $^oC$ and 235 $^oC$ in high pH environment [21]. α-$C_2SH$ has been also observed in PC cured above 110$^oC$ [14, 16]. Saout et al. also reported that an increase of pressure and temperature leads to form crystallise phases [22-24].

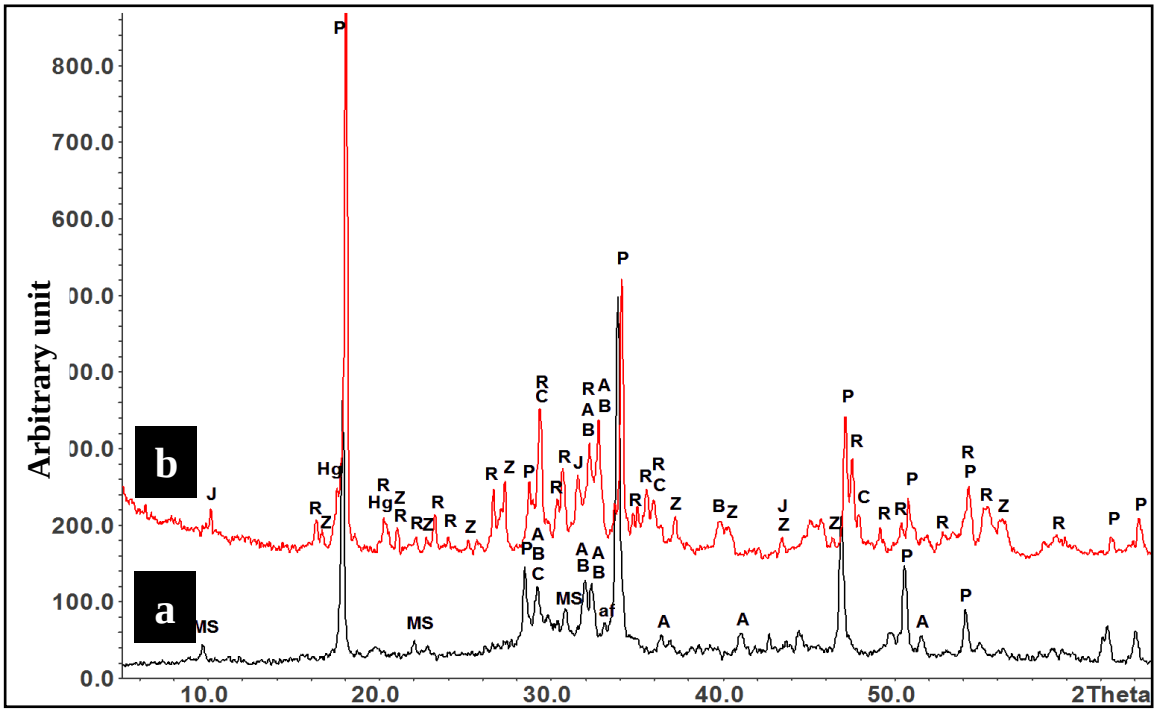


Figure 6.9 XRD trace of neat PC samples: (a) cured at 40°C, (b) cured under hydrothermal condition

Figure 6.10 shows TG and DTG data for the neat PC sample cured at 40°C and that cured under the hydrothermal condition for 28 days. The lack of the water loss below 300°C in the PC cured under hydrothermal condition confirms the absence of the C–S–H and AFm phases. The presence of hydrogarnet (Hg) is confirmed by a shoulder in the DTG curve at 370°C. A sharp peak due to the dehydroxylation of $Ca(OH)_2$ was observed between approximately 425°C and 475°C. The reduction of portlandite compared with the 40°C curing can be attributed to its reaction with the calcium silicates to form jaffeite and other Ca rich phases [18], which are previously identified through XRD (Figure 6.9 b). Further small peak at around 490-540°C is due to the decomposition of α-dicalcium silicate hydrate to dicalcium silicate which is slightly different from

clinker phase (β-$C_2S$) [6, 13, 19, 25]. Finally, the broad peak between 600°C and 700°C is attributed to the decomposition of calcium carbonates [26, 27].

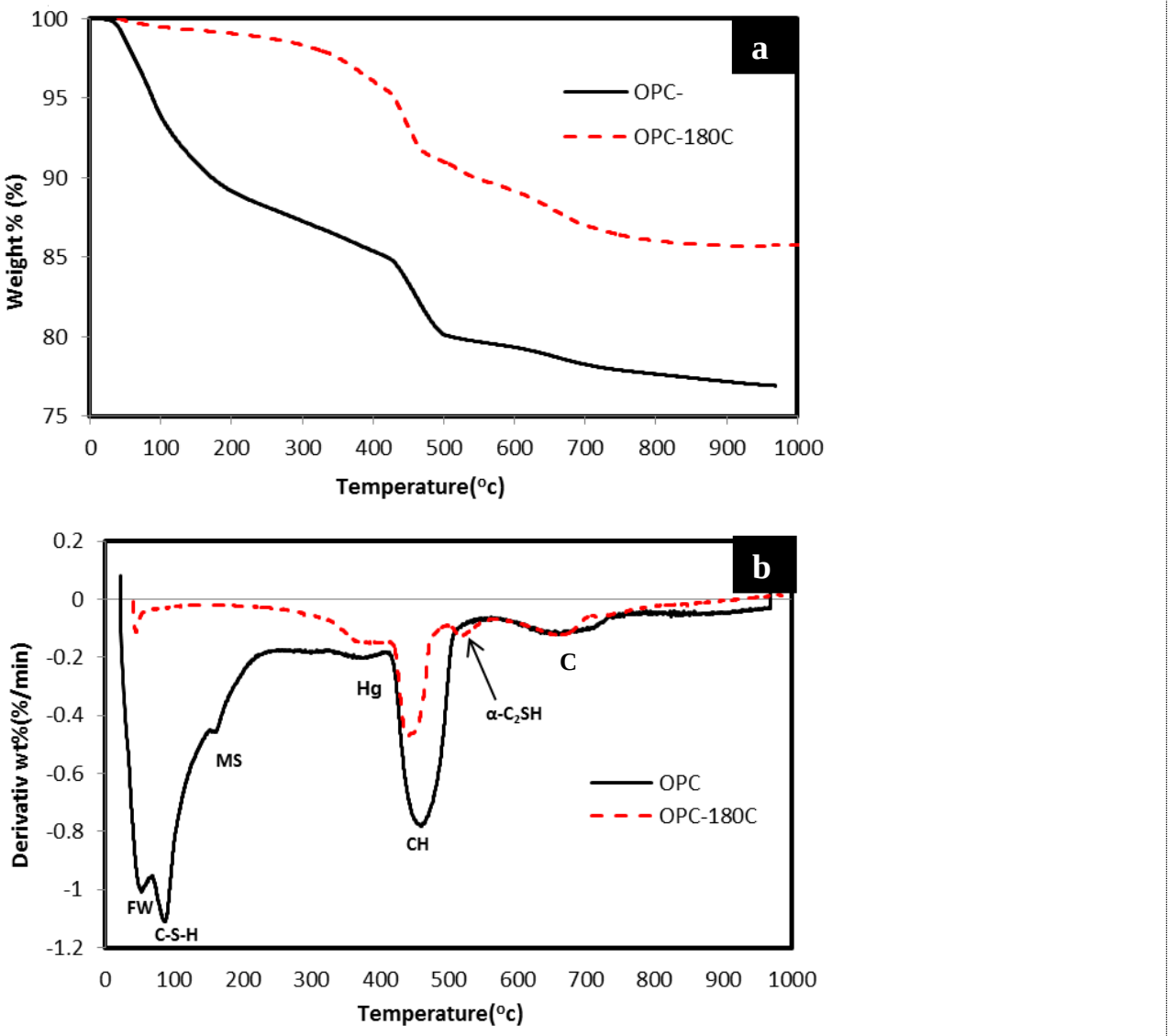


Figure 6.10 TG and DTG of neat PC cured at 40 °C and under hydrothermal condition

Figure 6.11 shows the BSE image of the neat PC cured at 40°C and that under hydrothermal condition for 28 days. The microstructure was clearly affected by the hydrothermal condition. The sample is much more porous when cured under hydrothermal condition. It has been reported that the curing of PC at

higher temperatures results in a non-uniform distribution of the hydration products in the microstructure [28]. A high concentration of hydration products tend to build up around the hydrating grains and retard the subsequent hydration at high temperatures, whereas the hydration products have sufficient time to diffuse at low temperatures and precipitate relatively more uniformly throughout the cement matrix [28]. In this particular case, however, this porous microstructure is more likely attributed to the lack of the usual C-S-H gel. The C-S-H gel formed in the early hydration reaction of $C_3S$ is known to lose its interlayer water under a similar condition (high pressure steam, 100-300°C) [16], which can be accompanied by a shrinkage of the layer thickness of C-S-H [13]. This usually leads to the formation of crystalline silicate hydrate phases with a high Ca/Si ratio such as Jaffeite and reinhardbraunsite by reacting with portlandite [13, 24], as observed in the XRD analysis (Figure 6.9). Because the C-S-H has less water content, the inner and outer products appear almost in the same grey level and are not easily identified at this magnification. It is believed that the unreacted β-dicalcium silicate ($C_2S$) directly changed to α-dicalcium silicate hydrate (α-$C_2SH$) rather than C-S-H gel when hydrated in the condition of the present study [18].

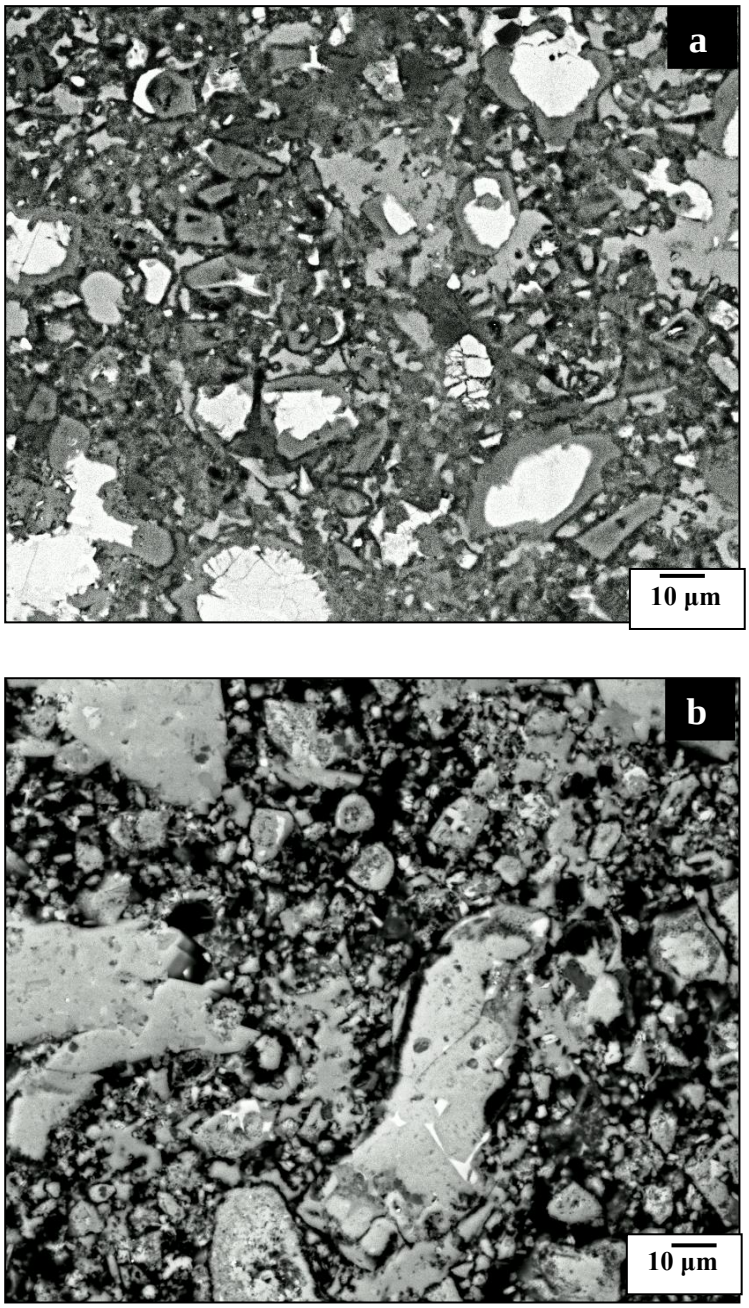


Figure 6.11 BSE images of PC, w/c=0.53: (a) cured at 40$^{o}$C, (b) under hydrothermal condition at 180 $^{o}$C

### 6.3.2 PC- $BaSO_4$ granule system

Figure 6.12 shows XRD trace of PC with 60 wt% $BaSO_4$ granule sample cured at 40°C and that cured at 180°C under hydrothermal condition for 28 days. The reaction products were similar to those observed in neat PC cured under

hydrothermal condition. Clear peaks of lime rich phases were also observed in addition to the high intensity peaks of $BaSO_4$ and calcite phase.

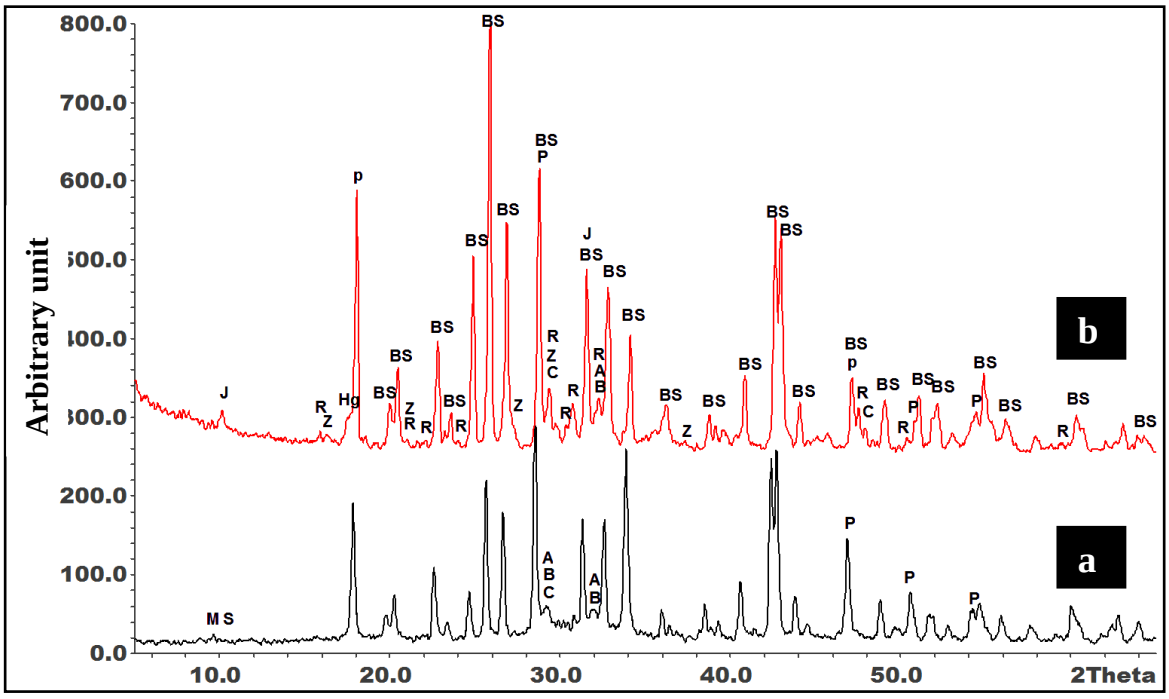


Figure 6.12 XRD trace for PC+ 60 wt% $BaSO_4$ granule w/c=0.53: (a) cured at 40°C, (b) cured under hydrothermal condition at 180 °C

Figure 6.13 shows TG and DTG for the same specimens. In the sample cured in the hydrothermal condition, the presence of hydrogarnet (Hg) is evident by a shoulder in the DTG curve at 350°C. The addition of $BaSO_4$ granule has increased the weight loss due to the decomposition of α-$C_2SH$ as clearly seen by the sharp peak at 530°C. The broad peak between 700°C and 800°C , which is attributed to the decomposition of calcium carbonates of varying crystallinity [26, 27], was also observed.

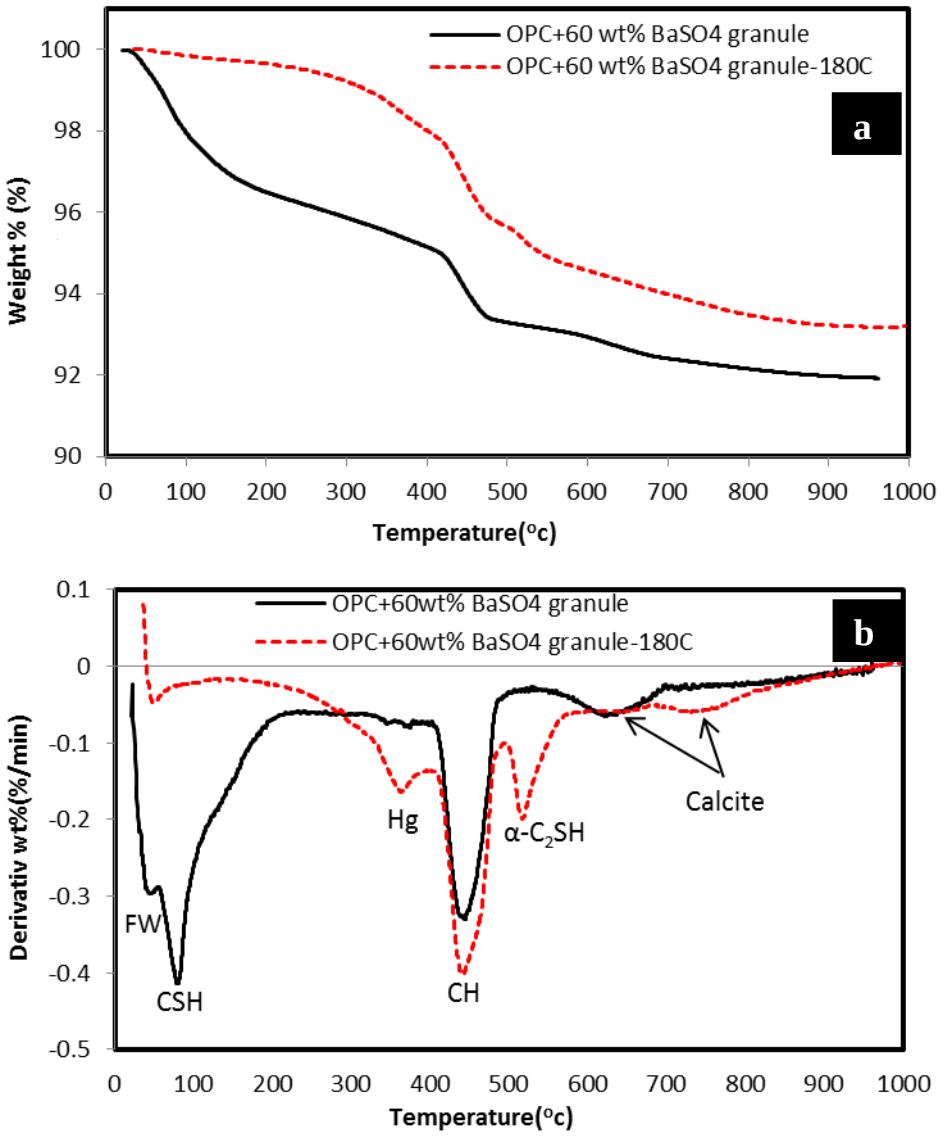


Figure 6.13 (a) TG and (b) DTG for PC+ 60 wt% $BaSO_4$ granule w/c=0.53, cured at 40°C and in hydrothermal condition at 180 °C for 28 days

Figure 6.14 shows the BSE image of the specimen. The effect of hydrothermal curing appeared to be less uniform in comparison to the neat PC sample (Figure 6.11b). The microstructure appeared more heterogeneous compared with the neat PC sample after the hydrothermal curing. This may be owing to the formation of the hydrogarnet and α-$C_2SH$ phases to fill some space produced by the reduction of C-S-H.

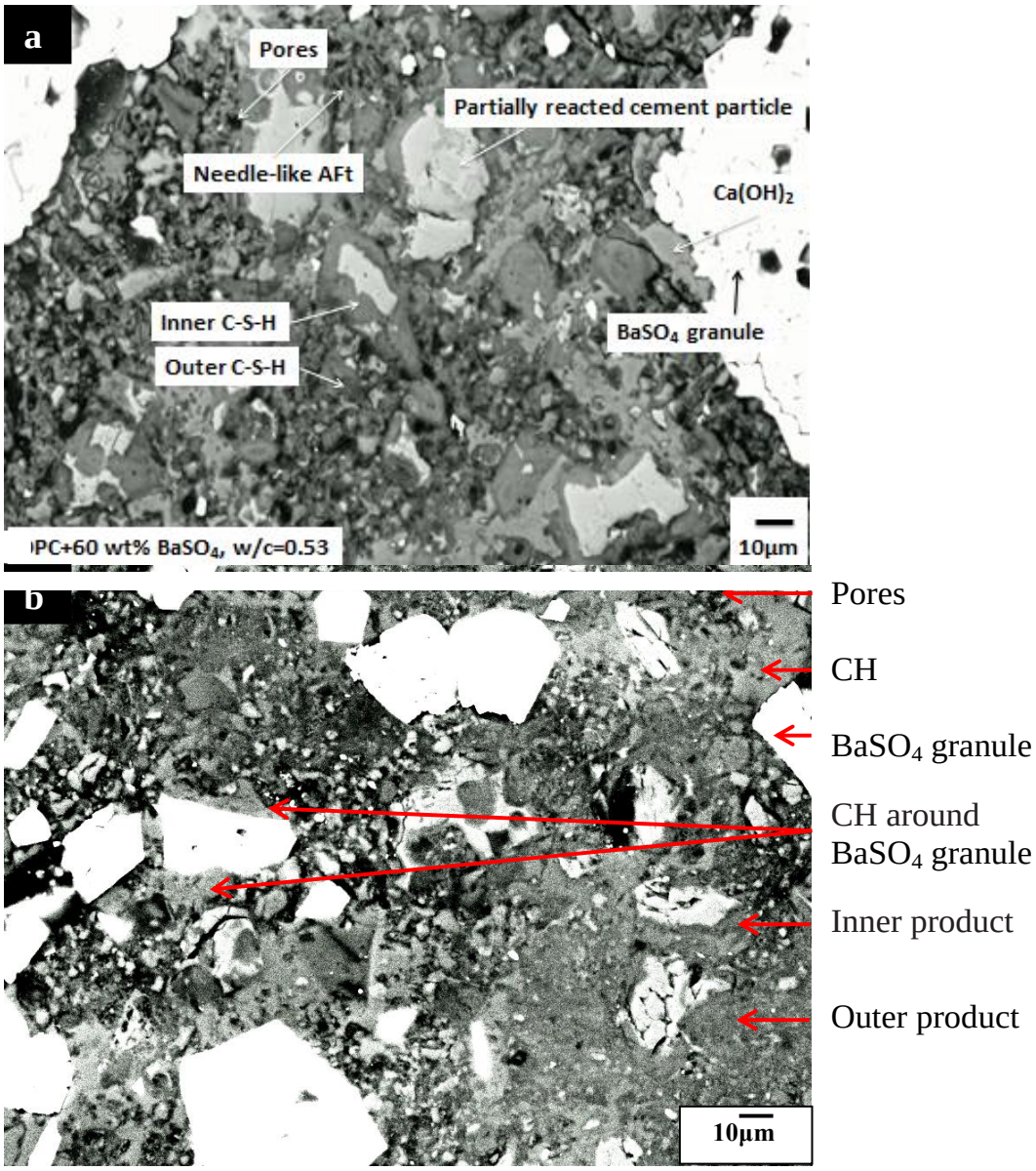


Figure 6.14 BSE image for PC+ 60 wt% $BaSO_4$ granule w/c=0.53: (a) cured at 40°C, (b) cured under hydrothermal condition at 180 °C

In general the area around $BaSO_4$ granules became more porous in the hydrothermally cured sample. This was confirmed by the EDS line scan as shown in Figure 6.15. The general decrease of the especially Ca is observed towards the $BaSO_4$ granule, suggesting that the less materials around $BaSO_4$ granule. Within the microstructure, anhydrous PC particles were observed

surrounded by slightly dark grey hydration rims which are considered to consist of Ca rich phase base on EDS analysis. It was difficult to distinguish between the inner and outer products.

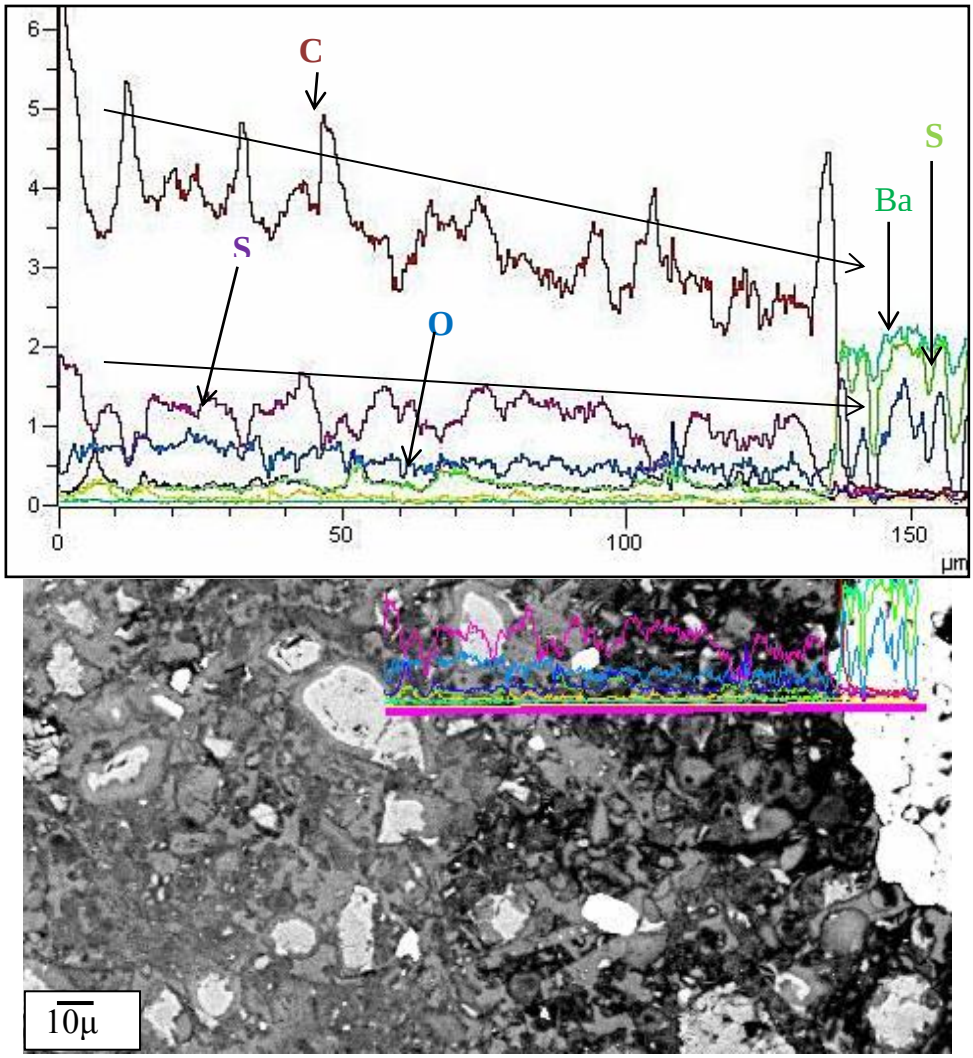


Figure 6.15 line scan for transition zone of PC+ 60 wt% $BaSO_4$ granule in hydrothermal condition

## 6.4 Hydrothermal curing with mineral admixtures

### 6.4.1 Visual observation

As discussed in chapter 5, mineral admixtures promote different properties of $BaSO_4$-containing cement materials. After the hydrothermal curing, as shown in Figure 6.16, the colour of the samples was different from that cured at 40$^{o}$C. A clear difference was observed in the sample containing metakaolin and slightly less in the PC-$BaSO_4$ powder system. The colour difference of the samples may be related to either the dehydration of hydrated phases or a less degree of hydration itself because a significant amount of water was found inside the container after the curing of these samples. The sample containing quartz powder did not show any obvious difference in the appearance and no water was found in the container after curing.

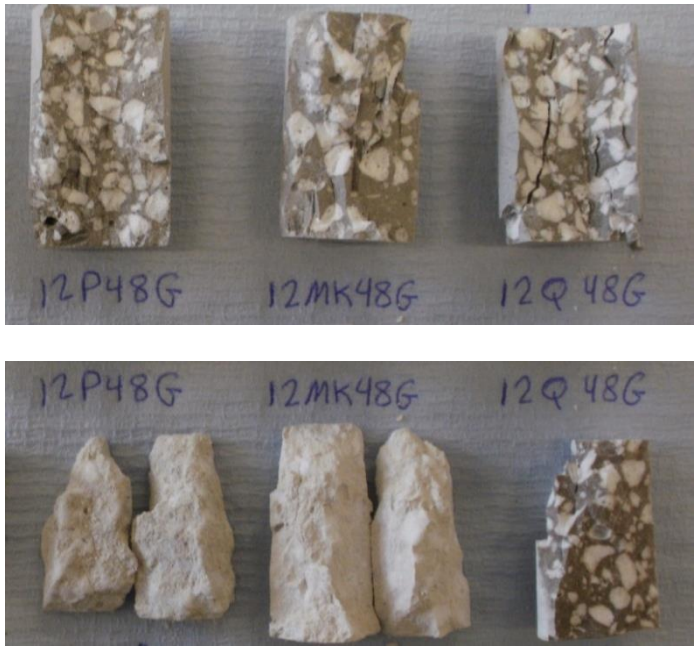


Figure 6.16 PC-mineral admixture samples cured at 40 $^{o}$C and cured under hydrothermal condition at 180 $^{o}$C

6.4.2 Phase analysis

Figure 6.17 shows XRD trace of the specimens after the hydrothermal curing at 180°C for 28 days. In samples containing 12 wt% $BaSO_4$ powder (Figure 6.17 a), reaction products were similar to those observed in the neat PC (Figure 6.9 b). Hydrogarnet, jaffeite and reinhardbraunsite were observed along with the formation of α-dicalcium silicate hydrate (α-$C_2SH$).

The replacement of the powdered $BaSO_4$ by metakaolin in the cement system (Figure 6.17 b) led to a slightly decrease in the intensity of portlandite, as a consequence of pozzolanic reaction took place with metakaolin [29]. One of the interesting effects of the hydrothermal curing to the 12MK48Gsample is the loss of the stratlingite which was observed in the same formulation cured at 40°C (Figure 5.13 and 5.15). It has been known that the high curing temperature contributes to the conversion of stratlingite to more stable hydrogarnet phase [30]. Formation Jaffeite, reinhardbraunsite and α-dicalcium silicate hydrate (α-$C_2SH$) phases were also observed.

The substitution of powdered $BaSO_4$ by quartz (Figure 6.17 c) led to a clear decrease in the portlandite peaks and the formation of tobermorite. It has been reported that autoclaving cement with finely ground quartz prevents the formation of portlandite, and results in the formation of tobermorite [31]. At high curing temperatures, the dissolution of quartz provides sufficient siliceous material to bring the Ca/Si ratio down to 1 or lower [6, 18]. The siliceous material reacts with $Ca(OH)_2$ initially, reducing the amount of $Ca(OH)_2$ [6]. Upon further dissolution of quartz and production of siliceous material, calcium from semicrystalline calcium-silicate hydrates reacts to give C-S-H (I) [6]. The Ca:Si ratios drop gradually to 0.8 as the reaction proceeds, and finally the C-S-H (I)

recrystallizes to 11A° tobermorite [6, 31]. XRD analysis for 12Q48G confirms that portlandite was totally consumed during the production of tobermorite as no peaks of $Ca(OH)_2$ was detected. The tobermorite formed appear to be poorly crystallined as it shows less defined peaks. Rather coarse quartz used in the present study must have caused the formation of tobermorite with a lower crystallinity [31]

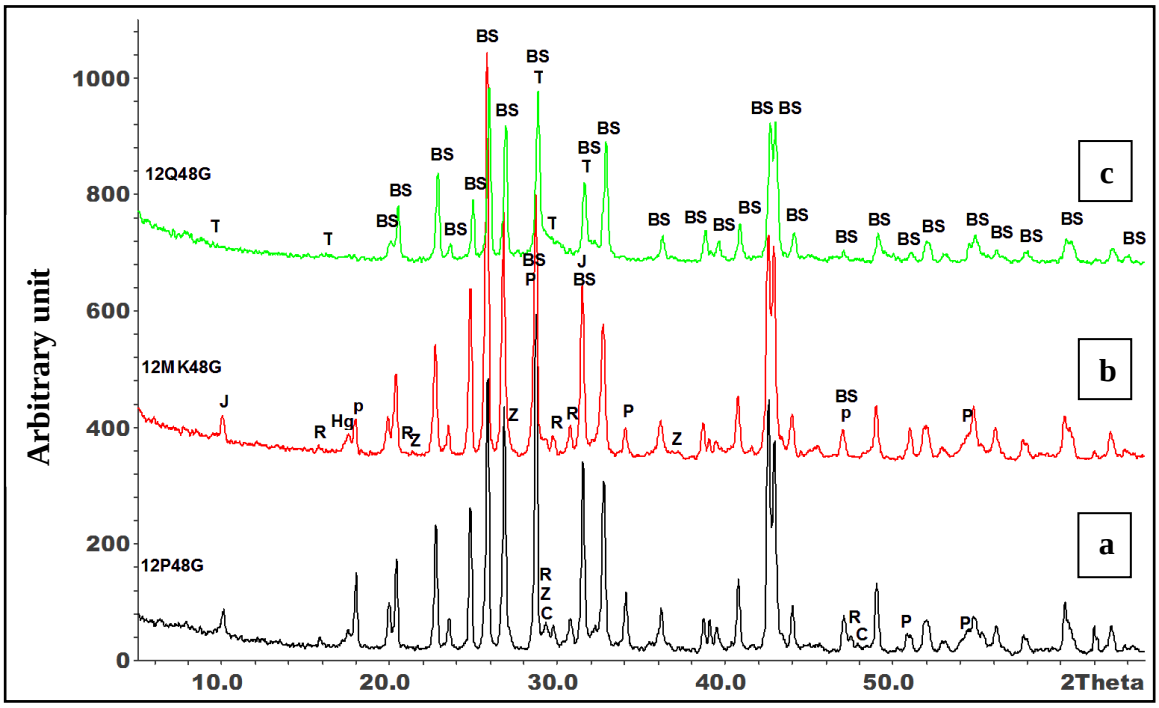


Figure 6.17 XRD trace of the specimens cured under hydrothermal condition at 180°C for 28 days.

TG-DTG data for the specimens are shown in Figure 6.18. The sample with 12wt% $BaSO_4$ and 12wt% metakaolin showed similar peaks in the DTG curves. A small peak observed at 370°C is assigned to the decomposition of hydrogarnet [5], in agreement with the XRD results (Figure 6.17). The weight

loss due to the dehydroxylation of $Ca(OH)_2$ at 450°C did not change significantly after the replacement of $BaSO_4$ powder by metakaolin, suggesting that the metakaolin had a weak pozzolanic reaction. This may be explained by the possible formation of an inhibiting layer of reaction product around the metakaolin particles under hydrothermal condition, which reduces their reaction with CH and further formation of hydration product as suggested by Khatib and Wild [32]. The peak assigned to the decomposition of α-dicalcium silicate hydrate phase was significantly increased in the 12MK48G sample. Metakaolin may have enhanced the formation of this phase by providing sufficient siliceous material. $CaCO_3$ was detected only in the 12P48G sample.

In the quartz-containing specimens (12Q48G), the mass losses between 70°C and 120°C are assigned to the loss of molecular water from tobermorite [6]. This specimen did not show a clear weight loss at 450, and thus CH may have totally consumed during the production of tobermorite, consistent with XRD observation. The peak of α-dicalcium silicate hydrate phase was not observed in this sample, suggesting that the most hydration product was tobermorite. Small peak for $CaCO_3$ was also detected.

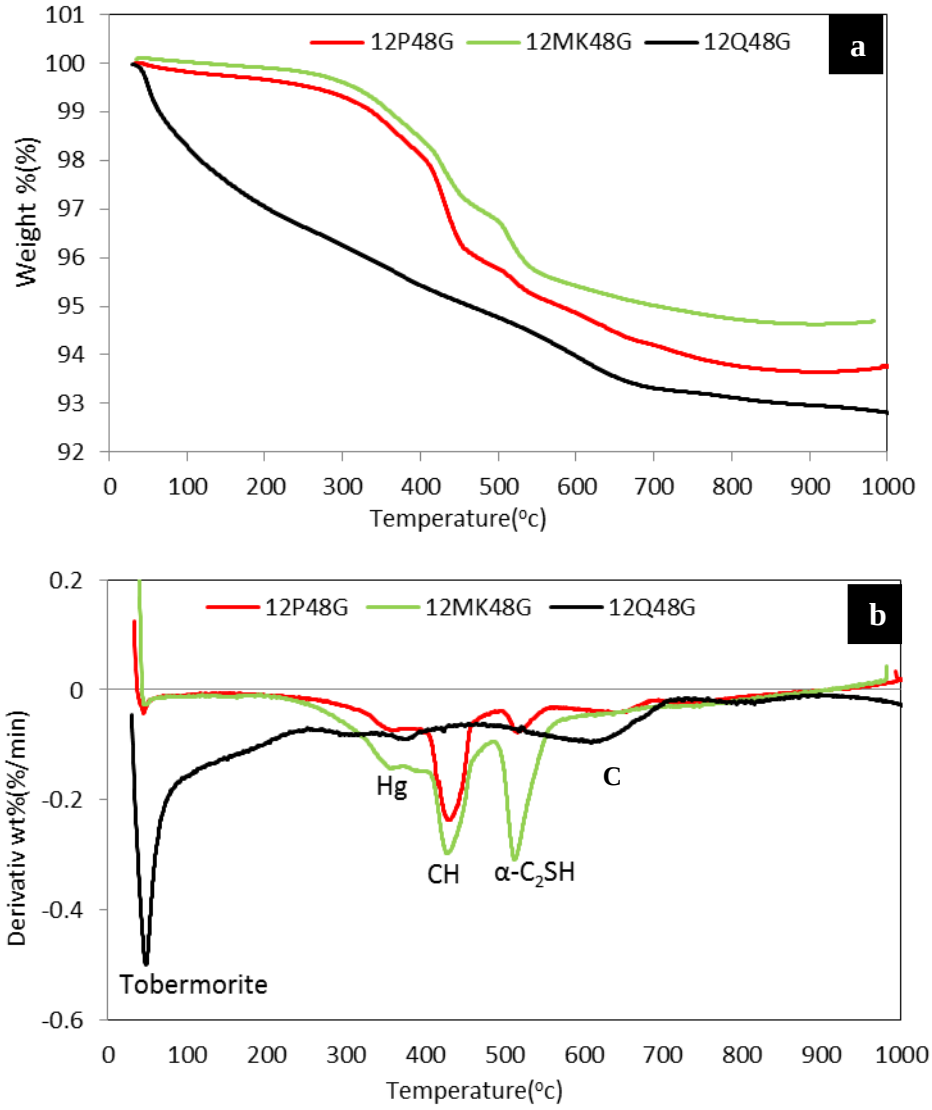


Figure 6.18 TG-DTG data for specimens cured under hydrothermal condition at 180°C for 28 days: (a) TG and (b) DTG

The total mass loss of each cement system, during the TG measurement are summarised in Table 6.4. In general, the total weight loss of all specimens significantly decreased when hydrothermally cured in comparison with the same samples cured at 40°C, suggesting that the hydrothermal curing had a significant effect on the cement hydration reaction. The specimen containing 12

wt% quartz presents a higher mass loss than the pastes formulated with 12 wt% $BaSO_4$ and 12 wt% MK, suggesting that the sample with 12 wt% quartz contained more bound water and was therefore hydrated to a greater extent. These results, in conjunction with XRD analyses, provide further evidence that the C-S-H formed in the samples with 12 wt% $BaSO_4$ and 12wt% MK are not stable during the hydrothermal curing.

Table 6.4 Total mass losses at 1000°C of PC-mineral admixture samples cured at 180°C for 28 days.

| **Sample ID** | **Total mass loss (%)** |
|---|---|
| 12 wt% P / 48 wt% G $BaSO_4$ | 6.23 |
| 12 wt% MK / 48 wt% G $BaSO_4$ | 5.38 |
| 12 wt% Q / 48 wt% G $BaSO_4$ | 7.77 |

### 6.4.3 Phase evolution

In order to assess the effect of curing time on cement hydration reaction under hydrothermal curing, TG analysis was performed on 12wt% $BaSO_4$ sample after 7 and 28 days of hydrothermal curing at 180°C. The result is shown in Figure 6.19. Differing from the sample cured for 28 days, the sample cured for 7 days showed the conventional cement hydration phases i.e. C-S-H and AFm. At 28 days, as already discussed, neither C-S-H nor AFm was observed, which suggests that the C-S-H phase progressively disappears during the hydrothermal curing and replaced by more stable phases with a higher Ca/Si ratio with a possible CH consumption [16]. In addition, more weight loss due to the decomposition of α-dicalcium silicate hydrate phase was observed after 7

days, compared with 28 days curing. The total weight loss of 12P48G cured for 7 days was significantly more than the same formulation cured for 28 days. The results show that the hydration products formed initially react each other to form more stable phases in this condition, and release the excess water as mentioned before.

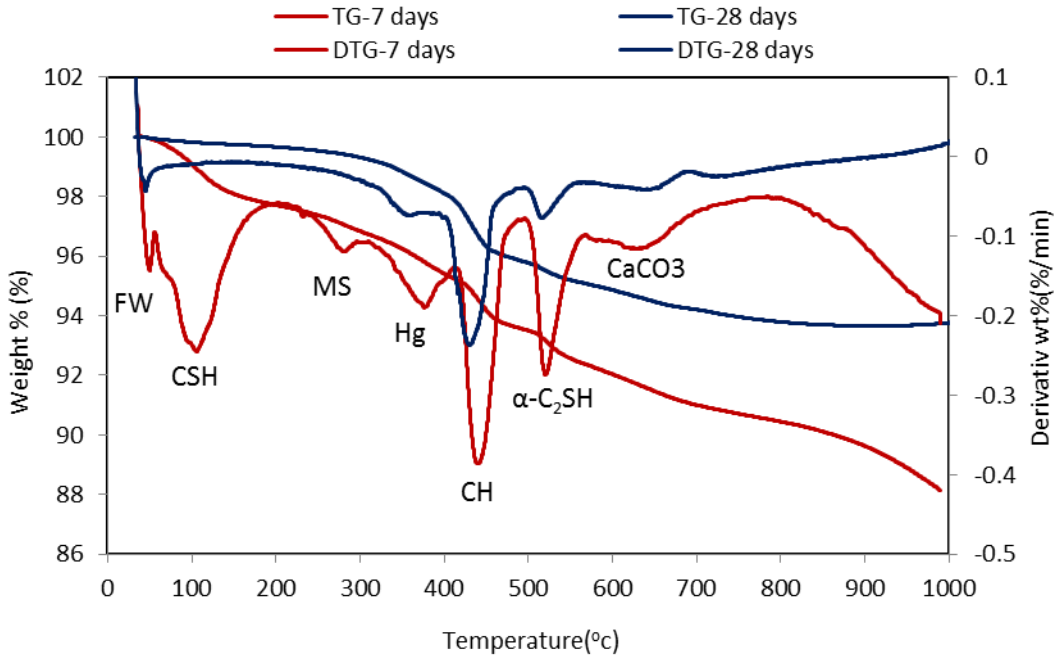


Figure 6.19 TG and DTG of 12P48G cured in hydrothermal condition for 7 and 28 days

### 6.4.4 Microstructure

Figure 6.20 shows the BSE of the 12P48G sample cured under hydrothermal for 28 days. The effect of hydrothermal condition on 12P48G was more uniform compared with the PC+60 wt% $BaSO_4$ granule sample (Figure 6.14b). The total porosity of 33.3% was also less than the 39% in the hydrothermally cured PC+60 wt% $BaSO_4$ granule system. The possible reason is the filler effect of fine $BaSO_4$ particles. The large surface area of $BaSO_4$ powder can enhance the

hydration reaction and fill the porous interfacial transition zone between the cement paste and $BaSO_4$ granule, resulting in more homogenous microstructure.

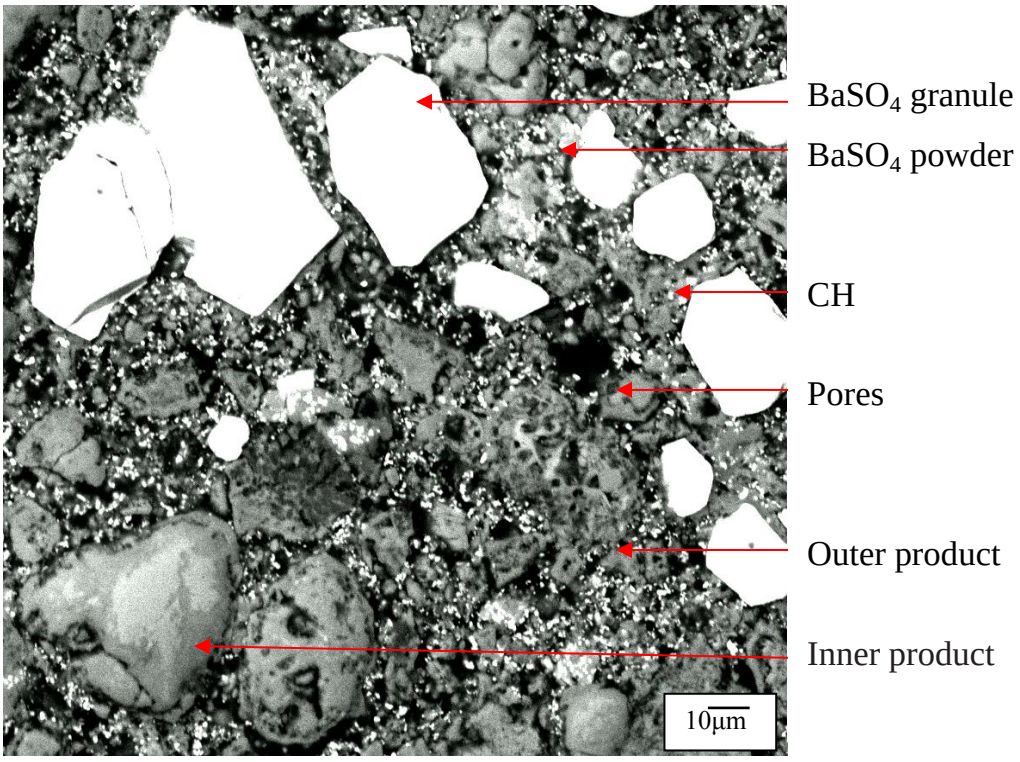


Figure 6.20 BSE images of 12P48G cured under hydrothermal condition for 28 days

EDS analysis for the same sample (Figure 6.21) shows that the outer product was mainly composed of calcium and silicon with a high Ca/Si ratio of approximately 2.88. This indicates that the matrix was most likely Jaffeite which has a Ca/Si ratio of 3 [18]. Higher silicon concentration was observed both in inner products and the anhydrous particles. The unreacted calcium silicate clinker phase was most likely $C_2S$ due to its lower reactivity compared to $C_3S$. The inner products had a significantly lower Ca/Si ratio than the outer products of approximately 1.83, implying that the inner products are likely α-$C_2SH$.

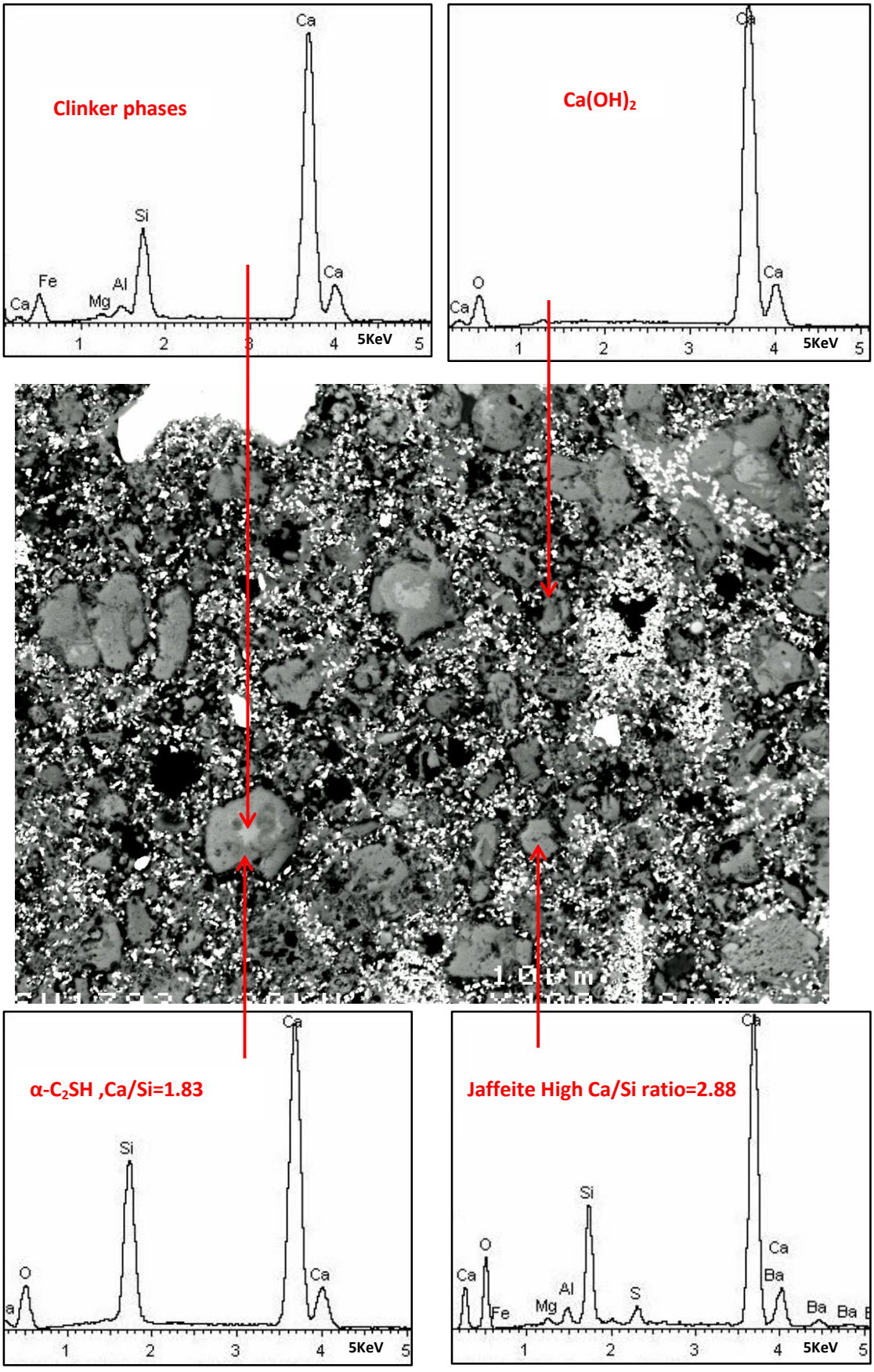


Figure 6.21 EDS of 12P48G cured under hydrothermal condition for 28 days

Figure 6.22 shows BSE images of 12MK48G. The microstructure is quite uniform with very fine porosity. The total porosity increased slightly compared to 12P48G sample. When used in cement pastes with a higher water content such as w/c=0.87, metakaolin causes smaller pore sizes but higher total porosity [33]. In addition, the shrinkage from the transformation of stratlingite to hydrogarnet also increases the porosity of the system. It has been reported that the transformation of this type can cause a reduction in the volume of cement hydration product approximately 13.3% [34]. Figure 6.23 shows EDS of the same sample. The point A corresponds to hydrogarnet, and point B α-$C_2SH$ phase.

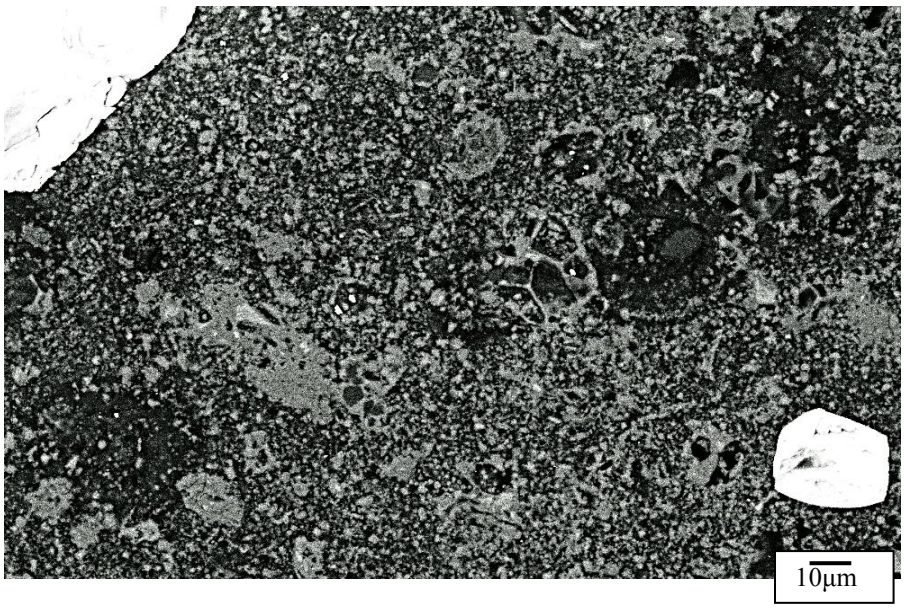


Figure 6.22 BSE images of 12MK48G cured under hydrothermal condition for 28 days

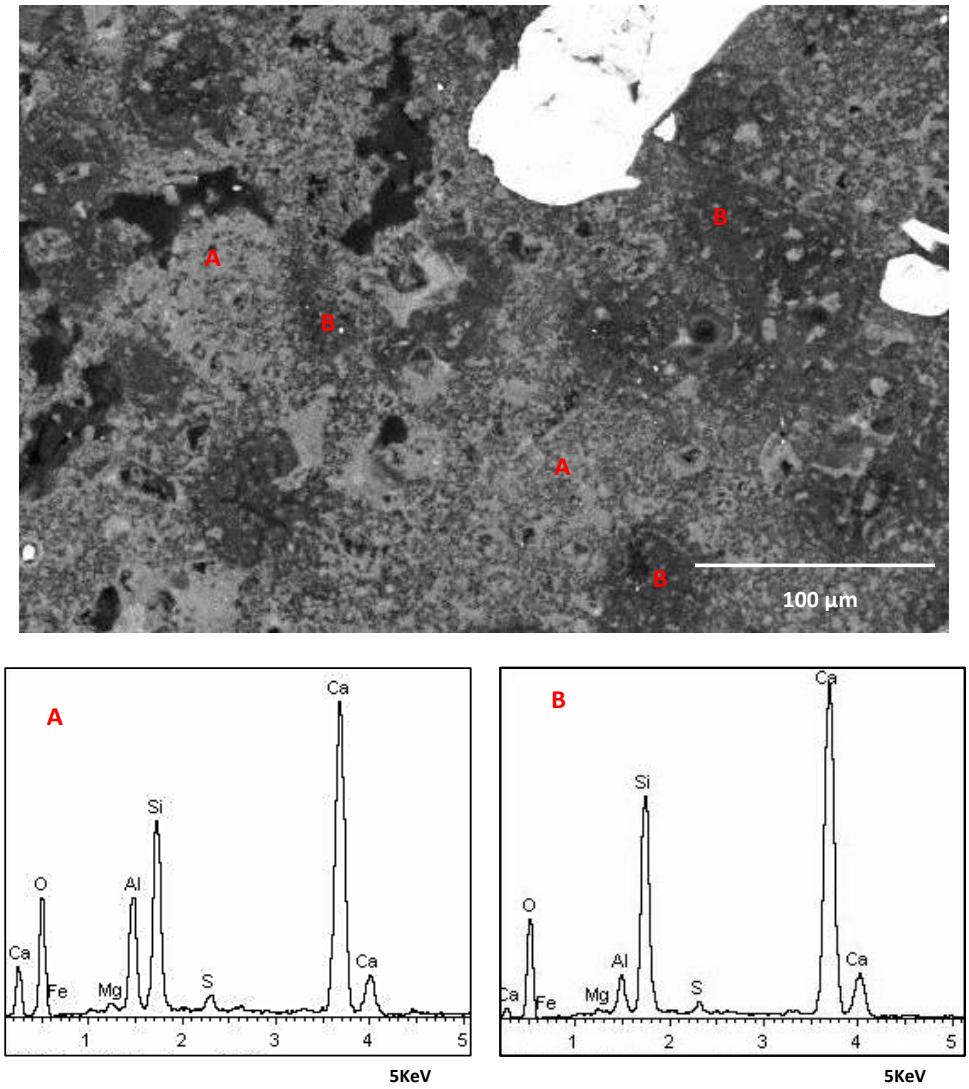


Figure 6.23 EDS of 12MK48G cured under hydrothermal condition for 28 days

Figure 6.24 shows BSE of the 12Q48G sample cured under the hydrothermal condition for 28 days. Fully hydrated cement grains can be easily distinguished and only a few partially hydrated grains are observed. It can be seen that the sample has a denser microstructure with small pores compared with the 12P48G and 12MK48G samples. The sample has limited amount of unreacted cement particles observed is likely because the pozzolanic reaction between portlandite and quartz took place to a higher extent in this sample as a result of

the steam effect under the curing condition so-called internal autoclaving effect [35]. Figure 6.25 shows EDS analysis of the same sample. The trace of point A shows the presence of fully reacted cement particle and that of B tobermorite phase.

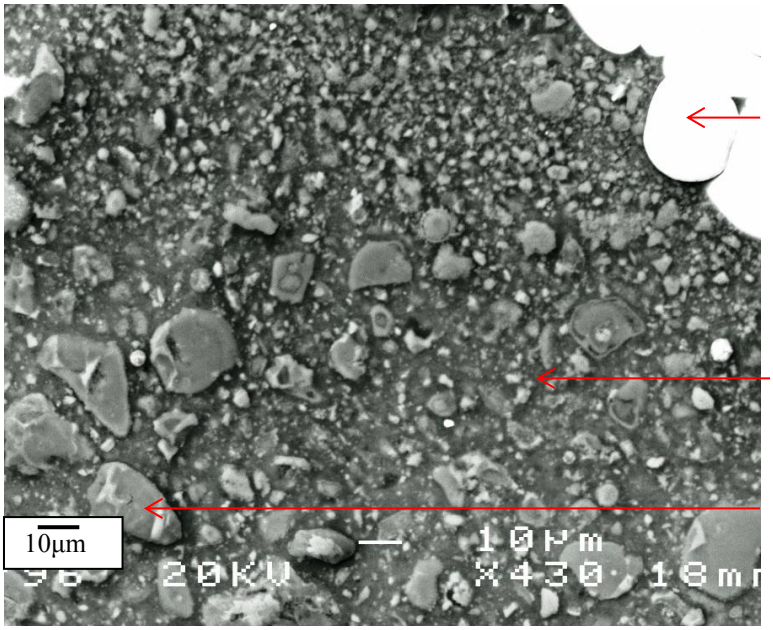


$BaSO_4$ granule

Tobermorite

Partially reacted cement particle

Figure 6.24 BSE images of 12Q48G cured under hydrothermal condition for 28 days

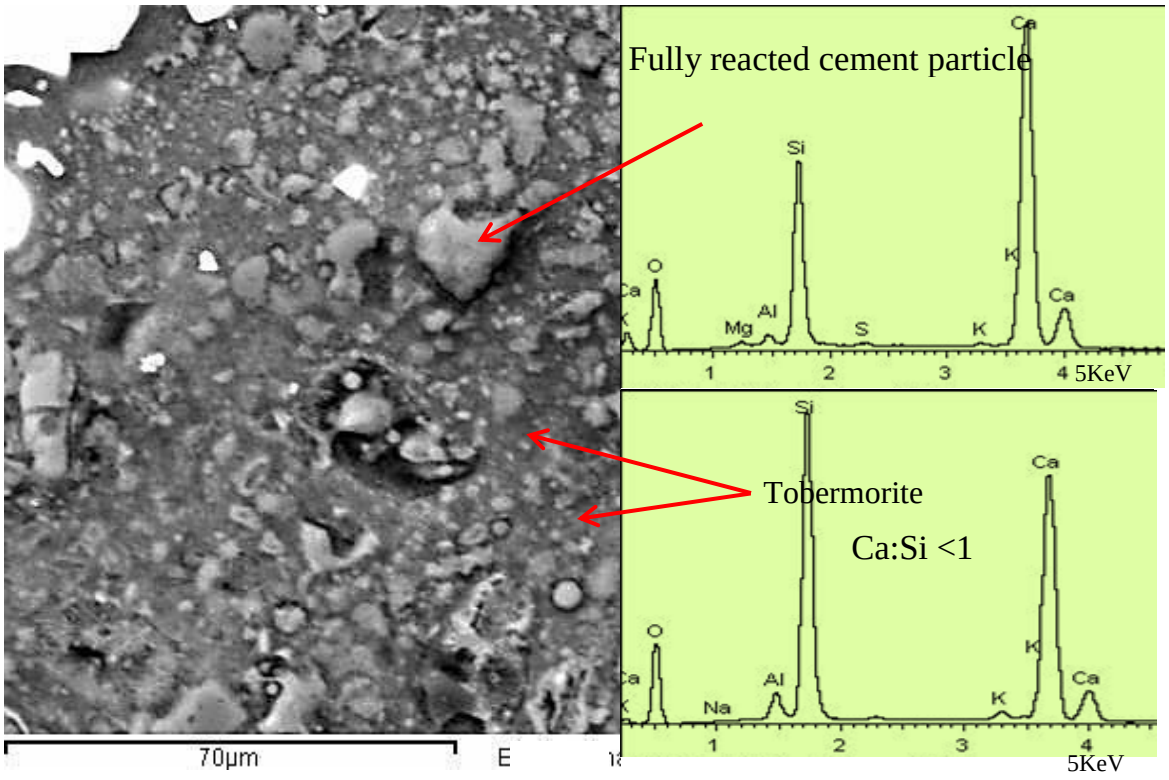


Figure 6.25 EDS of 12Q48G cured under hydrothermal condition for 28 days

Figure 6.26 compares the total porosity of the samples after the curing at 40°C and the hydrothermal treatment at 180°C for 28 days. The porosity was greater in all samples after hydrothermal curing, showing that the hydrothermal curing increases the porosity of the systems. The neat PC showed 48% increase in porosity. The 12P48G and 12MK48G samples showed a greater increase of 63% and 66%, respectively, whereas the 12Q48G sample had a smaller increase of approximately 39%.

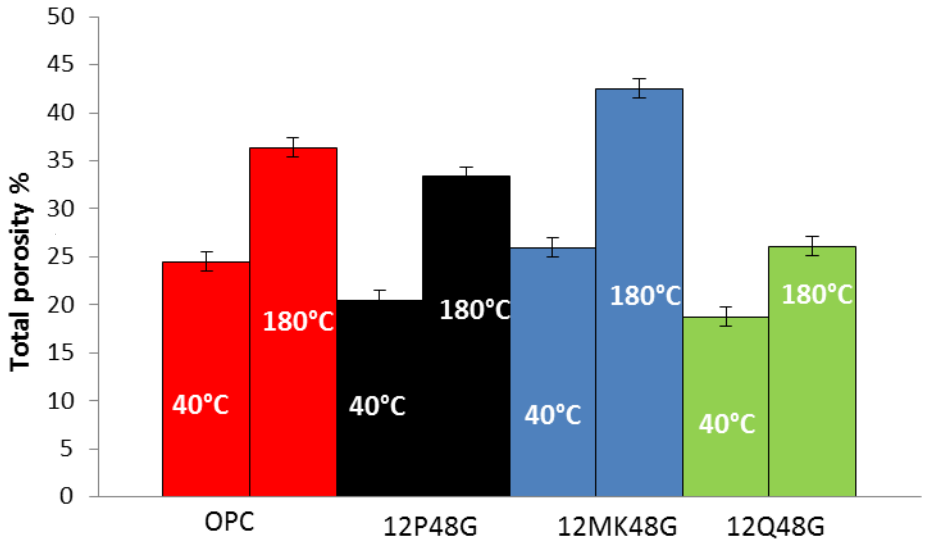


Figure 6.26 the total porosity of the samples before and after hydrothermal treatment at 180°C for 28 days

### 6.4.5 Strength regression

Figure 6.27 shows the compressive strength obtained for all samples cured under hydrothermal condition at 180°C for 28 days. All samples met the API recommended minimum of 6.9 MPa for compressive strength [20]. The values obtained ranged from just under 10 MPa to over 20 MPa, where PC has the lowest and 12Q48G has the highest strength value. The figure also shows the compressive strength data for these cured at 40°C for 28 days (same as in Figure 5.22). In hydrothermal curing, the mechanical strength clearly decreased compared to the same samples cured at 40°C. The impact of hydrothermal curing was significantly different depending on the samples. The impact of strength regression was most significant in the neat PC (76%). The 12P48G and 12MK48G showed a less strength regression of 59% and 63%, respectively, and the least strength regression was observed in the 12Q48G

(44%). As expected, the strength of neat PC sample was low, where the cement paste lost the main binding phase (C-S-H) as a result of the hydrothermal curing and formation α-$C_2SH$ [7, 8]. The α-$C_2SH$ has been known to increase in the permeability and strength reduction due to the volume reduction as a consequence of the formation of this phase under hydrothermal condition [6, 36]. The strength regression for the 12P48G sample probably because the less PC content in this system compared with the neat PC. The strength regression in the 12MK48G sample can be explained in terms of the extensive formation of α-$C_2SH$ and hydrogarnet, which is known to reduce the strength of cement paste [34]. It has been reported that metastable phases in PC-MK system can transfers to stable hydrogarnet phase with reduction in the cement paste volume about 13.3%, leading to the increase in porosity and decreasing the mechanical strength [34]. The 12Q48G sample indicated the least strength regression. It has been reported that the strength of the system in the hydrothermal condition can be maintained by the formation of crystalline tobermorite [37], while the low strength is usually ascribed to the presence of α-$C_2SH$ hydrate [13]. The formation of tobermorite phase was observed in this sample. Figure 6.28 show the general correlation between the strength regression and the porosity increase.

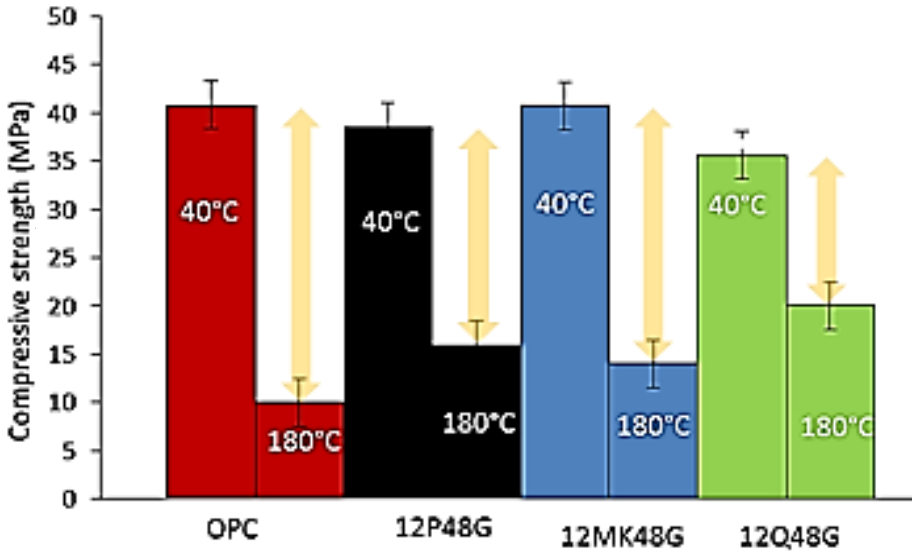


Figure 6.27 Compressive strength of the samples before and after hydrothermal treatment at 180°C for 28 days

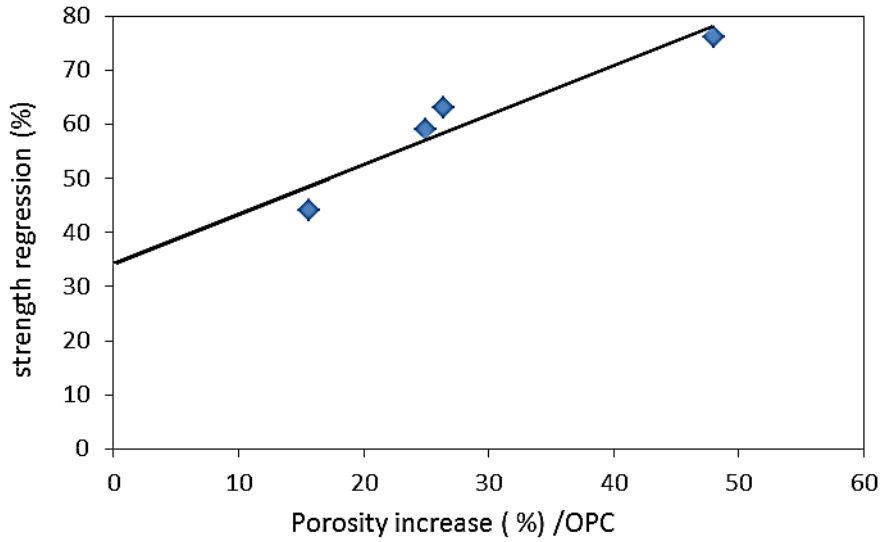


Figure 6.28 Correlation between the strength regression and the porosity increase of the samples after hydrothermal treatment at 180°C for 28 days.

## 6.5 Summary

The study on the heat treatment samples revealed that the neat PC and the PC with 60 wt% $BaSO_4$ granules indicated a similar response towards the heat treatment at 300ºC. After 24 hours of heat treatment, they lost a significant amount of the main binding phase C-S-H, as a result of the loss of chemically bound water from this phase and other cement hydration phases such as ettringite and monosulphate. This resulted in an increase of porosity, and a coarse pore structure that was significant in the system containing $BaSO_4$ granules.

The neat PC and the PC with 60 wt% $BaSO_4$ granules, when they were cured under hydrothermal condition at 180ºC for 28 days, did contain C-S-H or monosulphate phase, but showed the present of Jaffeite ($C_6S_2H_3$), reinhardbraunsite ($C_5S_2H$), and α-dicalcium silicate hydrate (α- $C_2SH$).

It was found that initially C-S-H and monosulphate forms through conventional hydration of PC cement, in addition to α- $C_2SH$ through direct hydration of $C_2S$. These phases are then replaced by more stable lime rich phases such as Jaffeite and reinhardbraunsite, possibly with a partial consumption of CH and α-$C_2SH$. The significant level of porosity after the hydrothermal curing is probably due to this phase evolution.

The formation of lime-rich phases, Jaffeite, reinhardbraunsite, and α-dicalcium silicate hydrate, was also observed when the fine $BaSO_4$ powder or metakaolin was introduced to the system. The amount of the hydrates was in proportion to the amount of PC in the system for the 12P48G sample due to the inert $BaSO_4$ powder. In the 12MK48G sample, increased α-$C_2SH$ and hydrogarnet were observed. These systems resulted in a similar level of porosity increase and

strength regression after the hydrothermal curing. On the other hand, the 12Q48G sample formed tobermorite without forming the lime-rich phases observed in the other systems. The low CH content may indicate a stronger pozzolanic behaviour of the quartz in the early stages of hydration, resulting in the formation of tobermorite. The formation of tobermorite instead of Jaffeite, reinhardbraunsite or α-dicalcium appeared to be very beneficial for the application of the cement paste under hydrothermal conditions as it indicated the minimal porosity increase and strength regression.

## 6.6 References


1. R. B. Gallaher and A. S. Kitzes, *Summary report on Portland cement concretes for shielding*. ORNL-1414. 1953: Oak Ridge National Laboratory
2. F. G. F. Gibb, N. A. McTaggart, K. P. Travis, D. Burley, and K. W. Hesketh, *High-density support matrices: Key to the deep borehole disposal of spent nuclear fuel.* Journal of Nuclear Materials 2008. **374** p. 370–377.
3. M. A. S. Anjos, A. E. Martinelli, and D. M. A. Melo, *Effect of sugarcane biomass waste in cement slurries submitted to high temperature and pressure.* Materials Science & Engineering, 2010.
4. F. G. F. Gibb, *High-temperature, very deep, geological disposal: a safer alternative for high-level radioactive waste?* Waste Management, 1999. **19** p. 207-211.
5. H. Taylor, *Chapter 7: Hydration of Portland cement* in *Cement Chemistry*. 1990, Thomas Telford London. p. 187-226.
6. V. S. Ramachandran, *Application of differential thermal analysis in cement chemistry*. 1969, New York: Chemical publishing company. 308.
7. M. C. R. Faragea, J. Sercombeb, and C. Galle, *Rehydration and microstructure of cement paste after heating at temperatures up to 300C.* Cement and Concrete Research, 2003. **33**( ): p. 1047–1056.
8. E. Annerel and L. Taerwe, *Revealing the temperature history in concrete after fir exposure by microscopic analysis.* Cement and concrete research, 2009. **39**: p. 967-970.
9. K. M. Haneefaa, M. Santhanama, and F. C. Parida, *Review of concrete performance at elevated temperature and hot sodium exposure applications in nuclear industry.* Nuclear Engineering and Design 2013. **258** p. 76-88.
10. L. Alarcon-Ruiz, G. Platret, E. Massieu, and A. Ehrlacher, *The use of thermal analysis in assessing the effect of temperature on a cement paste.* Cement and Concrete Research 2005. **35**: p. 609 - 613.
11. A. Mendes, J. G. Sanjayan, W. P. Gates, and F. Collins, *The influence of water absorption and porosity on the deterioration of cement paste and concrete exposed to elevated temperatures, as in a fire event.* Cement & Concrete Composites, 2012. **34**: p. 1067-1074.
12. J. Lee, Y. Xi, K. Willamb, and Y. Jung, *A multiscale model for modulus of elasticity of concrete at high temperatures.* Cement and Concrete Research 2009. **39** p. 754-762.
13. H. Taylor, *Chapter 11: Admixtures and special uses of cements*, in *Cement chemistry*. 1990, Academic Press: London. p. 365-371.
14. N. Meller, K. Kyritsis, and C. Hall, *The mineralogy of the CaO–Al2O3–SiO2–H2O (CASH) hydroceramic system from 200 to 350 °C.* Cement and Concrete Research 2009. **39**: p. 45–53.
15. M. Paul and F. P. Glasser, *Impact of prolonged warm (85ºC) moist cure on Portland cement paste.* Cement and Concrete Research, 2000. **30**(12): p. 1869-1877.
16. K. Luke, *Phase studies of pozzolanic stabilized calcium silicate hydrates at 180C.* Cement and Concrete Research, 2004. **34**( ): p. 1725 – 1732.
17. E. R. Buckle and H. F. W. Taylor, *The hydration of tricalcium and dicalcium silicates in pastes under normal and steam curing conditions.* Appl. Chem. , 1959. **9**: p. 163–172.
18. A. C. Jupe, A. P. Wilkinson, K. Luke, and G. P. Funkhouser, *Class H cement hydration at 180 °C and high pressure in the presence of added silica.* Cement and Concrete Research, 2008. **38**: p. 660–666.
19. K. Yanagisawa, X. H. A. Onda, and K. Kajiyoshi, *Hydration of β-dicalcium silicate at high temperatures under hydrothermal conditions* Cement and Concrete Research, 2006. **36**: p. 810–816.

20. N. B. Milestone, T. Sugama, L. E. Kukacka, and N. Carclello, *Carbonation of geothermal grouts-part 2: CO2 attack at 250°C.* Cement and Concrete Research, 1987. **17**: p. 37-46.
21. H. Sarp and D. R. Peacor, *Jaffeite, a new hydrated calcium silicate from the Kombat mineo Namibia.* American Mineralogist, 1989. **47**: p. 1203-1206.
22. G. L. Saout, E. Le´colier, A. Rivereau, and H. Zanni, *Chemical structure of cement aged at normal and elevated temperatures and pressures: Part I. Class G oilwell cement.* Cement and Concrete Research, 2006. **36**: p. 71-78.
23. C. Noik and A. Rivereau, *Oilwell cement durability*, in *The SPE Annual Technical Conference and Exhibition*. 1999: Houston-TX.
24. F. Meducin, H. Zanni, C. Noik, G. Hamel, and B. Bresson, *Tricalcium silicate (C3S) hydration under high pressure at ambient and high temperature (200 °C).* Cement and Concrete Research, 2008. **38**: p. 320–324.
25. H. Ishida, S. Yamazaki, K. Sasaki, Y. Okada, and T. Mitsuda, *α-Dicalcium Silicate Hydrate: Preparation, Decomposed Phase, and Its hydration.* American Ceramic Society, 1993. **7**(76): p. 1707–1712.
26. S. A. Bernal, R. M. Gutierrez, J. L. Provis, and V. Rose, *Effect of silicate modulus and metakaolin incorporation on the carbonation of alkali silicate-activated slags.* Cement and Concrete Research, 2010. **40**: p. 898–907.
27. J. M. Crennan, S. A. S. E.-. Hemaly, and H. F. W. Taylor, *Autoclaved lime-quartz materials. Some factores influncing strength.* Cement and concrete research, 1977. **7**: p. 493-502.
28. J. I. Escalante-Garcýa and J. H. Sharp, *Effect of temperature on the hydration of the main clinker phases in portland cement :part 1, neat cement.* Cement and Concrete Research, 1998. **28**( 9): p. 1245–1257.
29. B. B. Sabir, S. Wild, and J. Bai, *Metakaolin and calcined clays as pozzolans for concrete: a review.* Cement and Concrete Composites, 2001. **23**(6): p. 441-454.
30. F. W. Locher, *Stoichiometry of tricalcium silicate hydration*. 1966: Washington. p. 300-308.
31. D. S. Klimesch, A. Ray, and B. Sloane, *Autoclaved cement-quartz pastes: the effects on chemical and physical properties when using ground quartz with differnt surface areas. part 1:quartz of wide partical size distrbution* Cement and Concrete Research 1996. **26**(9): p. 1399-1408.
32. J. M. Khatib and S. Wild, *Pore size distribution of metakaolin paste.* Cement and concrete research, 1996. **26**: p. 1545–1553.
33. C. S. Poon, S. C. Kou, and L. Lam, *Compressive strength, chloride diffusivity and pore structure of high performance metakaolin and silica fume concrete.* Construction and Building Materials, 2006. **20** ( ): p. 858-865.
34. M. F. Rojas and M. I. S. n. d. Rojas, *Influence of metastable hydrated phases on the pore size distribution and degree of hydration of MK-blended cements cured at 60C.* Cement and Concrete Research, 2005. **35**: p. 1292– 1298.
35. M. S. Morsy, Y. A. Al-Salloum, H. Abbas, and S. H. Alsayed, *Behavior of blended cement mortars containing nano-metakaolin at elevated temperatures.* Construction and Building Materials, 2012. **35**( ): p. 900–905.
36. G. Bye, *Portland cement*, ed. 2. 1999: Thomas Telford.
37. A. Alhozaimy, M. S. Jaafar, A. Al-Negheimish, A. Abdullah, Y. H. Taufiq-Yap, J. Noorzaei, and O. A. Alawad, *Properties of high strength concrete using white and dune sands under normal and autoclaved curing.* Construction and Building Materials 2012. **27**: p. 218–222.

# Chapter 7: Conclusions

## 7.1 Characterisation of PC-$BaSO_4$ with high $BaSO_4$ loading

The present study investigated the effect of basic formulation on the PC-$BaSO_4$ system in particular $BaSO_4$ loading and water content using fine $BaSO_4$ powder and coarse granules. These data were used to establish the ability of cement matrix to encapsulate NORM scale waste. In the present study, both in PC-$BaSO_4$ powder and PC-$BaSO_4$ granule systems, it was possible to produce sold products up to 60 wt% of $BaSO_4$ loading which satisfied the minimum compressive strength of 7 MPa required for the radioactive cement wasteforms [1]. In both systems, the basic cement hydration products, C-S-H, portlandite, and monosulphate were formed, suggesting that $BaSO_4$ was encapsulated without obvious chemical reactions with the cement matrix.

Introduction of fine $BaSO_4$ powder, owing to the large surface area, resulted in an increased formation of $CaCO_3$ in the system investigated, which appeared to have significantly contributed to the compressive strength of the products. The amount of solid products in the system both hydration products and $CaCO_3$ appeared to contribute towards the strength of the system. The amount of water available in the system was found to be another important factor for $CaCO_3$ formation. A clear correlation between the w/c ratio of the system and the amount of $CaCO_3$ per unit PC was obtained. The $BaSO_4$ granules had different effects on the compressive strength of the products. The introduction of coarse $BaSO_4$ granules resulted in a significant decrease in strength due to the formation of highly porous interfacial transition zone. Increase of water in the system resulted in the increase in the porosity of products, which was more significant in the PC-$BaSO_4$ powder system than in the PC-$BaSO_4$ granule system. There was no significant difference in porosity between $BaSO_4$ powder

and $BaSO_4$ granule systems when w/c was 0.53. Maintaining the w/c ratio at this level would be beneficial to maintain a low porosity of the products.

Based on the obtained results, it is concluded that it is possible to achieve high $BaSO_4$ loadings whilst retaining the initial integrity of the wasteform products. It would be beneficial to incorporate small amount of fine $BaSO_4$ powder of about 12 wt% to maximise the strength of the product if the formation of $CaCO_3$ in the product is not an issue. $BaSO_4$ may be further incorporated, in the form of coarse granules to give a total of 60 wt% without reducing the strength of the product below 7 MPa. It is important to maintain w/c ratio at around 0.53 to keep the level of porosity in the final waste product around 25 % similar to the reference PC system.

## 7.2 Development of cement formulation for $BaSO_4$ NORM scale encapsulation

Sedimentation of $BaSO_4$ particles can occur in the cement paste due to its high density. Careful control of the setting time and the viscosity of cement slurry were necessary in order to avoid the sedimentation of $BaSO_4$ granules and obtain homogenous products.

The setting time of the neat PC was a function of the water content of the mixture, where the initial and final setting increased when w/c ratio increased. Introduction of fine $BaSO_4$ powder decreased both the initial and final setting times of the cement paste. Introduction of inert fine powder must have enhanced the hydration reaction owing to the large surface area. The introduction of metakaolin also resulted in the decrease in the initial and final

setting times. In this case, pozzolanic reaction must have contributed to the reduction of setting time in addition to increased surface area.

The study on the rheological properties revealed that the neat PC cement slurry with w/c=0.53 is capable of suspending $BaSO_4$ granules only with diameters less than 1.6 mm. Introduction of fine $BaSO_4$ powder was effective in improving the rheological properties of the cement paste. 12 wt% of $BaSO_4$ introduction was found sufficient to increase the viscosity and yield stress to give a cement paste which can suspend $BaSO_4$ granules 13.9 mm in diameter. The same amount of metakaolin or quartz was also found to be effective to suspend coarse $BaSO_4$ granules without sedimentation.

Based on the information gained, wasteform formulations were developed. Using both fine $BaSO_4$ powder and coarse $BaSO_4$ granules, it was possible to reduce the amount of highly porous interfacial zone around the coarse $BaSO_4$ granules, which resulted in the reduction of porosity, suppression of carbonation and improvement in the compressive strength. Replacing the fine $BaSO_4$ powder with metakaolin or quartz was also found effective to improve the microstructure of the wasteform. Although the metakaolin required more water, the pozzolanic reaction of metakaolin helped to maintain the strength of the product approximately at 40 MPa, a similar level as that of PC system.

The results of leaching tests were comparable with the literature data for nuclear wasteforms, suggesting that the developed formulation had sufficient durability. The amounts of Portlandite and C-S-H in the system have a significant effect on the leaching behaviour. The behaviour of Ba and S indicated a possible correlation with those of Ca and Si, respectively. Most of

the Ba found in the leachant was considered to be from the cement matrix, although this was not conclusive.

## 7.3 Behaviour of PC-$BaSO_4$ system in high temperature environment

The behaviour of PC-$BaSO_4$ cement system in high temperature environment was studied to assess the feasibility of using $BaSO_4$-containing cement systems as a potential support matrix for the deep bore geological disposal.

Both the neat PC and PC with 60 wt% $BaSO_4$ granules indicated a similar response towards the heat treatment at 300ºC. After 24 hours of heat treatment, the lost a significant amount of the main binding phase C-S-H, as a result of the loss of chemically bound water from this phase and other cement hydration phases such as ettringite and monosulphate. This resulted in an increase of porosity, and a coarse pore structure that was significant in the system containing $BaSO_4$ granules.

The neat PC and PC with 60 wt% $BaSO_4$ granules, when they were cured under hydrothermal condition at 180ºC for 28 days, did contain C-S-H or monosulphate phase, but showed the present of Jaffeite ($C_6S_2H_3$), reinhardbraunsite ($C_5S_2H$), and α-dicalcium silicate hydrate (α- $C_2SH$).

It was found that initially C-S-H and monosulphate forms through conventional hydration of PC cement, in addition to α- $C_2SH$ through direct hydration of $C_2S$. These phases are then replaced by more stable lime rich phases such as Jaffeite and reinhardbraunsite, possibly with a partial consumption of CH and α-

$C_2SH$. The significant level of porosity after the hydrothermal curing is probably due to this phase evolution.

The formation of lime-rich phases, Jaffeite, reinhardbraunsite, and α-dicalcium silicate hydrate, was also observed when fine $BaSO_4$ powder or metakaolin was introduced to the system. The amount of the hydrates was in proportion to the amount of PC in the system for the 12P48G sample due to the inert of the $BaSO_4$ powder. In the 12MK48G sample, increased of α-$C_2SH$ and hydrogarnet was observed. These systems resulted in a similar level of porosity increase after hydrothermal curing and strength regression despite having quite different microstructures. On the other hand, the 12Q48G sample formed tobermorite without forming the lime-rich phases observed in the other systems. The low CH content may indicate a stronger pozzolanic behaviour of the quartz in the early stages of hydration, resulting in the formation of tobermorite. The formation of tobermorite instead of Jaffeite, reinhardbraunsite or α-dicalcium appeared to be very beneficial for the application of the cement paste under hydrothermal conditions as it indicated the minimal porosity increase and strength regression.

Based on the obtained results, it is concluded that it would be possible to apply PC-$BaSO_4$ granule system as a high density support matrix for the deep borehole geological disposal. It is important to include quartz particles in the formulation to assure the sufficient rheological property and short-term strength.

## 7.4 References

1. Milestone, N.B., et al., *Carbonation of geothermal grouts-part 2: CO2 attack at 250°C.* Cement and Concrete Research, 1987. **17**: p. 37-46.

# Chapter 8: Future work

Future work

A number of questions remain unanswered from this project. If a complete understanding of the physical and chemical interactions between materials is required, further work should be performed in the following areas.

1. Both $BaSO_4$ powder and granule appeared to be incorporated into the cement hydration product without obvious chemical reactions with the cement matrix. However, there is a report suggesting the interaction between $BaSO_4$ and C3A [1]. More investigation is needed to confirm this.
2. Although the present study revealed that the initially formed C-S-H is replaced by Jaffeite, reinhardbraunsite later possibly with the aid of CH and α- C2SH, under hydrothermal condition, this reaction was not positively identified. It would be useful to understand the chemistry of these phase evolutions.
3. Most of the works in this project were up to 28 days. Considering the objective of the wasteforms or the high density support matrix, longe-term studies are necessary.
4. Most of the works in this project were focused on the pure $BaSO_4$ which would contain radioactive radium in the real NORM scale. Even though leach tests were performed on the PC doped with $BaSO_4$ acting as the representative of the scale, investigation on a cemented active $BaSO_4$ as (Ba, Ra) $SO_4$ scale would provide more accurate results on the durability of the wasteform produced in the industrial process.
5. Using radioactive Ra would be important to evaluate the stability of the cement matrix. Alternatively, gamma -ray irradiation can be used to study the effect of radiation on the cement wasteforms

Future work

## References

1. **Tsuyuki, N., et al.,** ***Effects of barium salt on the fixation of chloride ions in hardened mortars.*** **Cement and Concrete Research 2000. 30: p. 1435-1442.**

# Appendix- Publications

## Journal Papers

1. O. Hussein, C. Utton, M. Ojovan, H. Kinoshita. The effects of $BaSO_4$ loading on OPC cementing system for encapsulation of $BaSO_4$ scale from oil and gas industry, Journal of Hazardous Materials, 2013, 261, pp. 11-20.
2. O. H. Hussein, S. A. Bernal, C. A. Utton, H. Kinoshita, Mineral admixtures modifying the structure of $BaSO_4$-containing cement wasteforms, Journal of Hazardous Materials, 2013, waiting submission.
3. O. H. Hussein, S. A. Bernal, H. Kinoshita, High density support matrices for deep bore hole geological disposal, Journal of Hazardous Materials, 2013, this paper is waiting submission.
4. N. Mobasher, S. A. Bernal, O. H. Hussein, D. C. Apperley, H. Kinoshita, C. A. Sharrard, J. L. Provis, Characterisation of Ba(OH)2-Na2SO4-blast furnace slag cement-like composites. Currently being prepared for submission to Journal of Nuclear Materials, 2013
5. N. Mobasher, O. H. Hussein, S. A. Bernal, H. Kinoshita, J. L. Provis, Performance and structural changes induce by high temperature exposure of $BaSO_4$-Portland cement wasteforms. Currently being prepared for submission to Waste Management, 2013

## Conference Publications

1. Encapsulation of radioactive waste from oil industry in composite cement system, Conference of Engineering Sciences, London, UK (2011), (First prize for poster competition)
2. O. Hussein, M. Ojovan, H. Kinoshita, Immobilisation of $BaSO_4$: Phases and microstructure of OPC-$BaSO_4$ system cured at an elevated temperature, WM2011, Phoenix, AZ (2011)
3. O. Hussein, M. Ojovan, H. Kinoshita, Immobilisation of $BaSO_4$: the effect of fine $BaSO_4$ powder on the microstructure and strength of OPC- $BaSO_4$ cured at an elevated temperature, NEWCEM2011, Avignon, France (2011).